DYNAMIC INELASTIC RESPONSE AND FAILURE OF STRUCTURAL ELEMENTS

Failure Initiation, Criteria and Mechanisms

Qingming Li

THE UNIVERSITY
of LIVERPOOL

DYNAMIC INELASTIC RESPONSE AND FAILURE OF STRUCTURAL ELEMENTS

Failure Initiation, Criteria and Mechanisms

Thesis submitted in accordance with the requirements of

the **University of Liverpool**

for the degree of **Doctor in Philosophy**

by **Qingming Li**

November 1997

THE UNIVERSITY
of LIVERPOOL

to Guoqing, Xiang
and my parents

Acknowledgments

I would like to take this opportunity to express my sincere and deep gratitude to Professor Norman Jones for his outstanding and enthusiastic support and supervision throughout this study. His creative and rigorous attitude to scientific research is much appreciated and unforgettable.

Thanks also to Dr.R.S.Birch, from the Impact Research Centre, for his kind and efficient help on experimental techniques. To Dr.G.K.Schleyer for his concerning the progress of this work. My colleagues, Dr.H.M.Wen, Dr.M.Alves, Dr.C.C.Yang, Dr.M.White and Ms.C.Jones have contributed in various ways to this work.

My thanks are also due to all staff of the Impact Research Centre and Department of Mechanical Engineering, University of Liverpool for their dedication. In particular, Mrs.M.White, Mr.G.Swallow, Mr.P.Smith and Mr.J.Curran provided invaluable help throughout the course of this project.

The financial support from the Impact Research Centre, ORS Award, Christine King Memorial Trust, Henry Lester Trust, John Lennon Memorial Scholarship and the Great Britain-China Educational Trust throughout this study are gratefully acknowledged.

I also wish to express my gratitude to Taiyuan University of Technology, where I lectured previously, for concerning this research programme. Professor G.T.Yang, former president of Taiyuan University of Technology, gave me firm support and encouragement from the beginning of the project. Professor T.X.Yu from Hong Kong University of Science and Technology, Professor L.L.Wang from Ningbo University and Professor J.L.Yu from the University of Science and Technology of China provided various help in the early stage of this work.

Thanks to my parents with my deep indebtedness for their fundamental support and encouragement.

Finally, I dedicate this work to my beloved wife, Guoqing, and my lovely daughter, Xiang, for their great and consistent encouragement, patience and their love during my study for this thesis.

Dynamic Inelastic Failure of Structural Elements

------Failure initiation, criteria and mechanisms

Abstract

The dynamic shear response and failure of structural elements under transverse impact loads are studied in the present work.

The dynamic shear response is one of the important response modes in structural elements under transverse impact loads, which may lead to various shear failures depending on the loading rates and intensities. Transverse shear localization phenomena, which are represented by a shear hinge, have been observed in several structural elements when subjected to transverse dynamic loading and are studied in this thesis. The features of a stationary shear hinge are illustrated using a rigid, perfectly plastic simplification. The dimensions of a shear hinge for several structural elements are estimated both theoretically and numerically. It is shown that there exists a fixed shear hinge length for a given two-dimensional structural element. The length of a shear hinge is determined by its bending and shearing properties which can be obtained from a quasi-static analysis. When the shear hinge length has been determined, the conventional rigid-plastic method can be used to calculate the shear strain and shear strain rate within the shear hinge during the shear response phase. These theoretical results are employed to model Menkes and Opat's beam problem to find two possible failure mechanisms, i.e., ductile shear failure and adiabatic shear failure and the associated transition conditions.

A double-shear beam(DSB) subjected to a transverse projectile impact is studied experimentally and numerically in order to provide a more fundamental understanding on the features of structural failure in a localised shear zone. Both ductile tensile failure and adiabatic shear banding failure are found in the shear notch section. An analytical model and FEM simulation are developed to predict the DSB response and failures. The theoretical background of the strain energy density failure criterion is discussed and verified in this problem. Among the failure criteria examined in the current study, the strain energy density failure criterion is observed to give reasonable predictions for the failure initiation.

Contents

I. PREFACE

I.I Scope of the Problem

Unfortunately, structural failure is not an infrequent occurrence in modern society, and sometimes leads to a large loss of life, destruction of property and damage to the environment. The failure of structures due to an improper use of material has also caused many disasters. It is remarked in the preface of Wierzbicki and Jones(1989) that "It is the responsibility of scientists and engineers to determine the cause of failure, to describe the failure process, and to suggest measures of preventing the failure from recurring". In order to achieve this aim, many investigations have been conducted in the field of structural crashworthiness and hazard assessment. For example, three successive international symposia on structural crashworthiness(Jones and Wierzbicki(1983), Wierzbicki and Jones(1989) and Jones and Wierzbicki(1993)) have been held since 1983. These and many other conferences on the behaviour of structures and systems have reported valuable results which may be used for generating design methods and design data.

Frequently, external dynamic loads from impacts and explosions play an important role in many structural failures. Even when the structural failure is initiated sometimes from a static loading, the subsequent process is often a dynamic one. The dynamic behaviour of various structures is a complicated process particularly when material failure is involved. Therefore, an understanding of the basic failure modes of structures is important for assessing the safety of practical structures in extreme loading environments.

Generally speaking, every structural system consists of some basic structural elements. The most frequent structural elements are beams, plates and shells. Thus, investigations into the dynamic behaviour of these typical structural elements are important for understanding the dynamic behaviour of a structural system which is made of these elements. Basically, the dynamic behaviour of a structural element involves its dynamic response, the initiation of failure and the failure process up to complete collapse. Excessive deformations of structural elements may be an important type of failure from an engineering viewpoint, for example, ingress into

the minimum survivable occupant space in a vehicle. The dynamic response of structural elements under large dynamic loadings often gives rise to plastic deformations, which have been studied successfully using the well-developed rigid-plastic method of analysis. The basic principles and developments of this method have been introduced and reviewed by Jones(1989a,b). Many FEM softwares are also capable of solving these problems. When the plastic deformations in structural elements reach a critical value then a material failure will occur. The crucial point for predicting material failure in structural elements is how to develop an appropriate failure criterion and the corresponding analysis procedure, which can be used easily by an engineer. The post-failure process is much more complicated because of the interaction between the structural response and developments of material failure. Although some studies have touched upon this topic, there remain many difficulties requiring resolution in theoretical analyses, numerical methods and experimental techniques.

Developing a proper failure criterion is crucial for predicting the initiation of material failures in structural elements. Both analytical and FEM models need the material failure criterion in structural failure analysis. Although many failure criteria have been proposed for various practical applications there is still a shortcoming in their physical foundations. Furthermore, different failure mechanisms may lead to totally different failure types. A transition between two different failure mechanisms requires totally different failure criteria in failure analysis.

Generally, two major classes of external loadings for a structural element are associated with axial impact(or in-plane impact for plates) and transverse impact. One possible structural failure mechanism for the first situation is the occurrence of dynamic buckling, which may lead to material failure due to large localized strains. Some methods of analysis for the dynamic buckling response of structural elements have been discussed by Jones(1989a,b) though virtually no attention has been given to the consequences of material failure. Our particular attention in this research will focus on the dynamic ductile failure of structural elements under transverse loading which is a very common loading throughout many engineering industries. Investigations into the basic failure mechanisms of structural elements under

transverse impact loadings are important for understanding the complicated failure modes in many practical situations in the field of impact engineering.

As the simplest structural element, the behaviour of a beam under transverse dynamic loading yields some important characteristics for the response of other structural elements subjected to similar dynamic loadings. Therefore, an investigation into the failure modes of a beam under a transverse dynamic loading will assist our understanding of the failure mechanisms for more complex structural systems.

The scope of the present work is to study the localised shear deformation behaviours and various failure mechanisms in a transversely loaded structural element.

I.II Outline of the Current Work

Dynamic transverse loading is a common loading type in structural dynamics. Transverse shear localization and failures are frequently observed in practices, and are studied throughout this thesis. The behaviour of a transversely loaded structural element and various failure mechanisms and failure criteria are introduced in Chapter 1, in which both ductile shear failure and adiabatic shear failure as well as the possible transition between different failure modes are discussed. A rigid, perfectly plastic theory is proposed in Chapter 2 to illustrate the shear localization phenomena in structural elements when subjected to a dynamic transverse loading, which offers a theoretical foundation for using the concept of stationary shear hinge in the dynamic plastic response of structural elements. In order to estimate the deformation distributions in a shear hinge, Chapter 3 evaluates the size of a shear hinge for various structural elements. FEM simulations are conducted to describe the actual formation process of transverse shear localization. These results give important information for predicting the initiation of ductile shear failure and an adiabatic shear band. Transition between these two failure mechanisms in a fully clamped beam when subjected to an impulsive pressure loading is studied in Chapter 4 by using rigid, perfectly plastic analysis and the knowledge developed in Chapters 1 to 3. A similar discussion is conducted for circular plates and cylindrical shells, and projectile impact loadings.

In order to have a deep understanding on transverse shear response and failure phenomena, experiments and results on double shear beams under projectile impact are presented in Chapter 5. A thermo visco-plastic constitutive equation is also proposed there based on static tensile, dynamic compressive and high temperature test data. Both transformation and deformation shear bands are observed under different conditions. Two different failure mechanisms, i.e., tensile fracture failure and adiabatic shear band failure, are found at the notch corners. The response and failure phenomena observed in Chapter 5 are analyzed by using an analytical model and the FEM method in Chapter 6. Different failure criteria are verified using the experimental results.

Comments and main achievements are concluded in Chapter 7.

I.III Notation

A_k, P_{ij}, Y_{ij}	thermodynamic forces
B	beam width
c_e, c_p	elastic and plastic shear wave velocities
c_v	specific heat
D	damage parameter
e	half length of a shear hinge
E	Young's modulus
$\tilde{E}$	Young's modulus of the material when free from any damage
E_h	hardening modulus
f	void volume fraction
F_1, F_2, F_3	static, dynamic and temperature factors in a thermo-viscoplastic constitutive equation
H	thickness of structural element
I_r	rotatory inertia of a beam cross-section
J	volume ratio of material
K_v	thermal conductivity
l_m, l_s, l_n	length of the plastic bending, shear and membrane hinges
L	beam span
M	bending moment
P_0	pressure of the gas gun
q	parameter in Cowper-Symonds equation (5-3)
Q	transverse shear force
t	time
T	temperature
T_m	melting temperature
T_r	room temperature
u	axial displacement
V_0	initial velocity
V_c	critical velocity

V_k	plastic internal variables
w^p	inelastic strain energy density
w_c^p	critical value of w^p at failure
W_s	transverse shear displacement
β	Taylor-Quinney coefficient
γ	engineering shear strain
Δ	shear hinge length
ε_{ij}	strain
ε_e	von-Mises equivalent strain
ε_{EOf}	zero gauge length engineering strain
ε_{NOf}	zero gauge length natural rupture strain
κ	bending curvature
ν	Poisson's ratio
ξ	discontinuity interface location
ρ	material density
σ	effective stress
σ_0	yield stress
σ_e	von-Mises equivalent stress
σ_E	uniaxial engineering stress
σ_H	hydrostatic stress
σ_m	$3\sigma_H$
σ_T	uniaxial true stress
σ_{Tf}	uniaxial true stress at failure
σ_{TR}, T_p	defined in eq.(A14)
τ	shear stress
$\dot{\phi}$	intrinsic mechanical dissipation rate
$\dot{(\ )}$	d/dt
$(\ )'$	$\partial/\partial x$
$\|\|$	absolute value

1. INTRODUCTION

1.1. Introduction

Dynamic inelastic response and failure of structural elements under intensive loadings are of importance for safe design in the field of structural crashworthiness. Different dynamic loadings may lead to the development of a different response and failure modes. Three basic response and failure modes associated with a uniformly distributed impulsive pressure loading were observed by Menkes and Opat(1973) for a fully clamped beam, e.g.,

Mode I: Large inelastic deformations,

Mode II: Tearing(tensile failure) of outer fibres at or over the supports,

Mode III: Transverse shear failure at the supports,

which develop with an increase of loading intensity, as shown in Fig.1.1. Similar conclusions on a beam were reached by Ross, et al.(1977). Further experiments have confirmed the existence of three response and failure modes in square plates(Ross, et al.(1977), Olson, et al.(1991)), circular plates(Teeling-Smith and Nurick(1991)) and cylindrical shells(Ross, et al.(1977), Opat and Menkes(1974) and Stricklan, et al.(1976)), which have received considerable attention in recent years due to their widespread use in various engineering fields. A reasonable failure criterion together with a dynamic analysis procedure is necessary for understanding the responses and failure modes in order to assess the structural safety under transversely dynamic loads.

A theoretical analysis based on the rigid, perfectly plastic idealization together with an elementary failure criterion was suggested by Jones(1976,1989) to predict the occurrence of these response and failure modes in a fully clamped beam. A similar analysis was adopted by Duffy(1989) to predict the transverse shear failure at the hard-point of a cylindrical shell. Lately, a more universal theoretical procedure using the inelastic strain energy density failure criterion, as discussed in Appendix B, together with rigid, perfectly plastic analysis has been proposed to predict the observed response and failure modes in several structural elements(Shen and

Jones(1992), Shen and Jones(1993) and Jones and Shen(1993)). Material strain hardening and strain rate effects have been considered by Wen(1996) in an analysis of the response and tearing failure of a fully clamped beam. Alves(1996) incorporated damage mechanics into a rigid-plastic analysis to predict beam failures, while, some studies have combined FEM simulations with a failure criterion(Yu and Jones(1989), Clift, et al.(1990)). However, it appears that there are still many difficulties in incorporating failure criteria into a FEM procedure for a dynamic response and the failure of structures(Yu and Jones(1997)).

An important response feature of a structural element under a transverse dynamic loading is the localization of deformations, represented by bending and shear hinges, during the initial response period, which is followed by bending and membrane responses. Generally, a shear hinge may be initiated firstly by an intensive dynamic loading, followed by bending and then membrane responses if material failure does not occur. A bending hinge is normally associated with low loading rate and low to medium loading intensity, which develops into a membrane state with the increase of transverse displacement. However, material failure may occur at any time when a failure criterion is satisfied at the location of localized deformation. If material failure occurs during the transverse shear response phase, it is characterized by a Mode III failure. A mode II failure is associated with bending and membrane responses, although previous shear deformations may contribute to the final failure. Clearly, Mode I is not associated with an actual material failure. Because large permanent deformations of structural components may damage the contents in the structure, a Mode I response is considered as a particular safety criterion from the engineering view-point.

The failure criteria discussed in Section 1.3 may be used to predict material isothermal failure including Modes II and III, where equilibrium thermodynamic principles are applicable. However, the response characteristics associated with Mode III may lead to a different failure mechanism, known as an adiabatic shear band, which is initiated by material instability due to thermal softening. As pointed out previously, both Mode II and III failures result from localized deformations in a structural element related to bending and shearing hinges during the early response phases. The physical nature of bending and shearing hinges in a transversely loaded

structural element will be studied in Chapter 2 using a rigid, perfectly plastic idealization.

In the present chapter, a transverse shear localization and related failure mechanisms will be discussed. The possible failure mechanisms in a transverse shear hinge include isothermal fracture failure and an adiabatic shear banding failure. General features of a transversely loaded structural element will be discussed in Section 1.2. Various failure criteria that may be used to predict structural material failure are reviewed in Section 1.3. Shear banding phenomenon is discussed in Section 1.4. Failure transition between these two failure mechanisms is introduced in Section 1.5.

1.2 Transverse Shear Response and Failure

It has been shown that transverse shear forces may influence significantly the response of plastic structural elements under dynamic lateral loadings(Jones(1989)). Experimental and analytical results on the dynamic plastic response of structural elements have shown the existence of a transverse shear hinge which is an idealization of a localized shear zone. The critical conditions for the occurrence of transverse shear hinge(sliding) have been obtained for various structural elements(Jones(1989), Li and Jones(1994), Li and Jones(1995a,b)) using the rigid, perfectly plastic assumption. It appears that transverse shear localization is closely associated with the two dimensionless parameters for a sufficiently rapid loading

$$p=\frac{P}{P_0} \quad \text{and} \quad v=\frac{Q_0 R}{2M_0}, \tag{1-1a,b}$$

where P is the pressure intensity of the loading, P_0 is the static plastic bending collapse pressure, Q_0 and M_0 are the fully plastic generalized forces in structural elements, R is the dimension of structural element, i.e., radius for circular plate or the half length for a beam and a cylindrical shell(Li and Jones(1991), Li and Jones(1995b)). Critical curves for the initiation of a transverse shear hinge in several structural elements are shown in Fig.1.2 where a transverse shear hinge is initiated above the corresponding curve. Another important factor which influences the initiation of a transverse shear hinge is the loading rate described by V/c_p, where V

is the loading velocity and c_p is the propagation speed of transverse plastic shear deformations in a structural element, as shown in Chapter 3. Once a transverse shear hinge has been formed, the external energy will be dissipated mainly through shear deformations within the plastic hinge.

Symonds(1968) was the first to provide a theoretical illustration for the phenomenon of localized shear deformations in rigid, perfectly plastic beams. He discussed the influence of the transverse shear force on the dynamic plastic response of beams, and proved that a rigid-plastic shear interface remains stationary during the dynamic plastic response. Although, Symonds' results are based on a particular square yield curve which relates the bending moment and the transverse shear force, his conclusions have been extended in Chapter 2 to general regular and singular yield conditions, and furthermore, to circular plates and cylindrical shells. It is evident that the accumulated shear deformations at a stationary plastic hinge will be responsible for both the transverse shear failure observed by Menkes and Opat(1973) and the adiabatic shear banding mechanism discussed in Section 1.4.

The transverse shear hinge introduced into a rigid, perfectly plastic analysis is an idealization of rapid changes in transverse displacement across a short section of a beam. The distribution of transverse shear deformations within the shear hinge are complicated and cannot be determined with the aid of a rigid, perfectly plastic method of analysis. However, experimental evidence(Zener(1948), Jouri and Jones(1988)) suggests that the section which is deformed in shear is anti-symmetrical about its mid-point for a pure shear hinge and may be divided into two parts with rapid and slow changes of the transverse displacements in zones I and II, as shown in Fig. 1.3. Most of the transverse shear deformation occurs within the zone I so that the transverse shear sliding across a shear hinge is due mainly to the transverse displacement accumulated across this zone. The shear deformation within zone I is almost a simple shear flow, which is determined by

$$\gamma=\frac{W_s}{\Delta} \tag{1-2}$$

where W_s is the transverse shear sliding across the shear hinge and Δ is the length of shear hinge which will be determined in Chapter 3.

Within the shear hinge, plastic deformation is a simple shear flow associated with monotonic loading. Thus, the maximum shear strain failure criterion is

$$\gamma=\gamma_c, \tag{1-3}$$

where γ_c is the critical shear strain determined by a pure shear test.

Eqs.(1-2) and (1-3) lead to the so-called elementary failure criterion

$$W_s=W_s^c, \tag{1-4}$$

where W_s^c is the critical value of transverse shear displacement, determined from

$$W_s^c=\gamma_s\Delta=\lambda\gamma_s H=kH, \tag{1-5}$$

where, $k=\lambda\gamma_s$, and $\lambda=\Delta/H=2e/H$ is a constant which will be given in Section 3.2 for several structural elements. The validation of Eqs.(1-4) and (1-5) have been studied by Jouri and Jones(1988) through a series of tests on fully clamped double shear beams made from aluminium alloy and mild steel. The elementary shear failure criterion is given by

$$W_s=kH, \quad 0<k\leq 1 \tag{1-6}$$

which has been used in several applications(Jones(1976,1989)).

Practically, structural dimensions may have a slight influence on parameter k in eq.(1-6). Some results on beams and circular plates have been shown in Jouri and Jones(1988), Wen and Jones(1994), Jones, Kim and Li(1997).

1.3 Failure Criteria

Various failure criteria have been developed to predict the initiation of material failures in structural elements.

A general macroscopic failure criterion within the scope of continuum mechanics depends on some state variables, such as stress, strain and temperature, and some internal variables like plastic work. Among them, stress and strain failure criteria are the earliest phenomenological failure criteria used to predict material failures.

Early investigators suggested two general criteria for fracture, i.e., (a) fracture

occurs when a critical state of strain is achieved, and (b) fracture occurs when a critical state of stress is achieved. It is commonly accepted that stress failure criteria is suitable for material brittle failure and strain failure criteria is proper for material ductile failure because material brittle failure is controlled mainly by the existing stress state as the internal driving forces among atoms, while material ductile failure is dominated by the internal dissipation process preceding the failure.

Further investigations have shown that the critical strain and critical stress laws for material failure are individually incorrect. A general expression of a stress or strain failure criterion should be evaluated from the statement by Dorn(1948): *Material failure initiates when a critical value of the stress/strain state is achieved. But the stress/strain state for material failure depends upon the inelastic dissipation histories preceding the failure and some significant environmental variables.*

A general stress/strain failure criterion can be expressed by

$$F(\sigma_{ij})=F_c(\alpha_i,\beta_j), \quad \text{or} \quad F(\epsilon_{ij})=F_c(\alpha_i,\beta_j), \tag{1-7a,b}$$

where α_i and β_j are significant state and internal variables. The function F and its critical value F_c should be determined from experiments and a physical understanding of the failure mechanisms. Some frequently used stress and strain failure criteria are given below.

(a) Maximum normal stress failure criterion

$$F(\sigma_{ij})=\max(\sigma_1,\sigma_2,\sigma_3), \tag{1-8a}$$

where $\sigma_i(i=1\text{-}3)$ are principal stresses;

(b) Maximum shear stress failure criterion, or Tresca failure criterion

$$F(\sigma_{ij})=\tau_{max}=\frac{\sigma_1-\sigma_3}{2}; \tag{1-8b}$$

(c) Equivalent(Von-Mises) stress failure criterion

$$F(\sigma_{ij})=\sigma_e=\sqrt{\frac{3}{2}S_{ij}S_{ij}}, \tag{1-8c}$$

where $s_{ij}=\sigma_{ij}-p_{ij}$ and $p_{ij}=\sigma_{kl}\delta_{kl}\delta_{ij}/3=p\delta_{ij}$ are deviatoric and hydrostatic stresses, respectively;

(d) Hydrostatic tension failure criterion

$$F(\sigma_{ij})=\sigma_H=\frac{\sigma_{ij}\delta_{ij}}{3}; \tag{1-8d}$$

(e) Maximum plastic tensile strain failure criterion

$$F(\epsilon_{ij})=\max(\epsilon_1^p,\epsilon_2^p,\epsilon_3^p), \tag{1-8e}$$

where $\varepsilon_i^p(i=1\text{-}3)$ are principal plastic strains;

(f) Maximum plastic shear strain failure criterion

$$F(\epsilon_{ij})=\gamma_{\max}^p=\epsilon_1^p-\epsilon_3^p, \tag{1-8f}$$

where $\gamma_{ij}^p=2\varepsilon_{ij}^p$ is the engineering plastic strain;

(g) Equivalent plastic strain(Von-Mises) failure criterion

$$F(\epsilon_{ij})=\int_0^{\epsilon_{ij}^p}\sqrt{\frac{2}{3}d\epsilon_{ij}^p d\epsilon_{ij}^p}=\epsilon_e; \tag{1-8g}$$

(h) Plastic/damage volume expansion failure criterion

$$F(\epsilon_{ij})=\epsilon_{11}^p+\epsilon_{22}^p+\epsilon_{33}^p, \tag{1-8h}$$

which is identical to the void volume fraction failure criterion in damage mechanics.

The above failure criteria have been applied widely in engineering to predict the initiation of material failure. The four stress type failure criteria described above are illustrated in Fig.1.4. In a general sense, especially in engineering, a structural failure can be defined as either a material failure or a plastic flow instability, or sometimes simply excessive deformations. The proposed stress/strain failure criteria are capable of predicting both of them.

The inelastic strain energy density failure criterion has been used in several applications to predict material ductile failure initiation. The general expression of an inelastic strain energy density failure criterion is

$$\int_0^{\varepsilon_{ij}^p} \sigma_{ij} d\varepsilon_{ij}^p = w_c^p(\alpha_i, \beta_j) \quad , \tag{1-9}$$

in which, α_i and β_j are state and internal variables, which need to be identified in material failure test. More discussion on inelastic strain energy density failure criterion is given in Appendix B.

Some failure criteria are based on the theory of damage mechanics. The basic theory of continuum damage mechanics is introduced by Lemaitre and Chaboche(1990). The continuum damage mechanics approach is used by Alves(1996) for dynamic structural failure analysis. It should be noted that the macroscopic phenomenological failure criteria do not exclude the possible existence of material damage.

1.4. Adiabatic Shear Banding

The appearance of a shear hinge in a transversely loaded structural element is a type of shear localization from the viewpoint of a global structural response. However, the shear distribution within a shear hinge is still quite uniform if no material thermal instability occurs. However, the geometrical configuration of a shear hinge, shown in Fig.1.3 supplies an ideal environment for initiating a material thermal instability, or adiabatic shear banding.

The formation of adiabatic shear bands in metal structures subjected to rapid shearing through explosive or impact loading is an important deformation mechanism which usually results in a catastrophic fracture. The basic phenomenon of shear banding was pointed out by Zener and Holloman(1944) and has received increasing attention in recent years as it is a primary mode of ductile deformation and failure in a variety of materials at moderate to high rates of deformation. The current understanding of this topic is summarised by Bai and Dodd(1992).

An adiabatic shear band can form in a ductile material when thermal softening caused by the heat generated through plastic deformations dominates strain hardening,

strain rate hardening and all other hardening mechanisms combined[1]. A simple shear test on a Split Torsional Hopkinson Bar(STHB) is used frequently to generate simple shear flow, and, thus, to initiate an adiabatic shear banding mechanism. Based on their observations of the formation of shear bands in thin-walled HY-100 steel tubes, Marchand and Duffy(1988) have proposed that the localization of deformation into narrow shear bands occurs in three stages. During stage one, a simple shear flow develops homogeneously. Stage two begins when the shear stress attains a peak value, and the softening caused by the heating of the material is balanced by the strain and strain rate hardening. During stage two, the body deforms non-homogeneously. The initiation of stage three is indicated by a precipitous drop in the shear stress at a point in the body and the simultaneous localization of the deformation into a narrow band. These three stages of the deformation have also been confirmed by numerical studies of Molinari and Clifton(1987) and Wright and Walter(1987). These three stages can be described by a stress release model proposed by Grady and Kipp(1987) and Grady(1992) for a simple shear flow, as shown in Fig.1.5. The adiabatic shearing developed from a simple shear flow possesses the common features of adiabatic shearing evolved from any other plastic flow patterns, which are characterised by the localization of plastic shear deformations into a well-defined shear band and the anti-symmetric plastic deformations within and around a shear band, as shown in Figure 6.6 of Dodd and Bai(1987). Thus, conclusions obtained from a simple shear flow are generally valid, which, probably, is one reason why simple shear has been used by most researchers to study the formation of adiabatic shear banding.

According to the observations by Marchand and Duffy(1988), global instability is initiated from stage II when the maximum shear stress is reached. Afterwards, the subsequent adiabatic shear banding is a natural outcome if the input energy is supplied continuously. From an engineering viewpoint, the initiation of stage two in Figure 1.5 coincides with the loss of stability of a body in simple shear. It has been pointed out that this instability is due to the thermal softening caused by

[1] Material damage or textural effects may have a similar effect as thermal softening, and lead to an isothermal shear band or shear band in combination with thermal softening effects(Dodd and Atkins(1983)).

adiabatic heating[2]. Some linear(Costin, et al.(1979), Bai(1982)) and non-linear(Wright and Walter(1987), Fressengeas and Molinari(1987)) analyses have also shown that a localized shear deformation starts in a body after the peak homogeneous simple shear stress. Therefore, the maximum shear stress is used frequently as an approximate criterion for the formation of a shear band, as discussed by Dodd and Bai(1987), and Wang, et al.(1988).

If deformation history effects and changes in the structure of the metal are ignored, then the flow stress τ may be written as a function of the shear strain γ, the shear strain rate $\dot{\gamma}$ and the temperature T, i.e.,

$$\tau=f(\gamma,\dot{\gamma},T) \ . \tag{1-10}$$

The maximum shear stress criterion may be expressed as

$$d\tau=\frac{\partial\tau}{\partial\gamma}d\gamma+\frac{\partial\tau}{\partial\dot{\gamma}}d\dot{\gamma}+\frac{\partial\tau}{\partial T}dT=0 \ , \tag{1-11}$$

in which, $\partial\tau/\partial\gamma>0$, $\partial\tau/\partial\dot{\gamma}>0$ and $\partial\tau/\partial T<0$ represent strain hardening, strain rate hardening and thermal softening, respectively.

For adiabatic deformations, the increase of temperature with strain is given by

$$dT=\frac{\beta}{\rho C_v}\tau d\gamma \ , \tag{1-12}$$

where, β is the Taylor-Quinney coefficient defined as the fraction of the plastic work converted into heat(β=0.9-1.0)(see Taylor and Quinney(1934), Birch, Jones and Jouri(1988), and Oliferuk(1993)), τ is the flow stress, ρ is the density of the metal and C_v is the specific heat. Although, a constant β has been used by all publications known by the author, β may vary during an inelastic deformation process, which is still an open topic for further research.

By using eqs.(1-11) and (1-12), the maximum shear stress criterion can be expressed as

---

[2] Sometimes, a truly adiabatic condition is not obtained, but it is still known as adiabatic shearing.

$$f_c(\gamma,\dot{\gamma})=0 \ , \tag{1-13}$$

for an adiabatic process, where f_c depends on the particular form of the thermal visco-plastic constitutive equation.

The initiation of material failure in an adiabatic shear band is a complicated process, where both brittle and ductile modes of fracture are observed. Shear bands can be divided into two different types, i.e., deformation bands(without any micro-structural transformation) and transformation bands(with a micro-structural transformation). The majority of shear bands observed in nonferrous metals are deformation bands. Transformation bands are most commonly observed in ferrous alloys, in which they are associated with a ferrite-austenite transformation. Bai and Dodd(1992) give further details on the metallurgical and microscopic features of shear bands.

When an adiabatic shearing process occurs in a uniform shearing material section, the adiabatic shear banding criterion, eq.(1-13), could be applied easily because strain and strain rate are not related to wave propagation. However, when the loading rate is very high, the whole event may be completed within the time when wave effects are important. In this case, stress wave effects have to be considered for both fracture failure and adiabatic shear banding failure. If material failure or adiabatic shear banding occurs before the transverse shear wave reflects several times between two ends of the gauge section, wave effects must be considered in the deformation prediction and failure criteria. This is the case in Section 3.3.3(c) when $V>c_p$ and the situation in Section 4.3.2 when $V>V_{sw}$ which limits the method developed in Chapters 3 and 4 by using shear hinge concept within a proper impact velocity range.

In order to establish a criterion for initiating adiabatic shear banding, let us examine the "rate-independent" momentum equation

$$\frac{\partial^2 u}{\partial t^2}=c_p^2\frac{\partial^2 u}{\partial y^2}, \tag{1-14}$$

where u is the transverse displacement, and the transverse shear wave velocity, c_p, is determined by

$$c_p = \sqrt{\frac{1}{\rho}\frac{d\tau}{d\gamma}}. \tag{1-15}$$

The common concave τ-γ relationship in the isothermal case without a stress peak will give a decreasing wave speed with increasing stress or strain. However, it is unavoidable that an increase of shear strain at high strain rates may lead to a significant temperature rise, which causes the flow stress to decrease due to the so-called thermal softening effect. Texture softening, such as damage development, may also lead to strain softening, which is not important in the present problem. For a semi-infinite body loaded on its boundary surface with a monotonously increasing driving velocity, the deformations propagate by shear wave patterns. As soon as the shear stress reaches its maximum at a critical strain due to thermal softening, i.e., $d\tau/d\gamma=0$, the corresponding wave velocity is zero. Beyond the critical shear strain, which depends obviously on the loading rate, transverse shear disturbances cannot propagate into the semi-infinite body and are trapped at the location where $c_p=0$. This provides a strong discontinuity and, thus, an abrupt jump of particle velocities which leads to an adiabatic process and intensive shear strains at the location where $c_p=0$, and therefore, may be understood as the initiation of adiabatic shear banding. This phenomenon was termed "wave trapping" and was first noticed by Erlich, et al.(1980). According to the physical nature of wave trapping, the location of adiabatic shearing associated with shear wave propagation should be near the loading boundary(Wu and Freund(1984)), which is only possible when the loading rate and intensity are both sufficiently high.

Now, let us consider an idealized shear propagation model, where the input shear strain rate is constant[3] and the heat conduction is simplified by eq.(1-12). The balance of momentum in the absence of body forces is

[3]This is a simplification of the problem. After the occurrence of shear banding or wave trapping, the rate sensitivity must be considered, which results in a finite thickness of the shear band(Wu and Freund(1984)). It has been shown that this thickness varies with the boundary velocity in a certain region(Wu and Freund(1984)), which coincides with experimental observations that the shear band thickness varies from 10-100μm under different situations.

$$\rho\frac{\partial v}{\partial t}=\frac{\partial \tau}{\partial y}, \tag{1-16}$$

and the shear stress increment is

$$d\tau=(\frac{\partial \tau}{\partial \gamma}+\frac{\beta\tau}{\rho C_v}\frac{\partial \tau}{\partial T})d\gamma+\frac{\partial \tau}{\partial \dot{\gamma}}d\dot{\gamma} \tag{1-17}$$

according to eqs.(1-11) and (1-12). Before the occurrence of a shear instability, or wave trapping in this case, the assumption of a constant input shear strain rate may lead to $d\dot{\gamma}=0$ because the same relative velocity is imposed on the material particles by the travelling shear stress wave. Thus, eq.(1-14) can be evaluated from eqs.(1-16) and (1-17), in which the wave propagation velocity defined in eq.(1-15) is given by

$$c_p=\sqrt{\frac{1}{\rho}(\frac{\partial \tau}{\partial \gamma}+\frac{\alpha\beta\tau}{\rho C_v}\frac{\partial \tau}{\partial T})} \tag{1-18}$$

in the current case. $c_p=0$ implies that the input energy will be trapped at the place where this condition is satisfied first, which will lead to a localized shear deformation band.

It should be noted that the condition for wave trapping(or adiabatic shear banding), $c_p=0$, is identical to $d\tau=0$ when the strain rate change is neglected, which generally true before the initiation of adiabatic shear banding. After wave trapping occurs, $d\dot{\gamma}$ may not be zero. The term $d\dot{\gamma}$ in eq.(1-17) will be considered, as discussed previously by Wu and Freund(1984). It was shown that the strain rate effect leads to a viscous dissipation which makes the wave trap diffuse with a characteristic spatial length. The above analyses are only suitable for a limited period when the reflected plastic wave has not arrived at the loading boundary. Outside this period, the boundary conditions at the two ends of the shear section need to be considered, and eqs(1-16) and (1-17) require solving to predict the actual location of wave trapping. Therefore, the features of an adiabatic shear band formed by wave trapping during the early response period when the stress wave effect is important are different from those formed in the later phase when the stress wave effect may be neglected but dynamic effects(strain rate and inertia) are still important.

In the later case, the structure of a shear band is anti-symmetrical which has been observed in many cases(see Fig.6.9 on pp.152 of Bai and Dodd(1992)). However, in the wave trapping case, the distribution of deformation within the wave trapping layer is not anti-symmetrical(Wu and Freund(1984)). A detailed discussion on wave trapping is introduced by Bai and Dodd(1992).

Equation (1-18) is Klepaczko's(1994) results. Klepaczko used a rate-independent wave theory and rate-dependent constitutive equation in his evaluation, which appears to be contradictory. This contradiction is eliminated in the present evaluation when a characteristic strain rate is kept in the constitutive equation, but its transient changes are neglected.

By using the following relationship

$$dv \pm c_p d\gamma = 0 \tag{1-19}$$

along the non-linear characteristic lines, the critical impact velocity to initiate wave trapping may be obtained by

$$v_{ic} = \int_0^{\gamma_c} c_p d\gamma \tag{1-20}$$

where γ_c is determined by $c_p=0$(or $d\tau=0$), as shown by Klepaczko(1994).

1.5. Failure Mechanism Transition

It has been shown that isothermal fracture failure and adiabatic shear banding failure are two important failure mechanisms, which may develop within a shear hinge of a transversely loaded structural element. Previously, these two failure mechanisms were studied separately because isothermal fracture failure and adiabatic shear banding occur in different ranges of the loading rate and intensity.

Some recent studies have studied the interactions between an isothermal fracture failure and an adiabatic shear banding failure. Kalthoff(1987, 1990) observed two distinct failure mechanisms in double-shear beams when subjected to projectile impact. At a low loading rate, the usual opening fracture mode was observed. With an increase of loading rate(impact velocity), the opening fracture mode was transferee into an adiabatic shear mode, which is controlled by a totally different

failure mechanism. Wang, et al.(1994) treated this problem as an interaction between a dynamic opening fracture mode crack and an adiabatic shear band. The maximum stress criterion given in Section 1.3, and elastic fracture mechanics were used to predict the initiation of an adiabatic shear band. Good agreement is found between test and predicted results for a Ti-6Al-4V material, where the adiabatic shear band is triggered by an existing crack. In a structural element where no "crack trigger" exists, it is still possible to find the transition between these two failure mechanisms. Based on a rigid-plastic idealization and the maximum stress criterion, Wang and Jones(1996) gave a theoretical analysis for a simply supported beam under an impulsive loading, which is the first attempt to combine the studies on the dynamic plastic response of structural elements with the mechanics of adiabatic shearing, and gives some insight into the adiabatic shearing in an impulsively loaded beam. However, further experimental and theoretical studies are required due to the complexity of the problem.

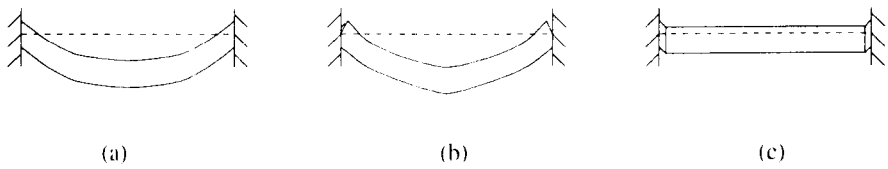

Fig.6.1

Fig.1.1 Three basic dynamic response and failure modes in a transversely loaded structural element, (a) Mode I; (b) Mode II; (c) Mode III.

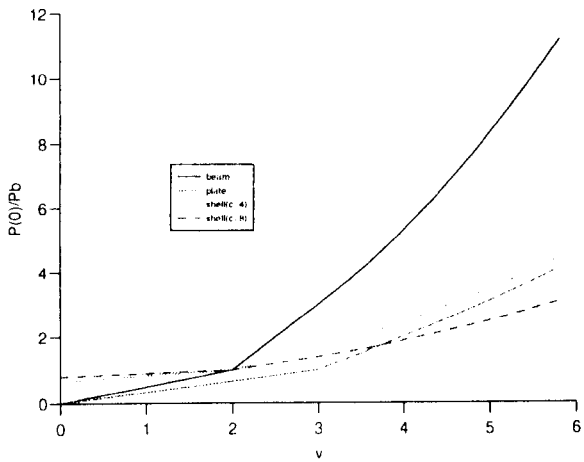

Fig.1.2 Critical curves for initiating transverse shear hinge in several structural elements.

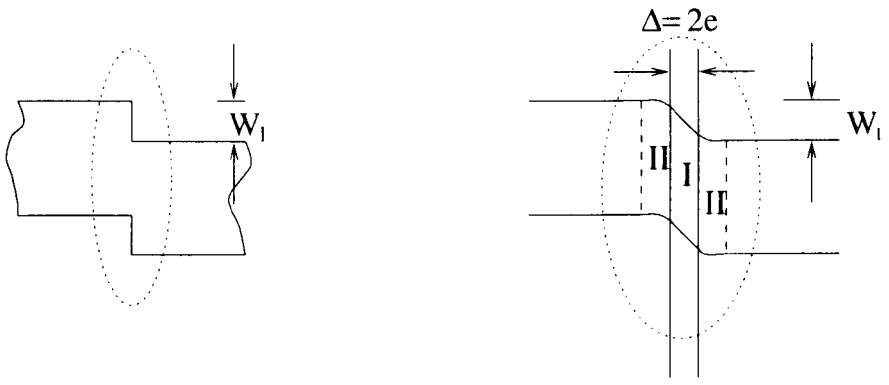

(a) (b)

Fig.1.3 (a) Idealized shear hinge; (b) Construction of a shear hinge.

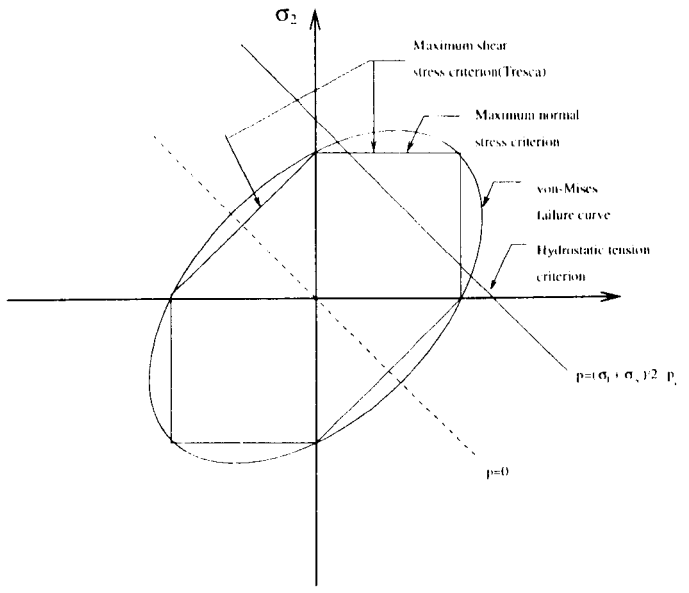

Fig.1.4. Stress failure criteria

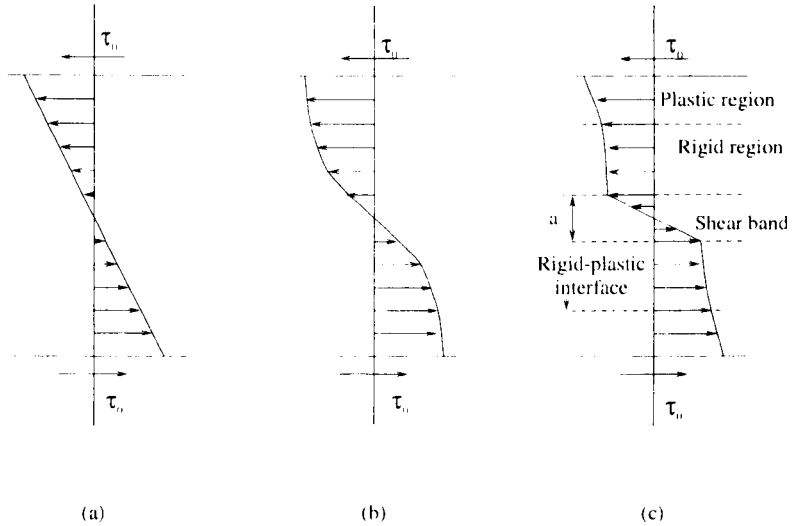

Fig. 1.5. Displacement distributions in a simple shear body corresponding to different stages of shear banding formation, (a) Stage I: uniform flow; (b) Stage II: non-uniform flow; (c) Stage III: localized shear flow(Grady(1992))

2. CONTINUITY CONDITIONS AT BENDING AND SHEARING INTERFACES OF RIGID-PERFECTLY PLASTIC STRUCTURAL ELEMENTS

2.1. Introduction

It has been shown in Chapter 1 that deformation localizations in a rigid, perfectly plastic structural element when subjected to a transverse dynamic load are represented by plastic hinges during the early response phase before a membrane state is reached. These plastic hinges, including bending and shearing hinges, are basically discontinuity interfaces of the generalized strains. For example, a bending hinge corresponds to a discontinuity interface of bending curvature, and a shear hinge is associated with the discontinuity interface of shear strain. Thus, the behaviour of these discontinuity interfaces determine the behaviour of plastic hinges, and therefore, the dynamic deformation localizations in a transversely loaded structural element.

Although, a discontinuity interface may appear in the dynamic response of structural elements, made from a rigid, perfectly plastic material, the bending and shearing hinges represent a general characteristic of dynamic plastic response of several structural elements under transverse load. The continuity conditions at an interface must satisfy the conservation of momentum across the interface and the kinematic admissibility of the motion at this interface. A large literature now exists for the dynamic plastic bending response of structural elements(Lee and Symonds(1952), Hopkins and Prager(1954), and Hodge(1955)), in which the continuity conditions at bending hinges in structural elements were discussed. These works are also be summarized by Jones(1989)(p.77-81 for beams; p.133-134 for circular plates; p.169-178 for cylindrical shells).

It has been shown that a transverse shear force plays an important role in the dynamic plastic response of structures(p.216-275 of Jones(1989)) when subjected to an intensive loading. Symonds(1968) discussed the continuity conditions at an interface in a beam when the influence of the transverse shear force is retained in the

yield condition, and these results have been used widely in the analyses of dynamic plastic response of beams(Jones and Oliveira(1979), Nonaka(1977), and Li and Jones(1995a)). However, Symonds' conclusions are based on a particular square yield surface, which are not applicable when the stress components at a rigid-plastic interface lie at a singular position of a yield surface, as pointed out by Jones and Oliveira(1979). The dynamic and kinematic continuity conditions at a discontinuity interface in axisymmetrically loaded circular plates and cylindrical shells have been obtained by Jones and Oliveira(1980, 1983) using generalized stresses and strains when transverse shear force and bending moments are retained in the yield surface, which is evaluated from the general dynamic and kinematic continuity conditions across a discontinuity surface in a continuum(Nowacki(1978)). Some further investigations on continuity conditions required across a discontinuity surface in an elastic-plastic solid have been discussed by Drugan and Shen(1987) and Nemat-Nasser and Gao(1988).

Although, the above mentioned continuity conditions at an interface have been used widely in theoretical and numerical analyses into the dynamic plastic response of structural elements, and predict reasonable results, they were, nevertheless, stated neatly for the convenient use in each case of rigid-plastic interfaces existing in rigid, perfectly plastic structural elements described with generalized stresses and strains. Symonds(1968) discussed the properties of both moving and stationary bending and shearing interfaces in rigid, perfectly plastic beams, which might be extended to axisymmetrically loaded, rigid perfectly plastic circular plates and cylindrical shells by a parallel analysis, but his proof is too restrictive to be used for a general yield condition.

The purpose of this chapter is to extend Symonds' results for a square yield curve between the bending moment and the transverse shear force in a beam to a more general yield condition which may be a regular or a singular one, and to present continuity conditions for each type of rigid-plastic interface. Furthermore, the conclusions for a rigid, perfectly plastic beam are proved to be valid for axisymmetrically loaded circular plates and cylindrical shells which are made from rigid, perfectly plastic materials, even though different generalized stresses are involved in the yield condition. The significance of these general results is to prove

that plastic shear deformation in a two-dimensional metal element has the localization feature when its plastic hardening modulus is relatively smaller than its elastic modulus, i.e., rigid, perfectly plastic simplification is applicable.

2.2. Basic Assumptions and Equations

When the local theory(Oliveira and Jones(1978)) is used in an analysis for the dynamic plastic response of beams without axial deformations, the generalized stresses and their associated generalized strains are M, Q, κ and γ, respectively, which should satisfy the material stability postulate proposed by Drucker(1951,1964)(also discussed by Martin(1975)). Therefore, for a regular yield surface $f(M,Q)=0$, we have

$$d\kappa=d\lambda\frac{\partial f}{\partial M} \tag{2-1a}$$

and

$$d\gamma=d\lambda\frac{\partial f}{\partial Q}, \tag{2-1b}$$

in which, $d\lambda=0$ for $f<0$(before yielding, or rigid case) or $f=0$ and $df<0$(unloading case), and $d\lambda\geq 0$ for $f=0$ and $df=0$(neutral loading case[1]) when the beam is made from a rigid, perfectly plastic material. In the plastic loading case, the flow directions of the generalized strains are in a direction normal to a regular yield surface, which has a unique normal direction at every point.

For a singular yield surface consisting of a number of n regular yield functions $f_p(M,Q)$, $p=1,...,n$, plastic yielding occurs as soon as at least one of the functions f_p is zero. It is evident that all the points on the yield surface, when only one function $f_p=0$, are regular and the corresponding generalized plastic strain increments are the same as those for a completely regular yield surface $f_p=0$. In those situations when the generalized stresses are at the intersection of two or more surfaces $f_p=0$, the flow rule of plastic yielding for such a singular point is obtained

[1] For a perfectly plastic material, the initial yield surface can not expand, therefore, only the neutral loading case exists.

by combining each yield function separately according to Koiter's suggestion(Koiter(1953)), which leads to

$$d\kappa=\sum_{1}^{n} d\lambda_p \frac{\partial f_p}{\partial M} \tag{2-2a}$$

and

$$d\gamma=\sum_{1}^{n} d\lambda_p \frac{\partial f_p}{\partial Q}, \tag{2-2b}$$

where,

$$\begin{aligned} &d\lambda_p=0, \quad for \quad f_p<0(\text{rigid case}) \quad \text{or} \quad f_p=0 \quad \text{and} \quad df_p<0(\text{unloading case}), \\ &d\lambda_p\geq 0, \quad \text{for} \quad f_p=0 \quad \text{and} \quad df_p=0(\text{neutral loading case}). \end{aligned} \tag{2-3}$$

Generally speaking, the flow directions of the generalized strains are uncertain at a singular point, but are bounded by the normal directions of each adjacent regular surface. This uncertainty is avoided by using the dynamic equations and the kinematic admissibility of the deformation field.

Furthermore, we assume that the final deformation of a beam is not influenced by the loading sequence of the bending moment and the transverse shear force, and therefore, the deflection of a beam is composed of two parts which are related to the bending and shearing behaviour

$$w=w_b+w_s \ . \tag{2-4}$$

Differentiation of equation(2-4) with respect to time leads to

$$\frac{\partial w}{\partial t}=\dot{w}=\dot{w}_b+\dot{w}_s \ . \tag{2-5}$$

From equations(2-4,2-5), we define the following quantities for small deformations

$$\frac{\partial w}{\partial x}=\psi+\gamma \tag{2-6a}$$

$$\frac{\partial^2 w}{\partial t \partial x} = \omega + \frac{\partial \gamma}{\partial t} \tag{2-6b}$$

and

$$\kappa = \frac{\partial \psi}{\partial x}, \tag{2-6c}$$

where, $\psi = \partial w_b / \partial x$, $\omega = \partial \psi / \partial t$ and κ are rotation angle, angular velocity and the curvature associated with bending, respectively, and $\gamma = \partial w_s / \partial x$ is the transverse shear strain.

The conservation of momentum across a discontinuity interface requires(p.230 in Jones(1989))

$$[Q]_\xi = -m\dot{\xi}[\frac{\partial w}{\partial t}]_\xi \tag{2-7a}$$

and

$$[M]_\xi = -I_r\dot{\xi}[\frac{\partial \psi}{\partial t}]_\xi \ , \tag{2-7b}$$

in which, ξ is the position of an interface, and $\dot{\xi}$ is the propagation velocity of a moving interface.

2.3. Results For Regular Yield Surface

Now, the kinematic continuity conditions across a moving interface are(p.230-231 in Jones(1989), also see Symonds(1968))

$$[w]_\xi = 0 \quad \text{and} \quad [\psi]_\xi = 0, \tag{2-8a,b}$$

which imply that

$$[\frac{\partial w}{\partial t}]_{\xi}+\dot{\xi}[\frac{\partial w}{\partial x}]_{\xi}=0 \tag{2-9a}$$

and

$$[\frac{\partial \psi}{\partial t}]_{\xi}+\dot{\xi}[\frac{\partial \psi}{\partial x}]_{\xi}=0 \tag{2-9b}$$

which allow equations (2-7a,b) to be written as

$$[Q]_{\xi}=m\dot{\xi}^{2}[\gamma]_{\xi} \tag{2-10a}$$

and

$$[M]_{\xi}=I\dot{\xi}^{2}[\kappa]_{\xi} \tag{2-10b}$$

when using equations (2-7a,b) and $[\partial w/\partial x]_{\xi}=[\psi]_{\xi}+[\gamma]_{\xi}=[\gamma]_{\xi}$.

Consider an interface moving from a perfectly plastic zone to a rigid segment, as shown in Fig.2.1(a). The points on the rigid side of the interface will yield when reached by the moving interface. Equations (2-10a,b) may be re-written as

$$dQ=m\dot{\xi}^{2}d\gamma \tag{2-11a}$$

and

$$dM=I\dot{\xi}^{2}d\kappa \tag{2-11b}$$

where, dA means the increment of a physical quantity A on the rigid side of an interface shown in Figure 2.1(a).

For a rigid, perfectly plastic material,

$$df=\frac{\partial f}{\partial Q}dQ+\frac{\partial f}{\partial M}dM=0 \tag{2-12}$$

during a loading process. According to equations (2-11a,b) and (2-1a,b), equation (2-

12) gives

$$\dot{\xi}^2 d\lambda[m(\frac{\partial f}{\partial Q})^2+I_r(\frac{\partial f}{\partial M})^2]=0 \tag{2-13}$$

which indicates that $d\lambda=0$ because $\dot{\xi}\neq 0$, $m>0$, $I_r>0$ and $\partial f/\partial Q$ and $\partial f/\partial M$ can not equal zero simultaneously. Thus, $d\gamma=d\kappa=0$ or $[\gamma]_\xi=[\kappa]_\xi=0$, which means that there is no discontinuity at such an interface in a rigid, perfectly plastic beam. It transpires that a discontinuity in γ or κ can not develop at an interface which moves from a plastic zone to a rigid segment. This conclusion has been presented by Symonds(1968) for a rigid, perfectly plastic beam. However, the proof given by Symonds(1968) is valid only for regular points on the square yield surface, as mentioned by Jones and Oliveira(1979).

If an interface in a rigid, perfectly plastic beam moves from a rigid segment to a plastic zone, as shown in Fig.2.1(b), the plastic side of the interface will become rigid as the interface moves across it. This is an unloading process for the region on the plastic side of interface, which, therefore, requires $d\lambda=0$ in equations (2-1a,b), or

$$[\gamma]_\xi=[\kappa]_\xi=0 \tag{2-14a,b}$$

and

$$[Q]_\xi=[M]_\xi=0. \tag{2-15a,b}$$

In this case, $\dot{\xi}$ may not be zero, as observed in many theoretical results for the dynamic plastic response of beams. One example is the second response phase for the simply supported beam in Section 3.2 of Jones and Oliveira(1979).

If $I_r=0$, equation (2-13) shows that $d\lambda$ is not required to be zero when $\partial f/\partial Q=0$. In this situation, $[\gamma]_\xi=0$, but $[\kappa]_\xi$ may not equal zero as an interface in a rigid, perfectly plastic beam moves from a plastic zone to a rigid segment. The appendix of Zhu, et al.(1986) gave an example of this case for the bending response of a simply supported beam subjected to a general pulse pressure loading. Similar results for a circular plate was obtained by Youngdahl(1971).

Equations (2-6a), (2-8b) and (2-14a) give $[\partial w/\partial x]_\xi=[\psi]_\xi+[\gamma]_\xi=0$, and, therefore,

$$[\frac{\partial w}{\partial t}]_{\xi}=0$$

according to equation (2-9a) whether I_r equals zero or not. Thus, the kinematic continuity conditions across a moving interface in a rigid, perfectly plastic beam(both cases in Fig.2.1) are

$$[w]_{\xi}=0 \quad \text{and} \quad [\dot{w}]_{\xi}=0, \tag{2-16a,b}$$

which, together with equations (2-15a,b) have been used in the previous theoretical analyses reported by Symonds(1968), Jones and Oliveira(1979), Nonaka(1977), and Li and Jones(1995a). It may be shown that equations (2-16a,b) are the sufficient and necessary conditions for the satisfaction of equations (2-8a,b) in the case of Figure 2.1(a), and equations (2-16a,b) are equivalent to equations (2-8a,b) for the case in Figure 2.1(b) under the assumption that $[\gamma]_{\xi}=0$ when $\dot{\xi}\neq 0$. Thus, equations (2-16a,b) may be used, instead of equations (2-8a,b), as kinematic continuity conditions across the interface in a rigid, perfectly plastic beam moving from a plastic zone to a rigid segment because a shear interface is always stationary which is an important conclusion of previous analyses.

The above analyses show that a shear interface in a rigid, perfectly plastic beam is always stationary whether or not $I_r=0$. This implies that the transverse shear deformation is always localized in its initially formed zone throughout the dynamic plastic response of beams. The characteristic length of this zone will be very small compared with the beam length, because the size of the shear deformation zone does not increase during the subsequent beam response. All transverse shear deformations will be localized in this zone, which, therefore, may be idealized as a plane with transverse shear sliding. The sliding displacement at an idealized plane is the relative displacement at two sides of the transverse shear deformation zone, as illustrated in Fig.1.3(a). Due to the antisymmetric property of the transverse shear force about the mid-plane of a shear deformation zone, the kinematic continuity condition across the transverse shear sliding plane is

$$[\psi]_\xi=0, \tag{2-17}$$

and equations (2-15a,b) should be satisfied for either $I_r\neq 0$ or $I_r=0$.

It should be noted that the assumption of shear sliding does not mean that the actual severance occurs at the shear sliding interface. $[w]_\xi\neq 0$ is an idealized result when we neglect the size of the transverse shear deformation zone, as discussed above.

For a stationary bending interface, only the transverse deflection need to be continuous, i.e., $[w]_\xi=0$ which is equivalent to $[w]_\xi=0$ according to equation (2-9a). Equations (2-7a,b) require $[Q]_\xi=[M]_\xi=0$.

In summary, the continuity conditions at an interface in a rigid, perfectly plastic beam may be expressed as

(a) Moving bending interface(does not exist for the case in Figure 2.1(a) when $I_r\neq 0$)

$$[Q]_\xi=0,\quad [M]_\xi=0,\quad [\dot{w}]_\xi=0 \quad \text{and} \quad [w]_\xi=0; \tag{2-18a-d}$$

(b) Stationary bending interface

$$[Q]_\xi=0,\quad [M]_\xi=0 \quad \text{and} \quad [\dot{w}]_\xi=0(\text{or } [w]_\xi=0); \tag{2-19a-c}$$

(c) Stationary shear slides

$$[Q]_\xi=0,\quad [M]_\xi=0 \quad \text{and} \quad [\psi]_\xi=0(\text{or } [\frac{\partial w}{\partial x}]_\xi=0); \tag{2-20a-c}$$

(d) Stationary bending and shear interface

$$[Q]_\xi=0 \quad \text{and} \quad [M]_\xi=0. \tag{2-21a,b}$$

All these continuity conditions in each case are identical to those presented by Li and Jones(1995a) and reduce to the special cases examined by previous studies on the transverse bending and shear responses of a rigid, perfectly plastic beam.

2.4. Results For A Singular Yield Surface

If one of the parameters $d\lambda_p=0(p=1,2)$ for a singular yield surface, then the associated terms in equations (2-2a,b) are eliminated, and the remaining terms in

equations (2-2a,b) are the same as equations (2-1a,b). Therefore, the results for this situation is the same as those for a regular yield surface.

In the case when $d\lambda_p>0 (p=1,2)$, then only the loading situation in Figure 2.1(a) requires discussion. The results for the unloading situation in Figure 2.1(b) are similar to those for a regular yield surface.

Now, equation (2-3) with $df_p=0$ for neutral loading requires

$$\frac{\partial f_1}{\partial Q}dQ+\frac{\partial f_1}{\partial M}dM=0, \tag{2-22a}$$

and

$$\frac{\partial f_2}{\partial Q}dQ+\frac{\partial f_2}{\partial M}dM=0. \tag{2-22b}$$

Equations (2-22a,b) with equations (2-11a,b) and (2-2a,b) may be expressed in the form

$$[m(\frac{\partial f_1}{\partial Q})^2+I_r(\frac{\partial f_1}{\partial M})^2]d\lambda_1+[m\frac{\partial f_1}{\partial Q}\frac{\partial f_2}{\partial Q}+I_r\frac{\partial f_1}{\partial M}\frac{\partial f_2}{\partial M}]d\lambda_2=0, \tag{2-23a}$$

and

$$[m\frac{\partial f_1}{\partial Q}\frac{\partial f_2}{\partial Q}+I_r\frac{\partial f_1}{\partial M}\frac{\partial f_2}{\partial M}]d\lambda_1+[m(\frac{\partial f_2}{\partial Q})^2+I_r(\frac{\partial f_2}{\partial M})^2]d\lambda_2=0 \tag{2-23b}$$

provided $\dot{\xi}\neq 0$.

The condition for $d\lambda_p\neq 0 (p=1,2)$ is

$$[m(\frac{\partial f_1}{\partial Q})^2+I_r(\frac{\partial f_1}{\partial M})^2][m(\frac{\partial f_2}{\partial Q})^2+I_r(\frac{\partial f_2}{\partial M})^2]-(m\frac{\partial f_1}{\partial Q}\frac{\partial f_2}{\partial Q}+I_r\frac{\partial f_1}{\partial M}\frac{\partial f_2}{\partial M})^2=0$$

or

$$\frac{\partial f_1}{\partial Q}\frac{\partial f_2}{\partial M}-\frac{\partial f_1}{\partial M}\frac{\partial f_2}{\partial Q}=0 \tag{2-24}$$

when $m\neq 0$ and $I_r\neq 0$.

Equation (2-24) implies that

$$\vec{n}_1 \times \vec{n}_2 = \left(\frac{\partial f_1}{\partial Q}\vec{i} + \frac{\partial f_1}{\partial M}\vec{j}\right) \times \left(\frac{\partial f_2}{\partial Q}\vec{i} + \frac{\partial f_2}{\partial M}\vec{j}\right) = 0 \tag{2-25}$$

where, $\vec{n}_1$ and $\vec{n}_2$ are the normal directions of $f_1(Q,M)=0$ and $f_2(Q,M)=0$ at the intersection point, respectively, and $\vec{i}$ and $\vec{j}$ are unit vectors of the local orthogonal coordinates. Equation (2-25) implies that $\vec{n}_1$ is parallel to $\vec{n}_2$. Therefore, the intersection point of $f_1(Q,M)=0$ and $f_2(Q,M)=0$ must be a regular point if equation (2-24) is satisfied, which has been discussed in Section 2.3. Thus

$$\frac{\partial f_1}{\partial Q}\frac{\partial f_2}{\partial M} - \frac{\partial f_1}{\partial M}\frac{\partial f_2}{\partial Q} \neq 0 \tag{2-26}$$

which leads to

$$d\lambda_1 = d\lambda_2 = 0$$

from equation (2-23), and following conditions are reached

$$[\gamma]_\xi = [\kappa]_\xi = 0 \quad \text{and} \quad [Q]_\xi = [M]_\xi = 0 \tag{2-27a-d}$$

at an interface in a rigid, perfectly plastic beam by using equations (2-2a,b) and (2-10a,b).

It transpires that all the conclusions for a moving interface at a singular yield point for a rigid, perfectly plastic beam are the same as those for the regular yield surface studied in Section 2.3 when $I_r \neq 0$. This conclusion is also true for the continuity conditions at both moving and stationary interfaces.

If $I_r=0$, then equation (2-10b) gives

$$[M]_\xi = 0 \ (\text{or } dM=0), \tag{2-28}$$

while, equations (2-22a,b) become

$$\frac{\partial f_1}{\partial Q} dQ = 0 \tag{2-29a}$$

and

$$\frac{\partial f_2}{\partial Q} dQ = 0 \tag{7-29b}$$

Equation (2-26) indicates that $\partial f_1/\partial Q$ and $\partial f_2/\partial Q$ can not equal zero simultaneously, and therefore, $dQ=0$, or

$$[Q]_\xi = 0 \tag{2-30}$$

which leads to

$$[\gamma]_\xi = 0 \tag{2-31}$$

from equation (2-10a).

Again, a shear interface must be stationary, and equation (2-10b) implies the possibility that a bending interface may move, which is the same conclusion as that reached for a regular yield surface. Thus, equations (2-18) to (2-21) are valid for both regular and singular yield surfaces.

2.5. Continuity Conditions for Circular Plates and Cylindrical Shells

The yield surface, which is shown in Figure 2.2, has the following properties

$$\frac{\partial f_1}{\partial P} = 1, \quad \frac{\partial f_1}{\partial M} = 0, \quad \frac{\partial f_1}{\partial Q} = 0 \quad \text{and} \quad \frac{\partial f_2}{\partial P} = 0 \tag{2-32a-d}$$

in which, $P=M_\theta$(or N) for circular plate(or cylindrical shell); where M_θ is the circumferential bending moment in a circular plate and N is the circumferential membrane force in a cylindrical shell.

For both an axisymmetrically loaded circular plate and an axisymmetrically loaded cylindrical shell, equations (2-1) to (2-11) will be satisfied according to the basic equations in Jones and Oliveira(1980,1983)[2]. Furthermore,

---

[2] For example, equations (2-7a,b) and (2-9a,b) here are the same as equations (2-4b,a) and (2-6b,a) in Jones and Oliveira(1980, 1983), respectively, when M, κ and x are replaced by M_r, κ_r and r for circular plate.

$$\kappa_\theta=\frac{\psi}{r}, \quad \text{for a circular plate} \tag{2-33a}$$

and

$$\varepsilon_\theta=-\frac{w}{R}, \quad \text{for a cylindrical shell} \tag{2-33b}$$

where, r is the radial coordinate of circular plate and R is the mean radius of a cylindrical shell.

In the following discussion, $f_2(Q,M,P)=0$ is assumed to be a regular surface. However, it does not influence the results when $f_2(Q,M,P)=0$ is a singular one because of the conclusions reached in Section 2.4.

The assumption of a rigid, perfectly plastic material requires

$$df_1=\frac{\partial f_1}{\partial Q}dQ+\frac{\partial f_1}{\partial M}dM+\frac{\partial f_1}{\partial P}dP=\frac{\partial f_1}{\partial P}dP=dP=0 \tag{2-34a}$$

and

$$df_2=\frac{\partial f_2}{\partial Q}dQ+\frac{\partial f_2}{\partial M}dM+\frac{\partial f_2}{\partial P}dP=\frac{\partial f_2}{\partial M}dM+\frac{\partial f_2}{\partial Q}dQ=0 \tag{2-34b}$$

while, the plastic flow rule from equation (2-2) gives

$$d\gamma=d\lambda_1\frac{\partial f_1}{\partial Q}+d\lambda_2\frac{\partial f_2}{\partial Q}=d\lambda_2\frac{\partial f_2}{\partial Q} \tag{2-35a}$$

$$d\kappa=d\lambda_1\frac{\partial f_1}{\partial M}+d\lambda_2\frac{\partial f_2}{\partial M}=d\lambda_2\frac{\partial f_2}{\partial M} \tag{2-35b}$$

and

$$dg=d\lambda_1\frac{\partial f_1}{\partial P}+d\lambda_2\frac{\partial f_2}{\partial P}=d\lambda_1 \tag{7-35c}$$

where, $g=\kappa_\theta$ (or ε_θ).

It is evident that equations (2-34b), (2-35a,b) together with equations (2-1) to (2-10) are the same as the corresponding equations for a beam. The extra equations

(2-33a,b) may be satisfied by adjusting $d\lambda_1$ which has no influence on $d\kappa$ and $d\gamma$. Thus, the continuity conditions for both a circular plate and a cylindrical shell are the same as those for a beam, except for the additional condition from equation (2-34a)

$$[P]_\xi=0. \tag{2-36}$$

It should be noted that the dynamic plastic response of circular plates and cylindrical shells usually lead to $f_1(Q,M,P)=0$ and $dg=d\lambda_1>0$ throughout the entire area of a plate or a shell. In this case, the continuity conditions(equations (2-18) to (2-21)) are not related to an interface between rigid regions and plastic zones in a rigid, perfectly plastic material, but to an interface in a plastic deformation zone. These conclusions have been examined for the dynamic plastic analyses of circular plates(Li and Jones(1994)) and cylindrical shells(Li and Jones(1995b)).

2.6. Comments

A rigid, perfectly plastic idealization has been used successfully to predict the dynamic plastic responses of various structural elements. An important concept in this analysis is plastic hinge, through which plastic deformations are propagated. Material failures always appear at deformation localization points, which are formed by the combination of bending and shear hinges, and sometimes, associated with the membrane deformation. The conclusion of this chapter shows that a shear hinge behaves like a "deformation trap" because of its stationary feature. Other analyses have shown that plastic deformations are easier to be consumed in a shear hinge than in a bending hinge or a membrane state. Thus, localized shear response and possible shear failure become the dominate mode when the transverse shear conditions discussed in Section 1.3 are satisfied, which are normally associated with dynamic loads with sufficient intensities. Therefore, the response and failure Modes I to III appear with an increase in the loading intensity.

Even when material strain hardening and strain rate effects are important, the basic response feature of a plastic structural element shows no significant change. Thus, a rigid, perfectly plastic analysis is sufficient for most engineering problems. The shortcoming of a rigid, perfectly plastic analysis is its limitation to give deformation distributions within a plastic hinge although some simplified methods

have been introduced to overcome this difficulty(Nonaka(1967), Jones and Shen(1993)). Most of them, unfortunately, concern the construction of a bending hinge, except Wang and Jones(1996) who proposed an one dimensional transverse shear propagation analysis based on rigid, plastic strain hardening model. The formation of a transverse shear hinge and its geometrical dimension will be studied in Chapter 3.

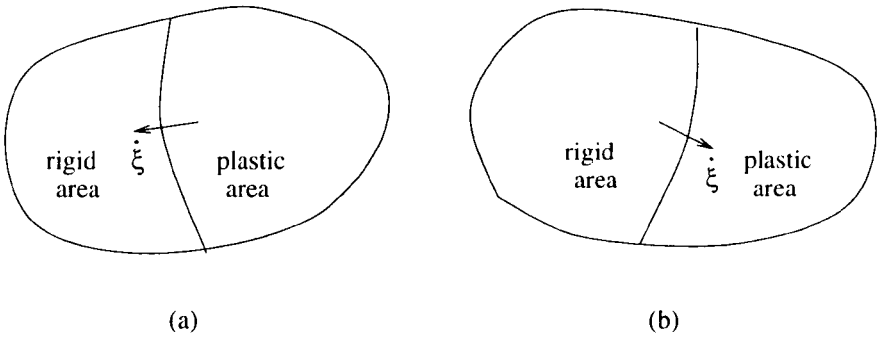

Fig.2.1 Discontinuity interfaces in a rigid, perfectly plastic material, (a) Moving from a perfectly plastic zone to rigid zone; (b) Moving from a rigid zone to a perfectly plastic zone.

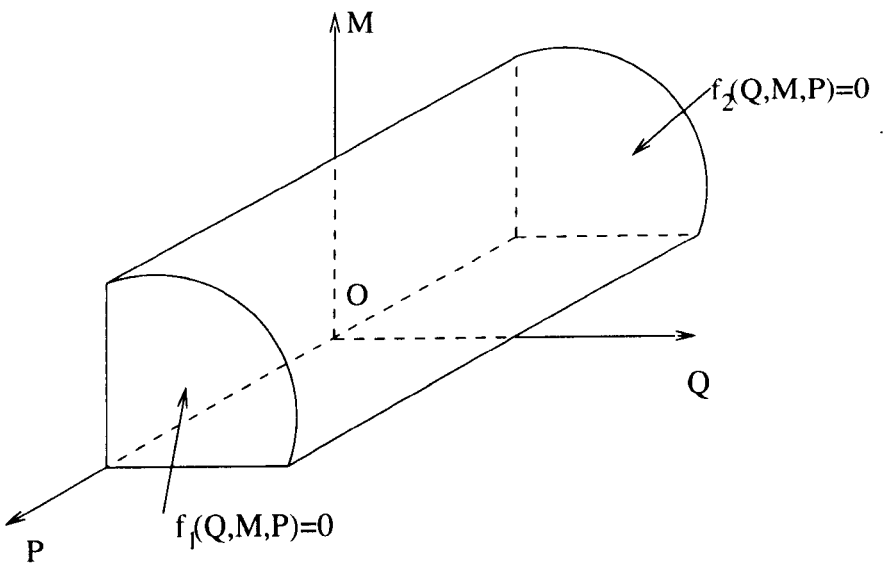

Fig.2.2 Yield surface.

3. FORMATION OF A SHEAR LOCALIZATION IN STRUCTURAL ELEMENTS UNDER TRANSVERSE DYNAMIC LOADS

3.1. Introduction

It is well-known that transverse shear becomes an important factor in the dynamic response and failure of transversely loaded structural elements with increasing dynamic loading rate and intensity and many studies have been published to examine the influence of transverse shear on the dynamic plastic response and failure of structural elements(Jones, 1989(a, b and c), Jones and Shen, 1993). The concept of a 'shear hinge(or shear sliding)' was employed in these studies to investigate the first stage of the response for those structural elements when shear deformation dominates the bending and membrane deformations. Usually, it is assumed that a shear hinge has an infinitesimal length for a rigid, perfectly plastic idealisation. This assumption emerges from Symonds(1968)' conclusion that a transverse shear hinge is always stationary in a rigid, perfectly plastic beam, which implies that transverse shear will be localized within its initially formed zone if the influence of material strain hardening can be neglected. Symonds' conclusion, which was originally based on a particular square yield surface, has been extended to arbitrary regular and singular yield conditions, and has been shown to be valid for symmetrically loaded circular plates and cylindrical shells, as shown in Chapter 2.

Either in Symonds' original proof or in the subsequent studies on structural elements, no efforts were made to explore the structure of a shear hinge. This situation occurs because these studies concentrated mainly on global structural responses, where the concept of shear and bending hinges can give a reasonable prediction of the energy consumed without knowing the exact size of shear and bending hinges in structural elements. In fact, the exact length of a shear or bending hinge is not necessary when the hinge concept is used in dynamic plastic response

analyses. The energy consumed within a shear or bending hinge may be estimated from the relative transverse displacement across the shear hinge, or the relative rotation angle across a bending hinge, respectively. However, if the results from rigid, perfectly plastic analyses are used to predict the initiation of local failures or local flow instabilities, then the size of shear and bending hinges are required in order to obtain the deformation details within these hinges.

Usually, combined bending and shearing responses develop first in a structural element under transverse dynamic loads(Jones(1985)). This is followed by a combined bending and membrane response and, finally, membrane behaviour dominates if no material failure has occurred during the response. However, a failure may initiate at any stage during the response, which defines different failure modes as observed by Menkes and Opat(1973) and clarified by Jones(1976, 1989(c)) for beams, which have been discussed in Chapter 6. The present investigation is confined within the early time response period when shearing and bending effects dominate the response, which often leads to shear failure or adiabatic shear instability depending on loading rate and material properties. A study on the transition between these two different shear failures will be given in Chapter 4.

A transverse shear localization might develop at the site of the impact loading and hard point support interfaces and is formed by the propagation of the transverse disturbance away from these interfaces. The propagation of transverse disturbances in one or two dimensional structural elements, such as beams, plates and shells, is complicated due to the existence of two free surfaces on the top and bottom of a structural element. However, when the loading rate is low, the inertia or wave propagation effect may be neglected. In this case, the formation of a shear localization might be treated as a quasi-static problem, as studied by Wen, et al.(1994) and Wen and Jones(1996) for a beam and a circular plate, respectively. These methods will be re-examined in Section 3.2 of the present paper with a more solid physical basis and will be extended to examine cylindrical shells. Several investigations have used the simplification of a quasi-static behaviour to determine the size of a shear hinge in order to study material failure, and observed encouraging results when compared with experimental results(see Wen, et al(1995) and Jones, et al.(1995)).

When the loading rate and intensity are high, material failure might occur while the transverse disturbance is propagating across a structure. The actual strain and strain rate cannot be determined from the shear hinge length predicted by a quasi-static analysis and wave propagation theory is necessary to provide a realistic prediction. Wang and Jones(1996) proposed a transverse shear propagation model within the scope of rigid, plastic analyses when retaining the influence of material strain hardening. It was assumed that the transverse shear disturbance will propagate with a constant velocity

$$c_p = \sqrt{\frac{E_t}{\rho}}, \tag{3-1}$$

where E_t is the linear hardening modulus in a pure shear test and ρ is the material density. Clearly, the influence of the top and bottom free surfaces of structural elements on the propagation of the transverse shear disturbance are neglected, which is, nevertheless, important for the actual shear wave propagation in a beam, as shown in Section 3.3. A possible relationship between the quasi-static method and a wave propagation analysis is studied numerically in Section 3.3 from this view-point, and, thus, a description of transverse shear localization in structural elements is presented, which might be used in material failure and flow instability analyses.

3.2. Quasi-static Analyses

3.2.1 Basic Equations

A shear dominant zone, which is described as a shear hinge in a dynamic plastic analysis, might develop in a beam section under the generalised forces shown in Fig.3.1(a) for the static case, which produce the same response as the problem specified in Fig.3.1(b). A necessary condition for the appearance of such a shear dominant zone is that the length of the beam section is sufficiently short. With an increase of the beam section length, a shear dominant deformation mode(Fig.3.1(c)) will become a bending dominant deformation mode(Fig.3.1(d)). The critical value of this length for the transition between these two deformation modes defines the shear hinge length in a quasi-static analysis, which will be evaluated in Sections 3.2.2 to

3.2.4 for beams, plates and cylindrical shells, respectively.

The validation of the above postulate is examined by using the finite-element code ABAQUS for the beam in Fig.3.1(a,b), which is idealized as a static plane strain problem. Four node bi-linear plane strain elements are used for a 6061-T6 aluminum-alloy beam. The material is modelled by elasto-plastic model with a yield stress σ_0=286.8MPa and a strain hardening modulus E_h=542.6MPa. Two typical results from the ABAQUS analyses are presented in Fig.3.2(a, b) for two different values of l/H, where l and H are the half length and the thickness of a beam section, respectively. It is evident that the deformation mode corresponding to a large value of l/H is a bending dominant deformation mode and the one corresponding to a small value of l/H is a shear dominant deformation mode. Therefore, it is assumed that there exists a transition point from a shearing dominant mode to a bending dominant mode with an increase of l/H. This transition condition is used to determine the shear hinge length in a beam.

The response of a beam under transverse static and dynamic loads is very different. In the static case, the bending deformation mode usually dominates the shear deformation mode if there is no hard-point restraints near to the loading point[1], because the small loading rate ensures that bending deformation starts first to absorb plastic strain energy rather than the shear deformation mode. However, with a rapidly increasing loading intensity in the dynamic case, the condition for initiating shear deformation may be satisfied first at the loading location, which starts to absorb plastic strain energy and leads to the subsequent propagation of a shear disturbance in the beam. The shear deformation will be confined within a limited distance because bending, and then membrane, deformations will prevent the further propagation of the shear disturbance. Thus, it is necessary to study the formation of a shear localization under various loading rates.

Experimental dynamic studies on beams have suggested that the main region of a shear hinge consists of anti-symmetrical simple shear flow. Zener(1948) provided a good demonstration of a typical shear dominant zone(see Fig.12 in

[1] The hard-point restraints may ensure the satisfaction of a short distance between a pair of the external opposite forces, which may initiate the shear deformation mode.

Zener(1948)). Similar results can also be found in Jones(1989(c)) although considerable bending deformations are introduced at both sides of the shear hinge. These anti-symmetrical features of the shear hinge are observed in the dynamic case when the loading rates are within the low to medium range since the propagation effects of a transverse disturbance may then be neglected. Now, the problem in Fig.3.1(b) has the following boundary conditions

$$w(x=e)=-w(x=-e) \tag{3-2}$$

when the place of anti-symmetry point is assumed to remain stationary[2]. The corresponding generalized stress system is shown in Fig.3.1(a). As mentioned above, such boundary condition or stress system may lead to another flow mechanism, i.e., bending deformations, as shown in Fig.3.1(d), which occurs often in transversely loaded thin sheet structures. If a generalized yield condition is described by

$$f(q,m,.....)=0 \tag{3-3}$$

where, $q=Q/Q_0$ and $m=M/M_0$, when Q_0, and M_0 are the static fully plastic transverse shear force and bending moment, respectively. The normality rule of plasticity requires

$$d\gamma=d\lambda\frac{\partial f}{\partial q} \quad \text{and} \quad d\kappa=d\lambda\frac{\partial f}{\partial m}, \tag{3-4a,b}$$

where $d\gamma$ and $d\kappa$ are the increments of transverse shear strain and bending curvature, respectively. Equations (3-4a,b) are associated with the transverse shear force and bending moment through the energy dissipation relations. Therefore, the generalized stresses on a yield surface satisfy the following requirements

$$\begin{aligned} &\left\|\frac{\partial f}{\partial m}\right\| > \left\|\frac{\partial f}{\partial q}\right\| \geq 0 \quad \text{for a bending dominated hinge} \\ &\text{and} \quad \left\|\frac{\partial f}{\partial q}\right\| > \left\|\frac{\partial f}{\partial m}\right\| \geq 0 \quad \text{for a shear dominated hinge.} \end{aligned} \tag{3-5a,b}$$

For many yield conditions between q and m, equations (3-5a,b) would require

[2] This does not lose any generality for a quasi-static problem.

$$\begin{array}{ll} \|m\|\approx 1 & \text{for a bending dominated hinge} \\ \text{and} \quad \|q\| \approx 1 & \text{for a shear dominated hinge.} \end{array} \qquad (3\text{-}6a,b)$$

In particular, an independent yield condition between q and m, shown in Fig.3.3, is used to simplify the following analyses and to provide an estimate for a shear dominated hinge length. In this case, Figs. 3.1(c) and (d) are two possible responses under condition (3-2) associated with equations (3-6b) and (3-6a), respectively. The maximum length for the occurrence of shear dominant deformation will be determined by a quasi-static method of analysis for three different structural elements.

3.2.2 Beam

The static equilibrium equations for a beam may be written in the form(Fig.3.4(a))

$$\frac{\partial Q}{\partial x}=0 \quad \text{and} \quad Q+\frac{\partial M}{\partial x}=0 \qquad (3\text{-}7a,b)$$

When a shear dominant zone(shear hinge) with length $\Delta=2D=2e$ is initiated in a beam, equations (3-5b) or (3-6b) must be satisfied according to the previous discussion. According to equations (3-6b) and (3-7a), $Q\approx Q_0$ within the shear hinge, so that integrating equation (3-7b) from x=-e to x=e gives

$$e=\frac{M(x=e)-M(x=-e)}{2Q_0}. \qquad (3\text{-}8)$$

The maximum value of e is determined when $M(x=e)=-M(x=-e)=M_0$,. In this case, bending dominant zones(bending hinges) will be formed at x=e and x=-e, which terminate the further propagation of shear deformations, and, thus, define the length of a shear hinge. Therefore,

$$e=\frac{M_0}{Q_0}=\frac{\sqrt{3}}{4}H=0.433H \qquad (3\text{-}9)$$

for a beam. A similar method was used by Wen, et al., (1995), in which M(x=e)=0 was assumed giving a value of e which is one-half of the present value, i.e., e=0.216H. An ABAQUS simulation of the idealized shear dominant zone in

Fig.3.1(a,b) has shown that a shear dominant behaviour will occur at e=0.3H. The value of e for a circular plate in Section 3.3.2 is around 0.325-0.342H, which is larger than Wen et al.(1995)'s value for a beam, but smaller than the value given by eq.(3-9). Because there are more restraints in a circular plate than in a beam, the value of e for a circular plate should be smaller than the value for a beam according to physical intuition. A similar conclusion is reached when comparing the values of e for a cylindrical shell and a beam. This evidence supports the present prediction, but further verification is necessary.

3.2.3 Circular Plate

The static equilibrium equations for a circular plate are(Fig.3.4(b))

$$\frac{d(Qr)}{dr}=0 \quad \text{and} \quad \frac{dM_r}{dr}+\frac{M_r-M_\theta}{r}+Q=0. \tag{3-10a,b}$$

Equation (3-10a) gives $Qr=-Q_0a$ if $Q=-Q_0$ is first reached at r=a. Therefore, $Q(r=a+\Delta r)=-Q_0/(1+\Delta r/a)$ where $\Delta r/a \le e/a$. If the problem can be treated as a plate problem, $e/a \sim H/a \ll 1$ is required in order to satisfy the plate assumptions. For example, a may be the radius of a circular plate for a uniform impulsive pressure loading, or the radius of blunt projectile for a mass impact problem. Thus, $Q \approx Q_0$ within the shear hinge.

Under the further assumption that $M_r=M_\theta$ in the immediate vicinity of the shear hinge, a static analysis has been presented by Wen and Jones(1996) to give a shear hinge length

$$e=\frac{1+\sqrt{3}}{8}H=0.342H \tag{3-11}$$

where the von-Mises yield condition was used to relate M_r and M_θ. If the Tresca yield condition is used instead, then a similar procedure gives the shear hinge length

$$e=\frac{3\sqrt{3}}{16}H=0.325H. \tag{3-12}$$

3.2.4 Cylindrical Shell

The static equilibrium equations for a cylindrical shell are(Fig.3.4(a) and (c))

$$\frac{dM}{dx}+Q=0 \quad \text{and} \quad \frac{dQ}{dx}-\frac{N}{R}=0, \tag{3-13a,b}$$

which may be written in the dimensionless forms

$$\frac{dm}{d\xi}=-2\nu q \quad \text{and} \quad \frac{dq}{d\xi}=\frac{c^2 n}{\nu}, \tag{3-14a,b}$$

where $m=M/M_0$, $n=N/N_0$, $q=Q/Q_0$, $\xi=x/L$, $\nu=Q_0L/2M_0$ and $c^2=N_0L^2/M_0R$.

An independent yield condition between m and (q,n) is shown in Fig.3.3. It is evident that a circumferential strain is always associated with a transverse shear flow, while strains associated with bending are expected to be small in a shear hinge, which means that material yielding only leads to significant circumferential and shear deformations in a shear hinge. Therefore, an interactive yield condition between transverse shear and the circumferential membrane force in a shear hinge is sufficient for predicting the distributions of shear force within a shear hinge, although the existence of a bending moment is important for satisfying the equilibrium equation (3-14a).

The stress states in a shear hinge, which may enter the interactive yield condition between q and n, are $\sigma_{11}=\sigma_\theta$ and $\sigma_{23}=-\tau$.

The von-Mises equivalent stress is

$$\sigma=\sqrt{\frac{3}{2}s_{ij}s_{ij}}\,, \tag{3-15}$$

$$\text{where} \quad s_{ij}=\sigma_{ij}-(\frac{1}{3}\sigma_{kl}\delta_{kl})\delta_{ij},$$

which leads to

$$\sigma_\theta^2+\frac{3}{2}\tau^2=\sigma_0^2 \tag{3-16}$$

or

$$n^2+\frac{1}{2}q^2=1 \tag{3-17}$$

when using $\sigma_0=\tau_0\sqrt{3}$, $N=\sigma_\theta H$ and $Q=\tau H$.

Substituting equation (3-17) into equation (3-14b) gives the dimensionless shear force

$$q=\sqrt{2}\cos(\frac{c^2}{\sqrt{2}v}\xi) \tag{3-18}$$

when using $q=1$ at $\xi=0$. Equations (3-14a) and (3-18) with boundary conditions $m=-1$ at $\xi=e/L$ and $m=1$ at $\xi=-e/L$ predict

$$\sin(\sqrt{\frac{3}{2}}\frac{e}{R})=\frac{3}{8}\frac{H}{R}. \tag{3-19}$$

Now, $e/R<<1$ for a cylindrical shell problem, which gives $\sin(e\sqrt{3}/R\sqrt{2})\approx e\sqrt{3}/R\sqrt{2}$, so that, equation (3-19) simplifies to

$$e\approx\frac{\sqrt{3}}{4\sqrt{2}}H\approx 0.306H \tag{3-20}$$

which is smaller than the shear hinge length of a beam in equation (3-9) due to the additional influence of the circumferential force.

3.3. Propagation of a Transverse Shear Displacement in a Beam

3.3.1 Description of the Problem

Within the scope of rigid, perfectly plastic materials, transverse plastic shearing is stationary according to Symonds(1968) and Chapter 2. However, when material strain hardening is considered, the transverse disturbance will propagate along the structural elements, as shown by Wang and Jones(1996), where a constant propagation velocity of transverse shearing is found in a linear strain hardening beam. This is a first degree approximation since reflections of a plane shear wave on the upper and lower free surfaces of a beam are neglected. In fact, a transverse shear

plane wave cannot propagate in a beam without scattering due to the existence of the two free surfaces on a beam. Even within the characteristic length of a localized transverse shear zone(shear hinge), this wave scattering is also important. In order to understand the propagation of a transverse disturbance in a beam, an idealized problem described below will be studied by using FEM simulations.

If the wave effects through the thickness of the structural elements are neglected in either impulsively loaded beams or in beams impacted by a projectile, the propagation of a transverse shear disturbance from the loading point may be simplified into the problem given in Fig.3.1(b), where the transverse shear disturbance at the loading location is represented by a transverse displacement history, W(t), described by

$$W(t)=W\frac{t}{T}, \quad \text{for} \quad 0\le t\le T \quad \text{and} \quad W(t)=W \quad \text{for} \quad t>T, \tag{3-21}$$

in which T can be adjusted to represent different loading rates. The beam material is elasto-plastic with a linear strain hardening relationship

$$\sigma_e=\sigma_0+E_h\varepsilon_e \tag{3-22}$$

where σ_0 and E_h are yield stress and hardening modulus given in Table 3.1. The strain rate effect may be included through the Cowper-Symonds relationship

$$\dot{\varepsilon}_e=D\left(\frac{\sigma_e}{\sigma_e^s}-1\right)^p \tag{3-23}$$

where $\dot{\varepsilon}_e$ is the equivalent plastic strain rate, σ_e^s is the equivalent stress under static loading condition, σ_e is the equivalent stress at a non-zero plastic strain rate and D and p are given in Table 3.1.

Plane strain four-node bi-linear elements(CPE4) in ABAQUS/standard-5.4 are used in the simulation. The plane strain element mesh is shown in Fig.3.5. Direct implicit time integration is used in the dynamic analysis in ABAQUS/standard. An automatic time step control based on the half-step residual concept is selected in the simulation. Newton's method was employed for solving the nonlinear equilibrium equations using the Hilber-Hughes-Taylor operator with the artificial damping

parameter α=-0.05 and Newmark's formula were used for the displacement and velocity integration. For more details of the numerical procedure the reader may refer to ABAQUS Theory and User's Manuals, Version 5.4(1994).

3.3.2 Dimensional Analysis

A complete group of independent dimensionless variables for the prescribed model are

$$\frac{B}{H},\ \frac{L}{H},\ \nu,\ p,\ TD,\ \frac{V}{c_e},\ \frac{V}{c_p},\ \frac{\sigma_0}{E},\ \frac{W}{H}, \qquad \text{(3-24a-i)}$$

where e=0.433H is the shear hinge length given by eq.(3-9). V=W/T is the driving velocity at one end of the beam. $c_e=\sqrt{(E/2(1+\nu)\rho)}$ and $c_p=\sqrt{(E_h/3\rho)}$ are elastic and plastic shear wave speeds[3], respectively. In the following analyses, further postulates are introduced, i.e.,

(i) Material strain rate effects are neglected. Thus, p and TD can be eliminated from the group.

(ii) The present beam problem may be treated as a plane strain problem because B/H=2.67. Therefore, B/H and ν are eliminated from the group.

(iii) The beam response is dominated by large plastic deformations, i.e., elastic effects are neglected in the analyses. Thus, σ_0/E and V/c_e are removed from the dimensionless groups.

(iv) L/H is an important factor in the transverse shear response(Jones(1989a)), which reflects the influence of the parameter $Q_0L/(2M_0)$=2L/H on the initiation of the transverse shear response mode in a beam with a rectangular cross-section. However, it is likely that the size of the transverse shear localization zone does not depend on this parameter if L/H>>1.

(v) The external work is determined by W/H, which may influence the characteristics of shear localization. When the driving velocity is a constant, the dimensionless time $T/(e/c_p)$ may be introduced to represent the input external work, equivalently, instead

---

[3] According to von-Mises yield condition, the linear hardening modulus in a pure shear test is given by $E_t=E_h/2(1+\nu')=E_h/3$ when the material is incompressible(ν'=0.5), where E_h is determined from a uniaxial tensile test.

of W/H.

Thus, only two dimensionless parameters are significant for describing a shear localization zone, i.e.,

$$\eta_v=\frac{V}{c_p} \quad \text{and} \quad \eta_t=\frac{T}{e/c_p}, \tag{3-25a,b}$$

where c_p=260m/s and $T^*=e/c_p$=15.85μs are the characteristic velocity and response time of the particular problem considered, respectively.

The FEM simulations show that three cases are possible, i.e., (a) $\eta_v<<1$, or $V<<c_p$; (b) $\eta_v<1$ and η_v ~o(1), or $V<c_p$ and V~o(c_p); (c) $\eta_v>1$, or $V>c_p$. These three cases correspond to a static or quasi-static process, a dynamic plastic response process and a transient wave propagation process, respectively, as shown in Figs.3.6(a-c). In case (c), two different situations, (c1) and (c2) are distinguished when $\eta_t\leq 1$ and $\eta_t>1$, which will be discussed in the subsequent section.

3.3.3 FEM Simulations

The three different cases (a)-(c) in Section 3.3.2 are simulated by the examples in Table 3.2.

(a) Bending response when $V<<c_p$

Two simulations are conducted with $V<<c_p$=260m/s. The parameters T=500μs and W=6.5mm are used for the first example, which gives V=13m/s and V/c_p=0.05. A second example with T=150μs and W=5.0mm gives V=33.3m/s and V/c_p=0.128. The final distributions of the equivalent plastic strains for these two examples are shown in Figs.3.7(a,b), respectively. It is evident that they both belong to a typical bending response, as shown previously in Figs.3.2(b) and 3.6(a). Thus, the response mode when $V<<c_p$ is a bending dominant deformation.

The unsymmetrical distributions of the equivalent strains on the upper and lower parts of the beam are due to the influence of the membrane force because the two ends of the beam are restrained in the horizontal direction.

(b) Plastic shear hinge formation when $V<c_p$ and V~o(c_p)

Propagations of both plastic equivalent strain and the transverse shear

component of the strain tensor are shown in Figs.3.8(a) and (b) for T=20μs and W=3.0mm with V=150m/s and V/c_p=0.58, respectively. The corresponding maximum shear stress(Tresca stress) and axial stress(S11) are presented in Figs.3.8(c,d). It is observed that there is a localised transverse shear zone near the loading end, in which an equivalent plastic strain consists mainly of the transverse shear component. This shear deformation is propagated at speeds of approximately 244m/s and 239m/s according to the first three simulation results in Fig.3.8(b) before T*=15.85μs. These speeds are approaching the plastic shear wave speed, c_p=260m/s, and, the propagation model proposed by Wang and Jones(1996) is adequate. However, after T>T*, the propagated shear deformations are trapped in a zone with a length, e≈0.433H, as determined by the quasi-static analysis. Stress distributions in the beam are complicated due to the existence of the upper and lower free surfaces. The propagation of the axial stress in Fig.3.8(d) indicates the formation of a bending mode in the beam, which is probably responsible for preventing any further propagation of shear deformation.

The concept of a shear hinge has been used by many authors to estimate the transverse shear strain when a uniform strain distribution is assumed. In order to verify the validity of this assumption, Fig.3.9(a) gives plastic shear strain histories at different locations across the length of a shear hinge where curves 1-10 correspond to the plastic shear strains in elements 386, 376, ... 306 and 296 shown in Fig.3.5. The size of each element is H/20. Therefore, these ten elements just cover the whole length of a shear hinge(0.433H) which is calculated by the quasi-static analysis. The shear hinge is completely established after a limited time. The shear strain development ceases sooner near the loading end than at the far side of the shear hinge, x=-e. The shear strain distribution in the shear hinge is not uniform. It consists of a main shear zone with nearly constant shear strain and a transition zone with decreasing shear strain, as shown in Figs.3.8(a,b) and 3.9(a).

It is interesting to check the validity of the traditional method for calculating the shear strain in a shear hinge, i.e.,

$$\gamma=\frac{W}{e}, \tag{3-26}$$

where γ is the engineering shear strain and W is the relative transverse displacement across the shear hinge. The relative transverse displacement across a shear hinge having a length(e) between nodes 5049 and node 5040 in Fig.3.5 is calculated by ABAQUS in Fig.3.9(b), which predicts γ=1.55/(0.433x9.52)=0.38. From Fig.3.9(a), the maximum engineering shear strain(ABAQUS always uses the engineering shear strain for the shear strain) is about 0.39. So that γ in equation (3-26) gives a good estimate of the maximum engineering plastic strain in a shear hinge. A similar conclusion is obtained from another example in Figs.3.10(a,b) with V/c_p=0.231 and γ_{max}=0.103 in Fig.3.10(a)[4], which is comparable with γ=0.447/(0.433x9.52)=0.11 from equation (3-26).

When the loading time is smaller than the characteristic time, $T^*=e/c_p$=15.85μs, the transverse shear deformation can only propagate a short distance before the input energy stops, which is smaller than the shear hinge length from the quasi-static method of analysis. Figs.3.11(a-d) demonstrate four different cases with the same impact velocity V=150m/s corresponding to (a) W=1.5mm and T=10μs, (b) W=3.0mm and T=20μs, (c) W=6.0mm and T=40μs and (d) W=9.0mm and T=60μs. It is evident that the length of a localised shear zone is smaller than the predicted shear hinge length, e, when $T<T^*$=15.85μs. The predicted maximum shear strain from equation (3-26) is 0.29, which is smaller than the numerically calculated one, i.e., γ_{max} =0.38 in Figs.3.12(a-d). Therefore, plastic shear wave propagation must be considered in this case. However, it should be noted that in most practical dynamic plastic problems, the imposed velocity is normally within the intermediate range and the loading time is much longer than T*. The maximum plastic shear strains corresponding to Figs.3.12(a-d) have almost a constant value of 0.38[5]. This implies

[4] Normally, the shear strain in the element near to the boundary(element 386) is not accurate due to the influence of the boundary on the strain calculation. Therefore, its connecting element(element 376) is used to give the maximum shear strain.

[5] The later slightly increasing value of shear strain is due to the large geometrical deformations which introduce a change of local co-ordinates and axial deformations. Here, a global reference frame is used in the ABAQUS simulation. Thus, γ_{12} represents the engineering shear strain in the original

that the maximum shear strain is determined mainly by the magnitude of the impact velocity.

(c) Shearing propagation when $V>c_p$

Figs.3.13 and 3.14 present similar results as in Figs.3.8 and 3.9 for the loading parameters T=5μs and W=1.5mm, which give V=300m/s and $V/c_p=1.15$. One important feature of this example is that shear deformations localize into a narrow zone which is smaller that the calculated shear hinge length e=0.433H. Because the loading time T is smaller than $T^*=e/c_p$, the transverse shear deformations cannot reach the distance, e, determined by a quasi-static method of analysis, before the input energy stops. In this case, a quasi-static analysis cannot be used to predict a realistic shear hinge length, i.e., eq. (3-26) is invalid for predicting the maximum strain in the localized shear zone. Thus, wave propagation of the transverse shear disturbance must be considered as suggested by Wang and Jones(1996). According to Fig.3.14(b) and eq.(3-26), the maximum shear strain in the shear hinge length(e=0.433H) is 0.39, which is much smaller that the numerical calculated maximum value of $\gamma_{max}=0.83$ in Fig.3.14(a) presented by the ABAQUS simulations.

When the loading time is longer than T*, the shear deformations are not trapped within the calculated shear hinge length and a large shear zone is observed, as shown in Figs.3.15(c,d). The propagation of shear deformations cannot be predicted by a shear wave theory for $T>T^*$. However, this situation rarely develops in practice because material failure occurs normally for high impact velocities, which prevents the input of any more external impact energy for $T>T^*$. Again, the maximum shear strains are the same for different loading parameters having the same imposed velocity, as shown in Fig.3.16, which confirms the observation that the imposed velocity is an important factor for determining the maximum shear strain.

3.4. Discussion

The actual transverse loads which act on structures are more complicated than the idealized case considered in the previous sections. Two typical loads in impact

---

1 and 2 directions.

engineering are projectile impacts and explosive pressure loads, in which a transverse shear localization may be formed at either the periphery of an impacted area or at the hard-points such as supports. The characteristic velocities and loading times in these cases are determined from the initial impact velocities and impact energies. Within the early stage of the response, a compressive wave propagates from the top surface to the bottom surface of a structural element and produces a transverse disturbance. When the impact velocity is sufficiently high, considerable indentation and local failure may occur during this stage. The interactions between the indentation/failure and shear propagation must be considered for a realistic prediction of the behaviour. Several practical models have been developed by Awerbuch and Bodner(1974) for this purpose and the perforated profiles of the plate cross-section in Figs 3 and 5 of Awerbuch and Bodner(1974) have a similar overall shape to the current simulations in Fig.3.6(c).

For rapid and intensive loading, the material properties may change significantly, which can only be simulated by a more complicated solid-fluid interaction model. Even within the dynamic plastic response range, strain rate and temperature effects are important for medium to high speed loadings. An adiabatic shear band may be initiated during the shear propagation period due to thermal softening of the material, which may prevent further extension of the conventional shear zone. Instead, a more severe shear localization with a band width around 10-100μm may be formed and material fractures initiate within the band. The band width is determined mainly by the material properties and is independent of the size of the conventional shear hinge. This feature is similar to a shear hinge which is determined mainly by the structural element properties, such as Q_0 and M_0 for a beam, and is independent of the size of the structural element, e.g., the beam length.

In many cases, the temperature effect becomes important only after considerable plastic work has been consumed, but, strain rate effects are always important for rate sensitive materials. Therefore, the influence of material strain rate sensitivity should be judged in the analyses of transverse shear propagation and the formation of a shear hinge in a strain rate sensitive material, which are studied by comparing the results with and without material strain rate effects when W=3.0mm and T=20μs, as shown in Figs.3.17 and 3.18. The distribution of transverse shear in

Fig.3.17(a) when the strain rate effect is neglected is larger than that in Fig.3.17(b) when strain rate effects are considered. Actually, the maximum shear strain has been given in Fig.3.9(a) as 0.38 when the strain rate effect is neglected, which is nearly double the value obtained from Fig.3.18(a) when the influence of material strain rate sensitivity is retained. Therefore, the stress state, or the yield stress, may be another important factor in the magnitude of the maximum shear strain in addition to the impact velocity. It is noted from Fig.3.18(b) that the maximum shear strain from eq.(3-26) is 0.22, which is comparable with γ_{max}=0.218 from the ABAQUS calculations.

Finally, it should be noted that the conclusions obtained in this study for a beam might be applied to plates and cylindrical shells when subjected to large dynamic transverse loads due to the similarities inherent in all transversely loaded structural elements.

Table 3.1 Material Properties of 6061-T6 Aluminum Alloy

E(GPa)	ρ(Kg/m^3)	σ_0(MPa)	ν	E_h(MPa)	p	D(1/s)
72.4	2686	286.8	0.32	542.6	4.0	6500.0

E, E_h, p and D: ABAQUS (1994b); ν: J. Appl. Phys, 72, 429-441(1992); ρ, σ_0: Jones(1976).

Table 3.2 Numerical Simulation Data

No.	W(mm)	T(μs)	V(m/s)	η_v	η_t	Type	Note
H1	1.5	5	300	1.154	0.32	(c1)	
H2	6.5	500	13	0.05	31.55	(a)	
H3	3.0	50	60	0.23	3.16	(b)	
H4	5.0	150	33.33	0.13	9.46	(a)	
H5	3.0	10	300	1.154	0.63	(c1)	
H6	3.0	20	150	0.58	1.26	(b)	
H7	1.5	10	150	0.58	0.63	(c1)	
H8	3.0	20	150	0.58	1.26	(b)	strain rate
H9	3.0	10	300	1.154	0.63	(c1)	
H10	6.0	20	300	1.154	1.26	(c2)	Fig.8.15(c)
H11	6.0	40	150	0.58	2.52	(b)	
H12	9.0	60	150	0.58	3.79	(b)	
H13	9.0	30	300	1.154	1.89	(c2)	Fig.8.15(d)

Note:(a):bending mode($\eta_v<<1$); (b): trapped shear hinge($\eta_v<1$ and $\eta_v\sim o(1)$); (c): transient shear wave propagation($\eta_v>1$), in which (c1) and (c2) correspond to $\eta_t<1$ and $\eta_t>1$, respectively.

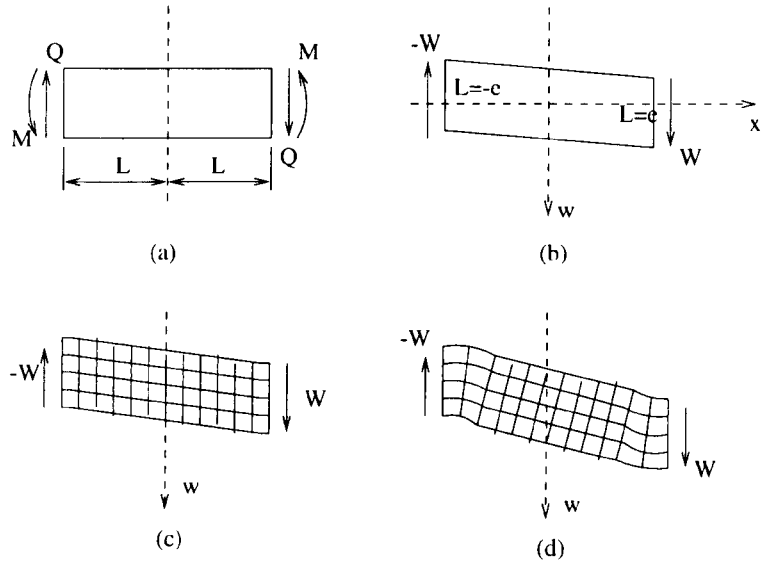

Fig.3.1 (a) Generalised forces on beam section; (b) Boundary condition of problem (a); (c) Shear dominant deformation mode; (d) Bending dominant deformation mode

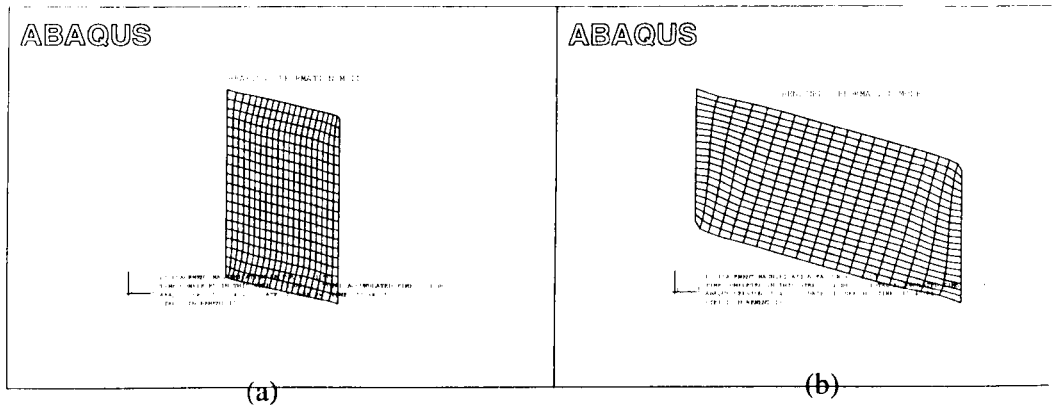

Fig.3.2 Static simulation of the plane strain problem in Fig.3.1(b) using ABAQUS, (a) Shearing deformation mode(l/H=0.3); (b) Bending deformation mode(l/H=0.8)

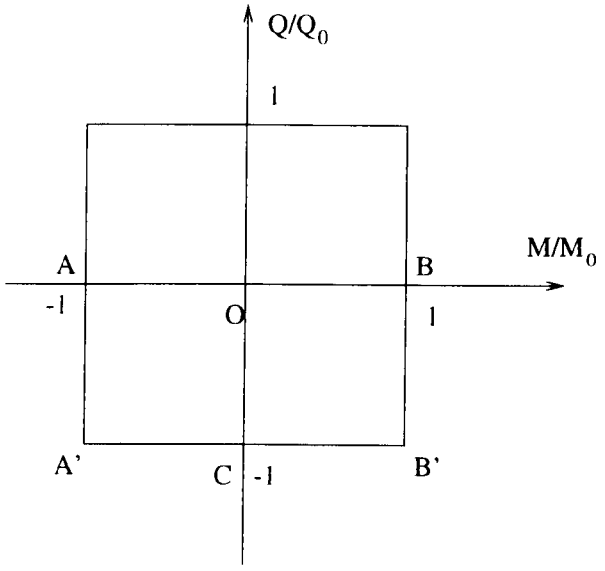

Fig.3.3 Independent yield curve for a beam.

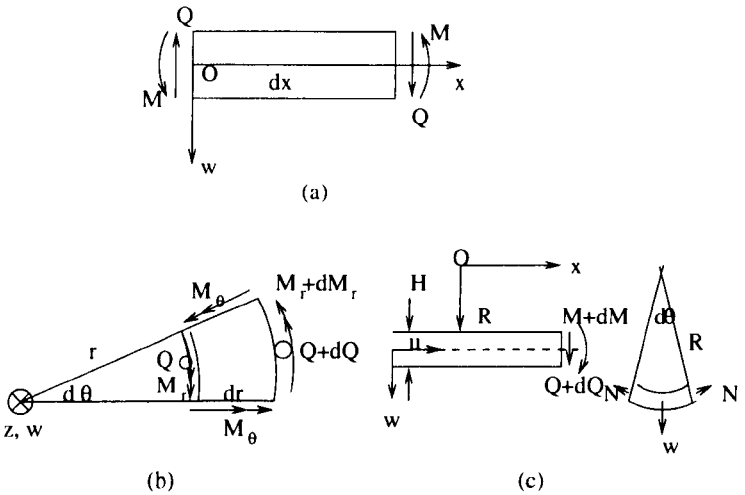

Fig.3.4 Structural elements, (a) Beam; (b) Circular plate; (c) Cylindrical shell.

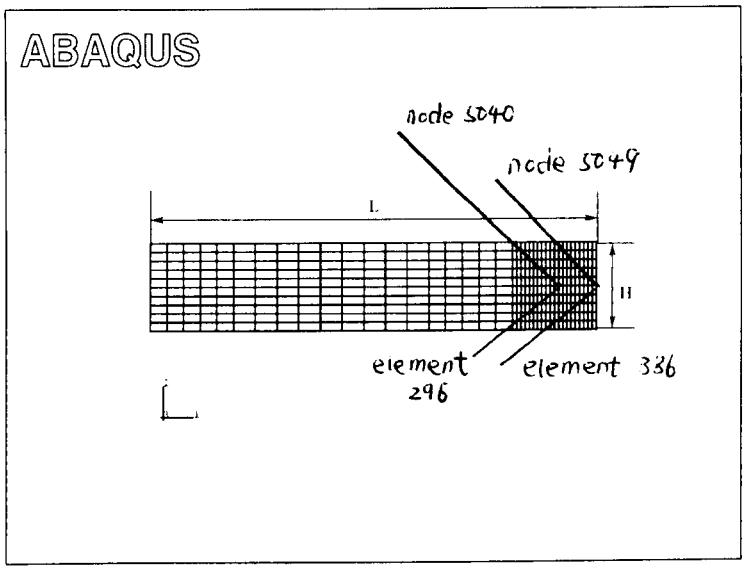

Fig3.5 Plane strain finite element of a beam.

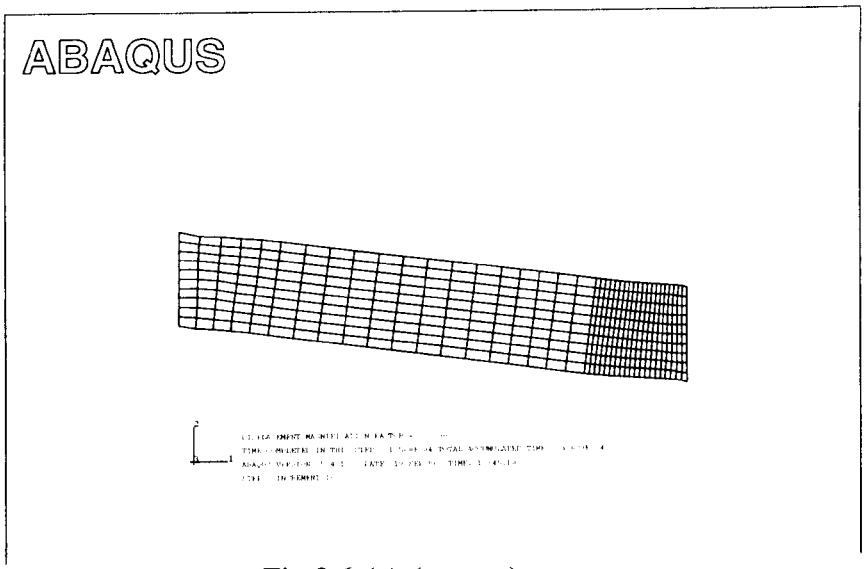

Fig.3.6 (a) (cont....)

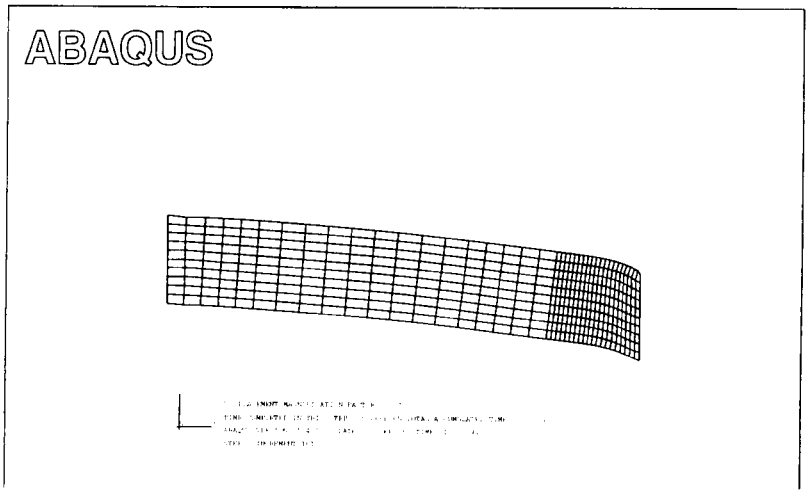

(b)

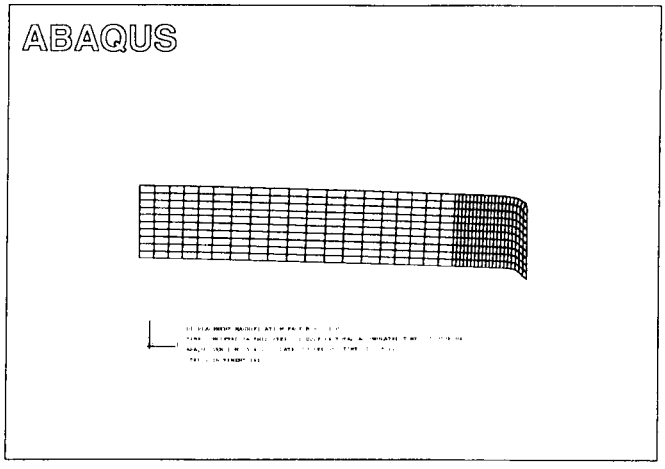

(c)

Fig.3.6 Response modes of a transversely loaded beam, (a) Bending dominant deformation(simulation No.H4); (b) Shear hinge at loading end(H6); (c) Shearing localization formed by shear wave(H1).

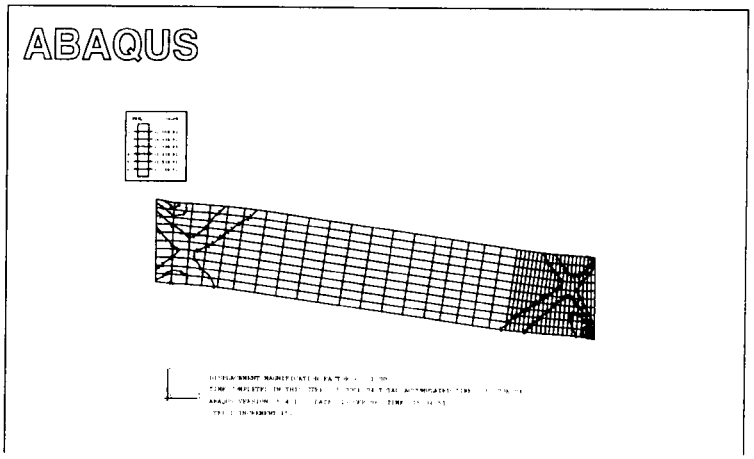

(a)

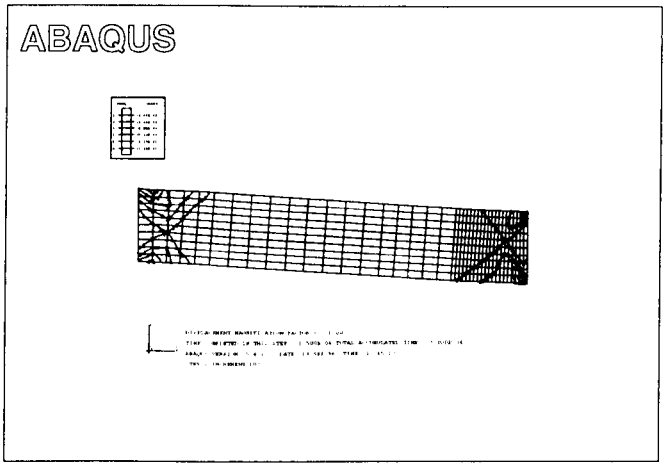

(b)

Fig.3.7 Bending response, (a) W=6.5mm and T=500μs(H2); (b)W=5mm and T=150μs(H4).

See the attachment(Eight pages)

Fig.3.8 Simulation results for W=3.0mm and T=20μs with V=150m/s(H6), (a) Propagation of equivalent plastic strain; (b) Propagation of engineering plastic shear strain(γ_{12}); (c) Propagation of the maximum shear stress; (d)Propagation of the axial tensile stress.

(a)

ABAQUS

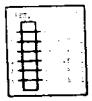

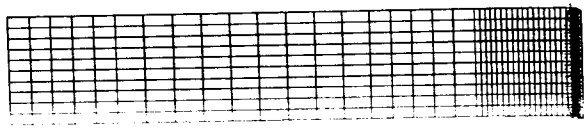

DISPLACEMENT MAGNIFICATION FACTOR = 1.00
TIME COMPLETED IN THIS STEP 0.1643E-04 TOTAL ACCUMULATED TIME 0.1643E-04
ABAQUS VERSION: 5.4-1 DATE: 20-SEP-96 TIME: 12:15:41
STEP 1 INCREMENT 10

ABAQUS

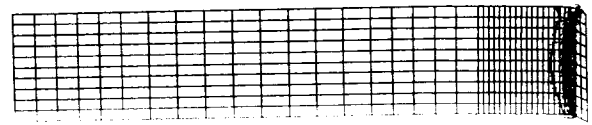

DISPLACEMENT MAGNIFICATION FACTOR = 1.00
TIME COMPLETED IN THIS STEP 0.1643E-04 TOTAL ACCUMULATED TIME 0.1643E-04
ABAQUS VERSION: 5.4-1 DATE: 20-SEP-96 TIME: 12:15:41
STEP 1 INCREMENT 10

ABAQUS

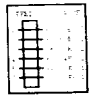

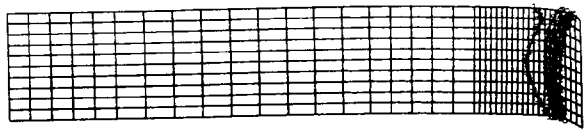

DISPLACEMENT MAGNIFICATION FACTOR = 1.00
TIME COMPLETED IN THIS STEP 1.047E-05 TOTAL ACCUMULATED TIME 1.047E-05
ABAQUS VERSION: 5.4-1 DATE: 20-SEP-96 TIME: 12:15:41
STEP 1 INCREMENT 30

ABAQUS

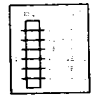

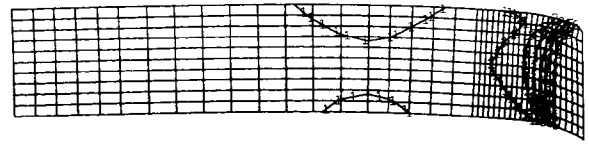

DISPLACEMENT MAGNIFICATION FACTOR = 1.00
TIME COMPLETED IN THIS STEP 1.855E-05 TOTAL ACCUMULATED TIME 1.855E-05
ABAQUS VERSION: 5.4-1 DATE: 20-SEP-96 TIME: 12:15:41
STEP 1 INCREMENT 40

(c)

ABAQUS

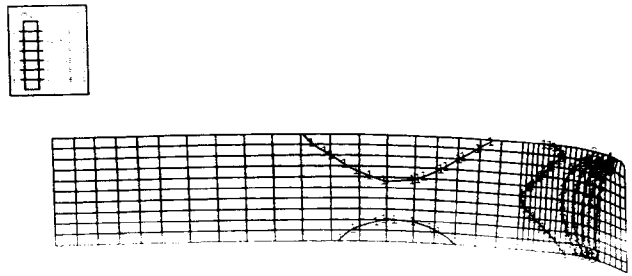

DISPLACEMENT MAGNIFICATION FACTOR = 1.00
TIME COMPLETED IN THIS STEP 1.972E-06 TOTAL ACCUMULATED TIME 1.972E-06
ABAQUS VERSION: 5.4-1 DATE: 20-SEP-96 TIME: 12:15:41
STEP 2 INCREMENT 12

ABAQUS

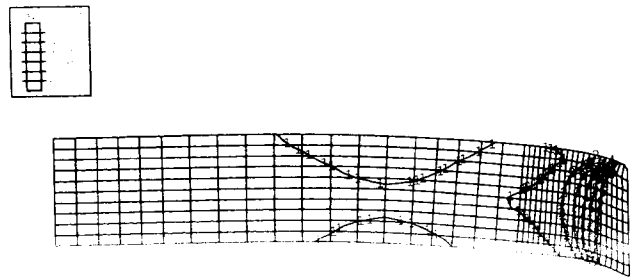

DISPLACEMENT MAGNIFICATION FACTOR = 1.00
TIME COMPLETED IN THIS STEP 4.486E-06 TOTAL ACCUMULATED TIME 4.486E-06
ABAQUS VERSION: 5.4-1 DATE: 20-SEP-96 TIME: 12:15:41
STEP 2 INCREMENT 19

ABAQUS

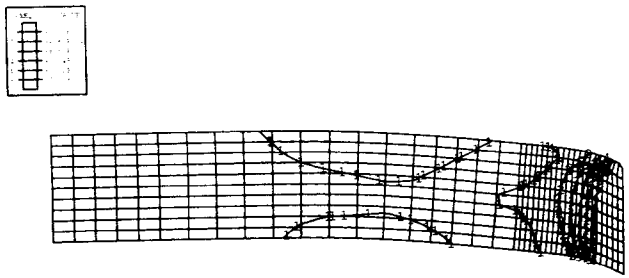

DISPLACEMENT MAGNIFICATION FACTOR = 1.00
TIME COMPLETED IN THIS STEP 7.258E-06 TOTAL ACCUMULATED TIME 2.726E-05
ABAQUS VERSION: 5.4-1 DATE: 20-SEP-96 TIME: 12:15:41
STEP 2 INCREMENT 36

ABAQUS

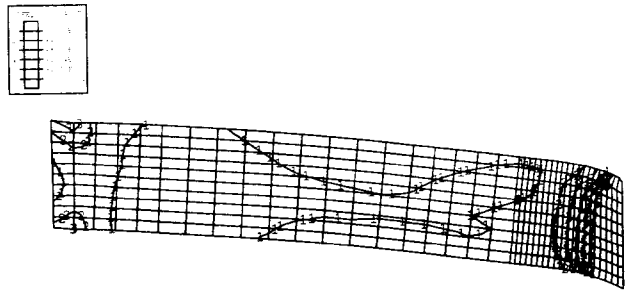

DISPLACEMENT MAGNIFICATION FACTOR = 1.00
TIME COMPLETED IN THIS STEP 5.000E-05 TOTAL ACCUMULATED TIME 7.000E-05
ABAQUS VERSION: 5.4-1 DATE: 20-SEP-96 TIME: 12:15:41
STEP 2 INCREMENT 101

ABAQUS

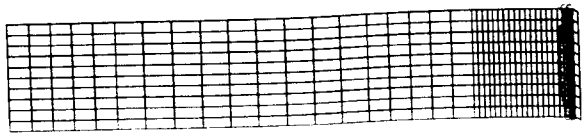

DISPLACEMENT MAGNIFICATION FACTOR = 1.00
TIME COMPLETED IN THIS STEP 1.841E-06 TOTAL ACCUMULATED TIME 1.841E-06
ABAQUS VERSION: 5.4-1 DATE: 20-SEP-96 TIME: 12:15:41
STEP 1 INCREMENT 10

ABAQUS

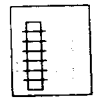

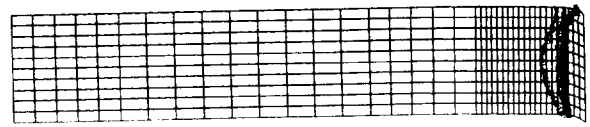

DISPLACEMENT MAGNIFICATION FACTOR = 1.00
TIME COMPLETED IN THIS STEP 6.147E-06 TOTAL ACCUMULATED TIME 6.147E-06
ABAQUS VERSION: 5.4-1 DATE: 20-SEP-96 TIME: 12:15:41
STEP 1 INCREMENT 20

ABAQUS

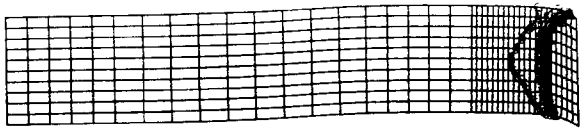

DISPLACEMENT MAGNIFICATION FACTOR = 1.00
TIME COMPLETED IN THIS STEP 1.047E-05 TOTAL ACCUMULATED TIME 1.047E-05
ABAQUS VERSION: 5.4-1 DATE: 20-SEP-96 TIME: 12:15:41
STEP 1 INCREMENT 30

ABAQUS

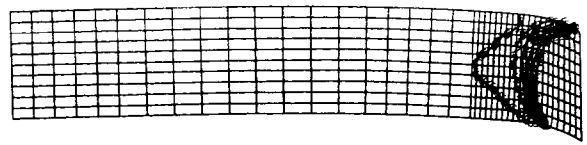

DISPLACEMENT MAGNIFICATION FACTOR = 1.00
TIME COMPLETED IN THIS STEP 1.855E-05 TOTAL ACCUMULATED TIME 1.855E-05
ABAQUS VERSION: 5.4-1 DATE: 20-SEP-96 TIME: 12:15:41
STEP 1 INCREMENT 40

(q)

ABAQUS

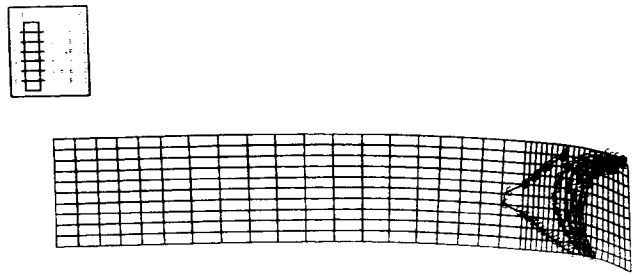

DISPLACEMENT MAGNIFICATION FACTOR = [illegible]
TIME COMPLETED IN THIS STEP [illegible] TOTAL ACCUMULATED TIME [illegible]
ABAQUS VERSION: 5.4-1 DATE: [illegible] TIME: 12:15:41
STEP 2 INCREMENT 12

ABAQUS

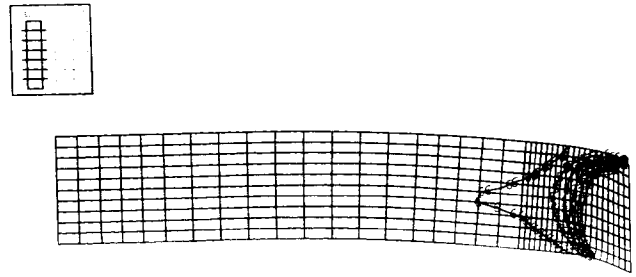

DISPLACEMENT MAGNIFICATION FACTOR = [illegible]
TIME COMPLETED IN THIS STEP [illegible] TOTAL ACCUMULATED TIME [illegible]
ABAQUS VERSION: 5.4-1 DATE: [illegible] TIME: 12:15:41
STEP 2 INCREMENT 34

ABAQUS

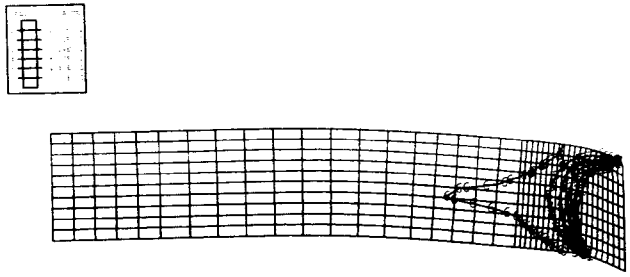

DISPLACEMENT MAGNIFICATION FACTOR = 1.00
TIME COMPLETED IN THIS STEP 7.258E-06 TOTAL ACCUMULATED TIME 2.726E-05
ABAQUS VERSION: 5.4-1 DATE: 20-SEP-96 TIME: 12:15:41
STEP 2 INCREMENT 36

ABAQUS

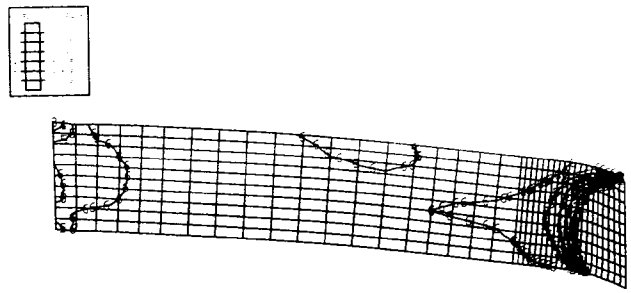

DISPLACEMENT MAGNIFICATION FACTOR = 1.00
TIME COMPLETED IN THIS STEP 5.000E-05 TOTAL ACCUMULATED TIME [illegible]
ABAQUS VERSION: 5.4-1 DATE: 20-SEP-96 TIME: 12:15:41
STEP 2 INCREMENT 101

(c)

ABAQUS

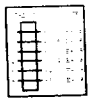

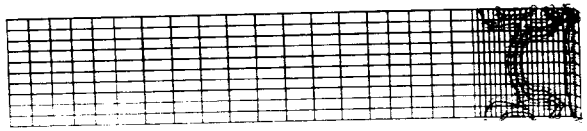

DISPLACEMENT MAGNIFICATION FACTOR = 1.00
TIME COMPLETED IN THIS STEP 1.184E-06 TOTAL ACCUMULATED TIME 1.184E-06
ABAQUS VERSION: 5.4-1 DATE: 20-SEP-96 TIME: 12:15:41
STEP 1 INCREMENT 10

ABAQUS

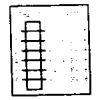

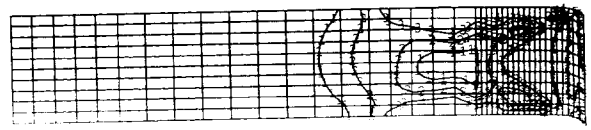

DISPLACEMENT MAGNIFICATION FACTOR = 1.00
TIME COMPLETED IN THIS STEP 5.917E-06 TOTAL ACCUMULATED TIME 7.101E-06
ABAQUS VERSION: 5.4-1 DATE: 20-SEP-96 TIME: 12:15:41
STEP 1 INCREMENT 20

ABAQUS

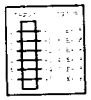

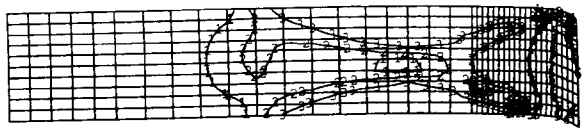

DISPLACEMENT MAGNIFICATION FACTOR = 1.00
TIME COMPLETED IN THIS STEP 1.047E-05 TOTAL ACCUMULATED TIME 1.047E-05
ABAQUS VERSION: 5.4-1 DATE: 20-SEP-96 TIME: 12:15:41
STEP 1 INCREMENT 30

ABAQUS

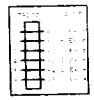

DISPLACEMENT MAGNIFICATION FACTOR = 1.00
TIME COMPLETED IN THIS STEP 1.855E-05 TOTAL ACCUMULATED TIME 1.855E-05
ABAQUS VERSION: 5.4-1 DATE: 20-SEP-96 TIME: 12:15:41
STEP 1 INCREMENT 40

ABAQUS

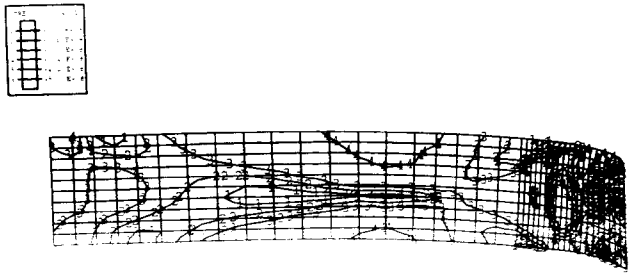

DISPLACEMENT MAGNIFICATION FACTOR = 1.00
TIME COMPLETED IN THIS STEP 2.726E-06 TOTAL ACCUMULATED TIME 2.726E-06
ABAQUS VERSION: 5.4-1 DATE: 20-SEP-96 TIME: 12:15:41
STEP 2 INCREMENT 12

ABAQUS

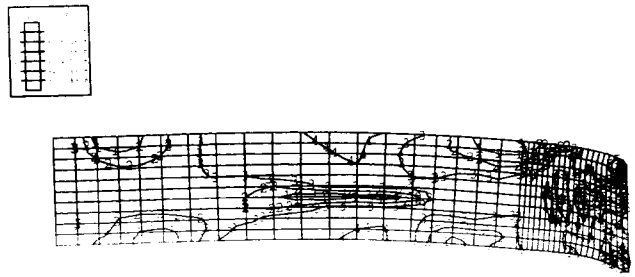

DISPLACEMENT MAGNIFICATION FACTOR = 1.00
TIME COMPLETED IN THIS STEP 4.000E-06 TOTAL ACCUMULATED TIME 1.726E-05
ABAQUS VERSION: 5.4-1 DATE: 20-SEP-96 TIME: 12:15:41
STEP 2 INCREMENT 24

ABAQUS

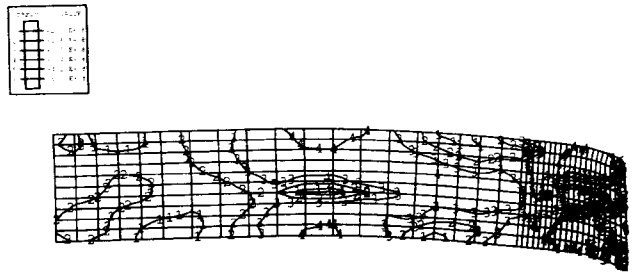

DISPLACEMENT MAGNIFICATION FACTOR = 1.00
TIME COMPLETED IN THIS STEP 7.258E-06 TOTAL ACCUMULATED TIME 2.726E-05
ABAQUS VERSION: 5.4-1 DATE: 20-SEP-96 TIME: 12:15:41
STEP 2 INCREMENT 36

ABAQUS

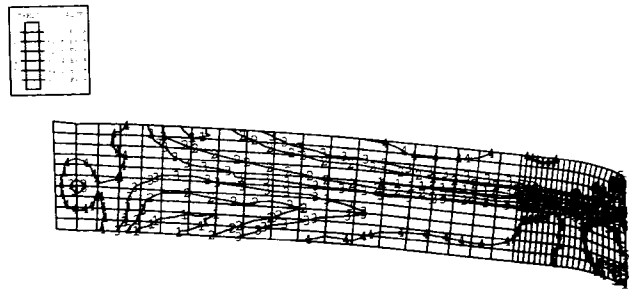

DISPLACEMENT MAGNIFICATION FACTOR = 1.00
TIME COMPLETED IN THIS STEP 5.000E-05 TOTAL ACCUMULATED TIME 7.000E-05
ABAQUS VERSION: 5.4-1 DATE: 20-SEP-96 TIME: 12:15:41
STEP 2 INCREMENT 101

(P)

ABAQUS

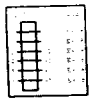

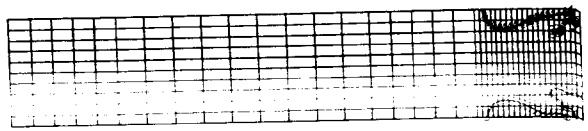

DISPLACEMENT MAGNIFICATION FACTOR = [illegible]
[illegible] COMPLETED IN THIS STEP [illegible] TOTAL ACCUMULATED TIME [illegible]
ABAQUS VERSION: 5.4-1 DATE: 20-SEP-96 TIME: 12:15:41
STEP 1 INCREMENT 10

ABAQUS

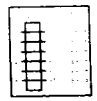

DISPLACEMENT MAGNIFICATION FACTOR = [illegible]
TIME [illegible] TOTAL ACCUMULATED TIME [illegible]
ABAQUS VERSION: 5.4-1 DATE: 20-SEP-96 TIME: 12:15:41
STEP 1 INCREMENT 10

ABAQUS

DISPLACEMENT MAGNIFICATION FACTOR = 1.00
TIME COMPLETED IN THIS STEP 1.047E-05 TOTAL ACCUMULATED TIME 1.047E-05
ABAQUS VERSION: 5.4-1 DATE: 20-SEP-96 TIME: 12:15:41
STEP 1 INCREMENT 30

ABAQUS

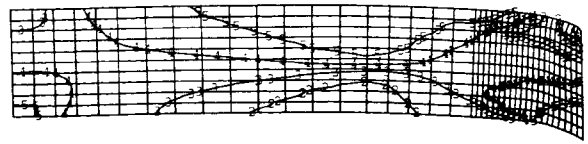

DISPLACEMENT MAGNIFICATION FACTOR = 1.00
TIME COMPLETED IN THIS STEP 1.855E-05 TOTAL ACCUMULATED TIME 1.855E-05
ABAQUS VERSION: 5.4-1 DATE: 20-SEP-96 TIME: 12:15:41
STEP 1 INCREMENT 40

(d)

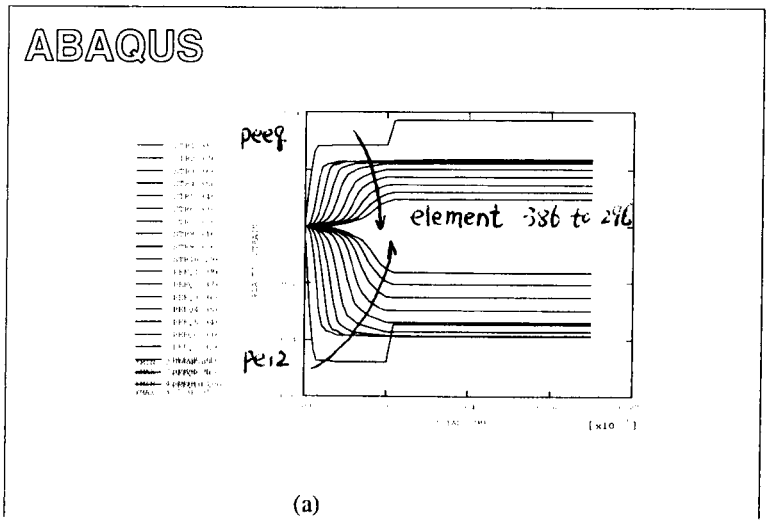

(a)

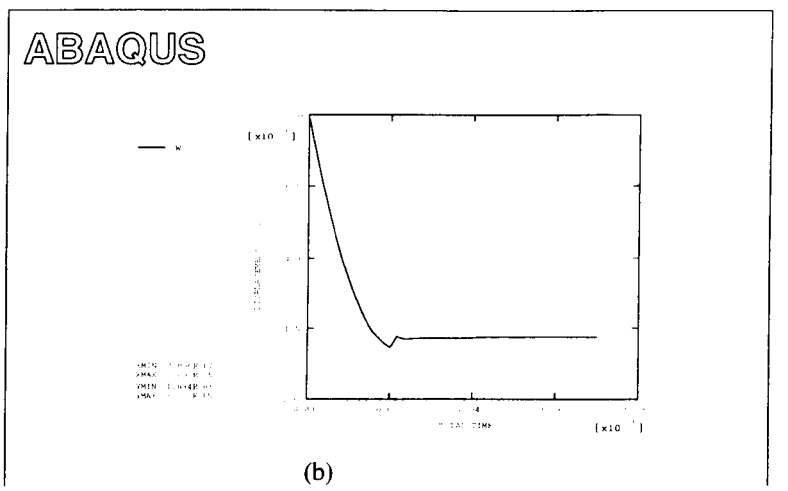

(b)

Fig.3.9 (a) Plastic shear and equivalent strain histories at different locations across the shear hinge length in simulation H6; (b) Relative displacement across the shear hinge length, e.

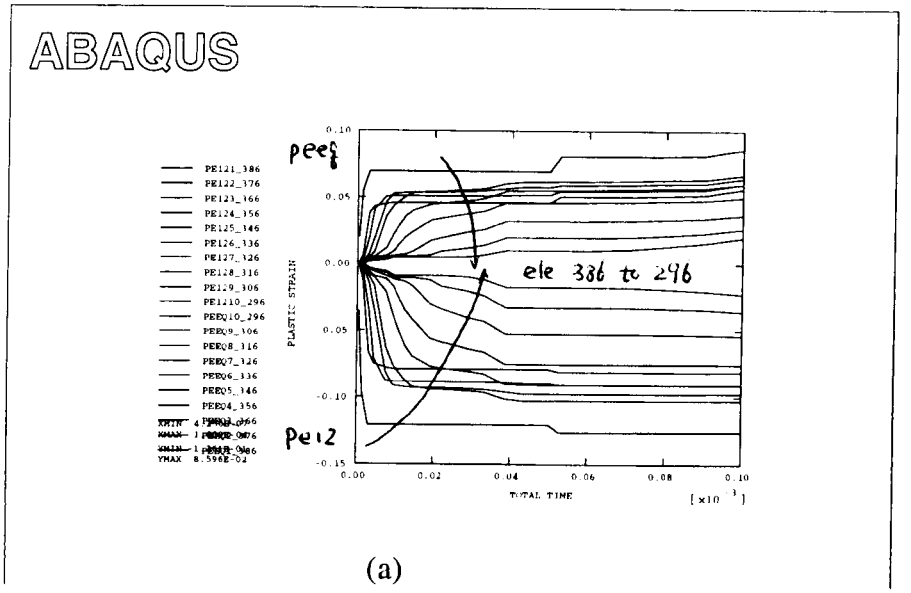

Fig.3.10 (a) Shear and equivalent strain histories at different location in shear hinge(H3); (b)Relative transverse displacement across shear hinge.

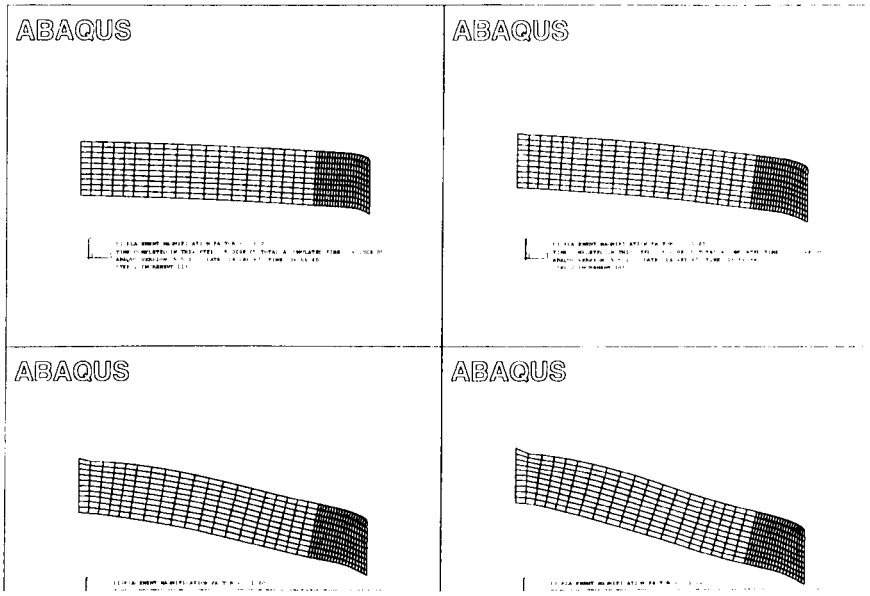

Fig.3.11 Deformation patterns of a beam with an imposed velocity of V=150m/s, (a) W=1.5mm and T=10μs(H7); (b) W=3.0mm and T=20μs(H6); (c) W=6.0mm and T=40μs(H11); (d) W=9.0mm and T=60μs(H12).

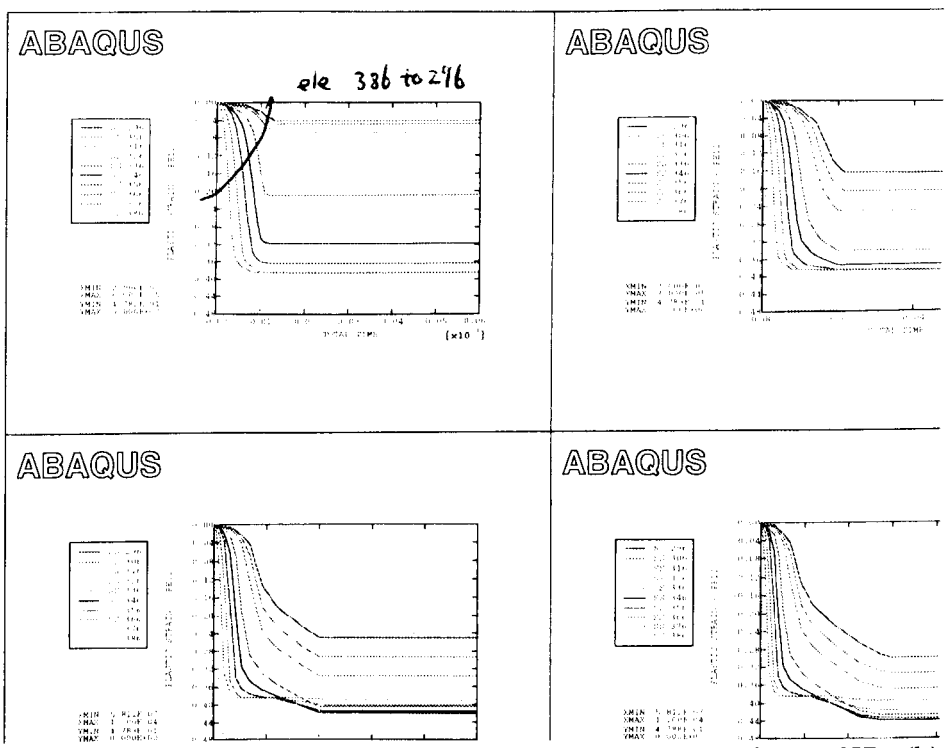

Fig.3.12 Shear strain histories with an imposed velocity of V=150m/s for (a) H7; (b) H6; (c) H11 and (d) H12, in Table 3.2, where γ_{max}=0.38 for (a)-(d).

See the attachment(Eight pages)

Fig.3.13 Simulation results for W=1.5mm and T=5μs with V=300m/s(H1), (a) Propagation of equivalent plastic strain; (b) Propagation of engineering plastic shear strain(γ_{12}); (c) Propagation of the maximum shear stress; (d)Propagation of the axial tensile stress.

(a)

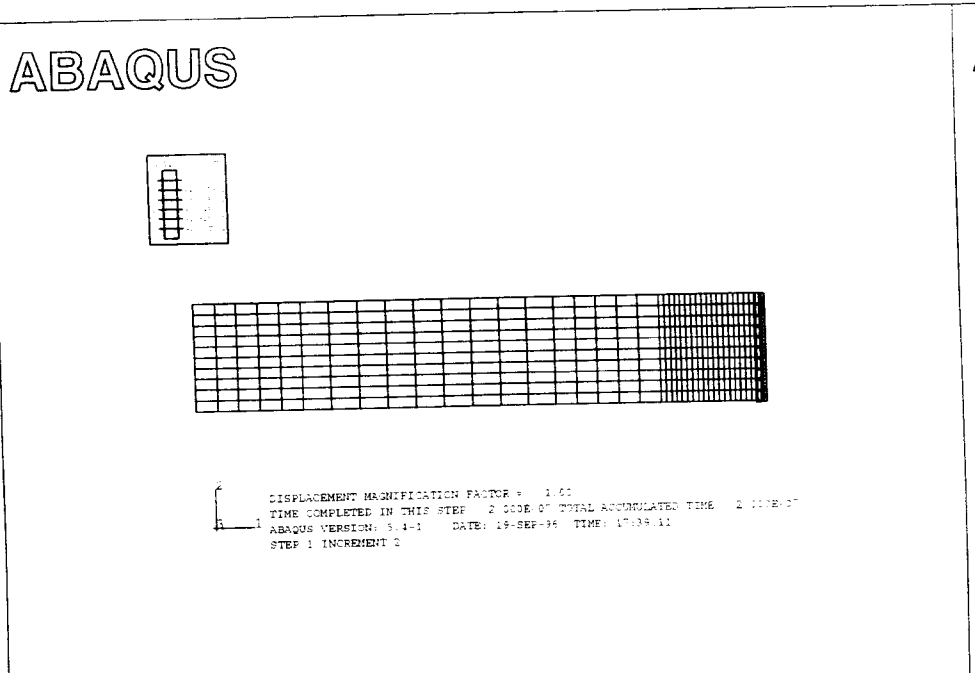
ABAQUS
DISPLACEMENT MAGNIFICATION FACTOR = 1.00
TIME COMPLETED IN THIS STEP 2.000E-07 TOTAL ACCUMULATED TIME 2.000E-07
ABAQUS VERSION: 5.4-1 DATE: 19-SEP-96 TIME: 17:39:11
STEP 1 INCREMENT 2

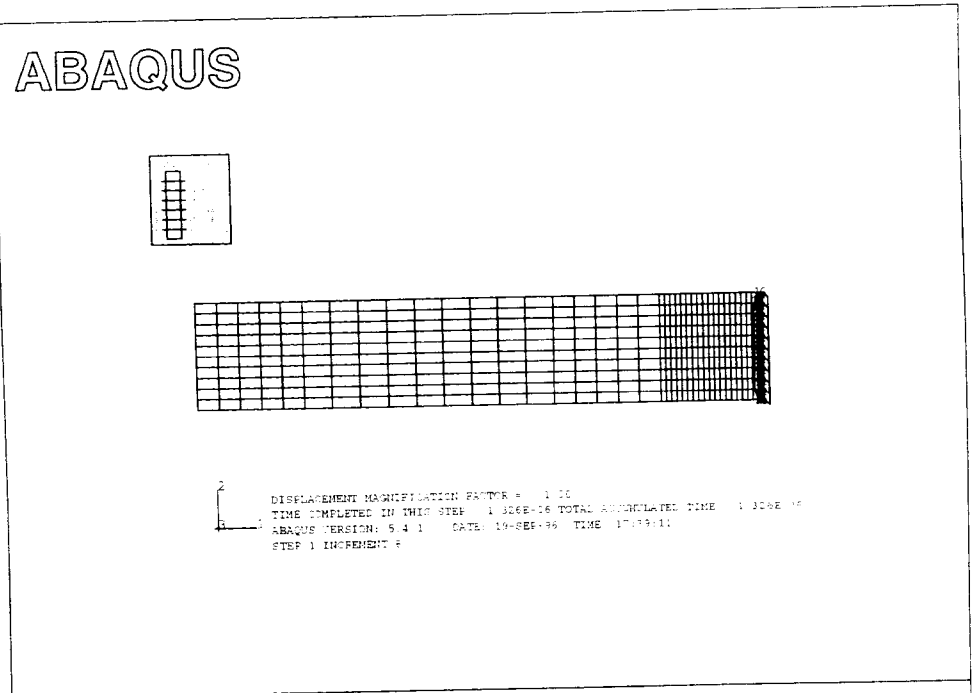
ABAQUS
DISPLACEMENT MAGNIFICATION FACTOR = 1.00
ABAQUS VERSION: 5.4-1 DATE: 19-SEP-96 TIME: 17:39:11
STEP 1 INCREMENT 8

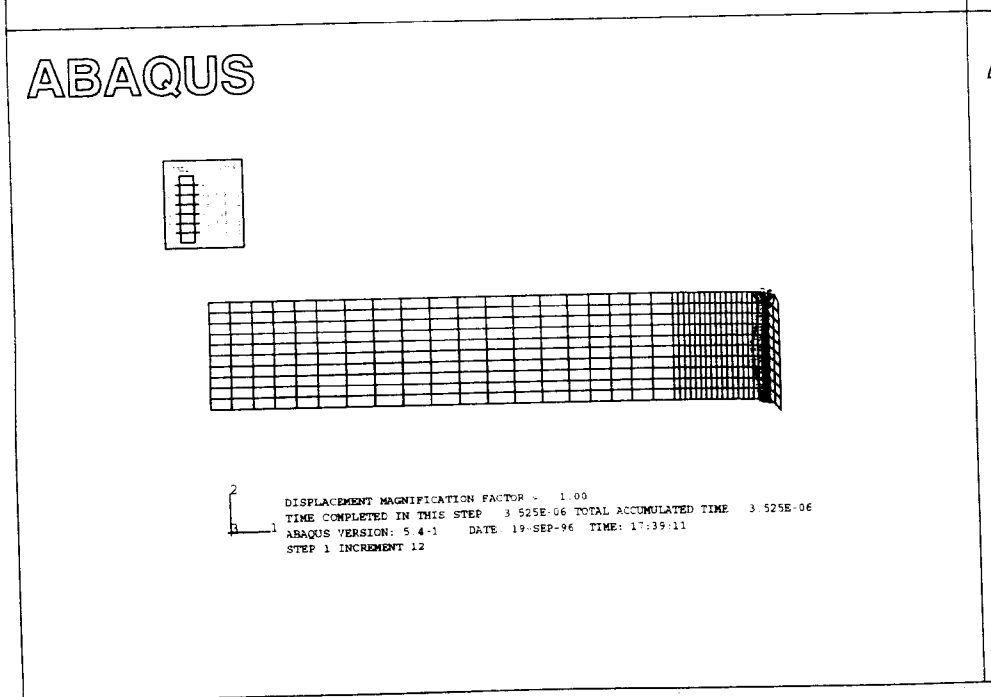
ABAQUS
DISPLACEMENT MAGNIFICATION FACTOR = 1.00
TIME COMPLETED IN THIS STEP 3.525E-06 TOTAL ACCUMULATED TIME 3.525E-06
ABAQUS VERSION: 5.4-1 DATE: 19-SEP-96 TIME: 17:39:11
STEP 1 INCREMENT 12

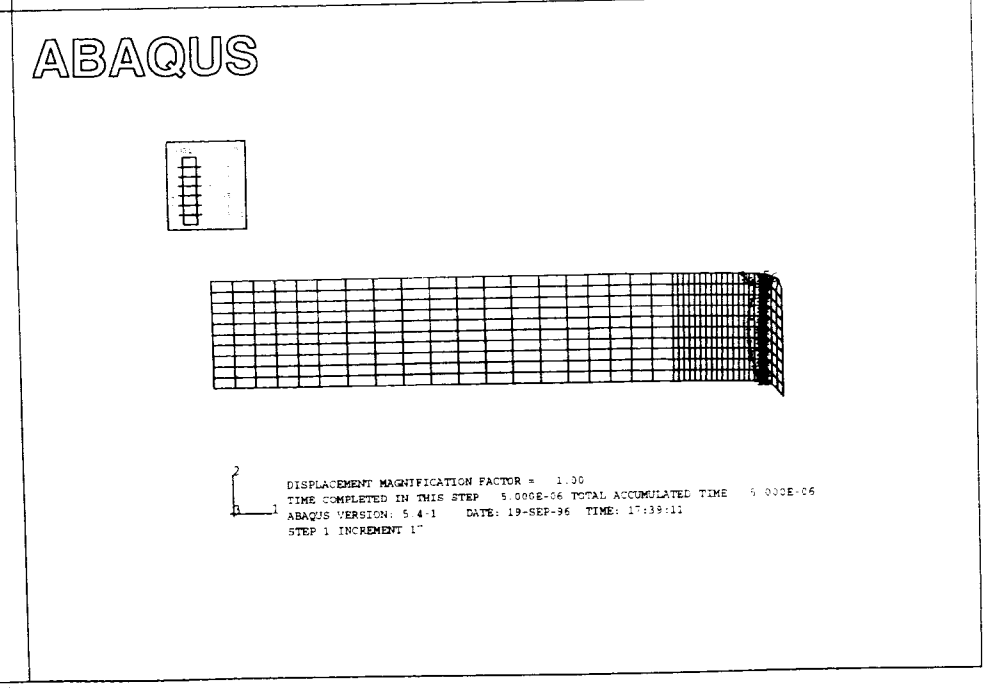
ABAQUS
DISPLACEMENT MAGNIFICATION FACTOR = 1.00
TIME COMPLETED IN THIS STEP 5.000E-06 TOTAL ACCUMULATED TIME 5.000E-06
ABAQUS VERSION: 5.4-1 DATE: 19-SEP-96 TIME: 17:39:11
STEP 1 INCREMENT 17

(a)

ABAQUS

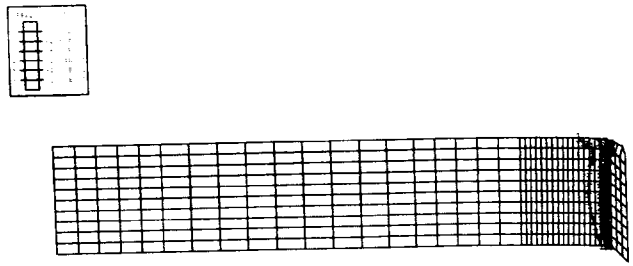

DISPLACEMENT MAGNIFICATION FACTOR = 1.00
TIME COMPLETED IN THIS STEP 1.561E-16 TOTAL ACCUMULATED TIME 5.561E-06
ABAQUS VERSION: 5.4-1 DATE: 19-SEP-96 TIME: 17:39:11
STEP 2 INCREMENT 10

ABAQUS

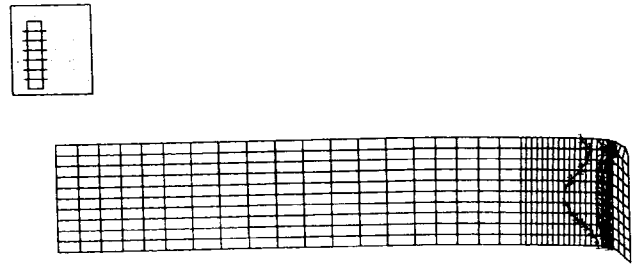

DISPLACEMENT MAGNIFICATION FACTOR = 1.00
TIME COMPLETED IN THIS STEP 4.423E-16 TOTAL ACCUMULATED TIME 5.429E-06
ABAQUS VERSION: 5.4-1 DATE: 19-SEP-96 TIME: 17:39:11
STEP 2 INCREMENT 30

ABAQUS

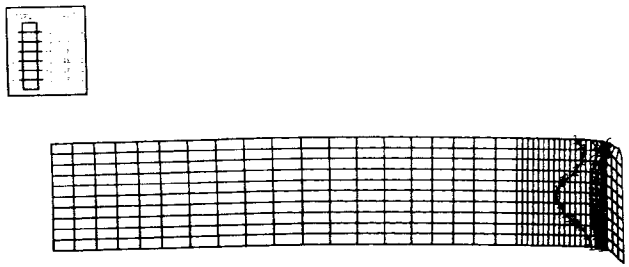

DISPLACEMENT MAGNIFICATION FACTOR = 1.00
TIME COMPLETED IN THIS STEP 1.200E-05 TOTAL ACCUMULATED TIME 1.700E-05
ABAQUS VERSION: 5.4-1 DATE: 19-SEP-96 TIME: 17:39:11
STEP 2 INCREMENT 70

ABAQUS

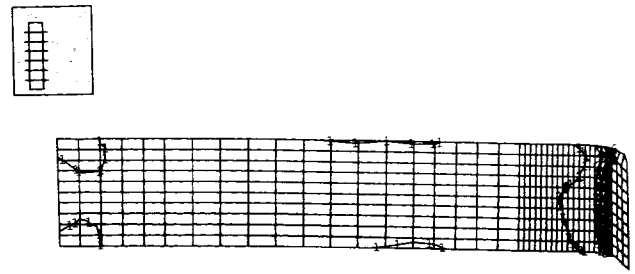

DISPLACEMENT MAGNIFICATION FACTOR = 1.00
TIME COMPLETED IN THIS STEP 1.000E-04 TOTAL ACCUMULATED TIME 1.050E-04
ABAQUS VERSION: 5.4-1 DATE: 19-SEP-96 TIME: 17:39:11
STEP 2 INCREMENT 141

(g)

ABAQUS

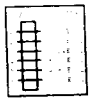

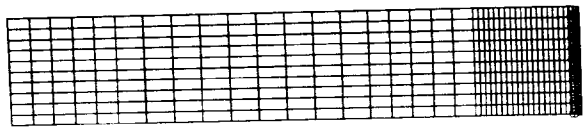

DISPLACEMENT MAGNIFICATION FACTOR = 1.00
TIME COMPLETED IN THIS STEP 2.000E-07 TOTAL ACCUMULATED TIME 2.000E-07
ABAQUS VERSION: 5.4-1 DATE: 19-SEP-96 TIME: 17:39:11
STEP 1 INCREMENT 2

ABAQUS

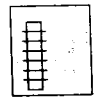

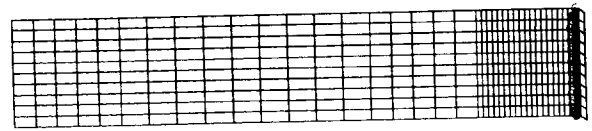

DISPLACEMENT MAGNIFICATION FACTOR = 1.00
TIME COMPLETED IN THIS STEP 1.824E-06 TOTAL ACCUMULATED TIME 1.824E-06
ABAQUS VERSION: 5.4-1 DATE: 19-SEP-96 TIME: 17:39:11
STEP 1 INCREMENT 9

ABAQUS

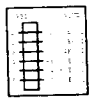

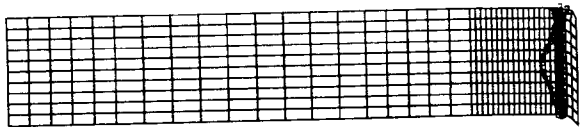

DISPLACEMENT MAGNIFICATION FACTOR = 1.00
TIME COMPLETED IN THIS STEP 3.525E-06 TOTAL ACCUMULATED TIME 3.525E-06
ABAQUS VERSION: 5.4-1 DATE: 19-SEP-96 TIME: 17:39:11
STEP 1 INCREMENT 12

ABAQUS

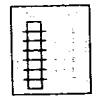

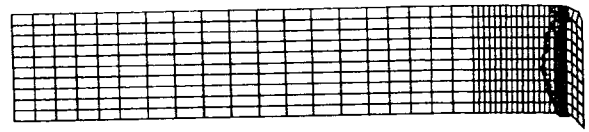

DISPLACEMENT MAGNIFICATION FACTOR = 1.00
TIME COMPLETED IN THIS STEP 5.000E-06 TOTAL ACCUMULATED TIME 5.000E-06
ABAQUS VERSION: 5.4-1 DATE: 19-SEP-96 TIME: 17:39:11
STEP 1 INCREMENT 17

(g)

ABAQUS

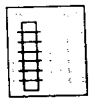

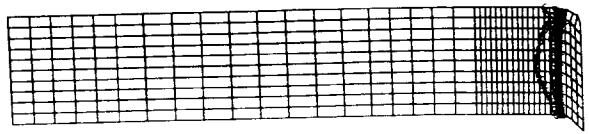

DISPLACEMENT MAGNIFICATION FACTOR = 1.00
TIME COMPLETED IN THIS STEP 1.561E-06 TOTAL ACCUMULATED TIME 6.561E-06
ABAQUS VERSION: 5.4-1 DATE: 19-SEP-96 TIME: 17:39:11
STEP 2 INCREMENT 10

ABAQUS

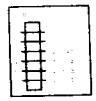

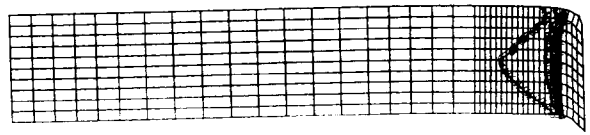

DISPLACEMENT MAGNIFICATION FACTOR = 1.00
TIME COMPLETED IN THIS STEP 4.429E-06 TOTAL ACCUMULATED TIME 9.429E-06
ABAQUS VERSION: 5.4-1 DATE: 19-SEP-96 TIME: 17:39:11
STEP 2 INCREMENT 20

ABAQUS

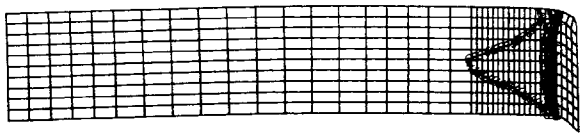

DISPLACEMENT MAGNIFICATION FACTOR = 1.00
TIME COMPLETED IN THIS STEP 1.200E-05 TOTAL ACCUMULATED TIME 1.700E-05
ABAQUS VERSION: 5.4-1 DATE: 19-SEP-96 TIME: 17:39:11
STEP 2 INCREMENT 70

ABAQUS

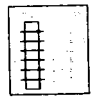

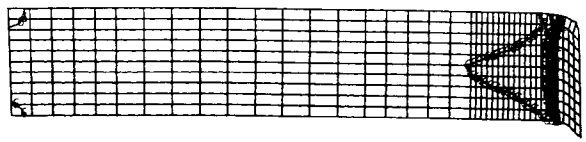

DISPLACEMENT MAGNIFICATION FACTOR = 1.00
TIME COMPLETED IN THIS STEP 1.000E-04 TOTAL ACCUMULATED TIME 1.050E-04
ABAQUS VERSION: 5.4-1 DATE: 19-SEP-96 TIME: 17:39:11
STEP 2 INCREMENT 141

(c)

ABAQUS

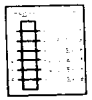

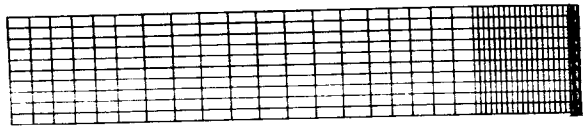

DISPLACEMENT MAGNIFICATION FACTOR = 1.00
TIME COMPLETED IN THIS STEP 2.002E-07 TOTAL ACCUMULATED TIME 2.002E-07
ABAQUS VERSION: 5.4-1 DATE: 19-SEP-96 TIME: 17:39:11
STEP 1 INCREMENT 2

ABAQUS

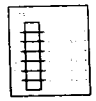

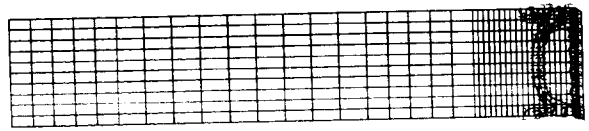

DISPLACEMENT MAGNIFICATION FACTOR = 1.00
TIME COMPLETED IN THIS STEP 1.324E-06 TOTAL ACCUMULATED TIME 1.324E-06
ABAQUS VERSION: 5.4-1 DATE: 19-SEP-96 TIME: 17:39:11
STEP 1 INCREMENT 8

ABAQUS

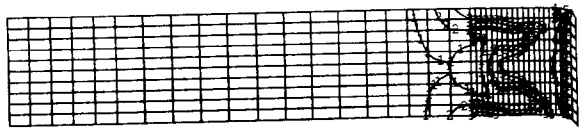

DISPLACEMENT MAGNIFICATION FACTOR = 1.00
TIME COMPLETED IN THIS STEP 3.525E-06 TOTAL ACCUMULATED TIME 3.525E-06
ABAQUS VERSION: 5.4-1 DATE: 19-SEP-96 TIME: 17:39:11
STEP 1 INCREMENT 12

ABAQUS

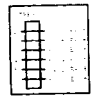

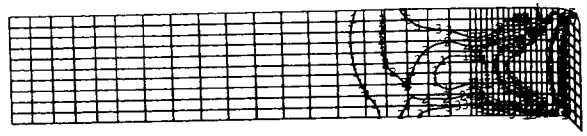

DISPLACEMENT MAGNIFICATION FACTOR = 1.00
TIME COMPLETED IN THIS STEP 5.000E-06 TOTAL ACCUMULATED TIME 5.000E-06
ABAQUS VERSION: 5.4-1 DATE: 19-SEP-96 TIME: 17:39:11
STEP 1 INCREMENT 17

(c)

ABAQUS

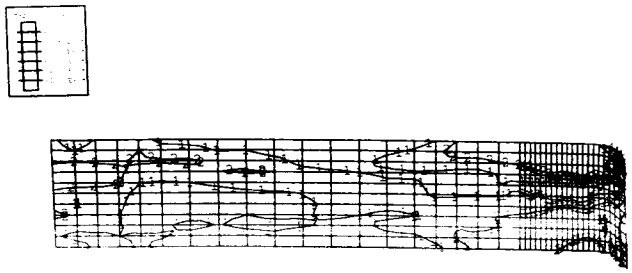

DISPLACEMENT MAGNIFICATION FACTOR = 1.00
TIME COMPLETED IN THIS STEP 1.000E-04 TOTAL ACCUMULATED TIME 1.050E-04
ABAQUS VERSION: 5.4-1 DATE: 19-SEP-96 TIME: 17:39:11
STEP 2 INCREMENT 141

ABAQUS

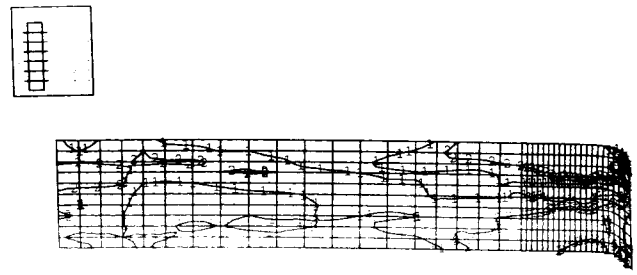

DISPLACEMENT MAGNIFICATION FACTOR = 1.00
TIME COMPLETED IN THIS STEP 1.000E-04 TOTAL ACCUMULATED TIME 1.050E-04
ABAQUS VERSION: 5.4-1 DATE: 19-SEP-96 TIME: 17:39:11
STEP 2 INCREMENT 141

ABAQUS

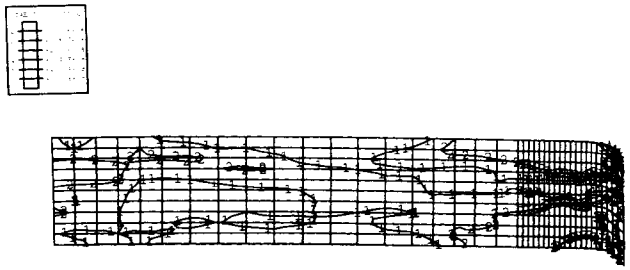

DISPLACEMENT MAGNIFICATION FACTOR = 1.00
TIME COMPLETED IN THIS STEP 1.000E-04 TOTAL ACCUMULATED TIME 1.050E-04
ABAQUS VERSION: 5.4-1 DATE: 19-SEP-96 TIME: 17:39:11
STEP 2 INCREMENT 141

ABAQUS

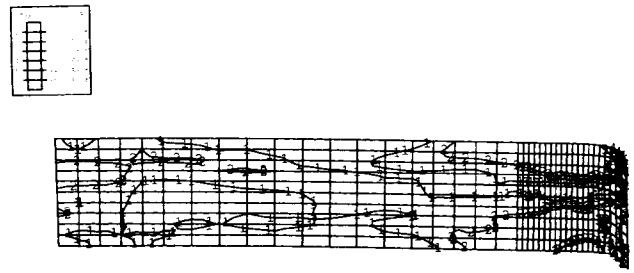

DISPLACEMENT MAGNIFICATION FACTOR = 1.00
TIME COMPLETED IN THIS STEP 1.000E-04 TOTAL ACCUMULATED TIME 1.050E-04
ABAQUS VERSION: 5.4-1 DATE: 19-SEP-96 TIME: 17:39:11
STEP 2 INCREMENT 141

(e)

ABAQUS

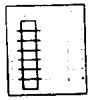

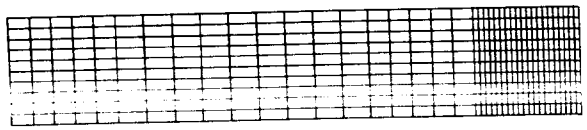

DISPLACEMENT MAGNIFICATION FACTOR = 1.00
TIME COMPLETED IN THIS STEP 0.000E+00 TOTAL ACCUMULATED TIME 0.000E+00
ABAQUS VERSION: 5.4-1 DATE: 19-SEP-96 TIME: 17:39:11
STEP 1 INCREMENT 2

ABAQUS

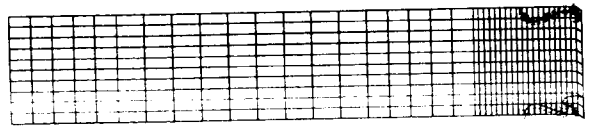

DISPLACEMENT MAGNIFICATION FACTOR = 1.00
TIME COMPLETED IN THIS STEP 1.000E-06 TOTAL ACCUMULATED TIME 1.000E-06
ABAQUS VERSION: 5.4-1 DATE: 19-SEP-96 TIME: 17:39:11
STEP 1 INCREMENT 6

ABAQUS

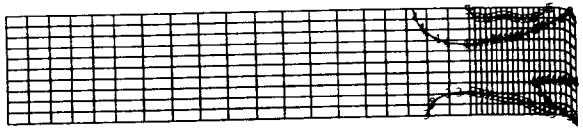

DISPLACEMENT MAGNIFICATION FACTOR = 1.00
TIME COMPLETED IN THIS STEP 3.525E-06 TOTAL ACCUMULATED TIME 3.525E-06
ABAQUS VERSION: 5.4-1 DATE: 19-SEP-96 TIME: 17:39:11
STEP 1 INCREMENT 12

ABAQUS

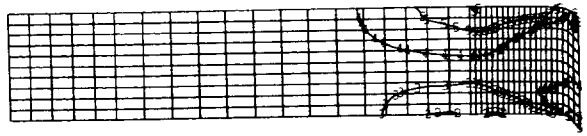

DISPLACEMENT MAGNIFICATION FACTOR = 1.00
TIME COMPLETED IN THIS STEP 5.000E-06 TOTAL ACCUMULATED TIME 5.000E-06
ABAQUS VERSION: 5.4-1 DATE: 19-SEP-96 TIME: 17:39:11
STEP 1 INCREMENT 17

(d)

ABAQUS

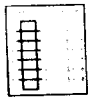

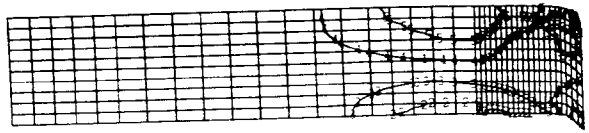

DISPLACEMENT MAGNIFICATION FACTOR = 1.00
TIME COMPLETED IN THIS STEP 1.200E-05 TOTAL ACCUMULATED TIME 1.700E-05
ABAQUS VERSION: 5.4-1 DATE: 19-SEP-96 TIME: 17:39:11
STEP 2 INCREMENT 70

ABAQUS

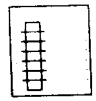

DISPLACEMENT MAGNIFICATION FACTOR = 1.00
TIME COMPLETED IN THIS STEP 4.429E-04 TOTAL ACCUMULATED TIME 4.429E-04
ABAQUS VERSION: 5.4-1 DATE: 19-SEP-96 TIME: 17:39:11
STEP 2 INCREMENT 80

ABAQUS

DISPLACEMENT MAGNIFICATION FACTOR = 1.00
TIME COMPLETED IN THIS STEP 1.200E-05 TOTAL ACCUMULATED TIME 1.700E-05
ABAQUS VERSION: 5.4-1 DATE: 19-SEP-96 TIME: 17:39:11
STEP 2 INCREMENT 70

ABAQUS

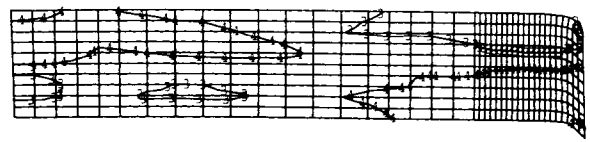

DISPLACEMENT MAGNIFICATION FACTOR = 1.00
TIME COMPLETED IN THIS STEP 1.000E-04 TOTAL ACCUMULATED TIME 1.050E-04
ABAQUS VERSION: 5.4-1 DATE: 19-SEP-96 TIME: 17:39:11
STEP 2 INCREMENT 141

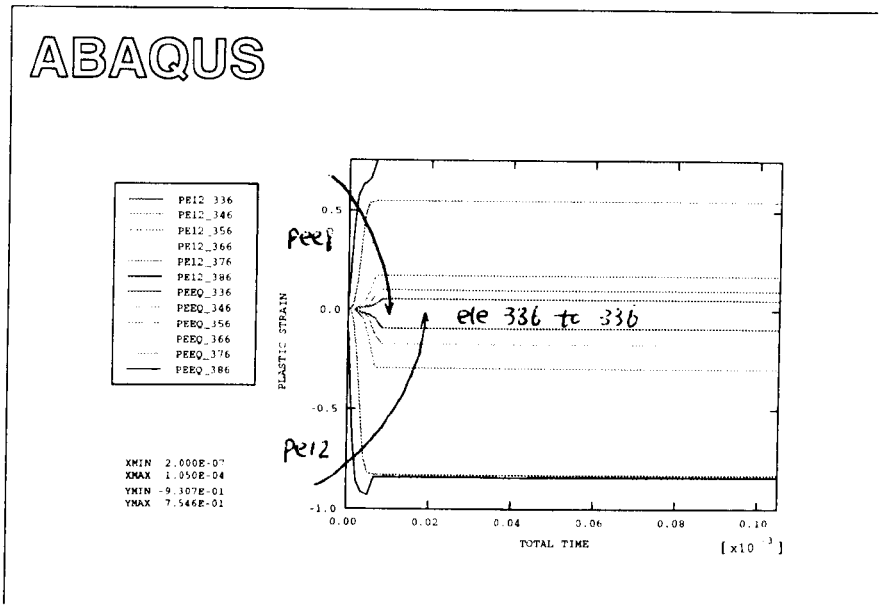

(a)

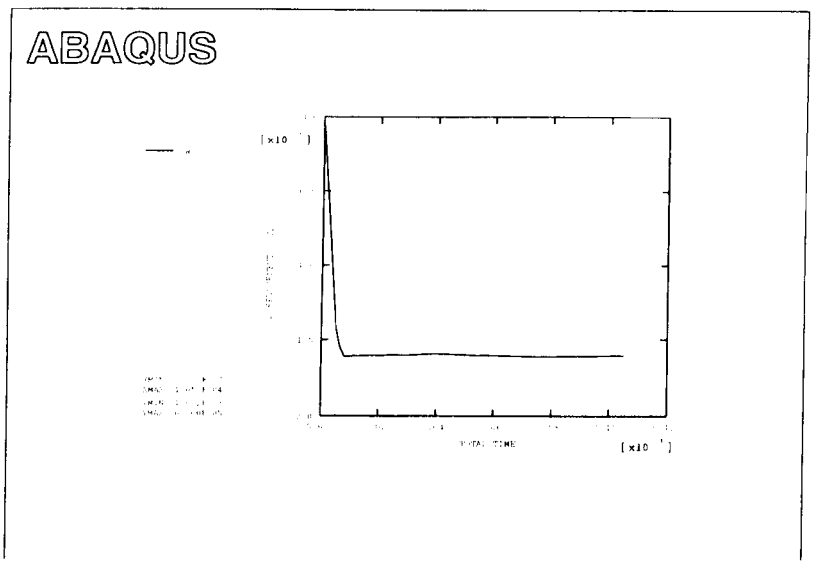

(b)

Fig.3.14 (a) Plastic shear and equivalent strain histories at different locations along the shear hinge length in simulation H1; (b) Relative displacement across the shear hinge length, e

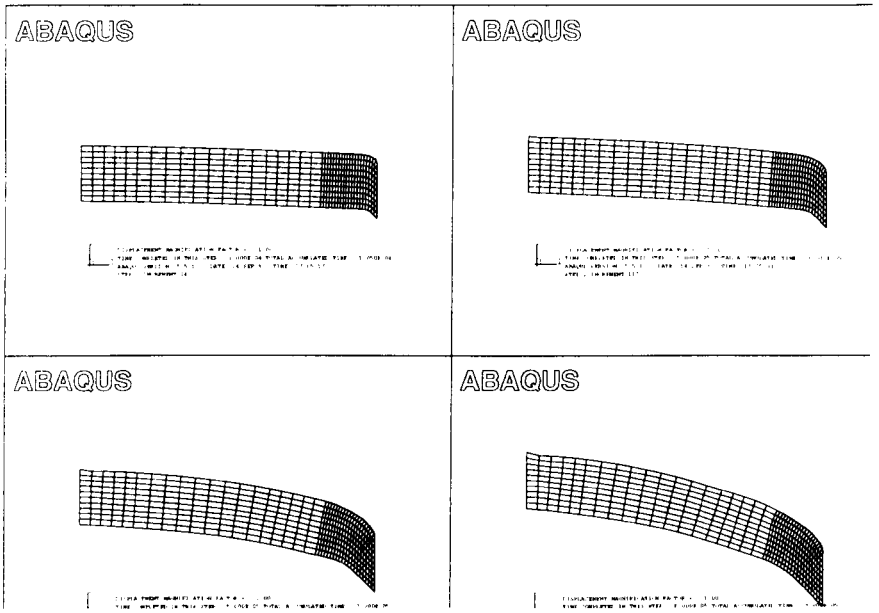

Fig.3.15 Deformation patterns of a beam with an imposed velocity of V=300m/s, (a) W=1.5mm and T=5μs(H1); (b) W=3.0mm and T=10μs(H9); (c) W=6.0mm and T=20μs(H10); (d) W=9.0mm and T=30μs(H13).

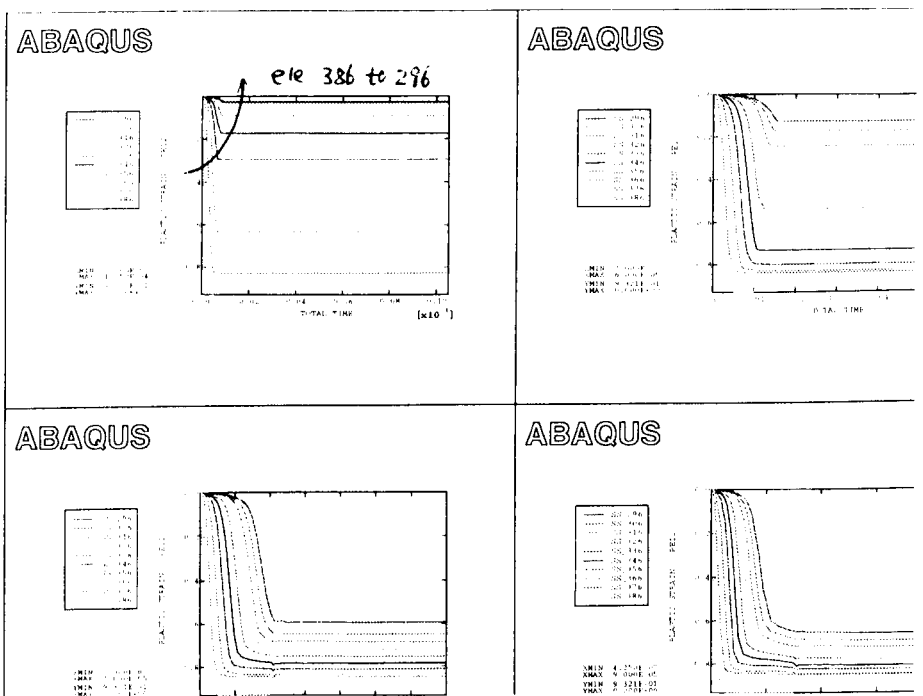

Fig. 3.16 Shear strain histories with an imposed velocity of V=300m/s, (a) γ_{max}=0.833(H1); (b) γ_{max}=0.844(H9); (c)γ_{max}=0.844(H10); (d) γ_{max}=0.850(H13).

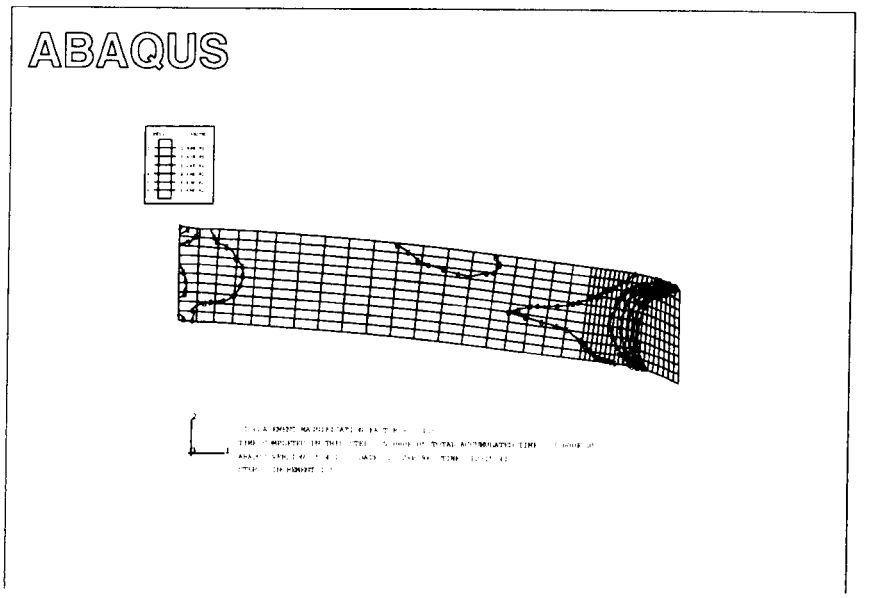

(a)

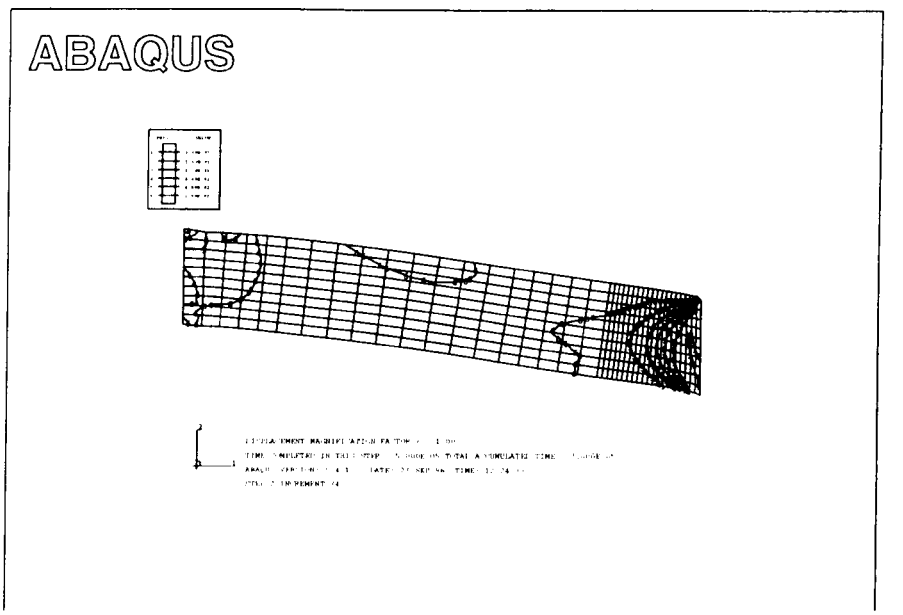

(b)

Fig.3.17 Shear strain distribution in a beam with W=3.0mm and T=20μs, (a) Without strain rate effects(H6); (b) With strain rate effects(H8)

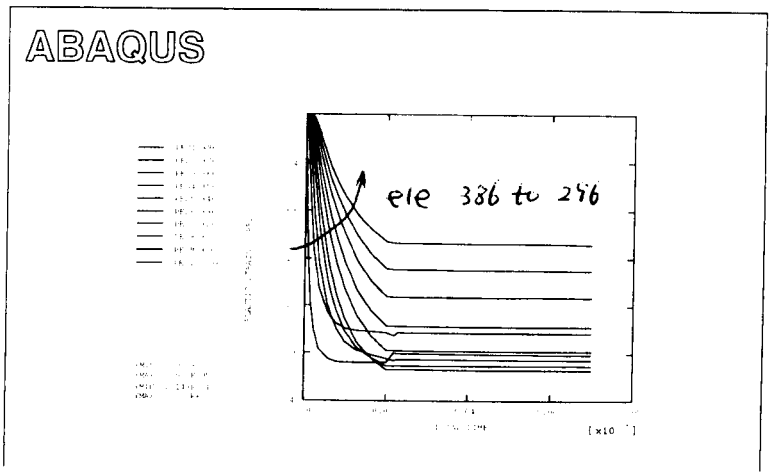

(a)

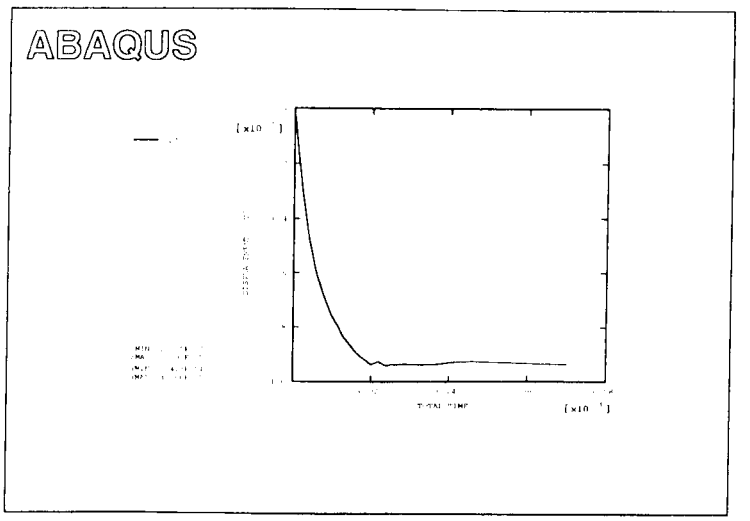

(b)

Fig.3.18 (a) Shear strain histories with strain rate effects(W=3.0mm and T=20μs in H8); (b) Relative displacement across the length of a shear hinge when retaining strain rate effects(H8).

4. SHEAR FAILURES IN A SHEAR HINGE IN A FULLY CLAMPED BEAM UNDER IMPULSIVE PRESSURE LOADING

4.1. Introduction

Localized shear, known as a shear hinge in transversely loaded structural elements, is an important deformation feature, which has been studied in Chapters 1-3. It has been shown in Chapter 1 that further developments of the localized shear deformation in a shear hinge might lead to either an isothermal fracture failure or an adiabatic shear banding failure, depending on the loading rate and intensity as well as the material properties.

Three failure modes have been observed by Menkes and Opat(1973) for a fully clamped beam under an impulsive pressure load. These three modes appear with an increase of the impulsive intensity. Jones(1976, 1989) has studied the failure mode transition using rigid, perfectly plastic analyses and elementary failure criteria outlined in Section 1.2. Dynamic plastic responses of an impulsively loaded beam have been studied by Jones and de Oliveira(1979) and Li and Jones(1995a). Wen(1996) predicted the tearing failure(Mode II) using a work-hardening model and an effective strain failure criterion. Failure maps of clamped beams and circular plates subjected to impulsive pressure loads are presented by Wen, et al.(1995a,b). These response and failure studies on an impulsively loaded beam and other similar studies on various structural elements are concentrated on isothermal response and failure without considering temperature softening effects, which is sometimes important, especially for high intensity loads. It has been shown that a failure transition between an isothermal fracture failure and an adiabatic shear banding failure may occur with continuously increasing loading rates and intensities. Thus, if the impulsive intensity in Menkes and Opat's problem is sufficiently high, a fourth response and failure mode, adiabatic shearing, is expected to appear, which has a different failure mechanism when comparing with Modes II and III failures. A failure transition between isothermal fracture and adiabatic shear banding has been observed

by Kalthoff, et al.(1987, 1990) for a pre-cracked steel plate subjected to projectile impact. Wang, et al.(1994) treated this problem as an interaction between a Mode II crack and an adiabatic shear band, and predicted failure transitions in Ti-6Al-4V specimen. The similar failure transition in a crack-free structural element is also possible when subjected to a sufficient high loading intensity. This view-point has been proposed by Wang and Jones(1996), where the possibility of adiabatic shearing in an impulsively loaded beam was studied briefly.

The occurrence of adiabatic shearing in Menkes and Opat's problem will be studied in this Chapter by combining the rigid, perfectly plastic analysis, the knowledge of shear hinge obtained in Chapters 2 and 3, and the maximum shear stress criterion introduced in Section 1.4. A description of failure mechanism transition from the isothermal shear failure(Mode III failure) to an adiabatic shear banding failure is presented. It transpires that the method developed here may be applied to other transversely loaded structural elements.

4.2. Description of the Problem

The original problem in Menkes and Opat(1973) is shown in Fig.4.1(a), where a sheet explosive is applied to the fully clamped beams over a neoprene buffer. This problem may be simplified as a fully clamped beam with a uniformly distributed initial velocity, as shown in Fig.4.1(b).

The initial velocity of the beam is determined by

$$V_0=\frac{I}{\rho H} \tag{4-1}$$

where I is the impulsive intensity of the explosion(impulse per unit area), ρ is the density of the beam material, 6061-T6 aluminium alloy, and H is the beam thickness.

The investigated beams have spans of L=203.2mm and 101.6mm, with a rectangular cross-section B=25.4mm width by three different depths, H=4.74mm, 6.35mm and 9.52mm, respectively.

The static isothermal constitutive equation is described by a linear strain hardening relationship, as shown in ABAQUS(1994b)

$$\sigma_e = \sigma_0 + E_h \varepsilon_e \tag{4-2}$$

where σ_0 and E_h are the yield stress and strain hardening modulus, given in Table 4.1, respectively, σ_e and ε_e are equivalent stress and strain, respectively. The strain rate effect is included by the Cowper-Symonds relationship(Wen(1996), ABAQUS(1994b))

$$\frac{\sigma_{de}}{\sigma_e} = 1 + \left(\frac{\dot{\varepsilon}_e}{D}\right)^{\frac{1}{p}} \tag{4-3}$$

where σ_{de} is the dynamic equivalent stress, and $\dot{\varepsilon}_e$ is the equivalent strain rate. D=6500.0s^{-1} and p=4.0.

The influence of temperature on the constitutive equation is included by the following factor

$$1 - \left(\frac{T - T_r}{T_m - T_r}\right)^q \tag{4-4}$$

where T_r=20°C is the room temperature, T_m=652°C is the melting temperature given by Boyer and Gall(1985) for 6061-T6 material. There is no available data on q for 6061-T6 aluminium alloy. However, Johnson and Cook(1983) conducted tests on 2024-T351 and 7039 aluminium alloy, and found q=1.0 for both materials. Thus, q=1.0 is used here for 6061-T6 aluminium alloy. One may use more realistic values when experimental data become available. Other material properties are described in Table 4.1.

Table 4.1 Material Properties of 6061-T6 Aluminium Alloy

ρ(kg/m^3)	C_v(J/kgK)	K_v(W/mK)	ν	E(GPa)	σ_0(MPa)	E_h(MPa)	Hardness(HB)
2686	937.4	167.3	0.32	72.4	286.8	542.6	95

Note: C_v and K_v are from Bai and Dodd(1992); Hardness is from Boyer and Gall(1985); others are from Table 3.1 in Chapter 3.

4.3. Modelling the Problem

4.3.1. Isothermal and Adiabatic Conditions

A deformation process may be idealised as either isothermal or adiabatic process depending on the physical properties of the material and loading conditions. It is the case that the deformation process is adiabatic for a well-developed shear banding. But, before the shear stress reaches a maximum value, it might be necessary to consider heat conduction aspects in order to determine the temperature from the consumed inelastic work. The general equations to describe momentum and energy balances for a simple shear deformation may be expressed by(pp.136 in Bai and Dodd(1992))

$$\rho\frac{\partial^2\gamma}{\partial t^2}=\frac{\partial^2\tau}{\partial x^2} \qquad \text{and} \quad \beta\tau\frac{\partial\gamma}{\partial t}=\rho C_v\frac{\partial T}{\partial t}-K_v\frac{\partial^2 T}{\partial x^2}, \tag{4-5a,b}$$

where, K_v is the thermal conductivity of the substance, and τ is determined by eq.(1-10). The dimensionless forms of eqs.(4-5a,b) are

$$a\frac{\partial\dot{\gamma}_d}{\partial t_d}=\frac{\partial^2\tau_d}{\partial x_d^2} \qquad \text{and} \quad \tau_d\dot{\gamma}_d=b\frac{\partial T_d}{\partial t_d}-d\frac{\partial^2 T_d}{\partial x_d^2} \tag{4-6a,b}$$

if the following dimensionless quantities are defined

$$T_d=\frac{T}{T_c},\ t_d=\frac{t}{t_c},\ x_d=\frac{x}{x_c},\ \tau_d=\frac{\tau}{\tau_c} \quad \text{and} \quad \dot{\gamma}_d=\frac{\dot{\gamma}}{\dot{\gamma}_c}, \tag{4-7a-e}$$

where T_c is the characteristic temperature, $\dot{\gamma}_c$ is a characteristic shear strain rate, τ_c is the characteristic shear stress, t_c and x_c are the characteristic response time and length which depend on the phenomenon of interest. The dimensionless coefficients in eqs.(4-6a,b) are

$$a=\frac{\rho\dot{\gamma}_c x_c^2}{\tau_c t_c},\quad b=\frac{\rho C_v T_c}{\beta\tau_c\dot{\gamma}_c t_c} \quad \text{and} \quad d=\frac{K_v T_c}{\beta\tau_c\dot{\gamma}_c x_c^2}. \tag{4-8a-c}$$

Similar equations have been obtained by Bai(1989) to study adiabatic shear bands. In a solid mechanics problem, it is necessary to determine the significance of both inertia and temperature effects. For a simple shear motion described by eqs.(4-6) to (4-8), the following situations in Table 4.2 may exist.

Table 4.2 Various Processes of a Simple Shear Motion

	I(isothermal)*	H(heat conduction)	A(adiabatic)
S(static)	a<<1, d>>1(or b>>1)	a<<1, b~d~1	a<<1, d<<1, d<<b
D(dynamic)	a~1, d>>1(or b>>1)	a~1, b~d~1	a~1, d<<1, d<<b

*: According to eq.(4-6b), either d>>1 or b>>1 satisfies the isothermal condition. However, b≈5.5~O(1) for the current test material in Chapter 5 when $\gamma_c=\dot{\gamma}_c t_c \sim 1$. Thus, d>>1 will be employed in Section 6.2.3 instead of b>>1.

Three typical cases are discussed in Bai and Dodd(1990)(pp.165), i.e., (1) isothermal case for a~d~1 and b~Pr, (2) quasi-static case for a~1/Pr and b~d~1, and (3) adiabatic case for a~b~1 and d~1/Pr, which are three special cases (i.e., D-I, S-H and D-A) in Table 4.2, where Pr is the effective Prandtl number defined by(Bai and Dodd(1990)) $Pr=C_v\tau_c/(K_v\dot{\gamma}_c)$ to represent the relative importance of the two dissipative mechanisms, i.e., rate dependent diffusion and thermal diffusion, in adiabatic shear band deformation, which is normally much larger than unity for metals within our strain rate range of interest(i.e., below $10^6 s^{-1}$). Wright and Ockendon(1996) used a scaling law and perturbation method to find a finite wavelength with a maximum growth rate that is claimed as the characteristic length of a shear band. In the current evaluation, analysis is focused on various stable mechanical-thermal processes of a simple shear motion before material thermal instability occurs when the effect of material thermal softness competes with other hardening effects on the shear stress.

According to Table 4.2, explicit strain rate conditions for isothermal and adiabatic process are given by

$$\begin{aligned} &\dot{\gamma}_c \ll \dot{\gamma}_{c1} \quad \text{for isothermal condition} \\ &t_c \ll t_{cd} \quad \text{and} \quad \dot{\gamma}_c \gg \dot{\gamma}_{c1} \quad \text{for adiabatic condition} \end{aligned} \tag{4-9a,b}$$

in which, $t_{cd}=\rho C_v x_c^2/K_v$ and $\dot{\gamma}_{c1}=K_v T_c/(\beta\tau_c x_c^2)$.

In other cases when heat conduction is significant, the temperature increase

may be expressed by

$$dT=\frac{\alpha\beta}{\rho C_v}\tau d\gamma$$
$$\text{with} \quad \alpha=1+d\frac{(\partial^2 T_d/\partial x_d^2)}{\dot{w}_d}, \qquad (4\text{-}10a,b)$$

where, $w_d=\tau\gamma/\tau_c\dot{\gamma}_c$ is the dimensionless strain energy dissipation rate. The value of parameter α depends on the particular problem. It is valuable to do further investigations to find an approximate expression for parameter α for different class of mechanical-thermal coupling problems. Particularly, within the current interesting range of $d<<1$, eq.(4-10b) gives $\alpha=1$, which, according to eq.(4-10a), leads to adiabatic expression of temperature rise in eq.(1-12).

4.3.2. Analytical Model

The dynamic plastic response of the beam will be predicted by using rigid, perfectly plastic analysis. This analysis is valid for predicting the global responses, such as bending rotation across a bending hinge and transverse shear displacement across a shear hinge when the actual size of these plastic hinges has no significant influence on the global response of structural elements. The existence of an interface between the shear hinge and outside rigid medium ensures the use of rigid, perfectly plastic analysis to give a valid prediction on the structural response outside shear hinge even when thermal softening becomes important within a shear hinge.

According to the results in Li and Jones(1995a), the shear response of a fully clamped beam in Menkes and Opat(1973) with $v=Q_0L/2M_0>3$ is shown in Fig.4.2. The relative transverse shear displacement across a shear hinge and the transverse shear response time are

$$W_1=V_0t-\frac{2\sigma_0}{9\rho H}t^2 \quad \text{and} \quad t_1=\frac{9\rho HV_0}{4\sigma_0}, \qquad (4\text{-}11a,b)$$

respectively. The maximum transverse shear displacement at $t=t_1$ is

$$W_{1f}=\frac{9\rho HV_0^2}{8\sigma_0} \tag{4-12}$$

The maximum engineering shear strain and the average shear strain rate within the shear hinge are

$$\gamma_1=\frac{W_{1f}}{2e}\approx 1.3\frac{\rho}{\sigma_0}V_0^2 \quad \text{and} \quad \dot{\gamma}_{av}=\frac{\gamma_1}{t_1}\approx 0.58\frac{V_0}{H}, \tag{4-13a,b}$$

in which, e=0.433H is given by eq.(3-9). It should be noted that the shear hinge length might depend on the propagation of transverse shear wave when the characteristic impact velocity is larger than the plastic shear wave speed, c_p=260m/s, as shown in Section 3.3. The characteristic velocity in the present case may be represented by the average transverse shear velocity, $V_0/2$. Thus, an approximate limitation for the valid application of the current analysis is $V_0<2c_p\approx$520m/s. Beyond this impulsive velocity, wave effects need to be considered to describe the transverse shear propagation, which is outside our interest.

Normally, strain rate effects are considered in the maximum shear stress criterion, eq.(1-11), by using the average strain rate to represent a constant strain rate process, which neglects the influence of strain rate change on the criterion, but includes the average strain rate hardening effects on flow stress(pp.126 in Bai and Dodd(1992), pp459 in Meyers(1994) and ppC8-35 of Klepaczko(1994)). Thus, eqs. (1-11) and (4-10) lead to

$$\frac{\partial\tau}{\partial\gamma}+\frac{\partial\tau}{\partial T}\frac{\alpha\beta\tau}{\rho C_v}=0 \tag{4-14}$$

for a simple shear constitutive equation, in which τ has the following form in the present case

$$\tau=(\frac{\sigma_0}{\sqrt{3}}+\frac{E_h}{3}\gamma)[1+(\frac{\dot{\gamma}}{\sqrt{3}D})^{\frac{1}{p}}][1-\frac{T-T_r}{T_m-T_r}]. \tag{4-15}$$

when $\sigma_e=\sqrt{3}\tau$ and $\varepsilon_e=\gamma/\sqrt{3}$ are substituted into eqs. (4-2) to (4-4). Eqs.(4-14) and (4-15) lead to

$$3\alpha\beta(\frac{\sigma_0}{\sqrt{3}}+\frac{E_h\gamma}{3})^2[1+(\frac{\dot{\gamma}}{\sqrt{3}D})^{\frac{1}{p}}]=\rho C_v E_h(T_m-T_r). \tag{4-16}$$

In order to find the minimum impulsive velocity, $\gamma=\gamma_1$ and $\dot{\gamma}=\dot{\gamma}_{av}$ in eqs.(4-13a,b) are substituted into eq.(4-16) to give

$$3\alpha\beta[0.577\sigma_0+\frac{0.433\rho E_h V_0^2}{\sigma_0}]^2[1+(\frac{0.335V_0}{DH})^{\frac{1}{p}}]=\rho C_v E_h(T_m-T_r), \tag{4-17}$$

which will be used to determine the critical impulsive velocity for the initiation of adiabatic shearing failure. In eq.(4-17), α should be determined according to discussion in Section 1.4. According to Table 1.1 or eq.(4-9b), the adiabatic condition in the present case is $d<<1$, or $t_c/t_{cd}<<1$, where $t_c=t_1=\gamma_c/\dot{\gamma}_c$ is the characteristic time of the transverse shear response in a shear hinge in the present problem determined by eq.(4-11b). While the characteristic time of heat conduction is

$$t_{cd}=\frac{\beta\tau_c\gamma_c x_c^2}{K_v T_c}=\frac{0.563\beta\rho V_0^2 H^2}{T_r K_v} \tag{4-18}$$

when $\gamma_c=W_{1f}/(2e)$, $\tau_c=\tau_0=\sigma_0/\sqrt{3}$ and $x_c=2e$ are used, where W_{1f} is given by eq.(4-12). Thus, the time ratio of t_c/t_{cd} is

$$\frac{t_c}{t_{cd}}=4.44\frac{T_r K_v}{\sigma_0 H V_0}, \tag{4-19}$$

when $\beta=0.9$ is used. It gives $t_c/t_{cd}\approx 1.7\times10^{-3}$ and 5.66×10^{-4} for $V_0=100$ and 300m/s, respectively, with material parameters given in Table 4.1, which are much smaller than the unit. Therefore, it is reasonable to assume an adiabatic condition during the transverse shear response process, i.e., $\alpha=1.0$ in eq.(4-17).

4.4. Results

4.4.1. Temperature Rise

According to eq.(4-10) with $\alpha=1.0$ and $\beta=0.9$, and eq.(4-15) with $\gamma=\gamma_1$ and $\dot{\gamma}=\dot{\gamma}_{av}$ in eqs.(4-13a,b), the temperature rise at the end of transverse shear response

phase is

$$T=T_m-\eta(T_m-T_r) \tag{4-20}$$

where

$$\eta=\exp[-\frac{\beta(\frac{\sigma_0\gamma_1}{\sqrt{3}}+\frac{E_h\gamma_1^2}{6})(1+(\frac{\dot{\gamma}_{av}}{\sqrt{3}D})^{\frac{1}{p}})}{\rho C_v(T_m-T_r)}]. \tag{4-21}$$

The temperature at the end of transverse shear response phase varies with the impulsive velocity, which is presented in Fig.4.3 for beams having three different thicknesses. It appears that the temperature may rise from room temperature to nearly 400°C when the impulsive velocity is 340m/s. Heat conduction may be important for low impulsive velocities, and need to be considered instead of the adiabatic condition for predicting the temperature rise. However, it has been shown in Section 4.3 that the adiabatic assumption is satisfied for the impulsive velocity range of V_0=100~300m/s. Thus, the predictions in Fig.4.3 give a realistic estimate of temperature rise within a shear hinge of the studied impulsively loaded beam.

It has been shown that Mode III shear failure occurs in the impulsive velocity range of 250-320m/s for three different thickness beams(Menkes and Opat(1973)). The temperature rise within this velocity range is between 150 and 250°C according to Fig.4.3. It is a common knowledge that material rupture strain increases significantly with temperature. According to the predictions given by Jones(1976), the shear rupture strain for Mode III failure is

$$\gamma_c=\frac{W_s^c}{2e}=1.153k \tag{4-22}$$

using eq.(1-5) for W_s^c and eq.(3-9) for e. Jones(1976) found k=1 gives a fairly good prediction for the critical impulse to initiate Mode III failure. Thus, the critical shear strain responsible for Mode III failure is γ_c=1.153, which is much higher than the value obtained by static tensile or shear test at room temperature. For example, Wen(1996) used ε_c=0.17 in his calculation for the tearing failure of 6061-T6 beam, which corresponds to γ_c=0.3 if von-Mises equivalent strain controls material failure.

Nevertheless, γ_c=1.153 becomes realistic at high temperature. It will be shown in Chapter 5 that the rupture strain in a tensile test at 500°C may go up to ε_c=2.14 for En24 steel while its static value is 0.65, approximately. Thus, the parameter k in an elementary failure criterion contains the influence of temperature rise on the failure initiation when it is significant, which has not been realised, previously.

The temperature rise in a shear hinge also leads to a decrease of the thermal conductivity(Bai and Dodd(1992)), which makes an adiabatic assumption more reasonable. On the other hand, the specific heat increases with temperature, as shown in FigB.5 of Bai and Dodd(1992) for 6061-T6 aluminium alloy, while the specific heat given in Table 4.1 is at room temperature. When the impulsive velocity is 300m/s, the temperature rise is about 200°C from Fig.4.3. The average specific heat of 6061-T6 from room temperature to 200°C is C_v≈1176J/kgK, approximately, according to Fig.B.5 of Bai and Dodd(1992), which will be used in predicting adiabatic shearing initiation in the following section.

4.4.2. Critical Velocities

The minimum impulsive velocity for a given beam thickness is determined by eq.(4-17). According to the discussion in Section 4.3 and 4.4.1, we have α=1.0, β=0.9 and C_v=1176J/kg.K. Other parameters are given in Table 4.1 and eqs.(4-3) and (4-4). Substituting all these parameters into eq.(4-17) leads to

$$(1+1.33\times10^{-5}V_0^2)^2(1+0.476\frac{V_0^{0.25}}{H^{0.25}})=14.65 \tag{4-23}$$

which determines the relationship between $V_0=V_{cs}$(m/s) and H(mm).

Jones(1976, 1989) suggested the following formula to predict a Mode III failure

$$V_{c3}=\frac{2}{3}(2k\frac{\sigma_0}{\rho})^{\frac{1}{2}} \tag{4-24}$$

for a fully clamped impulsively loaded beam with a rectangular cross-section, where a good agreement was reached when k=1.

Predictions on the minimum critical impulsive velocity to initiate adiabatic

shearing are presented in Fig.4.4. It is shown that the adiabatic shearing failure occurs at velocities higher than those for a Mode III failure. When the impulsive velocity $V_0>V_{cs}$, adiabatic shearing occurs before $t=t_1$. However, according to the discussion in Section 4.3.2, there is a limitation, $V_0<V_{sw}=520$m/s, for the validity of the analysis. Beyond this velocity, shear wave effects are significant for estimating localized shear deformations. These observations and previous studies(Menkes and Opat(1973), Jones(1976, 1989)), allow beam responses and failures under intensive dynamic transverse pressure loadings to be classified into the following modes,

(a) Large plastic deflection response(Mode I);

(b)Tearing failure from the combination of bending, shearing and membrane responses(Mode II);

(c) Shear failure by localised transverse shear response in a shear hinge(Mode III);

(d) Adiabatic shearing failure by localised transverse shear response in a shear hinge;

(e) Response and failure introduced by the propagation of a plastic shear wave.

These response and failure modes appear with increase of the imposed impulsive velocity. The first three modes have been confirmed by experimental results given by Menkes and Opat(1973), and Ross, et al.(1977). However, further systematic experiments are required to examined modes (d) and (e).

4.4.3. Adiabatic Shearing in Short Beams, Circular Plates and Cylindrical Shells

Similar analyses are possible for other structural elements under transverse impulsive pressure loadings. Rigid, perfectly plastic analyses have been given by Li and Jones(1994, 1995a,b) for the dynamic plastic response of a beam, circular plate and cylindrical shell under general blast pressure loading. A transverse shear hinge may develop for sufficiently large loading intensities, which depend on the parameter ν, as shown in Section 1.2. The parameter ν depends on the ratio of length and thickness for a solid cross-section structural element and determines the transverse shear response model. The beam problem of Menkes and Opat(1973) with $\nu>3$ has been studied in Sections 4.4.1 and 4.4.2. Here, the shear-only responses of a fully supported beam, circular plate and cylindrical shell corresponding to small length to thickness ratio will be studied.

(a) Beam($\nu<2$)

The maximum engineering shear strain and average shear strain rate within a shear hinge of fully clamped beam are

$$\gamma_1 \approx \frac{\rho}{\sigma_0}\frac{L}{H}V_0^2 \quad \text{and} \quad \dot{\gamma}_{av}=0.58\frac{V_0}{H} \tag{4-25a,b}$$

according to eq.(3-9) and Li and Jones(1995a). The critical velocity for the initiation of adiabatic shearing is

$$[1+0.476(\frac{V_0}{H})^{0.25}][1+0.0000102(\frac{L}{H})V_0^2]^2=14.65 \tag{4-26}$$

by using eqs.(4-25a,b) and (4-16).

(b) Circular Plate(ν<3)

A similar procedure gives

$$\gamma_1=0.633\frac{\rho}{\sigma_0}\frac{R}{H}V_0^2 \quad \text{and} \quad \dot{\gamma}_{av}=0.731\frac{V_0}{H} \tag{4-27a,b}$$

according to eq.(3-11) and Li and Jones(1994). The critical condition is

$$[1+0.505(\frac{V_0}{H})^{0.25}][1+0.00000646(\frac{R}{H})V_0^2]^2=14.65. \tag{4-28}$$

(c) Cylindrical Shell(ν<2)

Eq.(3-20) and the results in Li and Jones(1995b) predict

$$\gamma_1=\frac{1.415}{1+1.732L/r}\frac{\rho}{\sigma_0}\frac{L}{H}V_0^2 \quad \text{and} \quad \dot{\gamma}_{av}=0.817\frac{V_0}{H}, \tag{4-29a,b}$$

and the critical condition is

$$[1+0.52(\frac{V_0}{H})^{0.25}][1+\frac{0.0000144}{1+1.732L/r}(\frac{L}{H})V_0^2]^2=14.65. \tag{4-30}$$

In the above equations, the units of V_0 and H are m/s and mm, respectively. Fig.4.5 illustrates the relationship between the critical velocity for adiabatic shearing and structural thickness for a length(diameter)-thickness ratio of 1.7. It appears that a beam is the easiest one to be sheared adiabatically among the studied three structural elements, then the circular plate and cylindrical shell, provided their

length(diameter)/thickness ratios are the same. When the shell becomes slender, i.e., L/r increases, adiabatic shearing becomes more difficult. The extreme situation is L/r<<1, corresponding to a fully clamped ring, in which adiabatic shearing is easier than in a fully clamped beam, according to Fig.4.5.

4.5. Fully Clamped Beams Under Projectile Impact

The analytical procedure proposed in Sections 4.2 to 4.4 for an impulsive pressure loading may be used to predict the initiation of adiabatic shearing in a structural element under projectile impact. In the present case, a fully clamped beam subjected to a blunt projectile impact at the mid-span, as shown in Fig.4.6, will be studied.

According to the rigid, plastic results of Liu and Jones(1988), the transverse shear displacement across a shear hinge at the periphery of the projectile impact is

$$W_1=\frac{3GLgV_0^2}{8M_0\nu(\nu+3g)} \tag{4-31}$$

for a beam with $\nu>3$, in which, G is the projectile mass, V_0 is the impact velocity of the projectile; $g=\rho BHL/G$ and ν is defined as before. The shear response time is

$$t_1=\frac{3GLgV_0}{4M_0\nu(\nu+3g)}. \tag{4-32}$$

Thus, the maximum transverse engineering shear strain and the average shear strain rate are

$$\gamma_1=\frac{9}{8\delta}\frac{\rho}{\sigma_0}\frac{V_0^2}{1+2.6\frac{g}{L/H}} \quad \text{and} \quad \dot{\gamma}_{av}=\frac{V_0}{2\delta H}, \tag{4-33a,b}$$

when the width of shear hinge is given by

$$\Delta=\delta H, \tag{4-34}$$

where, $\delta=0.866$ according to eq.(3-9). However, in a practical projectile impact problem, δ may depends on both projectile and beam material properties, as well as

the impact velocity range. Some evidence has been shown by Jones, Kim and Li(1997) in an analysis of plate failure under projectile impact. As a qualitative analysis, δ=0.866 is used here. However, it is possible to use a more realistic value of δ in a particular problem if experimental data are available.

By using the material properties of 6061-T6 aluminium alloy, given in Table 4.1 and same simplifications of α=1, β=0.9 and C_v=1176J/kgK, the average specific heat with in 20-200°C, as discussed in Section 4.4.1, the minimum impact velocity for initiating adiabatic shearing is determined by

$$[1+1.33x10^{-5}\frac{V_0^2}{1+2.6\frac{g}{L/H}}]^2[1+0.476(\frac{V_0}{H})^{0.25}]=14.65. \qquad (4\text{-}35)$$

While, the minimum impact velocity for Mode III failure may be determined by the elementary failure criterion, eq.(1-6) proposed by Jones(1976, 1989), which leads to

$$V_0=\sqrt{\frac{8\sigma_0 k}{9\rho}(1+2.6\frac{g}{L/H})}\approx 308.1\sqrt{1+2.6\frac{g}{L/H}}\ . \qquad (4\text{-}36)$$

when k=1.0 is assumed.

Generally speaking, beam failures for small value of g(large projectile mass) and low impact velocity are mixed modes, in which both tensile, shear and bending deformations have contributions for beam failure(Jones(1989), Liu and Jones(1987,1988)). In the present case, we concentrate on the case of a large value of g(small projectile mass) and medium impact velocity. Figs.4.7(a,b) gives the predictions for the minimum velocities to initiate a Mode III failure and adiabatic shearing in the studied beam corresponding to different mass ratios and beam geometries. It is shown that there exists a transition impact velocity from Mode III failure to adiabatic shearing failure, which depends on the beam thickness, beam length and mass ratio, g. Adiabatic shearing may suppress a Mode III failure for a relatively thin beam. Generally, the critical velocity for both Mode III and adiabatic shearing failures increases with beam thickness, but decreases with projectile mass and beam length. It is interesting to point out that the adiabatic shearing suppresses a Mode III failure when the beam thickness is less than a given value which falls

within a narrow range of 1~2mm for a broad range of other parameters. This means that Mode III failure might not be found in a thin beam even a high impact velocity is imposed because Mode II failure transfers into adiabatic shearing failure with increasing impact velocity. Unfortunately, there are no experimental results available for comparison.

4.6. Remarks

A systematic analytical study on the transverse shear response and failure of a beam when subjected to a transverse dynamic loading has been presented in Chapters 1 to 3 and the current chapter. Most of the results for a beam are applicable for other structural elements, such as plates and shells under similar loading conditions. It is a common feature of these structural elements under transverse dynamic loadings that a transverse shear localization zone(or shear hinge) may be formed at some "hard points" like supports and at the impact loading periphery. Within the shear hinge, both shear rupture failure and adiabatic shearing failure may occur depending on loading rates and intensities as well as the thermal visco-plastic properties of the material. Comparing with the formation of a shear hinge, the formation of an adiabatic shear band is another type of shear localization due to material thermal softening. Both shear rupture failure and adiabatic shearing failures appear with increasing loading rate and intensity, and there may exist a transition between these two failure mechanisms that require different material and failure models in analyses and simulations. Thus, this observation should be considered seriously in relevant impact safety design.

Structural elements under projectile impact may introduce more difficulties than an impulsive pressure loading because the contact of a projectile with the structure may lead to considerable indentation. Indentation may result in a localized material failure, changes of material properties and structural element thickness and the absorbtion of projectile kinetic energy, which must be considered in order to use the proposed model correctly. Thus, modifications are necessary for a projectile impact problem, depending on the actual situation. For example, the transverse shear displacement determining shear failure initiation is accumulated through half shear hinge length given by eq.(3-11) in an aluminium alloy circular plate subjected to a

blunt projectile impact, as shown in Jones, Kim and Li(1997). Although, these problems are not discussed in the current study, it is obvious that incorporating dynamic indentation analysis into the current model is necessary for some practical impact problems.

It is well-known that the concept of a ballistic limit to perforate a structural element is an important design parameter for plate perforation and penetration. Many models in the low to medium velocity range have been proposed to predict the ballistic limit of given plate material and geometry based on various response and failure analyses, for example, Liu and Stronge(1995). However, as shown in the current analysis, adiabatic shearing may suppress other failure modes under proper conditions. Thus, the consideration of the adiabatic shearing mechanism in predicting the ballistic limit in a practically important impact velocity range may lead to an improved understanding of plate perforation and penetration problems.

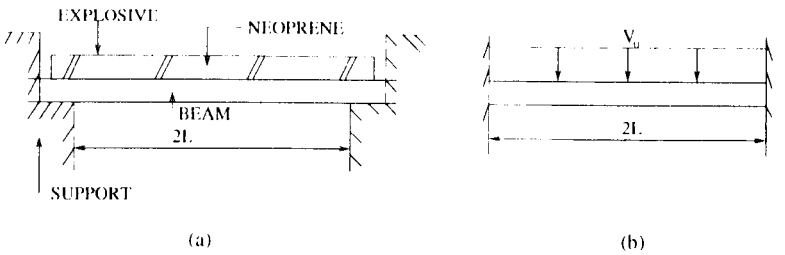

Fig.4.1 (a) Explosive tests on fully clamped beam; (b) Simplified fully clamped beam under uniformly distributed initial velocity.

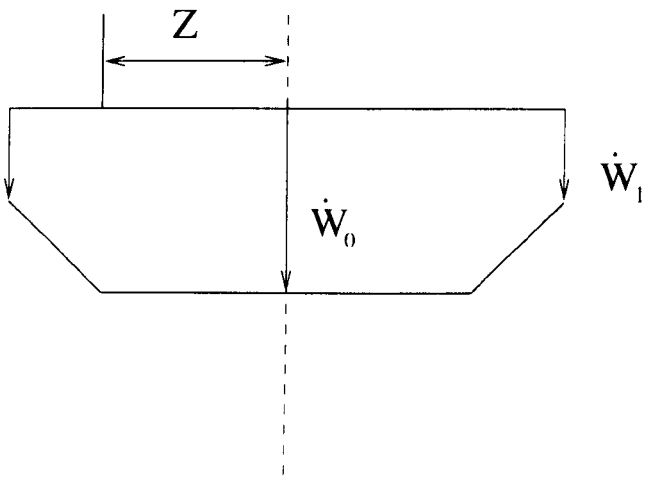

Fig.4.2 Velocity profile of a fully clamped beam under impulsive pressure loading when $v>3$.

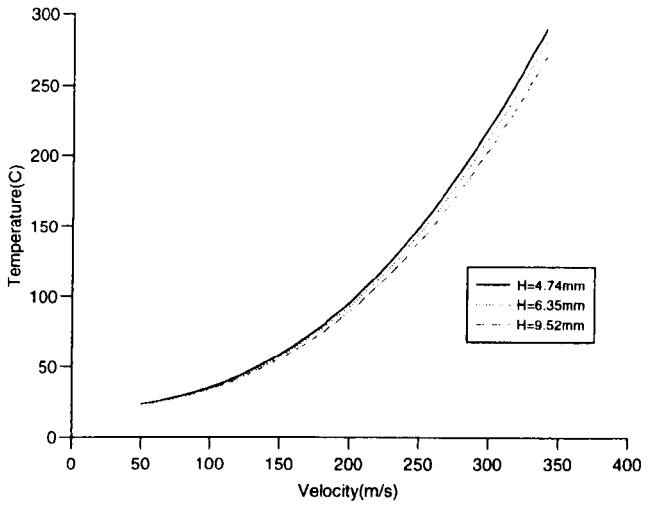

Fig.4.3 Temperature rise in the shear hinge of a beam under various impulsive velocities.

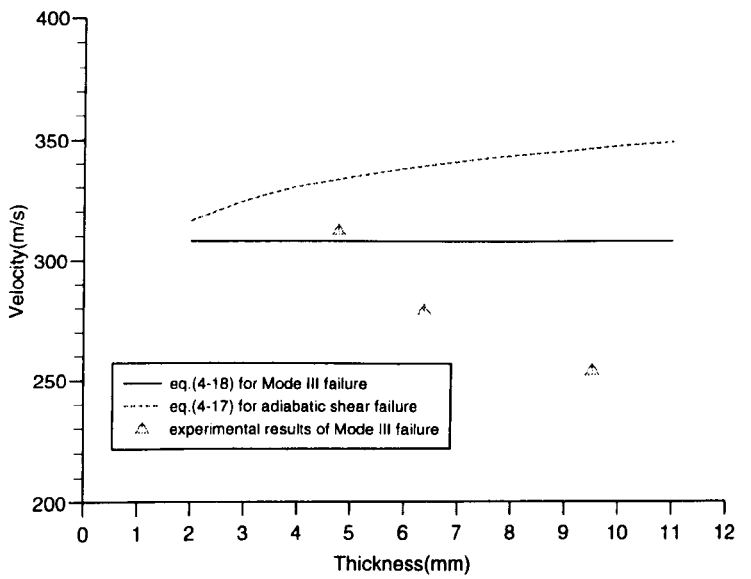

Fig.4.4 Critical conditions for adiabatic shearing and Mode III failures in tests of Menkes and Opat(1973).

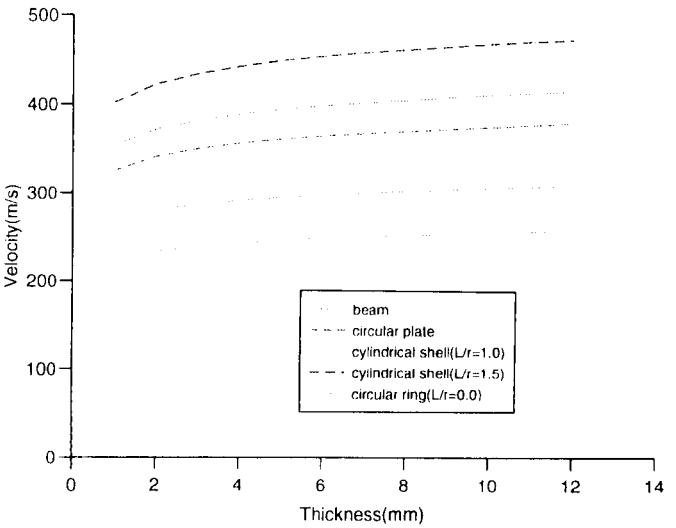

Fig.4.5 Critical condition for adiabatic shearing failure in a short beam, circular plate and cylindrical shell(L/H(or R/H)=1.7).

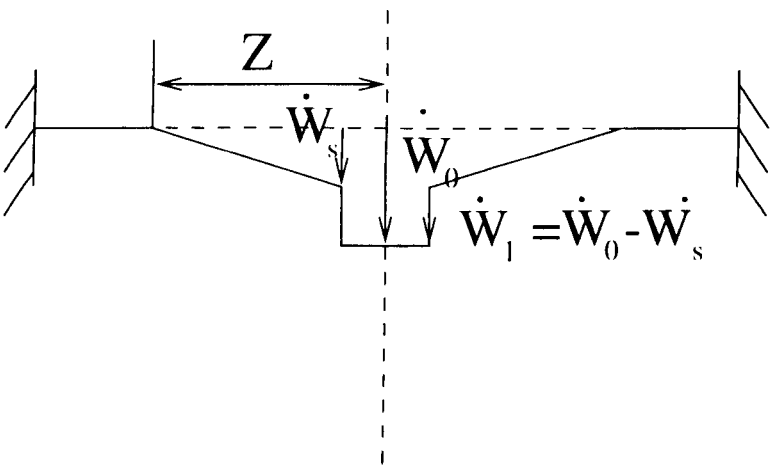

Fig.4.6 Velocity profile of a fully clamped beam under projectile impact when $v>3$.

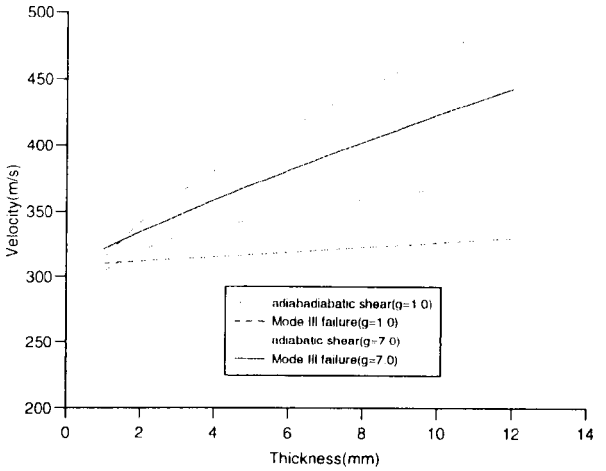

(a)

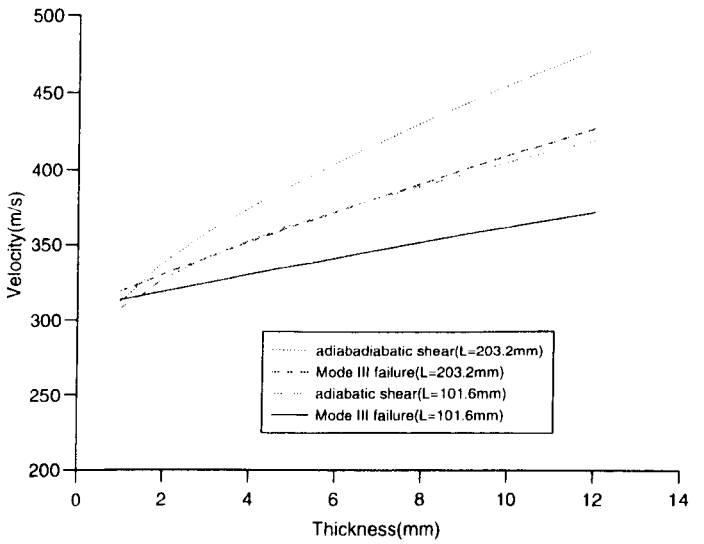

(b)

Fig.4.7 Variation of critical impact velocity of adiabatic shearing and Mode III failures with beam thickness for the problem in Fig.4.6, (a) L=203.2mm; (b) g=3.0.

5. EXPERIMENTS ON DOUBLE SHEAR BEAM UNDER PROJECTILE IMPACT

5.1. Material Properties

5.1.1. Physical Properties

The bar material used in the tests is BS970/En24(equivalent to AISI-4340 steel) medium carbon steel alloy. The composition of the material according to the supplier is shown in Table 5.1,

Other physical properties(at room temperature) are given in Table 5.2

The measured hardness of the present En24 material is RC-21, which is smaller than the value for 4340 steel given by Johnson and Cook(1983), and is probably due to the different heat treatment process. The specific heat of 4340 steel given by Johnson and Cook(1983) is C_v=477($JK^{-1}kg^{-1}$), which is very close to the value in Table 5.2 with a relative difference of 1%. The heat conductivity here is compared with the value given by Bai and Dodd(1992)(pp.305), where K_v=37.6 (Wm^1K^{-1}) for a 4340 steel which is only 1.4% smaller than the value in Table 5.2. Both specific heat and heat conductivity vary with temperature, which may be estimated according to Table 5.3

The value of C_v in Table 5.3 is the mean specific heat from 20°C to the temperature given in Table 5.3, which can be easily converted into their actual value, as shown in Table 5.4.

The mechanical properties and the constitutive equation for the material will be presented in Section 5.1.2.

5.1.2. Constitutive Equation

High-strain rate plastic deformation of a material is often described by a thermo-viscoplastic constitutive equation, which links stress with strain, strain rate and temperature. A general form of the rate and temperature dependent flow law may be expressed as

$$\sigma_e = F(\varepsilon_e, \dot{\varepsilon}_e, T, V_k) \tag{5-1}$$

for an isotropic material model, in which σ_e and ε_e are von-Mises equivalent stress and strain, T is temperature and V_k are some internal variables, such as a strain hardening parameter. The expression of function F is often identified by either a uniaxial tensile/compressive test or a pure shear test. In the first case, which will be used in the present research, eq.(5-1) is

$$\sigma = F(\varepsilon^p, \dot{\varepsilon}^p, T, V_k) \tag{5-2}$$

in which σ and $\varepsilon^p(\dot{\varepsilon}^p)$ are the uniaxial stress and plastic strain(plastic strain rate), respectively. It has been shown that the true stress and natural strain, defined in Appendix A1, are more convenient for metal plasticity to achieve consistency. The theory of dynamic plastic constitutive equation will not be discussed here, but may be found easily by an interested reader in many sources, such as, Harding(1988), Clifton(1983), Meyers(1994) and Walter(1992).

Normally, the function F in eq.(5-1) or eq.(5-2) satisfies the following inequalities, i.e.,

$$\frac{\partial F}{\partial \varepsilon_e} > 0, \quad \frac{\partial F}{\partial \dot{\varepsilon}_e} > 0 \quad \text{and} \quad \frac{\partial F}{\partial T} < 0 \tag{5-3}$$

to reflect strain hardening, strain rate hardening and thermal softening. Strain softening is also possible sometimes when void and texture softening mechanisms are more important, as discussed by Zbib and Tubran(1992).

Practically, it is very difficult to determine the function F by conducting limited experiments without further simplifications. Most proposed constitutive equations employ the following multiplicative form(Johnson and Cook(1983), Klepaczko(1994))

$$\sigma = F(\varepsilon^p, \dot{\varepsilon}^p, T, V_k) = F_1(\varepsilon^p, V_k) F_2(\dot{\varepsilon}^p) F_3(T), \tag{5-4}$$

where F_1 is determined from a quasi-static tensile test, F_2 is determined from a SHPB constant strain rate test, and F_3 will be obtained by a static constant temperature test, which will be described below. When eq.(5-4) is determined from uniaxial material

tests it may be converted into the general form of eq.(5-1) by using equivalent stress and strain definitions. Thus, at least two idealizations, i.e., (i) the influences of plastic strain, strain rate and temperature on the constitutive equation can be separated into the multiplicative form in eq.(5-4), and (ii) the constitutive equation is invariant with respect to the equivalent stress and strain, have been adopted here to obtain the material constitutive equation. The second idealization is based on the fact that the plastic flow of metal materials is controlled by the von-Mises equivalent stress and strain. The first idealization needs to be verified, which will be given in Section 5.1.3. Zerilli and Armstrong(1987,1990) proposed an another type of viscoplastic constitutive equation based on a micro-mechanics basis, which also indicated the uncoupled characteristics of plastic strain from strain rate and temperature, as discussed by Meyers(1994).

(a) Static Tensile Test

The static tensile tests were conducted on an INSTRON test machine with the axial loads being measured by a load cell installed in the machine. An extensometer with a gauge length of 50mm was used to measure the elongation up to ε_E=2%. Then, it was removed and the displacement was measured between the two crossheads.

The specimens were made from annealed BS970/En24 steel, which came from three different bars. The geometry of a test specimen is shown in Fig.5.1. The actual dimensions are given in Table 5.5 together with the final measurements of the diameter at the necked cross-section of a failed specimen.

The engineering stress-strain results are shown in Fig.5.2. Young's modulus, maximum engineering stress, the percentage elongation from the INSTRON machine, the zero gauge length rupture strain, defined by eq.(A-11a), and the true stress at failure are given in Table 5.6. Poisson's ratio is 0.29.

It was found that the test results for two bars(SP2 and SP3 for Bar 2 and Bar 3) were fairly close. But there are noticeable differences between the results of these two bars and Bar 1(SP1 and SP4). Generally, the average yield stress of Bar 1(421.45MPa) is about 8.7% higher than the average value of Bars 2 and 3(387.7MPa). Although, there is a noticeable discrepancy(about 22.02%) on the

percentage elongation of SP1 and SP4 from the same bar, the error based on zero gauge rupture strain is only 8.43% for SP1 and SP4. It is interesting to note that the values of the zero gauge length rupture strain give consistent results when compared with both UTS values and true stress values at failure(σ_{Tf}). It has been realised that the zero gauge length rupture strain is a more realistic index to measure material ductility than the percentage elongation index that is specimen dependent. The average value of ε_{N0f} for SP1 and SP4 is 78.72%, which is 21.56% higher than the average value of SP2 and SP3(ε_{N0f}=64.76%). It is reasonable to treat Bars 2 and 3 as the same material, but Bar 1 as a slightly different material. Thus, only Bars 2 and 3 are used in the DB beam test.

A relationship between true stress and natural strain for SP2 and SP3 is evaluated in Fig.5.3 according to the tensile theory in Appendix A1 when considering the influence of a superimposed hydrostatic tensile stress introduced by necking according to Bridgman's formula, equation (A-14). A straight line interpolation is used between the maximum stress point and final rupture point, which has been verified by Alves(1996). The modification factor in eq.(A-14) is given by

$$f_c=1.0224-0.0948\varepsilon_{eq} \tag{5-5}$$

according to Fig.2.13 in Alves(1996). This modification is not significant for the present material, where $f_c\approx 0.96$ for SP2 and SP3. However, when the material ductility(ε_{N0f}) is large, the stress value may be reduced more due to the further development of non-uniform stress distributions across the necked cross-section.

According to Fig.5.3, material static true stress-true plastic strain curve for Bars 2 and 3 may be described by

$$\begin{aligned} F_1&=\sigma_0 \quad \text{for} \quad 0\le\varepsilon^p<\varepsilon_1^p \\ F_1&=\sigma_0+A(\varepsilon^p-\varepsilon_1^p)^m \quad \text{for} \quad \varepsilon_1^p\le\varepsilon^p<\varepsilon_2^p \\ F_1&=B_1+B_2(\varepsilon^p-\varepsilon_2^p) \quad \text{for} \quad \varepsilon_2^p\le\varepsilon^p \end{aligned} \tag{5-6}$$

where σ_0=387.7(MPa), A=1182.7(MPa), B_1=784.08(MPa), B_2=749.2(MPa), m=0.45, ε_1^p=0.65% and ε_2^p=9.46%. The plastic strain energy density up to material failure is 606.64MJ/m^3 from eq.(5-6) when the average value of zero gauge rupture strain ε_{N0f}=64.76% is used. Eq.(5-6) is illustrated in Fig.5.3.

(b) Dynamic Compressive Test

A Split Hopkinson pressure bar(SHPB) is used for the dynamic compressive testing. The parameters used in the SHPB system, described in Fig.5.4, are presented in Table 5.7.

SHPB tests were conducted on specimens machined from three bars at various strain rates. Basic results are presented in Table 5.8.

A typical recording in SHPB test is given in Fig.5.5. It is evident that the strain rate, determined by the reflected waves in the incident bar, varies with time. Conventionally, the average strain rate may be calculated from eq.(A-18c) or eq.(A-20c). However, in practice, it may be obtained equivalently by measuring the total shortening of the specimen and the total loading time. For example, the average engineering strain rate is

$$\dot{\varepsilon}_E=\frac{(L_s-L_{sf})/L_s}{T_L} \tag{5-7}$$

in which T_L is the total loading time, which depends on projectile length and elastic wave speed. In our case, T_L=155.6μs. In Table 5.7, the average true strain rate is defined by

$$\dot{\varepsilon}=\frac{(L_s-L_{sf})/(\frac{L_s+L_{sf}}{2})}{T_L} \tag{5-8}$$

with a 4% difference when compared with the value from eq.(5-7).

The true stress-true strain relationships at various strain rates are demonstrated in Figs.5.6(a,b,c) for three bars. Various compressive strains were achieved for different strain rates. The maximum compressive strain is about 24% when strain rate is around $10^3 s^{-1}$. Some of them are less than 10% when strain rate is low. The dynamic yield stresses corresponding to different strain rates are presented in Fig.5.7.

From these results, the strain rate effect represented by F_2 in eq.(5-4) can be described by the Cowper-Symonds relationship when using yield stress to determine the parameters in it

$$F_2=1+(\frac{\dot{\varepsilon}}{D})^{\frac{1}{q}} \tag{5-9}$$

where q=4.41 for all three bars, D=186.7(1/s) for Bars 2 and 3, and D=378.3(1/s) for Bar 1. A comparison between Eq.(5-9) and the test results is shown in Fig.5.7. Again, a noticeable difference is observed between the results of Bar 1 and Bars 2 and 3.

If the dynamic stress at a fixed strain is used to determine the parameters in the Cowper-Symonds relationship, different parameters will be obtained. This implies that both D and q depend on the plastic strain. In order to verify the validity of the Cowper-Symonds relationship, the dynamic flow stress at 12% plastic strain is used to obtain the parameters, D and q. The experimental results used to obtain D and q at 12% plastic strain are given in Table 5.9, which, by using the minimum square method, leads to D=6948.3s^{-1} and q=5.132. Thus, D and q are plastic strain dependent, as noted by Jones(1989). The bigger the parameter D is, the smaller the strain rate sensitivity is. Both of the two sets of parameters obtained above will be verified in Section 5.1.3. Their influence on DS beam response and failure will be examined in Chapter 6.

(c) Temperature Effects

Static tensile tests were conducted at various temperatures from room temperature to 500°C on an INSTRON test machine. A specimen is heated by a 1.5mm diameter, nickel coil, model HBS050, made by H&B Sensors Ltd(UK), which has an inner heater wire and an outer sheath insulated by a magnesium oxide layer. The coil heater is wrapped around and along the gauge length of the test specimen. Two enlarged ends are screwed firmly to the specimen, which are used for installing a cooling pipe. The temperature of the coil heater can be adjusted by changing the input voltage. The complete test system is shown in Fig.5.8, and the specimen geometry is shown in Fig.5.9(a).

Typical stress-strain curves, based on the gauge length in Fig.5.9(a), are shown in Fig.5.10 for elevated temperatures. As expected the material yield stress decreases with increasing temperature. Further tests showed that the distinct yielding points disappears beyond 320°C. Table 5.10 presents the main test results.

The ratios of σ/σ_0 are plotted in Fig.5.11 against temperature, which are formulated by the temperature factor in the Johnson-Cook constitutive equation,

$$F_3=1-(\frac{T-T_r}{T_m-T_r})^n \tag{5-10}$$

where a single parameter n=0.65 fits all experimental results well, as shown in Fig.5.11.

Temperature also increases material ductility, which can be seen from comparing the values of ε_{N0f} at failure locations of T01 and T03. Unfortunately, other failures occur outside the heating section, and, thus, they cannot be used to show the dependence of ε_{N0f} on temperature. These limited results also show that the maximum tensile stress varies little with temperature before it reaches 300°C. More tests on tapered specimens, shown in Fig.5.9(b), are conducted in order to confine the failure location at the middle of the specimen. The results are given in Table 5.11.

According to the test results in Table 5.11, and the results of T11 and T03 in Table 5.10 for ε_{N0f}, which is defined using the zero gauge length given by eq.(A-11a) in Appendix A1, a relationship between material ductility and temperature up to 500°C is presented in Fig.5.12. It shows that the increase of material ductility with temperature is significant, especially when T>300°C.

5.1.3. Verification of the Constitutive Equation

In the proposed constitutive equation, the influences of plastic strain, strain rate and temperature on the constitutive equation are separated into a multiplicative form, as shown in eq.(5-4). Furthermore, the strain rate effect is included by using the Cowper-Symonds relationship, which was proposed originally for estimating the strain rate effect for the dynamic yield stress. Thus, it is necessary to verify the validity of eq.(5-4) when other functions, F_1, F_2 and F_3 are identified.

In our modelling, the function F_2 is assumed plastic strain independent. However, both the flow stress at zero and 12% plastic strains are used to obtain two sets of the parameters, D and q. The stress-strain predictions from them can be compared with the stress-strain result of a SHPB test to verify the proposed form of the constitutive equation. According to the discussion in Section 4.3.1, the

deformation process in a SHPB test can be idealized as an adiabatic process. The temperature rise during the test is estimated using eq.(1-12). The actual stress-strain curve in a SHPB test may be influenced by temperature, which, however, is not significant in the present case. Another factor is the variation of strain rate during the loading process. Fig.5.14(a) shows the measured incident, transmitted and reflected waves in SHPB test(specimen D22 in Table 5.8). The strain rate is proportional to the reflected wave. It is evident that strain rate is not constant during the test, and decreases monotonously from its maximum value to a minimum value that is less than half of the maximum value. The reflected wave in a typical SHPB record in Mayer(1994)(pp.310) also show this common feature of a SHPB test. Normally, the variation of strain rate during a test is neglected, and is replaced by the average value. The average strain rate, which is used in eq.(5-9), is about three-fifths of the maximum value. These factors should be considered in the verification. After considering both the temperature rise and the strain rate variation, the predicted result for $D=186.7s^{-1}$ and $q=4.41$ is higher than the test result, as shown in Fig.5.14. However, this difference tends to reduce with the increase of strain. The relative difference at 10% strain is about 20%, which reduces to about 10% at 24% strain. In the DS beam test programme, most of the material in the notch section of a DS beam experience plastic strain up to 25% to 50%, as shown in Chapter 6. It is expected that the proposed constitutive equation will give closer results for larger plastic strains. Unfortunately, the present capability of SHPB can only produce compressive strain of 24% in the specimen.

Predictions using $D=6948.3s^{-1}$ and $q=5.13$ are also shown in Fig.5.14. It is close to the experimental result at a plastic strain of 10%. The relative difference increases with increasing plastic strain. It is hard to judge which set of parameters offer a more accurate description of the strain rate effect from small to large plastic strains. However, it appears that these two curves for the two sets of parameters give upper and lower bounds on the test results. Their influences on DS beam response and failure will be verified in Chapter 6.

More complicated constitutive equations should include the variations of strain rate and temperature effects with plastic strain, which means that the function F_2 and F_3 depend on plastic strain as well. However, it is still difficult to fit material

behaviours in a range of strain rate and temperature. Alves(1996) obtained parameters for the Cowper-Symonds equation based on average values to fit yield stress, ultimate stress and failure stress simultaneously. However, the actual strain rate variation during the test was not discussed.

5.2. Experimental Description

The aim of the proposed experiments is to study the response and failure within the notch of a double shear(DS) beam under projectile impact in order to understand the features of the response and failure in a localised shear zone, or shear hinge, in the dynamic plastic response of a structural element. Responses and failures corresponding to different loading rates will be recorded and analyzed in order to supply the necessary information for further theoretical and numerical analyses. Experimental details are described in this section and the experimental results are presented in Section 5.3.

5.2.1. Loading System

A gas gun is used to accelerate the projectile. The velocity of the projectile is estimated according to an approximate formula derived from the gas pressure and Newton's second law of rigid body motion, which is expressed as

$$V_i = \frac{2.65\sqrt{P_0}}{\sqrt{M}} (m/s), \tag{5-11}$$

where M(kg) is the mass of the projectile and P_0(psi) is the initial pressure of the gas.

The actual impact velocities measured by the photocell system in Fig.5.15(a) are given in Table 5.12, which agree with the predicted results of Eq.(5-11), as shown in Fig.5.16.

The projectiles are made from an aluminium alloy shell with 20mm diameter and a hardened steel cap. The actual mass used in a test is shown in Table 5.12.

In order to achieve a normal impact and to prevent the barrel and the measuring device from being damaged by a projectile, the projectile is kept inside the barrel after hitting the beam. Two plates fixed beside the specimen are used as stoppers for this purpose, as shown in Fig.5.15(b).

5.2.2. Clamper and Specimen

A double shear beam is clamped by two 5mm screws and two clamps on a 255x152x24(mm^3) steel plate, which itself is clamped firmly on a massive steel block. The details of the clamping system are shown in Fig.5.15(b). Two hardened beam strips are used as stopper, which is on the same level as the top of double shear beam. A 10x10(mm^2) sheet with a given thickness is fixed on the top of the central block of the double shear beam to control the travelling distance of a projectile. The actual thickness of the sheet and its mass are given in Table 5.12.

The geometry of the double shear beam specimen is described in Fig.5.15(a). The notch width is 2mm.

5.2.3. Microscopic Observation Preparation

Specimen samples are prepared by sectioning, grinding, polishing and etching. After sectioning, it is mounted in resin. The mounted sample is ground, then, polished by a successively fine diamond paste down to 1μ until a mirror finish is achieved. The polished sample is etched by using 2% nital for 5 to 10 seconds which depends on experience to observe the colour of the etching surface.

Although there are different etching methods for various materials, the above reveals the deformation lines and both deformed and transformed adiabatic shear bands, which will be shown in Section 5.3.2.

5.3. Experimental Results

5.3.1. General Experimental Results

A detailed description of the experimental results on DS beams is given in Table 5.12 for various impact velocities and two different pad thicknesses.

Generally, simple shear dominates the deformations in the notch section. When the impact velocity is low, symmetrical shear deformations are observed in both notch sections. However, with increasing impact velocity, one of the two notches starts to fail. With further increase of the velocity, failures are observed in both notches. Normally, failures are initiated at the corners of a notch. A tensile failure appears at the upper-left(upper right) and lower-right(lower left) corners for

the left hand notch(right hand corner) of a DS beam(We will refer to a left hand notch in the following discussion), which are noted as upper-tensile(UT) and lower-tensile(LT) corners. While, a shear failure associated normally with adiabatic shear banding is observed at the upper-right and lower-left corners, which are noted as upper-shear(US) and lower-shear(LS) corners in the rest of this chapter and in Chapter 6.

It was found that there are negligible changes in the pad thickness and the thickness of the central block after impact. However, bending contributions to the displacement of the central block are noticeable. The bending displacements are measured after impact for some specimens, and are given in Table 5.12. These data are plotted in Fig.5.18 for impact velocities below 80m/s. The bending displacement reaches its maximum value at $V_i \approx 40$-50m/s, then starts to decrease due to the failure initiation at the notch corners. An approximate linear relationship between the bending displacement and the impact velocity is given in Fig.5.18. The shear displacement of the central block, W_f, is calculated from

$$W_f = \Delta_f - (d_p - \Delta_0) - W_b, \tag{5-12}$$

in which, the measured value of W_b is used when it is available, and the approximate relationship in Fig.5.18 is used when it is unavailable. The transverse displacement of the central block according to eq.(5-12) is given in Fig.5.19 for various impact velocities, which will be compared with the theoretical predictions in Section 6.3.

5.3.2. Observation of Tensile Failure and Shear Banding

The two failure mechanisms found within the notch of a DS beam specimen are a tensile failure and an adiabatic shear banding failure. Although, there is a small radius of 0.2mm at each corner of the notch, the stress concentration, and, thus, deformation concentration, is quite severe according to micro-observations presented in this section and the FEM simulations in Chapter 6. Thus, the failure of a DS beam, either a tensile failure or an adiabatic shear banding failure, is initiated from its four corners. This behaviour is different from the behaviour of a thin-wall tube tested in a torsional Hopkinson bar where failure is initiated in the middle of the gauge section, as shown by Marchand and Duffy(1988) for the adiabatic shear band

formation process.

(a) Tensile failure

Tensile failures are initiated in the tensile domain zones at either upper-tension(UT) or lower-tension(LT) corner(or both of them) when the impact velocity exceeds a critical velocity. The critical velocity to initiate tensile failure in the current DS beam tests is between 40 and 50m/s for both pad thicknesses. Normally, cracks appear in one of the two notches when the impact velocity just exceeds the critical velocity

Cracks extend in the direction of about 30 degrees, as shown in Fig.5.20. The crack extension length depends mainly on the input kinetic energy, or projectile impact velocity. It appears that the LT corner fails first because many experiments show that cracks at the DT corner extend more than the cracks at the UT corner. More discussion on this will be given in Section 6.4.

With a further increase of impact velocity, a third crack is found at the UT corner of the other notch. Obviously, this is due to the fact that cracks at the LT corner extend more than the cracks at the UT corner, which decreases the tensile concentration at the LT corner in the other notch. However, with a further increase of impact velocity, tensile failures are found at the UT and LT corners in both notches.

The microscopic examinations are conducted on the crack and its path. Crack propagation is irregular on the microscopic scale because the outline of a crack on a microscopic scale is characterised by fractal patterns, which is unpredictable on the macroscopic scale. The microscopic failure on the grain size is complicated, which may involve both tensile and shear effects. A microscopic tensile stress field over a finite region is consistent with the formation of a macroscopic tensile stress field. The observed macroscopic tensile crack seems to be in the vertical direction of the macroscopic tensile stress. Thus, it is believed that the macroscopic failure pattern can be determined by a macroscopic stress field at the front of a crack during the failure process. But, the failure in microscopic scale is determined by the microscopic local stress field. Thus, any failure phenomena and criteria have their associated spatial scale, which is necessary to be specified in any failure analysis. A proper

macroscopic failure criterion can predict the macroscopic failure initiation in structures if the failure index in a failure criterion is determined by a material test having the same failure mechanism.

In addition to the tests in Table 5.12 on the originally delivered En24 steel, some tests were conducted on a heat treated En24 steel with a hardness HRC 44-46 after heat treatment. No tensile failures were found at the UT and LT corners, but instead shear failures occurred at the upper-shear(US) and lower-shear(LS) corners, which will be described below.

(b) Adiabatic shear bands

Adiabatic shear bands are found in the shear domain zones at both the US and LS corners shown in Fig.5.21(a). Microscopic examinations are conducted for the post-test specimens and adiabatic shear bands are found in front of the cracks at the US and LS corners. It has been claimed in several publications(see pp.448 Meyers(1994)) that shear bands are precursors to fracture, which is true in some situations as in a SHTB test. However, it is highly possible that a pre-existing crack or an initiated crack may also play a precursor role for the development of an adiabatic shear band, which has also been confirmed by Kalthoff(1987, 1990). Shear band initiation in a DS beam is more complicated than in SHTB tube specimen because the local US and LS shear domain zones are not in a simple shear mode. It is also hard to find which phenomenon(crack or shear band) is initiated first, and then to be the precursor of another phenomenon. No matter which phenomenon occurs first, a failure transition between these two failure mechanisms are confirmed in the present test programme.

According to the microscopic observations in Fig.5.21(a), grains in a shear band are elongated into narrow strips along the shear band. The elongation of the grain decreases rapidly away from the core of a shear band. It is a practical view-point that an adiabatic shear band can only be achieved under rapid shear deformation, and it is hard to find evidence of shear bands in a macroscopic tensile stress field(that is why the term "shear band" is used for this material instability phenomenon). The elongation of the grains is much larger than that in macroscopic tension mode, shown in Fig.5.20. It appears that the compressive force created by the

macroscopic shear field could supply higher material ductility than a tensile stress field, which offers material an opportunity to consume more external energy to increase its temperature. Another advantage of a shear stress field to trigger adiabatic shear banding is its simultaneous deformation over a finite material domain, while a tensile failure mode is more likely to be a progressive process which makes it difficult to heat material up sufficiently to obtain a high ductility. Thus, adiabatic shear banding is more likely to be initiated in a shear stress field. Another factor is the loading rate. It is believed that the reason why grains can experience such high elongation is due to the rapid rise of temperature, which triggers the material instability to localize material deformations in this narrow zone, and, on the other hand, increases the material ductility significantly. The shear band length depends on the availability of input external energy and the material behaviour at the front of a shear band.

The maximum shear stress criterion has been used frequently to predict the initiation of an adiabatic shear band. If the adiabatic shear band is initiated in a simple shear field, the shear stress and strain of the simple shear motion can be used in the criterion because the local instability criterion is consistent with a global instability criterion in this case. SHTB can be used to create simple shear motion, and many analyses have been given to predict adiabatic shear bands in a SHTB specimen based on the maximum shear stress criterion. For a general stress field, the maximum shear stress criterion can be generalised as a maximum Tresca stress criterion. However, as discussed in Section 6.4, the maximum shear stress criterion is not always consistent with material instability because it could be satisfied during an unloading process without a material instability. Thus, the maximum Tresca stress criterion is one of the two necessary conditions to initiate adiabatic shear banding. More discussion on this topic will be given in Section 6.4.

The material around a shear band is sheared severely for about 20 times the shear band width in the present case. If this is taken as a characteristic size to model the initiation of a shear band(not the shear band itself), the FEM element size in this area should be the order of $10x\Delta_{sb}$ for an accurate simulation. For FEM simulations on instability development and the evaluation of an adiabatic shear band, finer elements are necessary.

There are two kinds of adiabatic shear bands, i.e., transformed shear band and deformed shear band. The first one is normally associated with hardening brittle materials, and the second one is frequently observed in ductile materials. In the current study, both the original delivered En24 steel and heat treated En24(H) are tested. The original delivered En24 can be classified as a ductile material, whose results have been reported above. The En24(H) is much more brittle than En24 with a high hardness. All the tested specimens on EN24(H) failed completely. Typical observations of an adiabatic shear band are shown in Fig.5.21(b). The failure surface is a shiny colour, which is believed to be fractured by failures in the shear band. In addition to the main failure surface, shear band branches are found beside the main failure surface, which satisfies the description for a transformed shear band from its white shiny colour. Because there is no material data available for the En24(H) material, most of the discussion is concentrated on the results obtained using the original delivered En24 material.

Table 5.1 Material Composition of En24 Mild Steel

Compositions	C	Cr	Mo	Ni
(%)	0.35-0.45	1.4	0.3	1.4

Table 5.2 Physical Properties

$\rho(kgm^{-3})$	$C_v(JK^{-1}kg^{-1})$	$K_v(Wm^{-1}K^{-1})$	$T_m(K)$	Hardness(Rockwell)
7830	482	38.13	1793	RC-21

ρ, T_m:Johnson and Cook(1983); C_v, K_v:Woolman and Mottram(1966);Hardness: from hardness test.

Table 5.3 Variations of Mean Specific Heat and Heat Conductivity With Temperature(Woolman and Mottram(1966))

T(°C)*	20	100	200	300	400	500	600	700	800	900
$C_v(JK^{-1}kg^{-1})$	481.2	481.2	502.1	514.6	531.4	556.5	585.8	627.6	707.1	690.4
$K_v(Wm^{-1}K^{-1})$	38.08	38.08	38.49	38.08	37.24	34.73	32.22	29.29	26.36	27.20

Table 5.4 Variation of Specific Heat with Temperature According to Table 5.3

T(°C)	20-100	150	250	350	450	550	650	750	850	950
$C_v(JK^{-1}kg^{-1})$	481.2	518.8	537.1	578.4	651.9	726.4	870.0	1247.7	560.1	608.1

Table 5.5. Diameter of the Test Specimens

	SP1	SP2	SP3	SP4
D_0(mm)	5.00	4.99	4.99	4.96
D_f(mm)	3.32	3.58	3.64	3.40
σ_{Ef}(MPa)	607.86	635.81	632.31	614.85
Note	Bar 1	Bar 2	Bar 3	Bar 1

D_0: initial diameter of the specimen; D_f: final diameter of the specimen at necking; σ_{Ef}: engineering stress at failure.

Table 5.6 Tensile Test Results(INSTRON)

	E(GPa)	σ_0(MPa)	UTS(Mpa)	elongation(%)	ε_{N0f}(%)	σ_{Tf}(MPa)
SP1	210.3	412.7	749.2	15.96	81.90	1378.7
SP2	212.8	391.5	719.5	13.44	66.42	1235.3
SP3	214.5	383.9	711.3	14.28	63.09	1188.3
SP4	215.4	430.2	746.3	13.08	75.53	1308.5

Table 5.7 Parameters of SHPB System

L_0	L_1	L_2	D	ρ(kg/m^3)	E(GPa)	c(m/s)	σ_0(MPa)	V_{max}(m/s)
400	750	450	23	7830	206.8	5140	531.65	26.42

D(mm): diameter of the incident and transmitter bars; L_0, L_1 and L_2(in mm) are shown in Fig.5.4; ρ, E, σ_0 and c are density, Young's modulus, yield stress and elastic wave speed of SHPB bars, respectively; V_{max} is the maximum impact velocity to ensure an elastic impact.

Table 5.8. SHPB Test Results

No.	V_i(m/s)	L_s	d_s	L_{sf}	d_{sf}	$\dot{\varepsilon}(s^{-1})$	Note
D01	14.60	4.315	9.990	3.980	10.410	519.0	Bar 1
D02	-------	4.315	9.980	3.760	10.750	883.2	Bar 1
D03	20.68	4.315	9.990	3.640	10.950	1090.4	Bar 1
D12	14.19	4.310	9.990	3.990	10.410	495.4	Bar 3
D13	16.74	4.310	9.980	3.840	10.630	741.0	Bar 3
D14	21.59	4.300	9.985	3.550	11.050	1226.2	Bar 3
D21	13.41	4.310	9.975	4.050	10.310	399.6	Bar 2
D22	21.90	4.310	9.970	3.565	11.050	1215.7	Bar 2

V_i: impact velocity of projectile; L_s and d_s(in mm) are defined in eq.(A-22), and L_{sf} and d_{sf} are their final values measured after test; $\dot{\varepsilon}$ is the average strain rate.

Table 5.9 Dynamic Flow Stress At 12% Plastic Strain

No.	ε^p(%)	σ_d(MPa)	σ_d/σ_s*	$\dot{\varepsilon}^p(s^{-1})$
D22	12.02	1342.0	1.721	1215.7
D13	12.01	1285.0	1.647	741.0
D14	12.02	1350.0	1.731	1226.2

*σ_s is the flow stress at 12% in quasi-static tensile test.

Table 5.10 Static Tensile Test Results At Various Temperatures

No.	d_0(mm)	d_f(mm)	T(°C)	σ/σ_0	ε_{N0f}	σ_{max}(MPa)	Note
T01	4.985	3.700	20.0	1.0	0.60	1104.8	Bar 1
T02	4.965	3.610	165.0	0.82	0.64	1046.5	Bar 1
T03	4.950	1.700	500.0		2.14		Bar 1,#1
T11	4.980	3.660	20.0	1.0	0.62		Bar 2
T12	4.960	3.610	115.0	0.81	0.64		Bar 2,#2
T13	4.940	3.670	240.0	0.64	0.60		Bar 2,#2
T21	4.970	3.570	320.0	0.68	0.66	1118.1	Bar 3

Note: #1: no yielding phenomenon; #2: failed outside heating section.σ and σ_0 are static yielding stresses at test temperature and room temperature, respectively.

Table 5.11 Variation of ε_{N0f} on Temperature

No.	T(°C)	D_0(mm)	D_f(mm)	ε_{N0f}	Note
TB1	340	6.09	3.88	0.90	Bar 2
TB2	430	6.01	3.28	1.21	Bar 2
TB3	250	6.09	4.16	0.76	Bar 2
TB4	175	6.12	4.29	0.71	Bar 2

Table 5.12 Experimental Results of DS Beam

No.	P(psi)	V_i(m/s)	d_p(mm)	Δ_0(mm)	Δ_f(mm)	W_b(mm)	W_f(mm)	Note
NT1	50	80.5	1.59	1.47	1.44	0.14	1.18	M_1, C
NT2	50	82.8	1.58		1.60	0.06		M_2, C
NT3	30	60.2	1.46	1.35	1.37		1.04	M_2, B
NT4	60	82.8	1.46	1.34	1.64		1.42	M_2, C
NT5	20	47.3	1.46	1.39	1.01	0.29	0.65	M_2, B
NT6	15	39.2	1.46	1.35	0.81	0.26	0.44	M_2, A
NT7	15	40.3	1.51	1.40	0.78	0.24	0.43	M_2, A
NT8	25	52.3	1.49	1.44	1.26		0.96	M_2, B
NT9	70	91.7	1.49	1.46	1.66		1.53	M_2, C
NT10	35	63.38				0.19		M_2, B
NT11	40	70.1	1.58	1.50	1.64		1.38	M_2, C
NT12	80	96.1	1.58	1.45	1.93		1.72	M_2, C
NT13	100	110.3	1.58	1.52	2.00		1.91	M_3, C
NT21	30	58.4	1.99	1.87	1.65	0.22	1.31	M_4, C
NT22	20	49.6	1.98	1.88	1.14	0.34	0.70	M_4, B
NT23	15	47.7	1.98	1.85	1.13	0.28	0.72	M_4, A
NT24	50	78.4	1.98	1.91	2.11	0.01	2.03	M_4, C
NT25	15	41.7	1.98	1.88	0.86	0.32	0.44	M_4, A
NT26			1.98	1.86	0.85	0.32	0.41	M_4, A
NT27	10	38.7	1.98	1.84	0.76	0.30	0.32	M_4, A
NT28	35	62.1	1.98	1.84	1.86	0.14	1.58	M_4, C
NT29	45	74.5	1.98	1.91	2.02	0.12	1.83	M_4, C
NT30	60	85.1	1.98	1.86	2.20	0.16	1.92	M_4, C
NT31	80	96.1	1.98	1.87	2.32	0.07	2.14	M_4, C
NT32	100	106.4	1.98	1.91	2.58	0.03	2.48	M_4, C

M_1=58.3g, M_2=62.0g, M_3=60.45g, M_4=62.38g;

A-symmetrical shear deformation in notch sections, B-failure occurrence in one notch, C-failure occurrence in both notches, as shown in Fig.5.17(a)

D- appearance of adiabatic shear band; E: appearance of tensile failure;

F: stopper plate(or impact pad or projectile) broken.

d_p: pad thickness, Δ_0: initial distance from pad top to the surface of stop plate, Δ_f: final distance from stop plate surface to the top of central block of DS beam, W_b: bending displacement of the central block, W_f: shear displacement of the central block, defined in Fig.5.17(b).

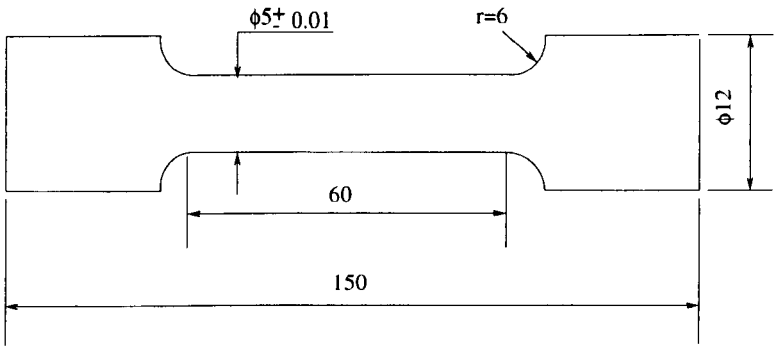

Fig.5.1 Geometry of the tensile specimen(Dimensions are not scaled, all units are mm)

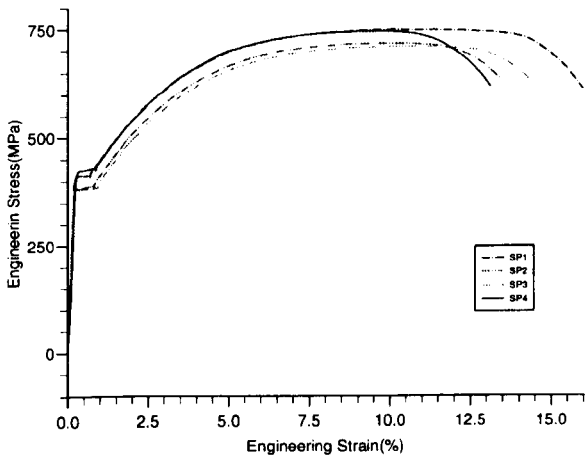

Fig.5.2 Engineering stress-strain curves for specimens SP1-SP4.

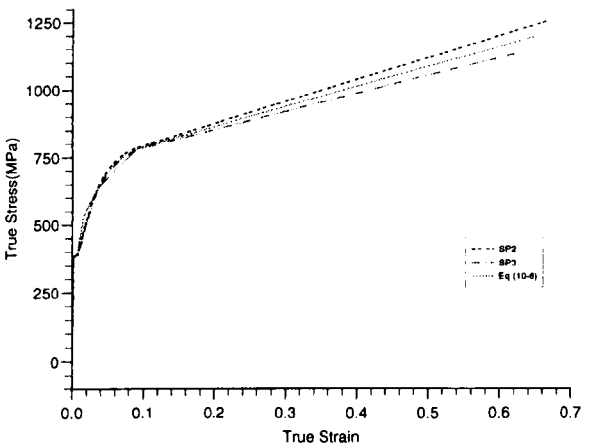

Fig.5.3 True stress-natural strain curves for specimens SP2 and SP3.

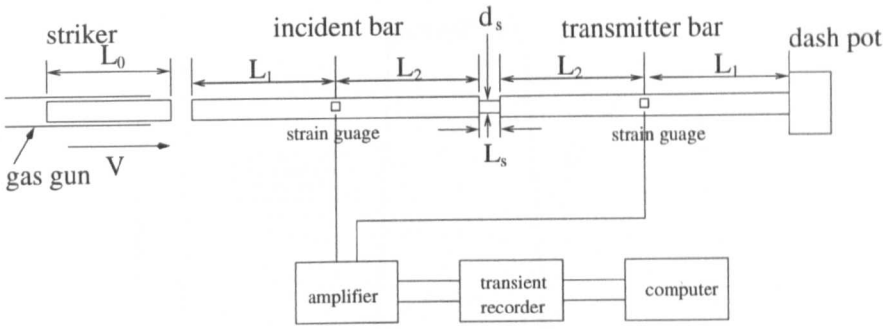

(a)

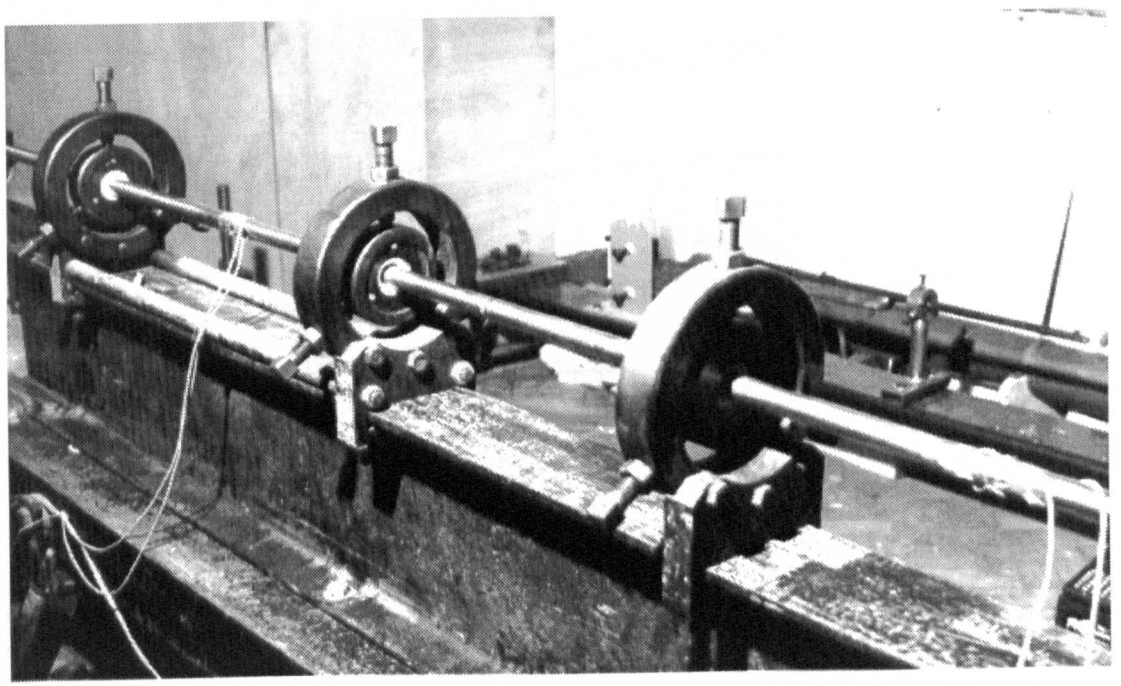

(b)

Fig.5.4 (a) A SHPB system; (b) An overall view of the SHPB system.

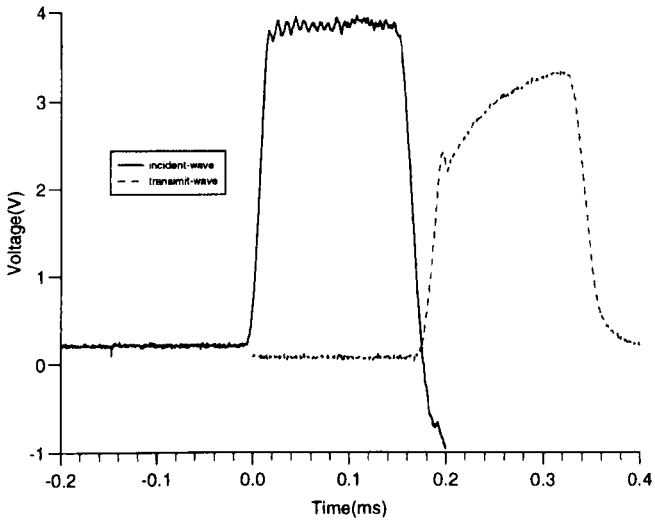

Fig 5.5 A typical recording from a SHTB test.

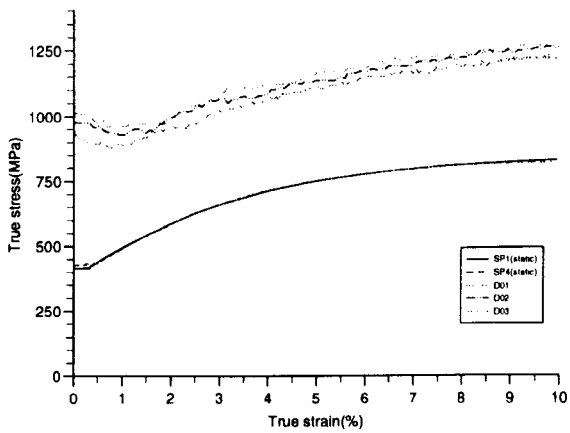

Fig.5.6 (a) (cont.)

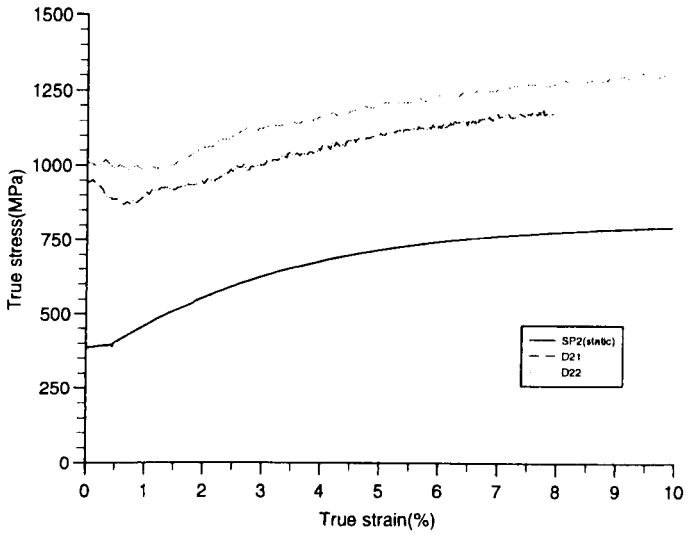

(b)

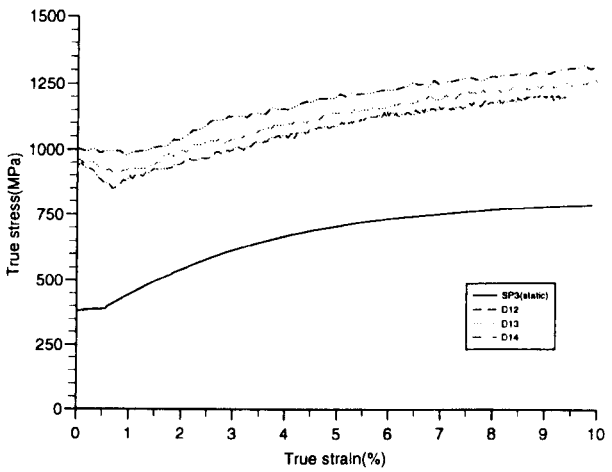

(c)

Fig. 5.6 True stress-strain curves at various strain rates, (a) Bar 1; (b) Bar 2; (c) Bar 3.

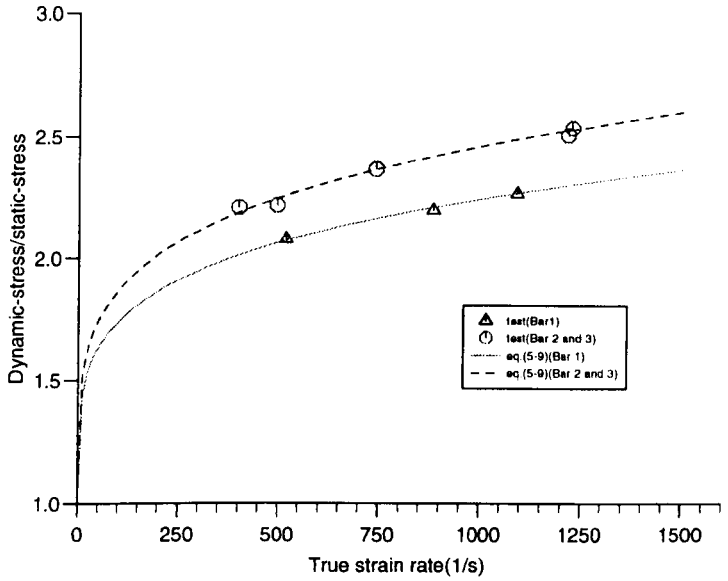

Fig. 5.7 Variation of dynamic yield stress with strain rate

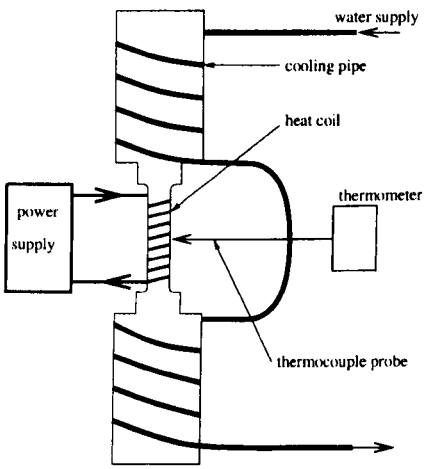

(a)

Fig. 5.8 (a) (cont.)

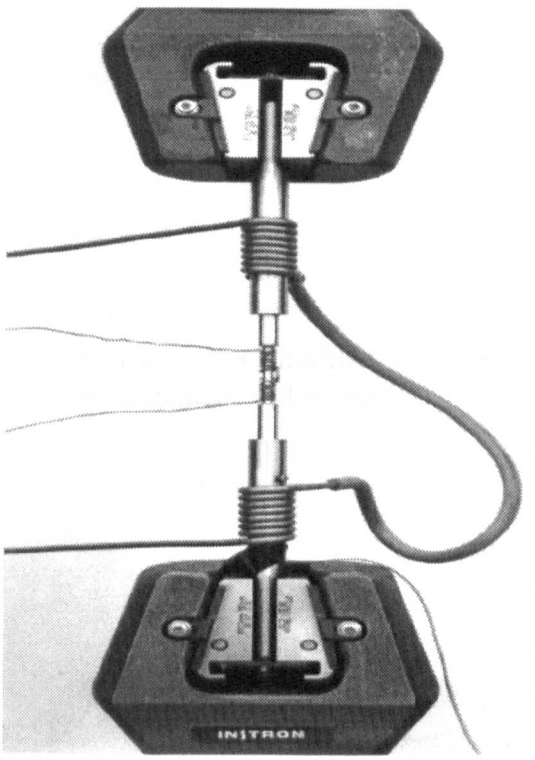

(b)

Figure 5.8 (a) High temperature test system; (b) An overall view of the heating and cooling system.

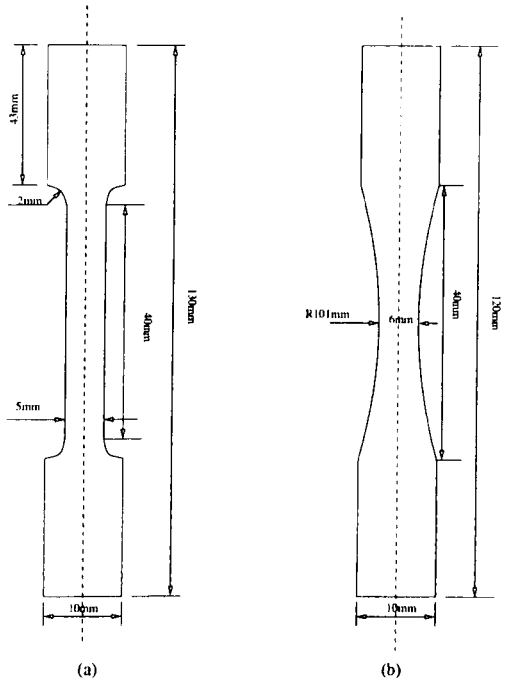

Fig. 5.9 Specimen geometries, (a) Cylindrical specimen; (b) Tapered specimen for failure test.

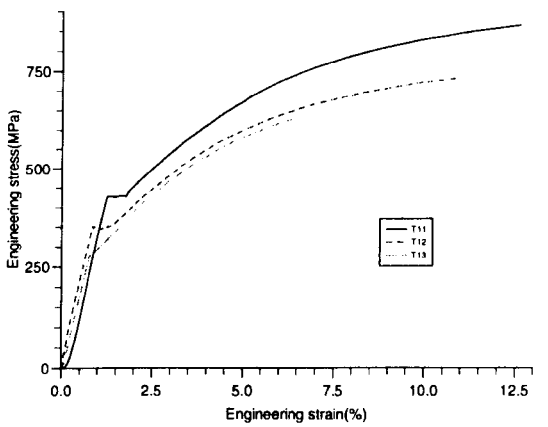

Fig. 5.10 Typical uniaxial tensile stress-strain curves with temperature.

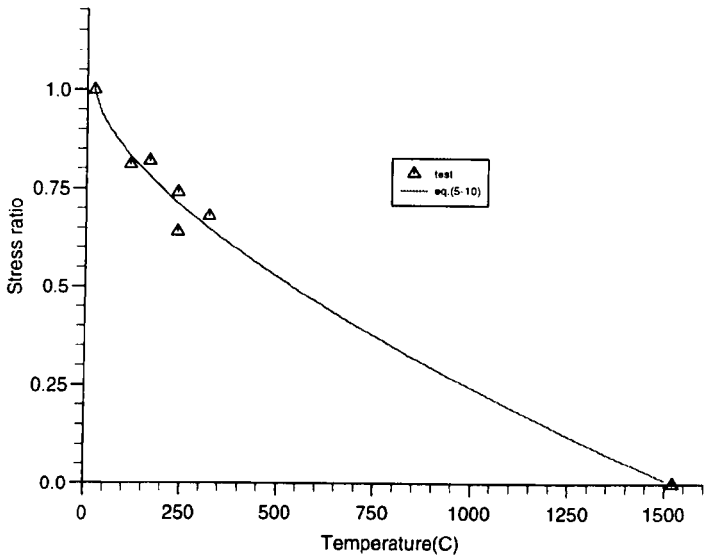

Fig. 5.11 Variation of yield stress ratio with temperature

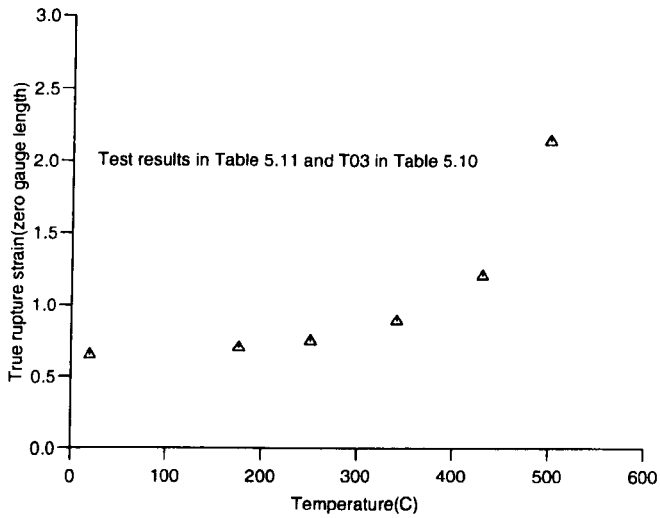

Fig. 5.12 Variation of zero gauge rupture strain with temperature.

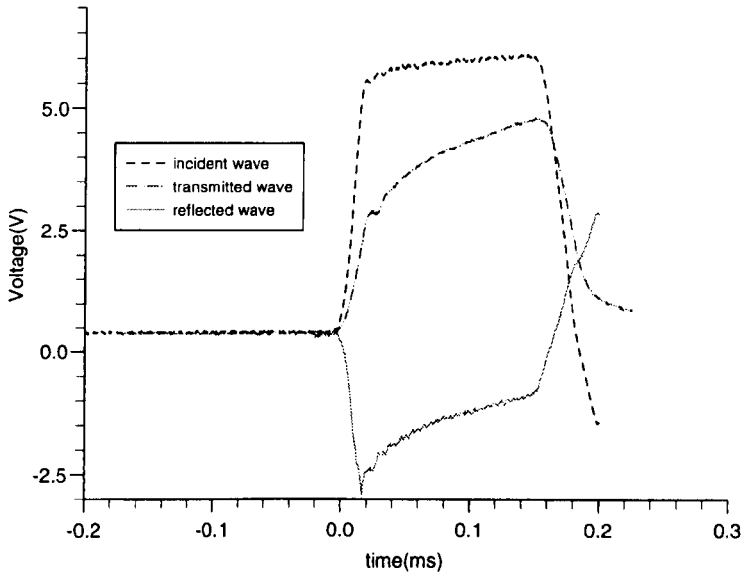

Fig.5.13 Incident, transmitted and reflected waves recorded for specimen D22.

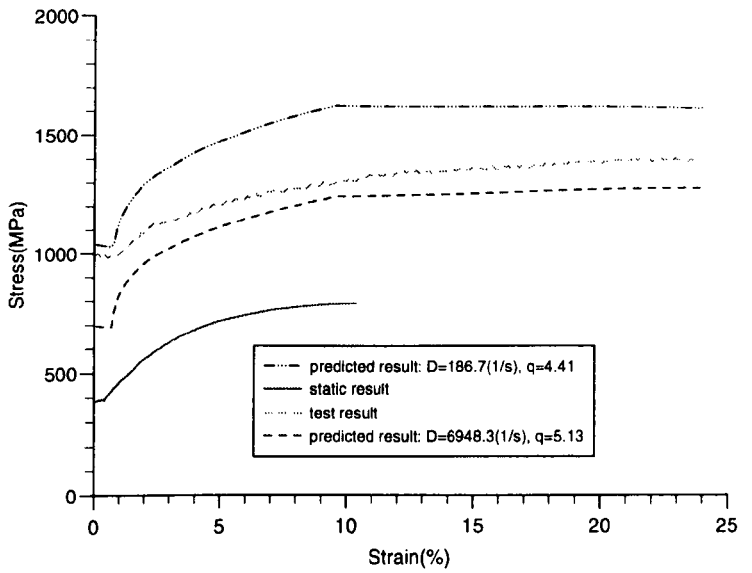

Fig.5.14 Comparison between predicted result with SHPB test result(specimen D22).

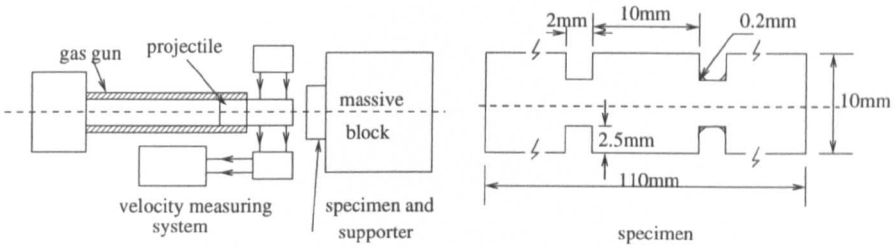

(a)

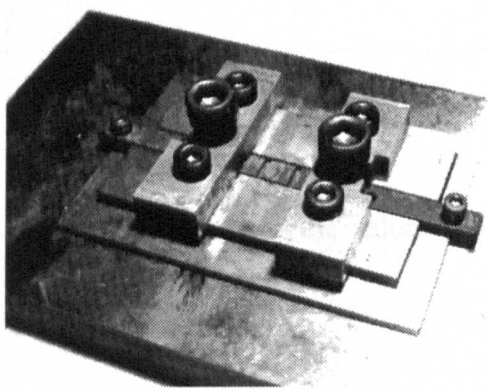

(b)

Figure 5.15 Experimental arrangement, (a) General description and specimen, (b) Clamps and stop plates.

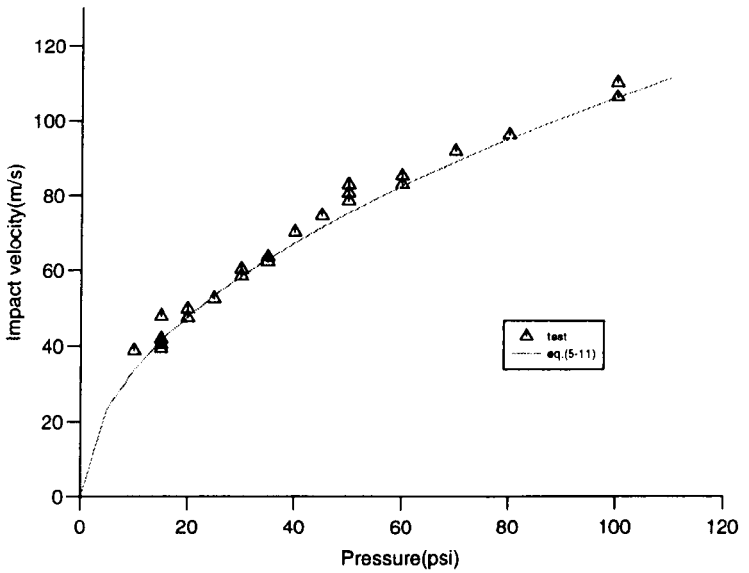

Fig. 5.16 Variation of projectile velocity with pressure.

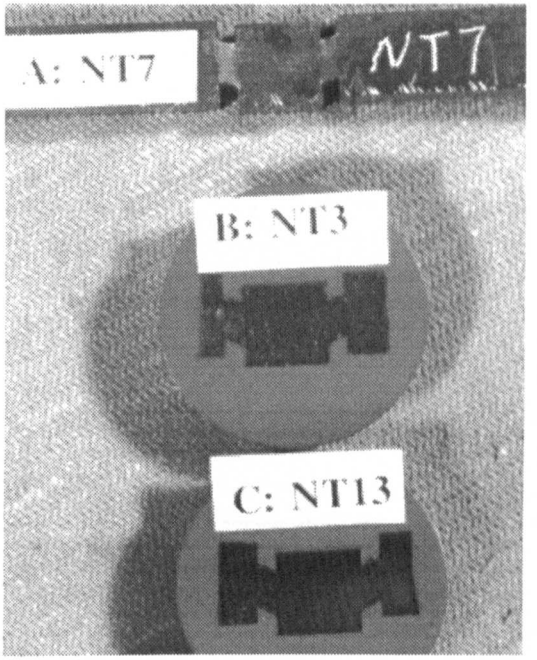

(a)

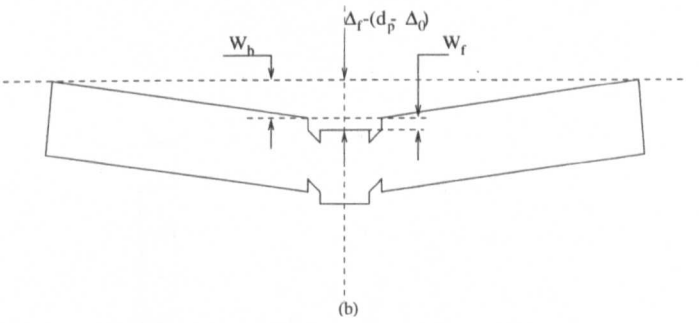

Fig.5.17 (a) Different deformation and failure modes in the notch section, A:symmetrical deformation(NT7); B:failure occurrence in one notch(NT3); C:failure occurrence in both notch(NT13); (b) Definition of bending displacement in DS beam.

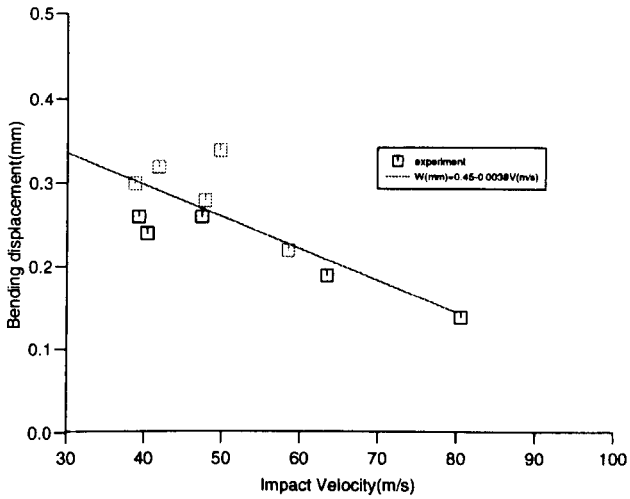

Fig. 5.18 variation of bending displacement with impact velocity.

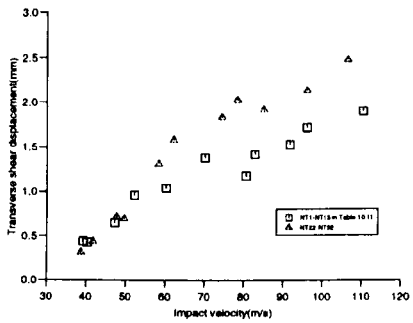

Fig. 5.19 Variation of transverse displacement of central block with impact velocity.

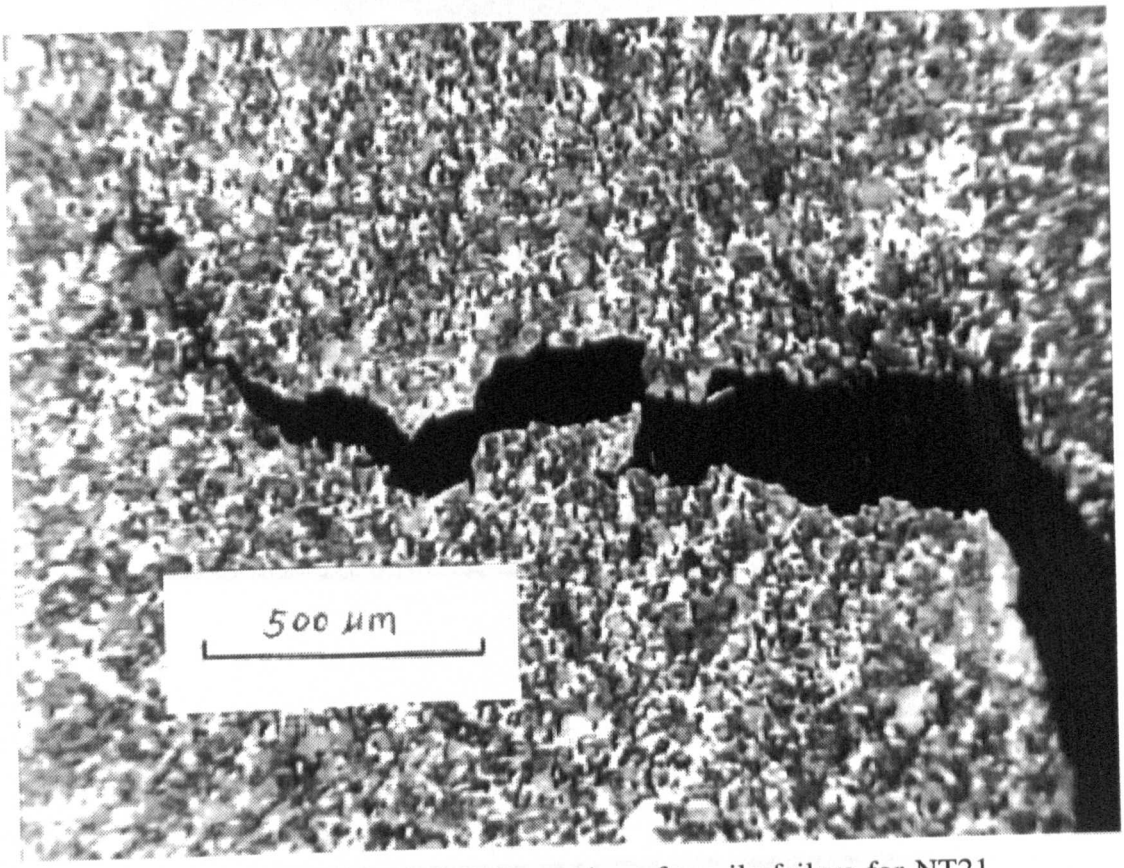

Figure 5.20 Microscopic observation of tensile failure for NT21.

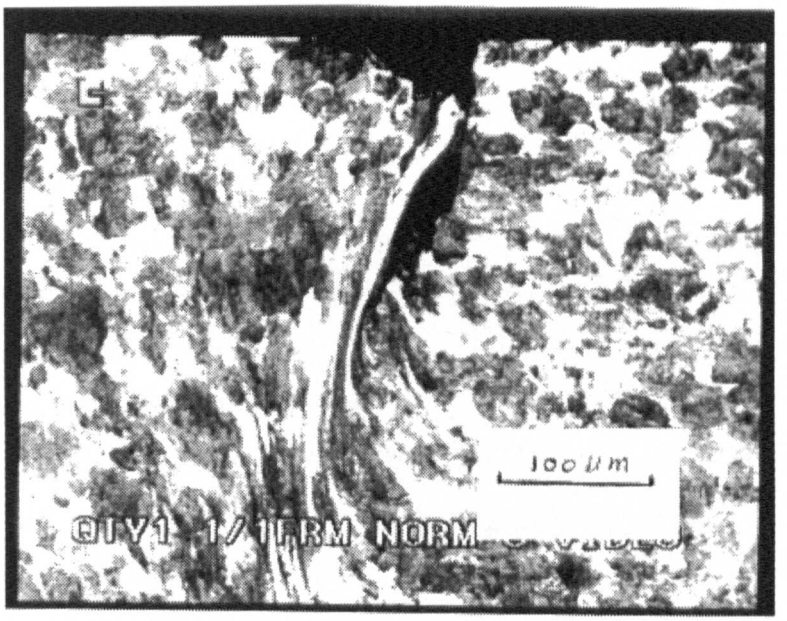

(a)

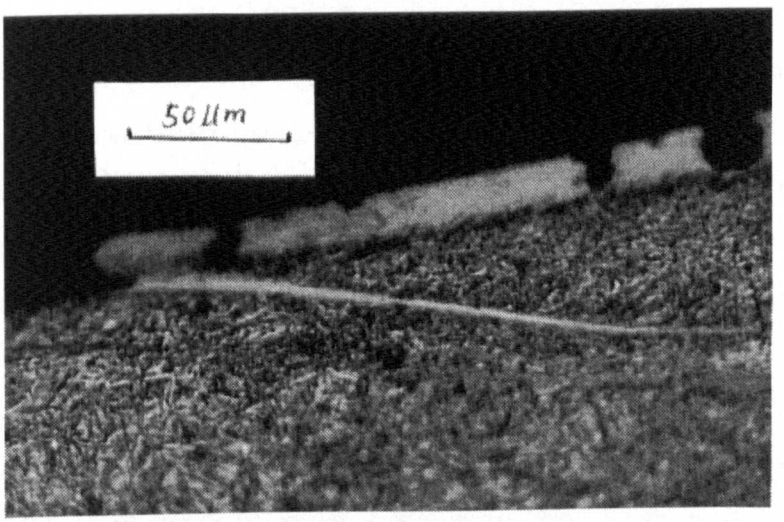

(b)

Figure 5.21 Microscopic observation of adiabatic shear bands, (a) Deformation shear band in original En24 steel(NT21), (b) Transformation shear band in heat treated En24(H) steel(T3).

6. RESPONSE AND FAILURE OF A DOUBLE SHEAR BEAM UNDER PROJECTILE IMPACT

6.1. Introduction

It is well-known that pure shear material tests conducted at different strain rates and temperatures can provide fundamental information for developing material constitutive equations. It is also an important way to investigate shear fracture and adiabatic shear band phenomena. Most experimental studies of both constitutive equations and adiabatic shearing were conducted by using Split Hopkinson Torsional Bar(SHTB) and pressure-shear impact(PSI) techniques. However, the strain rate limitation($\sim 10^3 s^{-1}$) for SHTB and maximum strain limitation(<few percent) for PSI actually introduce many difficulties for systematically investigating material dynamic behaviour(Klepaczko(1994)).

One of the most promising specimen configurations, which can be applied at low, medium and high strain rates in shear is the double-notch shear(DS) specimen. Such a specimen was first introduced by Ferguson(1967) to study the dynamic plasticity of single crystals. Later the DS specimen was applied with the Hopkinson bar technique by Campbell and Ferguson(1970), where nominal strain rates in excess of $10^4 s^{-1}$ were achieved with impact velocities from 1.2 to 11.0ms^{-1}. However, the determination of the shear strains in Campbell and Ferguson(1970) when they are higher than a few percent leads to large errors due to non-uniform shear and severe plastic deformations at the specimen supports, which have been shown by Ruiz, et al.(1989, 1991) by using photo-elasticity and ABAQUS FEM software. It was also shown that within the range of small strains the distribution of shear stresses in the shear zone(or gauge section) does not vary much, but stress concentration at the corners of the square notch of width 0.84mm is quite high. A modified double shear(MDS) technique was proposed by Klepaczko(1994) to overcome these shortcomings with a direct impact of a flat projectile on the MDS specimen to give greater flexibility to control the shear strain rate in the gauge length by changing impact velocities. However, the axial displacement of the central block of the MDS

specimen has to be measured by an optical method. The proposed MDS geometry has a wider gauge length, l_s=2.0mm(previously 0.84mm in Ferguson, Hauser and Dorn(1967), Campbell and Ferguson(1970), and Ruiz, Harding and Ruiz(1989, 1991)), and the sharp corner in previous use was changed into a round corner which substantially reduces stress concentrations near the notch corners. The extension parts were designed to be longer than before, and were clamped to the transmitter tube to prevent rotations. Such MDS geometry was analyzed statically by FEM at different stages of plastic deformation for low alloy steel XC18(French Standard).

It was shown that the shear strain fields up to 0.5 shear strain were quite uniform with a small asymmetry due to a bending component from the support. However, the extension part of the specimen outside the notch section also deformed plastically, causing an increasing tendency for rotation. A large width of the extension part may decrease this effect. Since the thickness of the gauge section in a MDS specimen is only 5mm, and the mean shear stress τ_s is assumed to be determined from an infinite layer, a calibration factor is introduced to calculate the actual shear stress in the uniform region of the gauge section from the mean shear stress. This calibration factor was found to be 1.2 approximately by Klepaczko(1994) for $0.05<\gamma<1.0$. No calibration factor for the shear strain was introduced. This experimental technique was used to investigate the initiation of adiabatic shear banding in the gauge section of a MDS specimen subsequently(Klepaczko(1994b, 1995)).

Although these studies have proposed the possibilities to use DS specimen as a standard material test technique at various strain rates, it is far from the mature technique like uniaxial tension or SHPB techniques. Previous studies have not given a systematic and complete description on the relationships between the shear stress/strain in the main part of the gauge section and the measurable force/displacement, which are crucial for calculating shear stress and shear strain. Temperature effects are neglected in these studies, which may be important for high strain rate tests and it is necessary to check its influence on the deformation of a DS specimen. Another interesting topic on the DS test is the initiation of failure at the notch corners where stress concentration is evident(even for a MDS specimen), which include both fracture and adiabatic shearing mechanisms. It has been shown that

only a fracture failure mechanism is involved in the failure process under a low velocity impact. The impact behaviour of a double shear specimen made from aluminium alloy and mild steel with a sharp triangle notch were studied by Jouri and Jones(1988). Only fracture failure was observed within the velocity range up to $12ms^{-1}$. However, Kalthoff(1987, 1990) observed failure transition in a specimen with two parallel edge notches when impact velocities varied from 50 to $100ms^{-1}$. It transpires that fracture and adiabatic shearing failures in a given DS specimen may appear with increasing impact velocities depending on the notch tip radius and material properties. Because fracture and adiabatic shearing are controlled by different criteria, it is significant for an engineering impact problem to determine the transition point when a new failure mechanism emerges. A general discussion on the failure transition has been given in Chapter 1, which has been used to study the failure transition in a fully clamped beam in Chapter 4.

In Chapter 5, a DS beam having a similar geometry(except the width of the gauge section) to Klepaczko(1994) has been tested by impact velocities within the range of 30 to 110m/s. Various deformation and failure modes have been recorded. In the present chapter, a combination of FEM simulation and analytical analysis are proposed to describe the behaviour of a DS beam under projectile impact. The advantages and disadvantages of using a DS beam for studying material dynamic properties and failure criteria are discussed. Section 6.2 studies the distributions of shear stress and strain in the gauge section, the temperature effects and the valid use of adiabatic condition. An analytical model is proposed in Section 6.3 for the motion of the central block based on the results from Section 6.2, which is compared with the test results and will be used as loading conditions in Section 6.4 where the actual response of a DS beam tested in Chapter 5 is simulated by using a FEM method. Various failure criteria are examined. The basic verification procedures proposed here may be used to modify other DS specimen results developed in any practical applications.

6.2. Stress/Strain and Temperature Distributions in a DS beam Under Various Strain Rates

6.2.1. Description of the Problem

Loading, clamping and specimen geometry of the DS test have been described in Section 5.2.2. Physical and mechanical properties of BS970/En24 are given in Section 6.1, which are incorporated into the ABAQUS material model. The coupled temperature-displacement procedure in ABAQUS is available for performing fully coupled heat transfer/stress analysis, where the thermal and mechanical solutions are obtained simultaneously. A set of elements are provided for this purpose, which generally use a lower-order(linear) interpolation for temperature than for displacement(linear or parabolic) in order to obtain a compatible variation of thermal and mechanical strain. The temperatures are integrated using a backward difference scheme, and the coupled system is solved using Newton's method. In the present study, 4-node bi-linear displacement and temperature plane strain element, CPE4T is used. The validity of using a plane strain assumption will be verified in Section 6.2.4. More details about fully coupled temperature-displacement elements in ABAQUS are given in ABAQUS User's Manual(Vol.1 Section 3.2.3).

With the option of coupled-temperature-displacement procedure, "inelastic heat fraction", "specific heat" and "conductivity" options are needed. Because there is no phase change in the present problem, the "latent heat" option is unnecessary. Data of specific heat and conductivity are given in Section 5.1.1, which depend on temperature. The coefficient of inelastic heat fraction, β, is taken as 0.9. Parameters in Cowper-Symonds relationship are $D=186.7s^{-1}$ and $q=4.41$. A parameter study on β, D and q will be conducted in Section 11.2.4 and Section 6.4.

Adiabatic analysis may be used in cases where mechanical deformation causes heating and the event is so rapid that this heat has no time to diffuse through the material. Generally, the adiabatic assumption can be used for very high strain rate events while isothermal assumption is valid for very low strain rate events. For inter-medium strain rate events, heat conduction should be considered. However, the present study indicated that adiabatic behaviour is a relative concept depending on the geometry scale of the phenomenon. For example, the dynamic deformation

process may be considered as an adiabatic phenomenon on the scale of the notch section. But, it may be invalid on the scale of the stress concentration area at notch corners. This problem will be discussed further in Section 6.2.1.

FEM mesh of the DS specimen is shown in Fig.6.1. It is not necessary to model whole specimen shown in Fig.5.15(a) In Fig.6.1(a), GH is the central line of the central block. The distance from AB to the notch edge is 2mm. AB and BC are assumed to be fully clamped. While a given velocity is imposed on FG and GH. In order to maintain a constant nominal strain rate, the imposed velocity must be held constant. However, in Section 6.4, the central block velocity calculated from Section 6.3, which varies with time, will be used. The notch has four round corners with radius, 0.2mm, which are modelled by six elements as shown in Fig.6.1(b).

Numerical simulation input data are given in Table 6.1, where t is the total simulation time, Δt is the fixed time increment, W_f is the maximum transverse displacement of the central block corresponding to maximum nominal shear strain, γ_n=1.0, $\dot{\gamma}_n$ is the nominal shear strain rate, V is the imposed velocity at the boundaries FG and GH, and INC is the total incremental number.

Table 6.1 ABAQUS Simulation Data-I

No.	$\dot{\gamma}_n(s^{-1})$	t(s)	$\Delta t(s)$	INC	W_f(mm)	V(ms^{-1})	Note
DS1	$2x10^{4}$	$50x10^{-6}$	$5x10^{-7}$	100	2.0	40.0	
DS2	$5x10^{4}$	$20x10^{-6}$	$2x10^{-7}$	100	2.0	100.0	
DS4	50	$20x10^{-3}$	$4x10^{-4}$	50	2.0	0.1	
DS5	$5x10^{-2}$	20.0	0.1	200	2.0	0.0001	

6.2.2. Stress/Strain Distributions

In a DS test, the displacements of the central block and the extension supports and the reaction force at the extension supports can be recorded. It is assumed that the total reaction force at the extension supports is the same as the total force on the cross-section DE. Thus, the nominal shear stress can be defined as

$$\tau_n = \frac{F_{ED}}{A}, \tag{6-1}$$

where A is the cross-section area of DE and F_{DE} is the total transverse shear force on a notch cross-section. It will be shown later that the total transverse shear force on the notch cross-section does not vary from the mid-point to the edge of the notch. Thus, F_{DE} may be understood as the total transverse shear force at the edge of notch, i.e., cross-section DE in Fig.6.1(a). The nominal shear strain is

$$\gamma_n = \frac{W}{\Delta}, \tag{6-2}$$

where W is the displacement of central block(the extension support has negligible permanent displacement) and Δ is the notch width.

It has been shown that there exists a shear area in the notch section where the shear stress and shear strain distributions do not vary much although the stress concentration in the corners of notch are quite high(Klepaczko(1994)). The mid-point of the notch section is always within this uniform shear area. Thus, the shear stress and strain at the mid-point of a notch section will be used to model the material response. In order to obtain the true shear stress(τ)/true shear strain(γ) at the mid-point of notch section from the nominal stress/strain, the following relationships are defined

$$\tau = \alpha_1 \tau_n \quad \text{and} \quad \gamma = \alpha_2 \gamma_n, \tag{6-3a,b}$$

where α_1 and α_2 will be determined by using FEM simulations.

Three constant nominal strain rate simulations, DS2, DS4 and DS5 in Table 6.1, have been conducted for strain rates of 0.05, 50.0 and 50000.0 s^{-1}. Time variations of the transverse shear strain at the mid-point of a notch section, τ, are shown in Fig.6.2. The mid-point of the notch is in the middle of elements 210, 211, 230 and 231. However, the transverse shear strain in these four elements are almost identical, as shown in Fig.6.2(a). Therefore, in Figs.6.2(b) and (c), the outputs from element 210 are used to represent the mid-point output. Because, these problems are simulated under a constant imposed velocity, the nominal strains can be calculated from the response time, and therefore, the relationships between γ and γ_n can be

evaluated from Fig.6.2, which are demonstrated in Fig.6.3. It shows that the strain calibration factor α_2 varies slightly with both plastic strain and strain rate. Thus, a constant value of α_2=0.718 can be used to obtain the actual shear strain at the mid-point of a notch section from the nominal shear strain. No strain calibrations are given by Klepaczko(1994). Ruiz, Harding and Ruiz(1991) introduced a calibration factor, but did not show its actual value on their DS beam tests.

Stress distributions are also analyzed in these simulations. Fig.6.4(a-c) compares the mean shear stress defined by eq.(6-1) at the mid-point(curve MA) and edge(curve BA) of the notch cross-section for three different strain rates. It is found that the total transverse shear forces at the different location of a notch section are almost the same although deformation distributions may vary significantly. Therefore, the constant transverse shear force assumption in eq.(6-1) is valid for these tests within the notch section.

Since the width of the notch section is finite while the nominal shear stress τ_n is defined for an infinite layer, a calibration factor α_1 has been introduced in eq.(6-3a). Klepaczko(1994) found that α_1 has a mean value of 1.2 for $0.05<\gamma_n<1.0$ according to a static FEM simulation. Ruiz, Harding and Ruiz(1991) also introduced a constant α_1 to calibrate the results, where the actual value of α_1 is not given. Fig.6.5 give the variations of α_1 throughout the response period for various strain rate simulations. Generally, α_1 varies within a narrow range from 1.06 to 1.22 for $0.0<\gamma_n<1.0$ depending on the nominal shear strain and strain rate. It increases from a low value to its maximum at $\gamma_n\approx0.25$, then starts to decrease. Practically, this small variation may be neglected by introducing an average value, $\alpha_1\approx1.1$, which is independent of both the nominal shear strain and strain rate, and can be used in eq.(6-4a) to obtain the mid-point shear stress before material failure or thermal instability occurs. Also, this value is very close to the value(α_1=1.2) obtained by Klepaczko(1994) using static FEM simulation.

6.2.3. Temperature Effects

The temperature rise is significant in most of the present impact tests. The temperature distributions in a DS beam are shown in Fig.6.6 for three simulations, DS1, DS2 and DS4 in Table 6.1. Even at a low impact velocity(DS4), the

temperature rise in the shear section is 139°C, which has a noticeable influence on the material mechanical properties according to Chapter 5. Thus, it is necessary to consider temperature effects in both the response and failure analyses.

According to Fig.6.6, there exist three distinct areas in which temperature rise is significant; namely the tensile notch corners(point E and its opposite corner E'), shear notch corners(point D and its opposite corner D') and the main shear zone in the middle of the notch section. Generally, when the strain rate is high(DS1 and DS2), the temperature at a shear notch corner is higher than the temperature at a tensile notch corner. In the low strain rate case(Fig.6.6(c) for DS4), the main shear zone has the highest temperature up to 139°C at γ_n=1.0, and the temperatures at the shear and tensile notch corners are 106°C and 97°C, respectively, although the plastic strain energy density at both the shear and tensile corners are higher than that in the main shear zone due to the stress and strain concentrations. This is because the stress concentration area of either shear or tensile notch corner are very small and the heat produced from the dissipative plastic strain energy in these localised areas is conducted into the surrounding material when the strain rate is low. In the main shear zone, the whole material experiences the same amount of plastic deformation, and, thus, is heated simultaneously from the dissipative plastic strain energy, in which the temperature decrease due to heat conduction is not as significant as at the localised shear and tensile north corners. It has been shown in Section 5.1.2 that the yield stress at 100°C is 15% less than the yield stress at room temperature. Therefore, it is recommended that a thermal-coupling analysis with temperature effects on material properties is necessary when the characteristic strain rate is over $10^2 s^{-1}$ in a similar problem.

For the high strain rate case, the temperature in the main shear zone is lower than the temperatures at both the shear and tensile notch corners. The temperature at the shear/tensile notch corners in Fig.6.6(a) and (b) are 859/439 °C and 1050/536 °C, respectively, which are significantly higher than the corresponding temperatures of 246°C and 298°C in the main shear zone in Fig.6.6(a, b). This feature indicates that thermal softening phenomenon is more likely at the shear notch corner which coincides with the experimental observations.

According to the material property test criterion proposed in Appendix A1,

the response in the main shear zone of a DS beam before material failure could be used to evaluate the dynamic mechanical properties of the material. However, temperature effects should be taken into account in the material constitutive equations for medium/high strain rate test depending on the physical properties of the tested material. This is a common problem in any dynamic material test techniques.

Isothermal and adiabatic assumptions may simplify calculations for the temperature rise in a thermal-coupling dynamic problem. However, it is necessary to find the valid range of strain rates to use these simplifications. There are various ways to define the accuracy of a simplification depending on applications. One of them is to use the relative difference of temperature, i.e.

$$e_i=\|\frac{T-T_i}{T}\| \quad \text{and} \quad e_a=\|\frac{T-T_a}{T}\|, \tag{6-4a,b}$$

where, T is the temperature at the mid-point of a notch section when mechanical-thermal coupling and heat conduction are considered, $T_i=T_r=20^oC$ is the isothermal temperature at the same location, and T_a is the adiabatic temperature calculated from

$$T_a=T_r+\frac{\beta w_p}{\rho C_v}, \tag{6-5}$$

where, w_p is the plastic strain energy density at the mid-point of a notch section calculated by ABAQUS. It should be noted here that the "adiabatic analysis procedure" in ABAQUS assumes no heat conduction on any geometrical scale which is not suitable for the present problem, as mentioned in Section 6.2.1. The results obtained by "adiabatic analysis procedure" are obviously unrealistic even when the strain rate is high, in which plastic deformations are largely concentrated in the shear corners of the notch. This is probably due to the occurrence of material instability which prohibits large deformations. However, adiabatic behaviour is valid within the scale of a notch section, which will be discussed below based on eq.(6-5).

According to the dimensional analysis results in eq.(4-9) of Section 4.3.1, $t_{cd}=0.4(s)$ and $\dot{\gamma}_{c1}=14(s^{-1})$. Thus, principally, if the characteristic strain rate, $\dot{\gamma}_c$ is much larger than $\dot{\gamma}_{c1}$, the adiabatic assumption could be used. On the other hand, when $\dot{\gamma}_c$ is much less than $\dot{\gamma}_{c1}$, the isothermal assumption is valid, which means that the temperature rise can be neglected. When $\dot{\gamma}_c$ is in the same order as $\dot{\gamma}_{c1}$, any heat

conduction effects need to be considered. These three situations are examined by using ABAQUS FEM simulations. Table 6.2 gives data on the simulations and Table 6.3 gives the corresponding results.

It was shown by simulations using the current FEM mesh in Fig.6.1(a) that the isolated boundary has no influence on the temperature rise and distribution when $\dot{\gamma}_n \geq 10^2 s^{-1}$. When $\dot{\gamma}_n < 10^2 s^{-1}$, the heat conduction on boundaries AB, BC and FG is considered by introducing extra material to conduct heat. The dimensions of the introduced material are represented approximately by the real dimensions of the clamps, in which the temperature at the extended boundaries is fixed at room temperature. This is accurate enough to model the heat conduction at the boundaries. There is an obvious improvement on the temperature distributions from the model in Fig.6.1(a) according to our simulation results.

Table 6.2 ABAQUS Simulation Data-II

No.	$\dot{\gamma}_n(s^{-1})$	t(s)	Δt(s)	INC	W_f(mm)	V(ms^{-1})	Note
TT1	10^{-3}	1000	2	500	2.0	$2x10^{-6}$	#a
TT2	10^{-2}	100	0.5	200	2.0	$2x10^{-5}$	#a
TT3	10^{-1}	10	0.1	100	2.0	$2x10^{-4}$	#a
TT4	1	1	0.01	100	2.0	$2x10^{-3}$	#a
TT5	10	0.1	0.001	100	2.0	$2x10^{-2}$	#a
T6	10^2	0.01	10^{-4}	100	2.0	0.2	
T7	10^3	0.001	10^{-5}	100	2.0	2	
T8	10^4	10^{-4}	10^{-6}	100	2.0	20	
T9	10^5	10^{-5}	10^{-7}	100	2.0	200	

#a: Extra materials are introduced to eliminate boundary effects on heat conduction.

Table 6.3 Simulation Results From Table 6.2

No.	TT1	TT2	TT3	TT4	TT5	T6	T7	T8	T9
T	20.1	21.4	26.6	46.7	119.6	150	184	230	314
T_a				122	133.9	153	184	230	314
T_c				48	76	130	245	437	699
T_{ca}				536	556	610	754	996	1358
e_i(%)	0.5	6.5	24.8	57.2	83.3				
e_a(%)				161.	12.0	2.0	0.0	0.0	0.0
Note	#b	#b	#b	#b	#b	#b	#c	#c	#c

T_c is the average temperature at the upper-shear notch corner and T_{ca} is the adiabatic value of T_c according to eq.(6-5). All temperatures have unit °C.
#b: Maximum temperature occurs at the mid-point of notch section when the strain rate is low
#c: Maximum temperature occurs at the up-shear notch corner with high strain rates.

Two typical curves for the variation of T and T_a with response time up to γ_n=1.0 are shown in Fig.6.7. It indicates that the adiabatic simplification in eq.(6-6) for the notch section response is accurate when $\dot{\gamma}_n \geq 10^2 s^{-1}$, as shown in Fig.6.7(b). However, the difference between the adiabatic simplification and the heat conduction analysis becomes significant for a decreasing strain rate, as shown in Fig.6.7(a). Variations of e_i and e_a with logarithm strain rate are shown in Fig.6.8. If the accuracy of isothermal and adiabatic simplifications are controlled by 10% of e_i and e_a, it is found that isothermal and adiabatic simplifications based on the scale of the notch section can be used for $\dot{\gamma}_c < 10^{-2}(s^{-1}) << \dot{\gamma}_{c1}$ and $\dot{\gamma}_c > 10^2(s^{-1}) >> \dot{\gamma}_{c1}$, respectively, and heat conduction should be considered for $\dot{\gamma}_c \sim \dot{\gamma}_{c1}$, which agree with the dimensional analysis results in eq.(4-9). It is necessary to remember that the scale of a notch section is used in the dimensional analysis. Thus, the result obtained is valid on this scale. In Table 6.3, the temperature at the upper-shear corner of the notch where localised stress concentration is very severe is compared with the adiabatic temperature. Although the difference between T_c and T_{ca} decreases with increasing strain rate, there is still quite a large difference at $\dot{\gamma}_n = 10^5(s^{-1})$, which means that adiabatic simplification for the localized stress concentration at the upper-shear corner of the notch is not valid up to $\dot{\gamma}_n = 10^5(s^{-1})$. A much smaller space scale should be used in dimensional analysis to find the valid strain rate range of the adiabatic simplification in this local area, which will not be discussed here. It is expected that the

observations in this particular problem are generally true, but, more verification on other dynamic problems are necessary before they can be accepted.

6.2.4 Verifications on Plane Strain Modelling and Material Parameters

The actual geometry of the modelling specimen does not belong to either plane strain or plane stress. However, due to the intensive "in-plane" deformation within the notch section, the effect of "out-plane" constraint may be neglected. Thus, it is expected that plane strain and plane stress elements give similar results, which will be verified through an example.

The FEM model DS4 in Table 6.1 is simulated after changing the plane strain element type, CPE4T, into plane stress element type, CPS4T. As expected, the variations due to employing the plane stress assumption are negligible when comparing with the corresponding plane strain results. One calculated example is shown in Fig.6.9 for von-Mises equivalent stress. The maximum relative difference between using plane strain and plane stress assumptions is 3.3% after yielding.

In the DS beam test, material failure is found in the notch corner when the impact velocity is in the range of 40m/s to 50m/s. Thus, DS1 in Table 6.1 with imposed boundary velocity, 40m/s, is used to verified the influence of Taylor-Quinney coefficient β and the parameters, D and q in the Cowper-Symonds relationship on the response of a DS beam. The parameters used in simulation are shown in Table 6.4. Fig.6.10 (a,b) show the plastic equivalent strain and histories in the middle and tensile corner of a notch section. The maximum relative differences on final equivalent plastic strain and final plastic strain energy density for β=0.0 and β=0.9 is 10% and 4.4%, respectively. Thus, the influence of β on deformations in the notch section within the discussed impact velocity range is negligible. It is also shown that the influence of the parameters in Cowper-Symonds relationship on plastic equivalent strain history is very small. More parameter verifications will be presented in Section 6.4 according to the DS beam test results.

Table 6.4 Parameters Used in Verification

Curve No.	β	D(s^{-1})	q
EM_210	0.9	186.7	4.41
ERM_210	0.9	6948.3	5.132
EB00M_210	0.0	186.7	4.41
EB05M_210	0.5	186.7	4.41
ECA	0.9	186.7	4.41
ERCA	0.9	6948.3	5.132
EB00CA	0.0	186.7	4.41
EB05CA	0.5	186.7	4.41

6.3. Analytical Model of Central Block Motion

The problem is simplified as a fully supported DS beam, shown in Fig.5-15. A projectile travelling with a velocity V_0 impacts on the impact pad, a given thickness square sheet which is made from hardened steel and used to control the travelling distance of the projectile. After impact, the projectile, impact pad and the central block move together with a common velocity when ignoring stress wave propagation effects. The initial velocity of the central block is estimated by momentum conservation,

$$V_i=\frac{M}{M+m_p+m}V_0 \tag{6-6}$$

in which, M is the mass of projectile, m is the mass of central block, and m_p is the mass of impact pad. According to the analysis in Section 6.2, the transverse shear force along the notch section is almost constant. Thus, the force acting on the boundary of the central block is $\tau_n A$, where τ_n is the nominal shear stress defined by eq.(6-1), A=bh, where b and h are the width and thickness of a notch section.

Therefore, the movement in this stage is governed by

$$(M+m+m_p)\frac{dV}{dt}=-2\tau_n A, \tag{6-7}$$

where, V is the velocity of the central block of the DS specimen. The initial conditions are

$$V(t=0)=V_i \quad \text{and} \quad W(t=0)=0, \tag{6-8}$$

where, V_i is given by eq.(6-6) and W is the transverse displacement of the central block.

After travelling a fixed distance determined by the thickness of the impact pad, the projectile is stopped by the surrounding stoppers and the impact pad is separated from the central block. Thus, the equation of motion is

$$m\frac{dV}{dt}=-2\tau_n A \tag{6-9}$$

after $t=t_1$, which is determined by

$$W(t=t_1)=d \tag{6-10}$$

from eqs.(6-7) and (6-8), where d is the thickness of the impact pad.

In the above formulation, deformations of the impact pad and projectile are neglected because their stiffness is relatively larger than the stiffness of the DS specimen. Wave propagation effects in the specimen are not considered because the characteristic time of wave propagation in the central block is only about 4μs which is much shorter than the response time.

Relationships between the nominal shear strain(rate) and the true shear strain(rate) at the mid-point of a notch section are

$$\gamma_n=\frac{W}{\Delta} \quad \text{and} \quad \dot{\gamma}_n=\frac{V}{\Delta}, \tag{6-11a,b}$$

in which, Δ is the width of notch section.

Shear stress-strain relationship in Section 5.1.2 can be expressed by

$$\tau=\tau_{st}[1+(\frac{\dot{\gamma}(s^{-1})}{323.4})^{\frac{1}{4.91}}][1-\frac{(T(^{o}C)-20)^{0.65}}{116}] \qquad (6\text{-}12)$$

where, the temperature is obtained from eq.(1-12) by using the adiabatic simplification which has been proved to be valid in Section 6.2 for the present impact velocity range, and τ_{st} is given by

$$\begin{gathered}\tau_{st}=223.84(MPa) \quad \text{for} \quad 0\le\gamma\le 0.01126,\\ \tau_{st}=223.84(MPa)+533.29(MPa)(\gamma-0.01126)^{0.45}\\ \text{for} \quad 0.01126<\gamma\le 0.16,\\ \text{and} \quad \tau_{st}=411.8(MPa)+249.7(MPa)\gamma \quad \text{for} \quad \gamma>0.16.\end{gathered} \qquad (6\text{-}13)$$

The final displacements of a DS beam have been obtained in Section 5.3, which are compared with the current theoretical predictions, as shown in Fig.6.11. Generally, the theoretical predictions for both the 1.5mm and 2.0mm pad thickness tests are lower than the experimental results. One important factor responsible for this phenomenon is the local shear and tensile failures at the notch corners which reduce the transverse strength of the notch section, which is not considered in the analytical model. However, in general, the agreement between experimental and theoretical results is fairly reasonable, which gives a good assessment on observations obtained in Section 6.2. The method proposed in this section will be use to predict the velocity-time history that can be used in the next section for a FEM simulation on the DS beam tests.

6.4. FEM Simulation On the Failure behaviour of a DS Beam

The dynamic response of a DS beam under projectile impact described in Chapter 5 is simulated by using ABAQUS FEM software with the input impact velocity-time history predicted in Section 6.3. A typical deformation process of the notch section of specimen NT6 is shown in Figs.6.12(a-d). It shows that most of the notch section experiences transverse shear deformations. The transverse shear deformations in the middle area are quite uniform throughout the duration of response, which is one of the advantages of DS beam specimens for material testing. The equivalent stress, strain, strain rate, plastic strain energy density and temperature histories at the middle point of the notch section are given in Figs.6.13(a-e). The

average strain rate is about $4x10^3s^{-1}$. The plastic strain energy density and temperature curves are related each other according to eq.(6-5). Thus, the response of the notch section can be classified as an adiabatic response.

Two failure modes have been observed in Section 5.3 on a DS beam under projectile impact. Shear failure appears at the upper-shear(US) and lower-shear(LS) notch corners, as shown in Section 5.3.1. While tensile failure occurs at the upper-tensile(LT) and lower-tensile(LT) notch corners. It is not the purpose of this section to describe the whole post-failure process of the DS-beam, which would need mesh reconstructing by removing failed elements and redefining boundary conditions. This is still a difficult topic for many failure problems. However, the mechanical conditions to initiate these failure modes can be studied by using FEM simulations, which is the primary in a structural failure problem, and has not been fully understood with satisfactory confidence for most practical problems.

It has been shown that adiabatic shear banding appears when the impact velocity approaches 60m/s. The location of adiabatic shear banding is at either the upper-shear(US) corner or lower-shear(LS) corner(or both of them) within the notch section, where the stress concentration is very severe and would not be predicted on the basis of the nominal shear stress and strain. Thus, using a DS beam to study the shear banding phenomenon is unrealistic in the present experimental configurations unless the stress concentration at the shear corner is understood well.

A shear band normally originates from a non-homogeneous deformation phase followed by a localization phase, which was observed by Marchand and Duffy(1988) for the formation of shear bands in a thin-walled steel tube. It is generally accepted that the maximum shear stress criterion predicts the initiation of the non-homogeneous deformation phase, and thus, has been used as the criterion for the initiation of an adiabatic shear band. However, this has been confirmed only on a system where the deformation within the gauge length is one-dimensional, such as the tube test on SHPB. In the present case, where the formation of an adiabatic shear band is very local and has little influence on the global response of the DS beam, this criterion does not predict the initiation of a shear band. In Fig.6.13(a), the von-Mises equivalent stress at the mid-point of a notch section, which consists mainly of transverse shear stress, reaches its maximum value at $t \approx 17.5\mu s$. However, it does not

correspond to the initiation of an adiabatic shear band. The decrease of the shear stress is due to the decrease of strain rate controlled by the external energy input, but not due to the thermal softening of the material. Thus, the maximum stress criterion should be reconsidered in these situations.

In order to simulate the formation of a shear band, a special mesh design is necessary. Most of the FEM simulations are based on some well-defined plastic deformation patterns determined by given boundary condition, such as simple shear. The loading rate, or external energy input is continuous. In this case, the drop of the resistant force, or shear stress, is purely from a thermal softening factor. Therefore, it could be used to predict the initiation of a shear band. In the present case, it is extremely difficult to determine the boundary conditions around the local shear corner in the notch section of a DS beam. The current mesh design is also too coarse to model the shear banding phenomenon. Further efforts are necessary on the shear banding initiation in a DS beam. The following discussion is concentrated on the tensile failure in the notch.

It has been shown in Chapter 1 that there are various failure criteria which may be used to predict material ductile failure. Six different failure criteria discussed in Section 1.3 will be examined here, which are maximum normal stress failure criterion, maximum shear stress(or Tresca) failure criterion, von-Mises equivalent stress failure criterion, maximum plastic tensile strain failure criterion, equivalent plastic strain failure criterion, maximum plastic shear strain failure criterion and plastic strain energy density failure criterion. The following simulations are based on the velocity-time history developed in Section 6.3 and the FEM model is the same as that in Section 6.2.

According to the experimental observations on material tensile failure in a DS beam, all tensile failures initiate from the UT and LT notch corners. The critical impact velocity is between 40.3m/s(specimen NT7 without failure) and 47.3m/s(specimen NT5 with failure), as shown in Table 5.12. The maximum failure indexes under this critical impact velocity, such as equivalent plastic strain and maximum plastic strain energy density, occur at the middle elements at the corner of a notch described in Fig.6.1(b), will be used to examine the validation of the available failure criteria.

Table 6.5 gives the predicted values from DS beam tests and ABAQUS FEM simulations, which are compared with the measured values in material tests described in Table 5.6. The impact velocities for NT5 and NT7 are 47.3m/s and 40.3m/s, respectively. Tensile failures are found in all specimens when the impact velocity is higher than 47.3m/s. But, there is no any tensile failure when the impact velocity is lower than 40.3m/s. One exception is NT23 that does not fail at an impact velocity of 47.7m/s. The impact pad for NT23 is 1.98mm, which is different from the pad thickness used for NT5 and NT7. Thus, it is believed that the critical velocity to initiate tensile failure at the corner of a notch is between 40.3m/s and 47.3m/s. The predictions for various failure indices at these two impact velocities are given in Table 6.5.

It observed that plastic strain energy density failure criterion obtained from static tensile test gives a reasonable prediction for failure initiation. Stress failure values from material tests are smaller than the values at failure in the tensile notch corner. But, strain failure values are higher than the predicted values at failure. The variations of the maximum values of ε^p_{eq} and w^p with the impact velocities are calculated using ABAQUS, and compared with the critical values of ε^p_{eq} and w^p, as shown in Fig.6.14(a,b). The FEM simulation results show that the maximum values of ε^p_{eq} and w^p occur at the upper tensile corner, which is contrast to the experimental observations that tensile failures are more likely to initiate from the lower tensile corner. However, the difference in the maximum value for ε^p_{eq} and w^p is not significant between the UT and LT corners according to the ABAQUS simulations. For example, the maximum values of w^p are 652.4MJ/m^3 and 576.5MJ/m^3 at UT and LT corners, respectively, when the impact velocity is 40m/s. Thus, their average value will be used to give the maximum value in failure prediction. Obviously, bending effects cause the LT corner to fail more easily than the UT corner. The critical value of ε^p_{eq}, ε^p_{eqc}, is the static natural strain based on the zero gauge length defined in Appendix A1, which has an average value of 0.648 according to Table 5.6 for specimens SP2 and SP3 at room temperature. This value increases with temperature, as shown in Fig.5.12. The critical value of w^p, w_c^p, is calculated from the uniaxial true stress-true strain relationship at room temperature given by eq.(5-6).

Table 6.5 Critical Values of the Failure Indices(β=0.9, D=186.7s^{-1}, q=4.41)

Failure Criterion	Material Test Value	Predicted Value(NT7)	Predicted Value(NT5)
σ_{max}(MPa)	1211.8*	3230.0	3410.0
σ_{Tresca}(MPa)	605.9*	1512.0	1595.5
σ_{Mises}(MPa)	1211.8*	2619.0	2763.0
ε^p_{max}	0.648	0.264	0.294
ε^p_{eq}	0.648#	0.231	0.337
ε^p_{max}-ε^p_{min}	0.972#	0.461	0.587
w^p(MJ/m^3)	606.64	599.0	816.0

*:$2\sigma_{Tresca}=\sigma_{max}=\sigma_{Mises}$ in uniaxial tensile test; #: For plastic incompressible material.

Table 6.6 Critical Values of the Failure Indices(β=0.9, D=6948.3s^{-1}, q=5.132)

Failure Criterion	Material Test Value	Predicted Value(NT7)	Predicted Value(NT5)
σ_{max}(MPa)	1211.8	2109.0	2163.0
σ_{Tresca}(MPa)	605.9	986.0	1011.5
σ_{Mises}(MPa)	1211.8	1708.0	1752.0
ε^p_{max}	0.648	0.341	0.430
ε^p_{eq}	0.648	0.394	0.473
ε^p_{max}-ε^p_{min}	0.972	0.680	0.815
w^p(MJ/m^3)	606.64	598.7	747.6

Table 6.6 gives simulation results using $D=6948.3s^{-1}$ and $q=5.132$ in order to examine the validity of parameters used in Cowper-Symonds relationship. Similar conclusions are obtained from the results in Table 6.6, i.e., only plastic strain energy density failure criterion gives a reasonable failure prediction. It should be noted that these two sets of Cowper-Symonds parameters used in Tables 6.5 and 6.6 offer upper and lower bounds of the actual property of material strain rate sensitivity, as discussed in Section 5.1.3. Thus, the strain energy density failure criterion is the only suitable one in the current problem to predict material failure at the tensile corner of a notch section.

According to the results from Table 6.5 and Fig.6.14(a), the equivalent strain failure criterion does not agree with the experimental results. The actual tensile failure appears at a value of ε^p_{eq} which is much lower than 0.648. The local temperature at the failure site is about 150°C when the impact velocity is 45.0m/s, which leads to less than 10% increase on ε^p_{eqc}. The strain rate effect is another important factor that may reduce material ductility significantly. Thus, the actual value of ε^p_{eqc} at the failure site is between 0.3-0.35 corresponding to an average strain rate of $\sim 10^4(s^{-1})$ according to ABAQUS analyses, which is much lower than the static one. Generally speaking, two factors may contribute to this result. One is the strain rate effect on failure strain, which has not been studied thoroughly. Another factor is the stress triaxiality, which may reduce the failure strain. In uniaxial tensile test, the value of stress triaxiality, σ_H/σ_e, is 0.33. The time history of the average stress triaxiality at the upper-tension corner is calculated by using ABAQUS, as shown in Fig.6.15 for specimen NT7. The value of σ_H/σ_e is 0.655 at the end of response, which is the double of the value in uniaxial tensile test. It has been shown by Alves(1996) that the equivalent fracture plastic strain goes down from 1.0 at $\sigma_H/\sigma_e=0.4$ to 0.5 at $\sigma_H/\sigma_e=0.8$(see Fig.3.11 in Alves(1996). A similar observation on this phenomenon is reported by Holmes, et al.(1993). Thus, this may be the important reason for the reduction of the equivalent plastic strain at failure.

w_c^p gives a good prediction for the tensile failure initiation. The actual failure occurs at w_c^p between 599-816MJ/m^3, which is somewhat higher than $w_c^p=606.64$MJ/m^3 obtained in a static tensile test. However, the static critical value of plastic strain energy density is reasonably close to the predicted value in an actual

failure. This result supports the postulate proposed in Appendix B that both temperature and strain rate effects on w^p_c are small. Thus, a plastic strain energy density failure criterion appears to be a more promising procedure in the present work for predicting failure than other stress and strain type failure criteria examined in the present paper. It is possible that other failure criteria are applicable when other influencing factors, such as strain rate, temperature and hydrostatic effects, are identified in material failure tests. However, this requires more advanced measuring techniques and extra tests.

ABAQUS simulations indicated that the maximum temperature at the critical impact velocity of the corner tensile failure is around 150°C, which has little influence on the uniaxial failure strain, as shown in Fig.5.12. The temperature effects on uniaxial failure stress up to 300°C are negligible according to the recorded data in Table 5.10. It has been shown in Section 6.2.4 that the Taylor-Quinney coefficient has little influence on the DS beam response when the impact velocity is around 40m/s. This conclusion is confirmed by Fig.6.16 where the variations of maximum plastic strain energy density at critical impact velocities (for both NT5 and NT7) with coefficient β are presented.

6.5. Conclusions

The response and failure of a DS beam when subjected to a projectile impact are studied in the present Chapter. With the aid of a FEM simulation, the details of the stress and strain distributions in the notch section are obtained, and are used to set up relationships between the nominal values of stress/strain and their actual values in the major shear zone within the notch section. This information is particularly useful when using a DS beam for a dynamic shear test. Temperature effects are discussed in the present analysis by using a coupled-temperature-displacement procedure in ABAQUS.

Due to the high stress intensity at the notch corners in a DS beam, two types of material failures may be initiated easily in these locations, i.e., tensile and shear failures. Among several failure criteria examined in the present work, i.e., the failure criteria defined by maximum normal stress, maximum normal plastic strain, von-Mises equivalent stress, equivalent plastic strain, maximum shear stress and

maximum plastic shear strain, the plastic strain energy density failure criterion gives a good prediction for the initiation of a tensile type failure. Parameter verifications are conducted to ensure correct material property modelling is used in the simulation. A shear failure is normally associated with adiabatic shear banding due to material instabilities. Comments are made on further studies on simulating adiabatic shear band initiation in the notch section of a DS beam.

It is concluded that a DS beam specimen satisfies the requirement for a material property test, proposed in Appendix A1. However, this is only applicable up to the initiation of material failure. It is difficult to obtain a material failure index from a DS beam test because it fails due to stress concentration locations at the notch corners.

Both FEM and analytical models are used in the analyses. Predictions are compared with experimental results with reasonable agreement for the central block motion and tensile failure initiation.

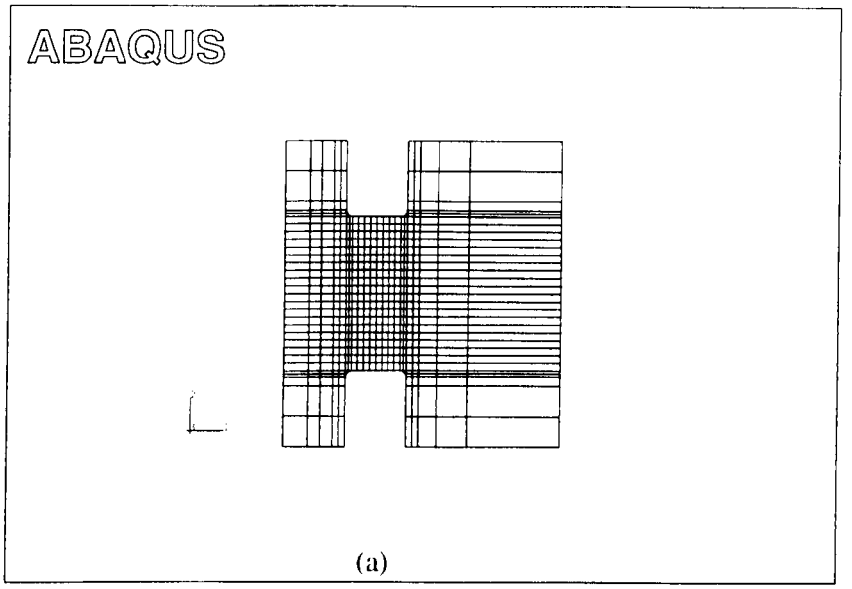

(a)

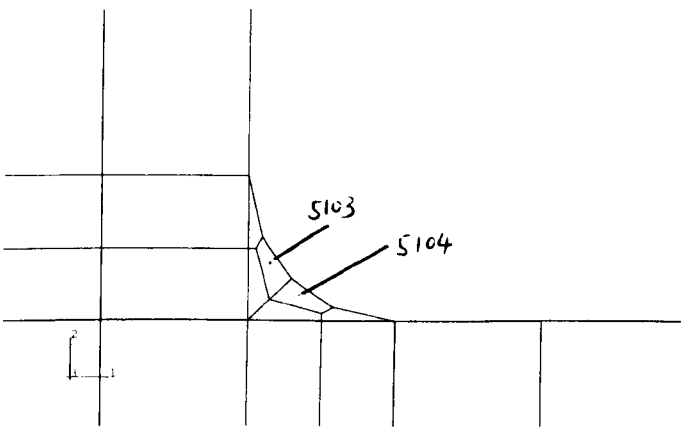

(b)

Fig.6.1 (a) FEM model of a DS beam; (b) Mesh of the notch corner.

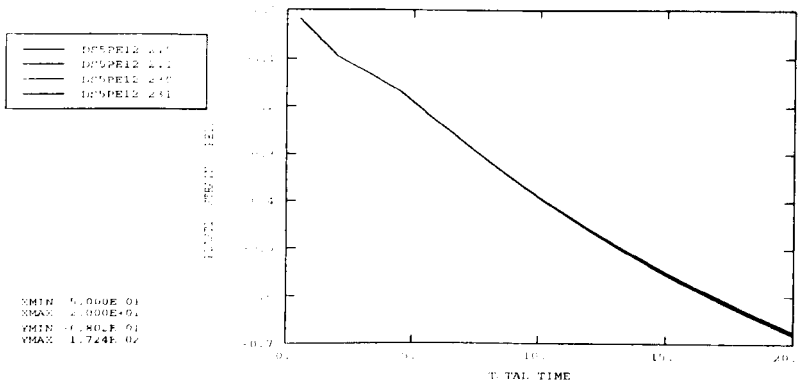

(a)

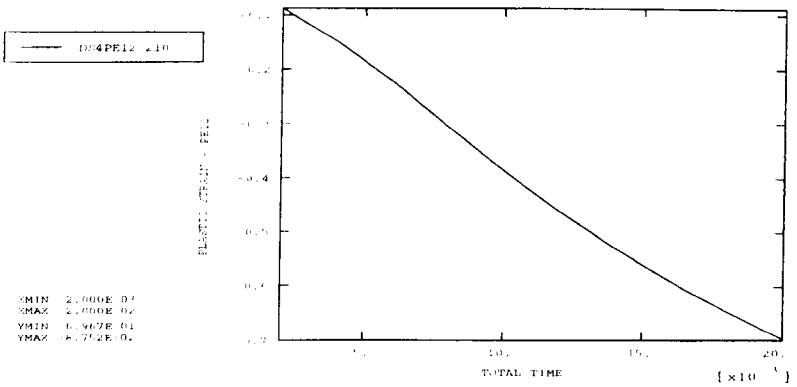

(b)

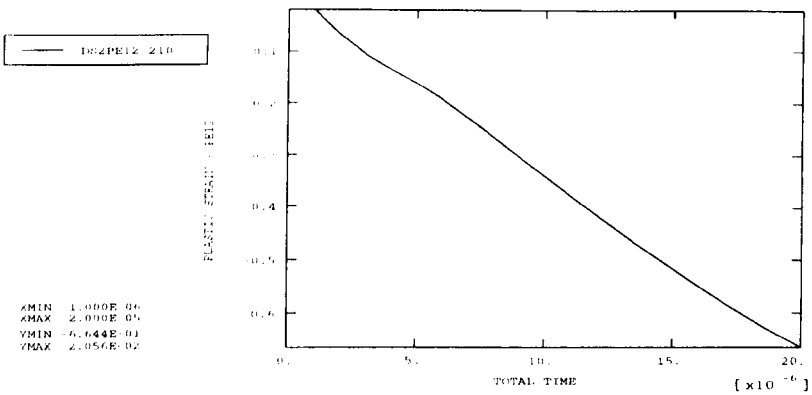

(c)

Fig.6.2 Variations of plastic shear strain with time(s), (a) DS5; (b) DS4; and (c) DS2.

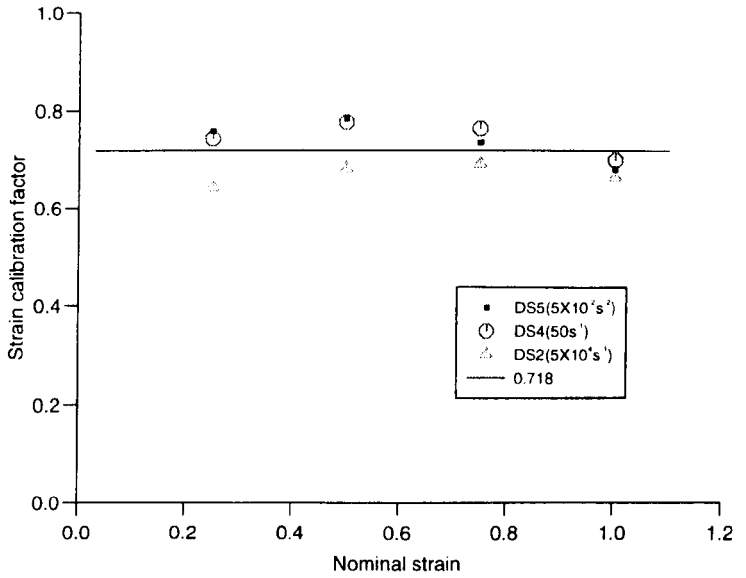

Fig.6.3 Variation of shear strain calibration factor with nominal shear strain for different strain rate simulations, ■: DS5; ○: DS4; ▲: DS2.

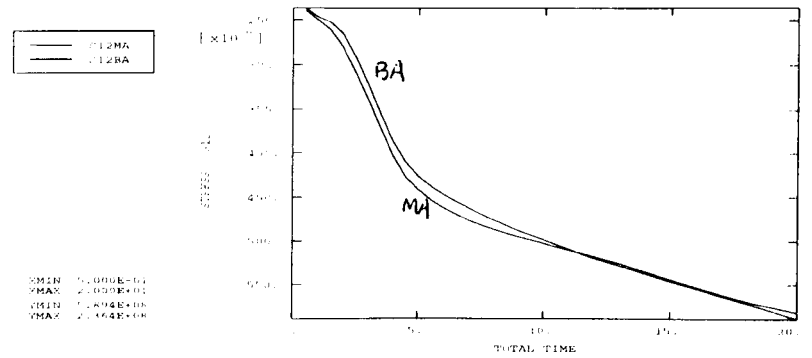

(a)

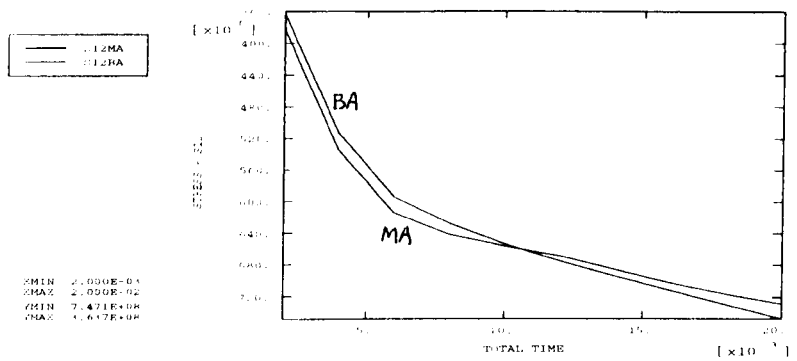

(b)

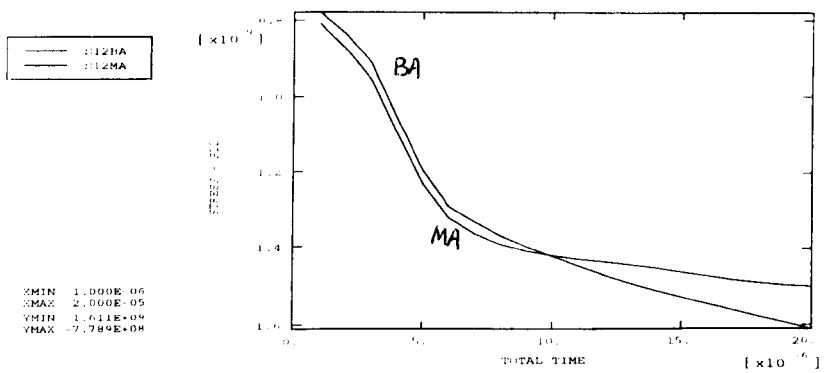

(c)

Fig.6.4 Variation of the mean shear stress on the cross-section of notch with time, (a) DS5; (b) DS4; and (c) DS2, MA: at the mid-point of notch, BA: at the edge of notch.

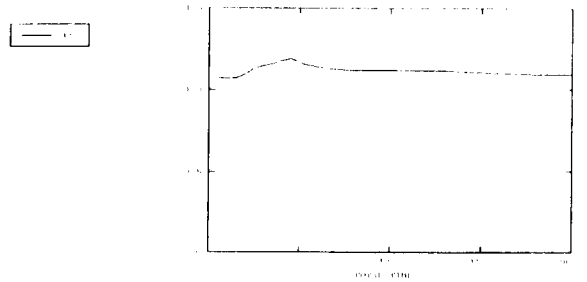

(a)

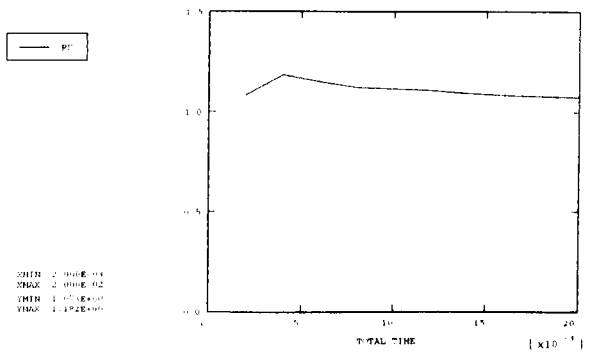

(b)

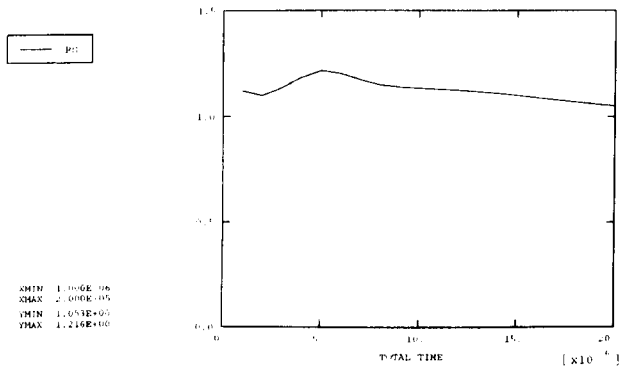

Fig.6.5 Variations of shear stress calibration factor with time(nominal shear strain) for different strain rates, (a) DS5(average value α_I=1.108); (b) DS4(average value α_I=1.108); (c) DS2(average value α_I=1.118).

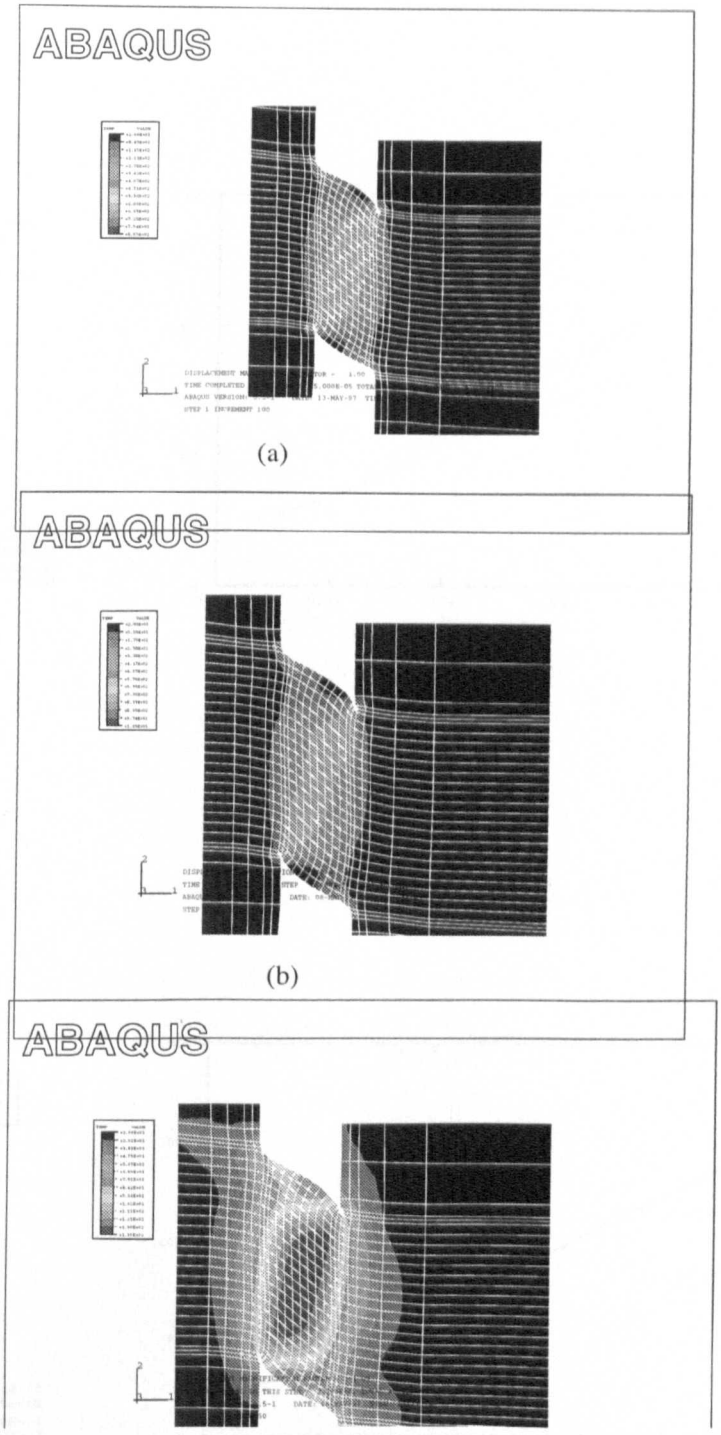

Fig.6.6 Temperature distribution in a DS specimen at nominal shear strain, γ_n=1.0, (a) DS1(V=40m/s, $\dot{\gamma}_n$=20000s^{-1}); (b)DS2(V=100m/s, $\dot{\gamma}_n$=50000s^{-1}); (c) DS4(V=0.1m/s, $\dot{\gamma}_n$=50s^{-1}).

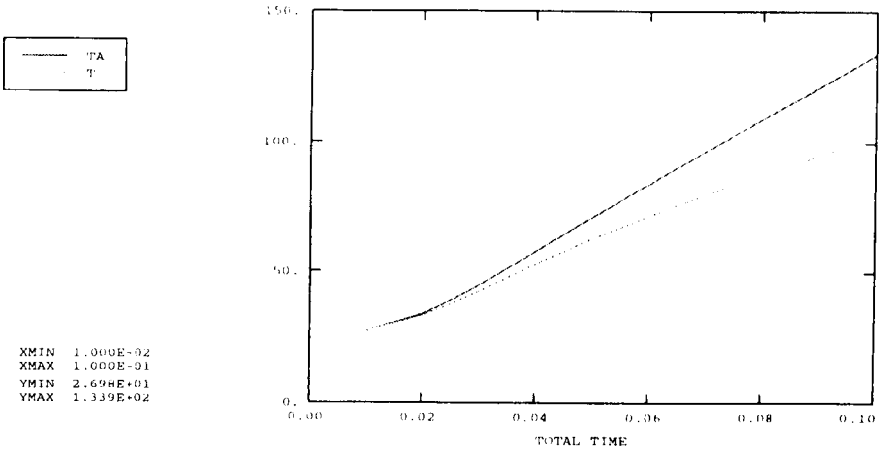

(a)

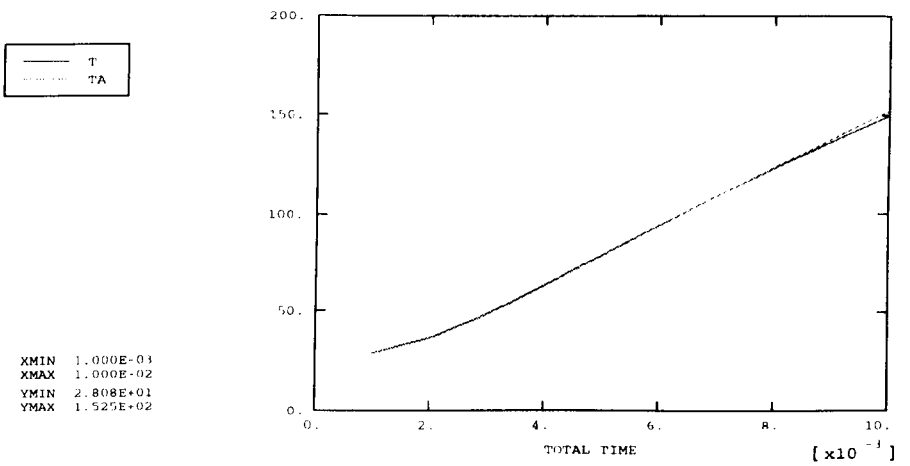

(b)

Fig.6.7 Variations of T(with heat conduction) and T_a(adiabatic simplification) with time, (a) TT5; (b) T6 in Table 6.2.

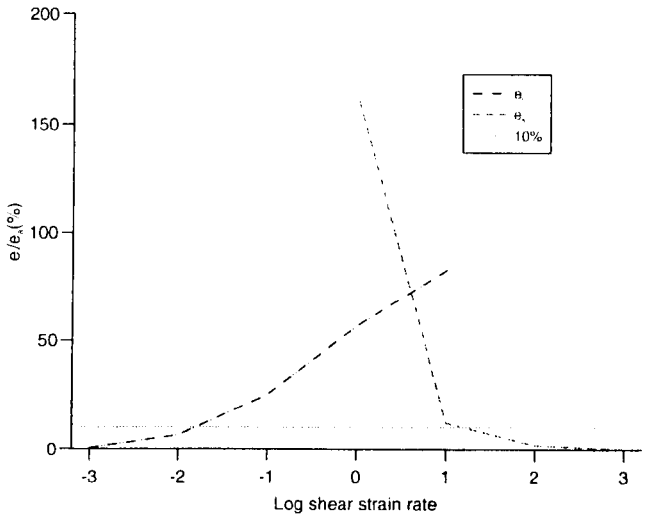

Fig.6.8 Variation of e_i and e_a with logarithm strain rate according to Table 6.3.

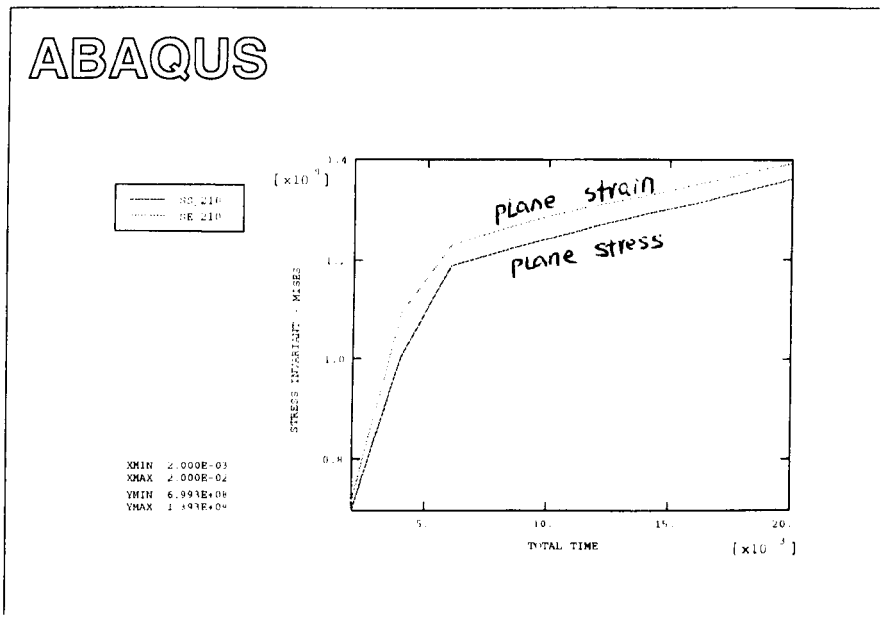

Fig.6.9 Comparison between plane strain and plane stress idealizations.

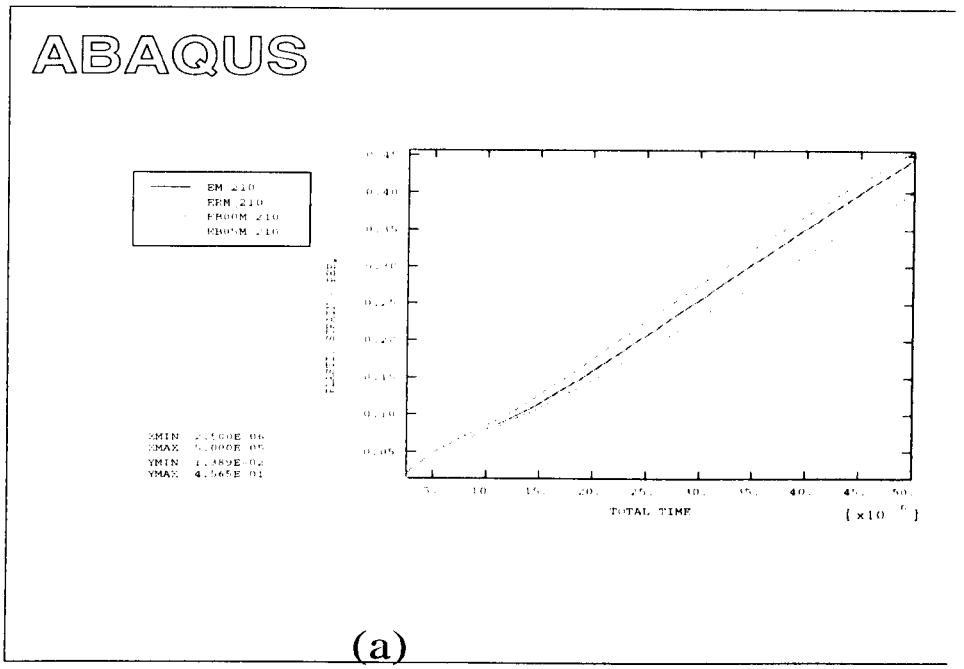

(a)

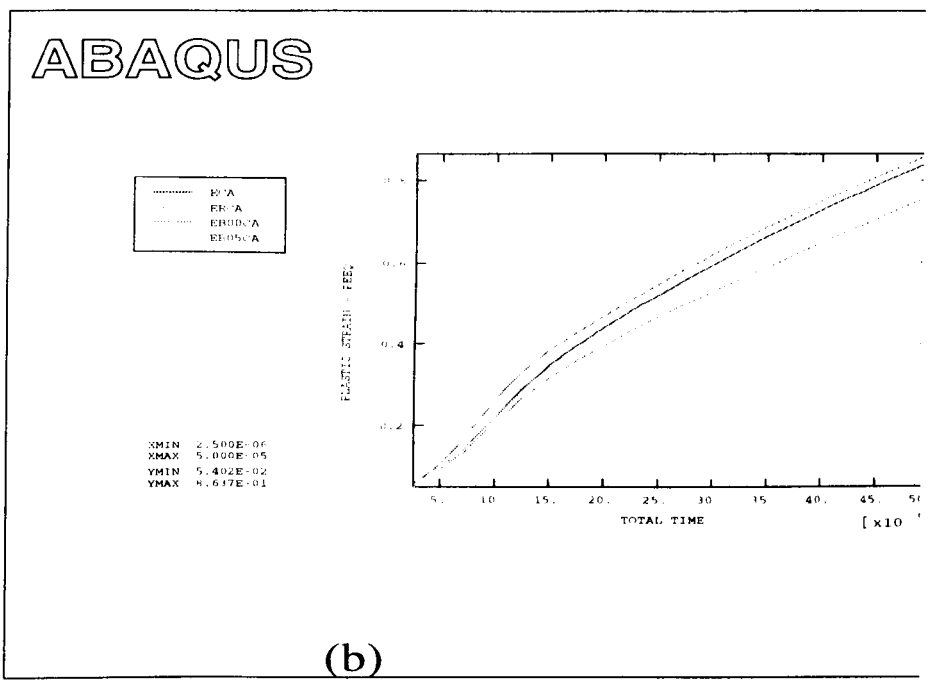

(b)

Fig.6.10 Equivalent plastic strain histories at (a) middle, (b) Tensile corner, of the notch section for various material parameters in Table 6.4.

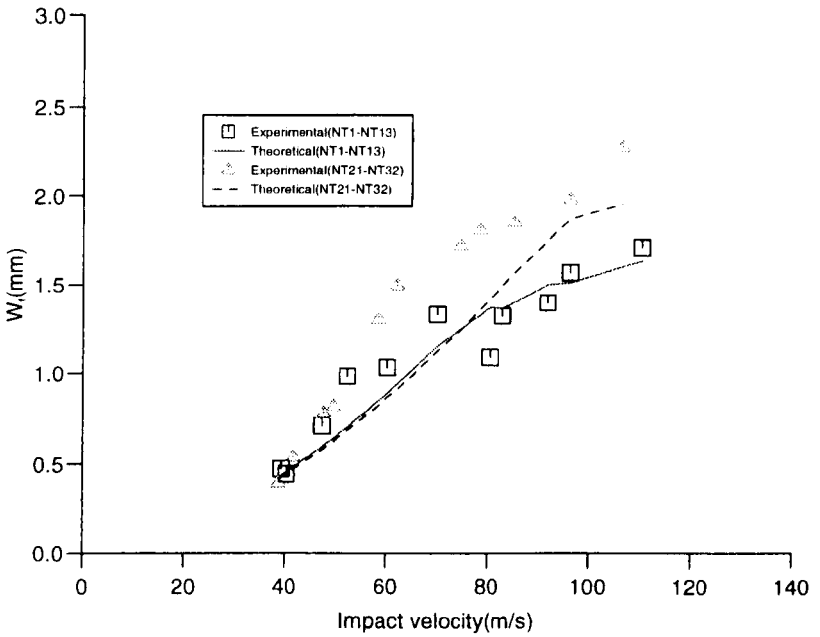

Fig.6.11 Comparison between experimental and theoretical results on final transverse displacement of DS beam.

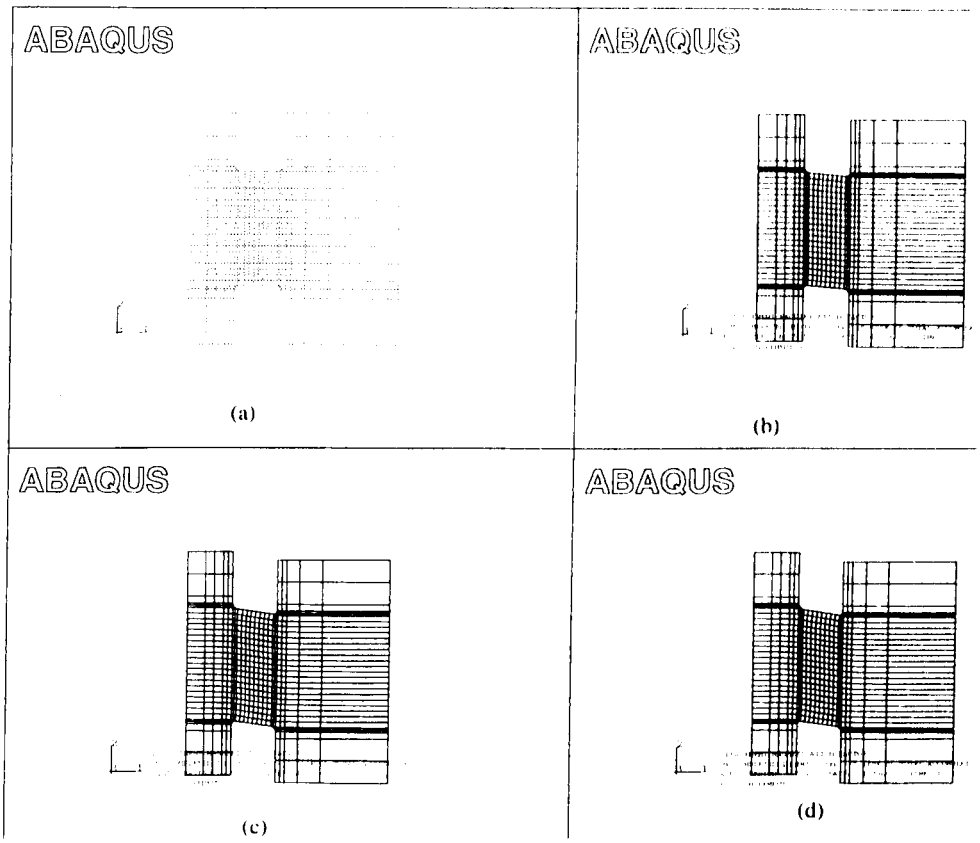

Fig.6.12 Deformations of the notch section of NT6 at, (a) t=0μs; (b) t=8μs; (c) t=16μs, and (d) t=25.6μs.

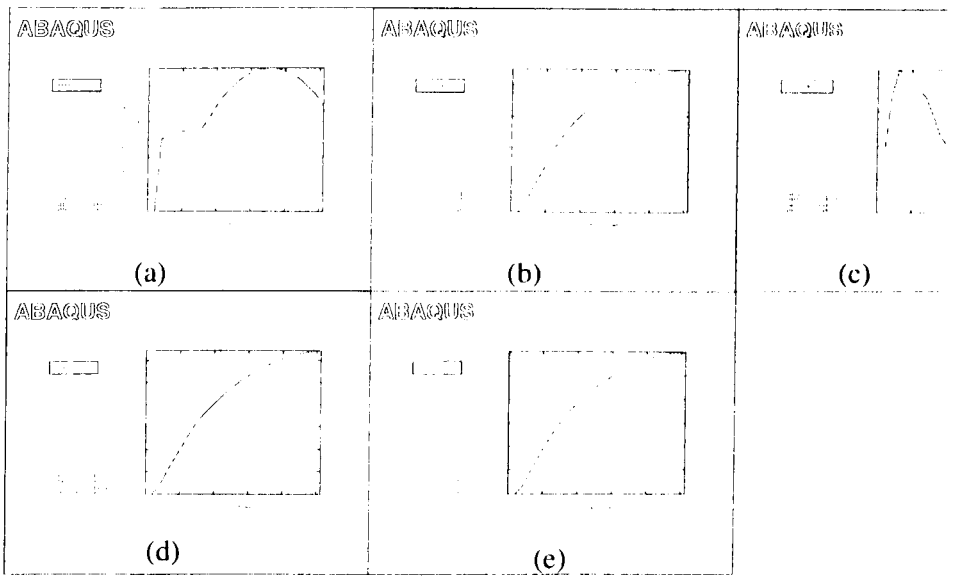

Fig.6.13 Response histories of (a) Mises equivalent stress; (b) Plastic equivalent strain; (c) Plastic equivalent strain rate; (d) Plastic strain energy density, and (e) Temperature, at the middle point of notch section of NT6.

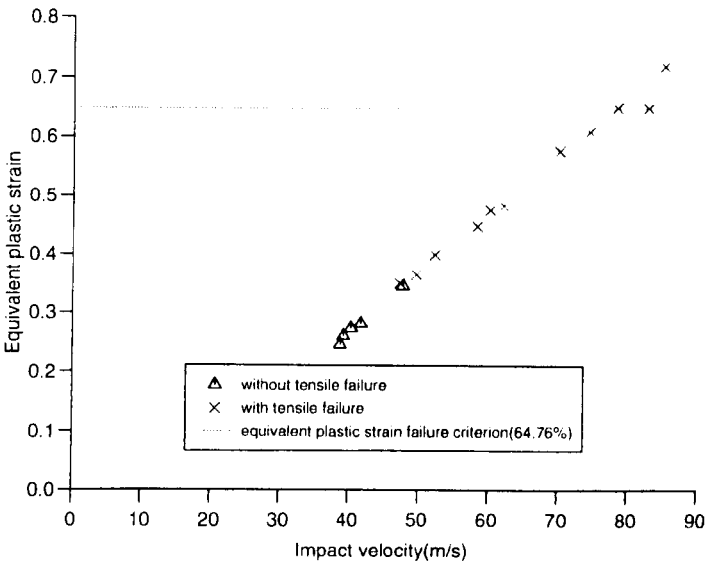

(a)

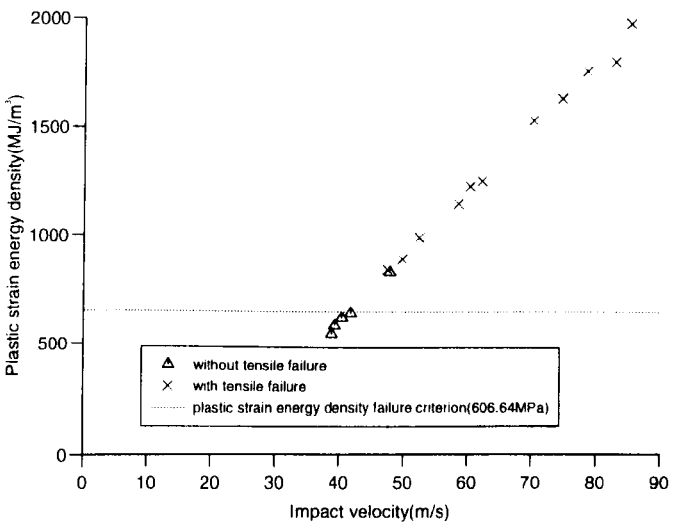

(b)

Fig.6.14 Predictions of tensile failure initiation in notch section of a DS beam, (a) Equivalent plastic strain; (b) Plastic strain energy density.

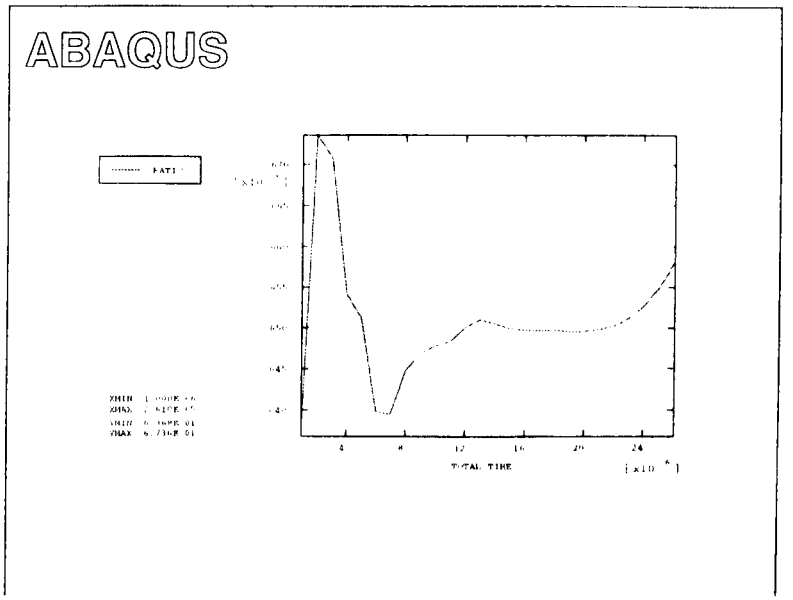

Fig.6.15 Variation of stress triaxiality, σ_H/σ_e, at the upper tension corner of specimen NT7.

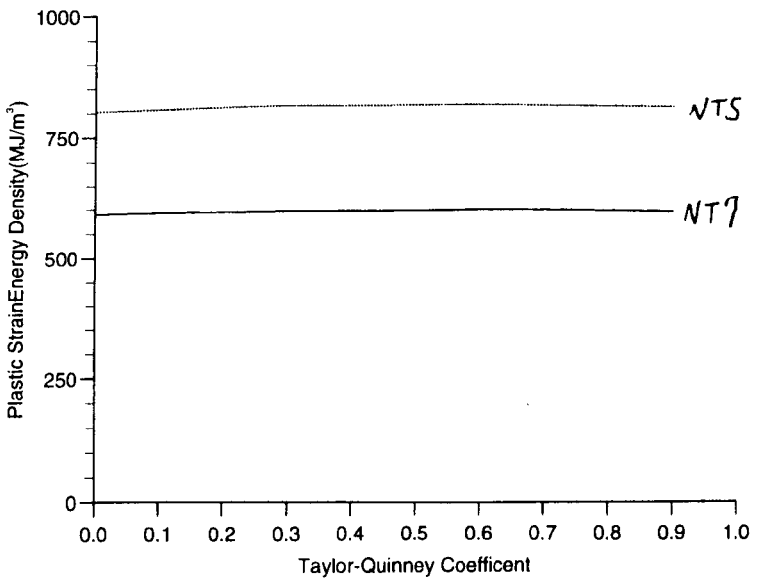

Fig.6.16 Dependence of the predicted plastic strain energy densities for NT5 and NT7 on the Taylor-Quinney coefficient.

7 CONCLUSIONS

Structures used to sustain transverse dynamic loads have been used widely in many applications. Transverse shear localization in some basic structural elements under transverse dynamic loads may reduce significantly structural strength, which is studied in the present thesis. The main achievements of the present work are given below with a discussion on existing problems and suggestions for further work.

7.1 Dynamic Shear Localization in Transversely Loaded Structural Elements

In dynamic plastic structural response, shear localization is represented by a so-called shear hinge. The existence of a shear hinge is based on experimental observations and Symonds'(1968) proof that a shear interface in rigid, perfectly plastic beam is always stationary when its yielding behaviour is based on a condition which has no interaction between bending and shearing. Symonds' conclusion on a shear interface is extended into several frequently used structural elements, including beams, plates and cylindrical shells in Chapter 2. Furthermore, the restrictions on yielding surface are removed. Thus, the shear localization in dynamic plastic response of structural elements is an intrinsic property of a transversely loaded, two-dimensional ductile material that can be characterized by a rigid, perfectly plastic model. This conclusion is applicable for many metals when their plastic hardening effect is not very significant. Complete continuity conditions at both bending and shear hinges are obtained in Chapter 2, which should be satisfied in a dynamic plastic response of structural elements.

In the dynamic plastic response of structural elements, both bending and shearing hinge sizes are neglected. This leads to a discontinuity in the transverse displacement across a shear hinge, and a discontinuity on the rotation angle across a bending hinge. This idealization does not influence the dynamic plastic analysis because the idealized hinge concept caters for the consumed plastic energy within the hinge. This idealization faces a challenge when dynamic plastic analyses are

combined with failure predictions. In this case, it is necessary to understand a hinge as a finite deformation zone. Its dimension is an important parameter to describe the hinge.

Chapter 3 evaluates the shear hinge length for beams, plates and cylindrical shells using a quasi-static method proposed by Wen, et al.(1994). The validity of the results from quasi-static method is verified by FEM simulations on a elastic, linear plastic hardening beam. After a dimensional analysis, two dimensionless parameters given in eq.(3-25) are found to be significant for the propagation of shear deformations. Three distinct cases are identified for different characteristic transverse loading rates that can be determined by eq.(3-25), i.e., (1) Bending response mode for low loading rate; (2) Stationary shear hinge mode for medium loading rate, and (3) Plastic shear wave mode for high loading rate. The shear hinge size obtained by a quasi-static method is applicable in Case (2), where the shear wave is trapped within the shear hinge. The shear wave mode proposed by Wang and Jones(1996) belongs to Case (3).

The current understanding of the geometrical structure of a bending hinge is based on some simple slip line analyses. It would not be difficult to use the FEM method to explore the forming process of these localized deformations and their geometry structures, which can supply useful information when conducting failure analysis together with a rigid, perfectly plastic model analysis.

7.2 Strain Rate and Temperature Effects on Structural Response and Failure

It has been confirmed that the flow stress increases with strain rate and decreases with temperature. On the other hand, material ductility decreases with strain rate and increases with temperature. These features have been observed in the material tests in Chapter 5, which may influence structural response and failure. The strain rate and temperature effects in the proposed constitutive equations on the DS beam response and failure are verified by comparing theoretical and numerical predictions on material response and failure with test results.

A portion of the mechanical deformation work will be converted into heat, which may lead to a temperature rise when the characteristic time for heat conduction

is longer than the characteristic response time. There exist two extreme cases, i.e., isothermal and adiabatic processes, which can greatly simplify the analysis. Isothermal and adiabatic processes are normally associated with low and high strain rates, respectively. A dimensional analysis is given in Chapter 4 to obtain strain rate conditions for these two processes. These conditions, which are verified in Chapter 5 using FEM simulations, have been employed in Chapter 4 to predict the temperature rise in an model analysis of Menkes and Opat's beam problem. It shows that the temperature rise is significant when the impulsive intensity is high. Temperature may go up to 200°C when the impulsive velocity is around 300m/s, which is about the velocity corresponding to mode III failure for these particular tests. This temperature rise leads to an increase of material ductility. This gives a reasonable explanation for the successful application of the elementary failure criterion to predict mode III failure, where the temperature effect is not included explicitly, but the choice of parameter k takes into account temperature.

Few papers report the observation that failure transition from ductile fracture failure to adiabatic shearing failure is possible with increasing loading rate. This failure mechanism transition is confirmed in the double shear beam test. It is believed that this is an important issue in failure predictions because a totally different failure criterion and modelling method have to be used for different failure mechanisms. For example, adiabatic shearing failure is associated with material thermal instability, which may become very localised, and thus, need to refine the element mesh to its characteristic dimension. In Chapter 4, critical conditions for this transition are obtained for Menkes and Opat's beam problem using a model analysis, which is applicable for other structural elements under similar loading conditions including both impulsive and projectile impact loadings. The predicted velocity is in a reasonable range beyond the critical velocity for mode III failure, which needs to be confirmed by experiments.

7.3 Failure Criteria

With the rapid developments of computational capabilities and expert systems, problems of structural deformation and failure could be solved based on valid

fundamental physical foundations and material property descriptions. The incorporation of a failure criterion into a FEM code is a promising way forward to allow engineers to duplicate the actual failure possibilities at the design stage.

Several failure criteria, which have been used in various cases, are examined in modelling the failure of a double shear notch in Chapter 6. Equivalent plastic strain, maximum normal plastic strain and maximum plastic shear strain failure criteria overestimate the failure initiation. This is partly due to the influence of hydrostatic stress according to the numerical modelling results. Strain rate effect on material ductility is another cause. Stress type failure criteria are maximum normal stress failure criterion, equivalent stress failure criterion, and maximum shear stress failure criterion. The predicted values are much higher than the corresponding material values. It is shown that plastic strain energy density failure criterion is the most promising failure criterion in the present case. Several successful applications of the plastic strain energy density failure criterion for both static and dynamic structural failure predictions have been reported previously in the literature. Thus, the plastic strain energy density failure criterion is capable of predicting a range of macroscopic failure phenomena, and therefore, it is worth exploring the physical base of the plastic strain energy density failure criterion. A general strain energy density failure criterion based on continuum thermodynamics is proposed in Appendix B. It is assumed that material failure is basically a "brittle failure" process initiated by the local internal forces or a specified elastic strain energy density. Inelastic dissipations, including the plastic strain energy density, influence material failure by reducing the material resistance to the local internal forces through a continuous change of material internal states. When the ductile failure is controlled mainly by plastic dissipation, the plastic strain energy density failure criterion is expected to give a good prediction. However, several other issues, such as the influence of strain rate and temperature on the critical value of plastic strain energy density, hydrostatic effect, etc., need to be studied further.

The maximum stress criterion has been recognised as the criterion for predicting the initiation of a shear band. The FEM modelling in Chapter 6 indicates that the maximum stress criterion is only a necessary condition for shear banding

initiation. During a practical loading process, equivalent(or maximum shear) stress may reach its maximum due to the decrease of strain rate(not the thermal softening that is associated with increasing strain rate). Further studies are necessary on this topic.

One of the vital problems concerning the combination of FEM and failure criterion is to find the correct volume of material, or the correct mesh size of the element, on which the failure criterion can be expressed correctly. This requires a good-understanding of the physical nature of material failure and a proper design of material property and failure tests.

7.4 Response and Failure Features of a Double Shear Beam

Experiments on a double-shear(DS) beam are reported in Chapter 5. Because the DS beam has been used for the purpose of material property test, the relationships between its measurable quantities and the actual responses are important for evaluating material property data. For the current design of the DS test, the two factors are identified to convert the measurable nominal stress and strain into the actual stress and strain at the mid-point of notch section by using FEM method. Although the obtained factors may vary for different design of DS specimen, the procedure used in the present study is general.

The localised shear in the notch section of a DS beam can be used to explore the shear response and failure occurred in a shear hinge of a structural element. In impulsively loaded or impact loaded structural elements, the localised shear zone, or shear hinge, is not as evident as in the notch of DS beam. The current results show that the basic shear response in the notch section is similar to the deformation in a shear hinge. Two failure mechanisms in the notch section has been reported separately in other impulsive and impacted problems. In the shear section of a notch, tensile failure is on one side of the notch and shear failure is on another side of the notch where the external force is applied. These observations may be helpful for understanding failures in a shear hinge.

The temperature effect has to be considered during the response process of a DS test. In the current case, a strain rate of $50s^{-1}$ can lead to a temperature rise of

139°C at a unit shear strain according to the simulation in Section 6.2.3. With a further increase of strain rate, the temperature rise may lead to thermal softening which develops into an adiabatic shear band. The local stress concentration at the notch corner may lead to material failure, which has been shown in Chapter 5 and simulated in Chapter 6. These limitations should be considered when using DS test as a material property test.

Due to the high localisation of stress and deformation at the notch corners, the failure index obtained from a DS test is difficult to interpret, and thus, it is not recommended as a material failure test.

7.5 Closure

Material failure is a long term interest of material and structural engineers and researchers. Gradually, engineers change their previous design criterion from "yielding" to "failure" with accumulated confidence in their predictions. The basic purpose of the current study is to add some more understanding to this difficult yet important field.

In some cases, shear response and failure can be distinguished from other response and failure modes, which offers a simple environment to study the response and failure features. Other response and failure modes are equally important in a practical problem and are interactive with shear modes. For example, a shear response is only one of the three phases in a transversely loaded beam. While, material failure within the DS notch is actually a tensile failure. Therefore, it is believed that some conclusions in the present study are not confined to an increased understanding of shear response and failure.

APPENDIX A: MATERIAL TEST THEORY

A1. Tensile Test

The behaviour of a material under a uniaxial tensile load is very important for the understanding of material properties. In a tensile test, the specimen is subjected to a tensile force along its axis. Specimens, in the form of cylindrical rods, or flat sheets, usually have a reduced section, or gauge length, to obtain a uniform state of stress and strain.

Typical tensile curves for ductile nonferrous and steel metals are presented in Figs. A1(a,b), respectively. The concepts of engineering(nominal) stress(σ_E) and engineering strain (ε_E) are used in these curves and are defined as

$$\sigma_E=\frac{P}{A_0} \tag{A-1}$$

and

$$\varepsilon_E=\eta-1 \ ,\eta=\frac{l}{l_0} \ , \tag{A-2}$$

respectively, where P is the axial load, A_0 is the initial cross-section area, η is the stretching ratio defined as the ratio of the current(l) and the original(l_0) gauge lengths. The physical interpretations for the different regions of Figs.A1(a,b) have been discussed in detail by Dodd and Bai(1987) and Nadai(1950). A mechanics interpretation for a common tensile curve up to failure was given by Duffy(1989), as depicted in Fig.A2. The initially unloaded sample (A_0) is loaded elastically from stress free state A to B, the tensile yield point of the material. From B to D, the material continues to flow plastically and to strain-harden, carrying increased load. This increased load capacity is counteracted in part by a reduction in area caused by thinning of the material in the transverse directions. At D, the maximum load-carrying capability due to strain-hardening exactly equals the loss in capacity due to

the reduction in area. Following this point of neutral stability, local necking occurs(E) followed at a later point(F) by complete separation of the material(sometimes due to the growth and coalescence of voids in the material).

The engineering stress-strain curve is important for understanding the various deformation mechanisms which occur during a uniaxial tensile test. Two parameters are normally taken as measures of material ductility in a tensile test(Dodd and Bai(1987))

$$e=\frac{l_f-l_0}{l_0}=\varepsilon_{Ef}\ ,\quad R_i=\frac{A_0-A_f}{A_0}, \tag{A-3a,b}$$

where l_f and A_f are the final length of the original gauge length(l_0) and the final cross-sectional area in the necked region at specimen failure, respectively. ε_{Ef} is the value of ε_E at failure. However, for a uniaxial tensile test, the reduction in area, R_i, is a more significant measure of material ductility than the extension of the gauge length to fracture(Dodd and Bai(1987)).

Natural strain is defined by the expression

$$\varepsilon_N=\ln\eta=\ln\frac{l}{l_0}=\ln(1+\varepsilon_E)\ , \tag{A-4}$$

and is commonly used with true stress in constitutive equations for metal plasticity. It is evident that $\varepsilon_N\approx\varepsilon_E$ for small strains. Some applications for using natural strain were given by Nadai(1950).

The engineering stress in uniaxial tension is defined using the original configuration of the test specimen as one of the components of the Lagrangian stress tensor. The corresponding component of the Eulerian stress tensor is defined using the current configuration of the test specimen and is called a true stress in a tensile test(σ_T)

$$\sigma_T=\frac{P}{A} \tag{A-5}$$

where A is the current area of the cross-section. When material is incompressive, one has $lA=l_0A_0$, or $A=l_0A_0/l=A_0/(1+\varepsilon_E)$. Therefore,

$$\sigma_T=\frac{P}{A_0}(1+\epsilon_E)=\sigma_E(1+\epsilon_E). \tag{A-6}$$

From the σ_T-ε_N(or ε_E) curve shown in Fig.A2, one cannot distinguish easily the critical point for the onset of necking in a uniaxial tensile test because the effect of the reduction of cross-section area is eliminated by the definition of the true stress. A continuation of the true stress beyond *D* in Fig.A2 is difficult due to experimental difficulties in measuring the minimum cross-section during the necking process. Even if the whole range of the true stress-strain curve could be obtained, it is only significant before point *D'* in Fig.A2 because of the non-uniform deformations introduced into the test specimen after the initiation of necking. The true stress-strain curve according to equations (A-4) and (A-5) may be used only as the uniaxial stress-strain relationship before the maximum stress point in an engineering stress-strain curve.

The strains in equations (A-2) and (A-4) are defined on finite gauge length in a uniaxial tensile test, and are a valid description of the local deformations within the gauge length only when the deformation is uniform along the gauge length. After the occurrence of necking, the deformation within a finite gauge length is nonuniform. Thus, a valid strain measure should be defined on an infinitesimal length, which is called a zero gauge length strain throughout this report[1]. Let l_{i0} represents an infinitesimal length at any given location within the gauge length in the original configuration of the tensile test specimen, which lengthens to l_i in the current configuration of the test specimen. Therefore, the zero gauge length natural strain in uniaxial tension is

[1] In this report, zero gauge length strain and rupture (or failure) strain are represented by subscripts 0 and *f*, respectively. For example, zero gauge length engineering strain and its critical value at failure are ε_{E0} and ε_{E0f}, respectively.

$$\varepsilon_{N0}=\ln(\frac{l_i}{l_{i0}}) \ , \tag{A-7a}$$

while the zero gauge length engineering strain[2] in uniaxial tension is

$$\varepsilon_{E0}=\frac{l_i-l_{i0}}{l_{i0}} \tag{A-7b}$$

and they are assumed to remain constant within the infinitesimal length l_i in the current configuration of a test specimen. Equation (A-4) gives a relationship between them.

If it is assumed that the material is incompressible, then

$$l_iA=l_{i0}A_0=\text{const}, \tag{A-8a}$$

or

$$Adl_i+l_idA=0, \tag{A-8b}$$

where, A_0 and A are respectively the original and the current cross-sectional areas at the location where l_{i0} and l_i are measured in the test specimen. Thus,

$$\varepsilon_{N0}=\ln(\frac{A_0}{A}) \tag{A-9a}$$

which yields

$$\dot{\varepsilon}_{N0}=-\frac{1}{A}\frac{dA}{dt} \ , \tag{A-9b}$$

when eqs.(A-8a,b) are used and $\dot{(\ )}$ represents differentiation with respect to time t.

Before the initiation of a localized neck, a tensile specimen deforms uniformly along the gauge length and, therefore, the σ_T-ε_N and σ_T-ε_{N0} curves are identical. The advantage of using the zero gauge length natural strain is its capability for describing

[2] The zero gauge length engineering strain defined here was called effective elongation by Ludwik(see Timoshenko(1956)).

the local uniaxial deformation between necking and material failure. Equation (A-3b) can be expressed in terms of the zero gauge length rupture strain ε_{N0f} when failure occurs, which is defined by equation (A-9a) when substituting A by A_f

$$R_i=1-e^{-\varepsilon_{N0f}}=\frac{\varepsilon_{E0f}}{1+\varepsilon_{E0f}} . \qquad \text{(A-10)}$$

where

$$\varepsilon_{N0f}=\ln(\frac{A_0}{A_f}) \quad \text{and} \quad \varepsilon_{E0f}=\frac{A_0}{A_f}-1 . \qquad \text{(A-11a,b)}$$

This is why equation (A-3b) is more significant than equation (A-3a) for measuring the material ductility, as mentioned before.

The measurement of σ_T, ε_{N0} and ε_{N0} after necking may be obtained by using a transient image recorder, for example, a high-speed camera, as implied by Dodd and Bai(1987)(pp.26), to record continuously the specimen configuration in the area of necking. However, majority of the experimental results published previously did not give this information. One published result based on this method were given by Alves(1996) for dynamic tensile tests up to $\dot{\varepsilon}=239.9s^{-1}$. But, it seems that an engineering strain rate instead of a natural strain rate in equation (A-9b) was used there. Nevertheless, it confirmed that a straight line could be used to connect the necking point and the failure point on true stress-strain curve, as suggested by Yu and Jones(1991).

Although the σ_T-ε_{N0} relationship reflects more the nature of a material than the σ_E-ε_E curve, the σ_E-ε_E curve is useful when necking is the basic failure mechanism on the macroscopic scale.

The critical strain energy density within a characteristic unit volume of the material at the failure location is

$$w_c=\int_0^{\varepsilon_{N0f}}\sigma_T d\varepsilon_{N0}=\int_0^{\varepsilon_{E0f}}\sigma_E d\varepsilon_{E0} . \qquad \text{(A-12)}$$

according to eqs. (A-4) and (A-6).

Historically, there are different strain definitions for a uniaxial loading test, for example, true strain and logarithmic strain are used by different authors instead of natural strain. These strains are usually defined over a finite gauge length which cannot describe local deformation features after the maximum point of the engineering stress-strain curve. Furthermore, these definitions should be consistent with the general strain definitions for a three-dimensional solid continuum(ABAQUS(1994a)). In order to clarify these strain definitions in a tensile test and connect them to the general definitions in a three-dimensional solid continuum, a strain, which is defined across an infinitesimal length, is called a zero gauge length strain. The definition of stress should be a conjugate quantity in the sense that the product of stress and strain gives strain energy density. Conventionally, in a uniaxial loading test, the Eulerian stress component, which has the conjugate quantity, ε_{N0}, is called a true stress(σ_T), and the Lagrangian stress component, which has the conjugate quantity, ε_{E0}, is called an engineering stress(σ_E), as shown in eq. (A-12).

The general expression of eq. (A-12) in three dimensional stress state is

$$W_c = \int_0^{t_f} \sigma_{Tij} V_{ij} dt = \int_0^{D_{ij}^f} \sigma_{Eij} dD_{ij}, \qquad \text{(A-13)}$$

where σ_{Tij} and σ_{Eij} are Eulerian and Lagrangian stress tensor, respectively. While, D_{ij} and V_{ij} correspond to the displacement gradient tensor defined on original configuration and the deformation rate tensor. t is the internal time scale. t_f and D_{ij}^f are the value of t and D_{ij} at material failure. In metal plasticity, Eulerian stress tensor and deformation rate tensor are commonly used. Therefore, true stress and zero gauge length natural strain should be used in a uniaxial tensile test.

Once necking develops in a cylindrical rod specimen, a rotationally symmetric triaxial tensile stress state is induced in the region, which is shown in Fig.A3. In this case, it has been shown that the strain distribution is still uniform across the necking cross-section. The stress system in the neck consists of two parts, a superimposed hydrostatic tension stress($T_p=\sigma_{rr}=\sigma_{\theta\theta}=\sigma_z-\sigma_{TR}$) whose magnitude varies with radius,

increasing from zero on the outside of the neck to a maximum on the axis, and a longitudinal constant stress σ_{TR} across the necking cross-section, which is given by

$$\sigma_{TR}=\frac{\sigma_T}{(1+2\frac{R}{a})ln(1+\frac{a}{2R})}=f_c\sigma_{TR} \cdot \qquad \text{(A-14)}$$

according to Bridgman(1944)(also see Dodd and Bai(1987)), where a and R are defined in Fig.A3 and $\sigma_T=P/\pi a^2$ is the true stress.

Strictly speaking, the uniaxial true stress obtained from eq. (A-5) or (A-6) should be modified by eq. (A-14) after necking. And the method for calculating the strain energy density over the characteristic necking volume in eq. (A-12) need to be modified too. The superimposed hydrostatic tensile stress

$$T_p=\sigma_{rr}=\sigma_{\theta\theta}=\sigma_z-\sigma_{TR}=\sigma_{TR}ln(\frac{a^2+2aR-r^2}{2aR}) \qquad \text{(A-15)}$$

has negligible influence on the plastic flow of material, which has been confirmed by the uniform distribution of uniaxial strain across necking cross-section. However, hydrostatic stress is one of the important factor to influence material failure, which has been confirmed by many test results.

A tensile test is one of the important material mechanical property tests used to establish the constitutive equation and failure parameters although there are many other ways to achieve the same purpose. These tests normally use the global responses of a finite volume of material to predict deformation or failure parameters. The following criterion could be used to judge the validation of a material test

Material Property Test Criterion: *When conducting a material property test, there should exist a fixed collection of materials whose internal mechanical responses are predictable from the measurable global responses until material failure is initiated.*

A uniaxial tensile test is capable to satisfy this requirement due to Bridgman's brilliant contributions.

Although the standard tensile test has been used for a long time to obtain the mechanical properties of materials, there is still an incomplete understanding of the results from this simple test, as realised by Orowan half a century ago, 'The tensile

test (is) very easily and quickly performed but it is not possible to do much with its results, because one does not know what they really mean. They are the outcome of a number of very complicated physical process ... ... The extension of a piece of metal (is) in a sense more complicated than the working of a pocket watch and to hope to derive information about its mechanism from two or three data derived from measurement during the tensile test (is) perhaps as optimistic as would be an attempt to learn about the working of a pocket watch by determining its compressive strength.'(E.Orowan, Proc. Instn. Engrs Vol.151, p133, 1944).

Therefore, there are still many research works being conducted on the investigation of uniaxial tensile test until today.

A2. Split Hopkinson Pressure Bar(SHPB)

SHPB has been widely used to determine dynamic constitutive equations of various materials over a strain rate range of 10^2-$10^4 s^{-1}$. The SHPB apparatus for compression testing consists of a striker bar, an incident bar and a transmitter bar, made from the same material with same diameter, and associated instrumentation for recording data as shown schematically in Fig.5.4. The incident and transmitter pressure bars are mounted in teflon or nylon bushings to assure accurate axial alignment while permitting stress waves to pass without dispersion. The striker bar is fired from a gas gun. Its velocity is measured by two photocells and light sources at a known distance apart. When the striker bar impacts the incident bar, constant amplitude compressive pulses are generated in both bars. The length or duration of the compressive pulse generated in the incident bar is twice the wave-transit time in the striker bar and the magnitude is directly proportional to the striker velocity, determined by

$$\sigma_I=\frac{1}{2}\rho c V \quad \text{or} \quad \epsilon_I=\frac{V}{2c}, \qquad \text{(A-16a,b)}$$

where $\sigma_I(\epsilon_I)$ is the incident stress(strain) magnitude in the incident bar, ρ is the density of the bar material, c is the longitudinal elastic-wave velocity in the Hopkinson bars, and V is the impact velocity of the striker bar. In order to keep the Hopkinson bar system in elastic range, it requires that $\sigma_I<\sigma_0$, or,

$$V<\frac{2\sigma_0}{\rho c}, \tag{A-17}$$

where σ_0 is the yield stress of the bar material.

Under the following postulates

(a) The dispersion of a longitudinal wave in the Hopkinson bar system is negligible, which means that a one-dimensional wave theory is applicable;

(b) An uniaxial compressive stress state can be achieved in the specimen, which demands an ideal interface between Hopkinson bars and specimen to eliminate transverse friction, and requires that the transverse inertia effects are negligible in the specimen;

(c) The stress and strain are uniform along the specimen, which requires that the wave transit time in the specimen is much smaller than the pulse duration and that there no failures or flow instabilities occur in the specimen during the measurement;

the engineering strain, stress and strain rate in the specimen are

$$\sigma_E=E\frac{A}{A_s}\epsilon_t,\quad \epsilon_E=\frac{-2c}{L_s}\int_0^t\epsilon_r dt \quad \text{and} \quad \dot{\epsilon}_E=\frac{-2c}{L_s}\epsilon_r, \tag{A-18a,b,c}$$

where L_s and A_s are the original length and area of the specimen, A is the area of incident and transmitter bars, and E is the Young's modulus of the Hopkinson bars. It should be noted that $\epsilon_r(>0)$ and $\epsilon_t(<0)$ are the reflected and transmitted strain pulses in strain gauges located at incident and transmitter bars.

It has been mentioned in Section A1 that true stress-natural strain curve is required to describe the plastic behaviour of a metal. Therefore, eqs. (A-18a-c) need to be modified according to eqs. (A-4) and (A-6) together with the natural strain rate described by

$$\dot{\epsilon}_N=\frac{\dot{\epsilon}_E}{1+\epsilon_E}, \tag{A-19}$$

according to eq. (A-4). The modified formulas are

$$\sigma_T=E\frac{A}{A_s}(1-\frac{2c}{L_s}\int_0^t\varepsilon_r dt\ )\varepsilon_t\ ,\quad \varepsilon_N=\ln(1-\frac{2c}{L_s}\int_0^t\varepsilon_r dt\ )$$

$$\text{and}\quad \dot{\varepsilon}_N=-\frac{2c\varepsilon_r}{L_s-2c\int_0^t\varepsilon_r dt}. \qquad \text{(A-20a,b,c)}$$

These equations are based on material incompressibility of the specimen material, which is generally correct for metal materials in moderate plastic deformations. Some researchers did not do these modifications when they evaluated the material constitutive equation by using the results from SHPB, which is correct only for small strains.

Normally, the SHPB system requires $L_1 \geq L_2 \geq L_0 \rightarrow L_s$, as shown in Fig.5.4. It was recommended that the system be calibrated dynamically by passing a known stress wave through the strain gauges on both the incident and transmitter bars without a specimen. The magnitude of the strain pulse set up in the bars is V/2c, which can be compared with the output from strain gauges on both incident and transmitter bars to give a calibration factor. This method is employed in the present studies. An alternative method of calibration is sometimes used to check the dynamic calibration. This merely involves shunting a known calibration resistor across one arm of the strain-gauge bridges. This produces a simulated strain of

$$\varepsilon_c=\frac{1}{f}\frac{R_g}{R_c+R_g}, \qquad \text{(A-21)}$$

where f is the gauge factor and R_g and R_c are the gauge and calibration resistances. This method verifies the dynamic calibration to within several percent[Nicholas(1982)].

Considerable studies have been conducted to check the conditions when the pre-assumed postulates are satisfied(see Bertholf and Karnes(1975), Nicholas(1982), and Follansbee(1985)). It is generally accepted that SHPB technique is very accurate and can be reliably used for the measurement of dynamic properties. The optimum specimen dimension proposed by Davies and Hunter(1963) and confirmed by Bertholf and Karnes(1975) is

$$\frac{d_s}{L_s} = \frac{4}{\sqrt{3}}, \tag{A-22}$$

where d_s and L_s are the diameter and length of the cylindrical specimen. Some work has been conducted using strain gauges or non-contact methods directly to measure the strain on the specimen. One of them was published recently by Ramesh and Narasimhan(1996).

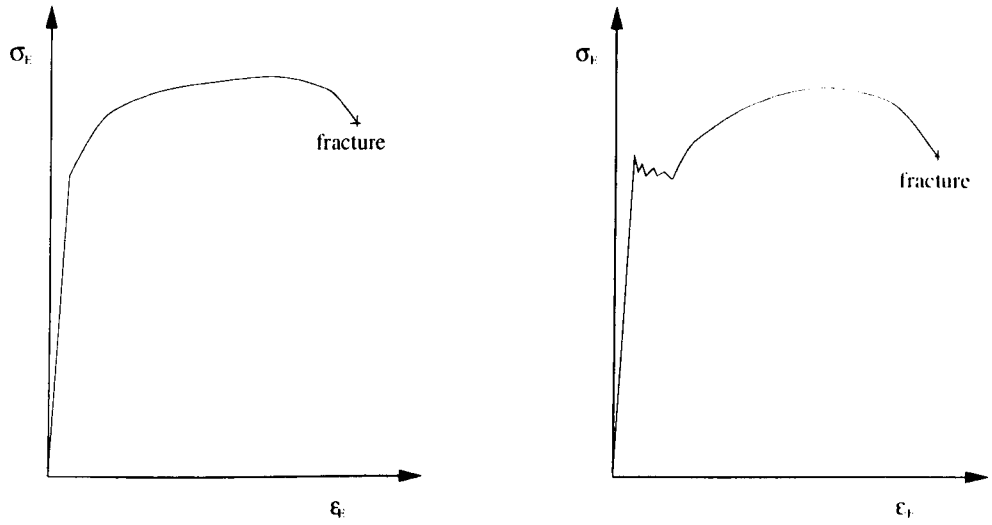

(a) (b)

Fig.A1 Engineering stress-strain curves under uniaxial tension, (a) Non-ferrous metal;
(b) Mild steel

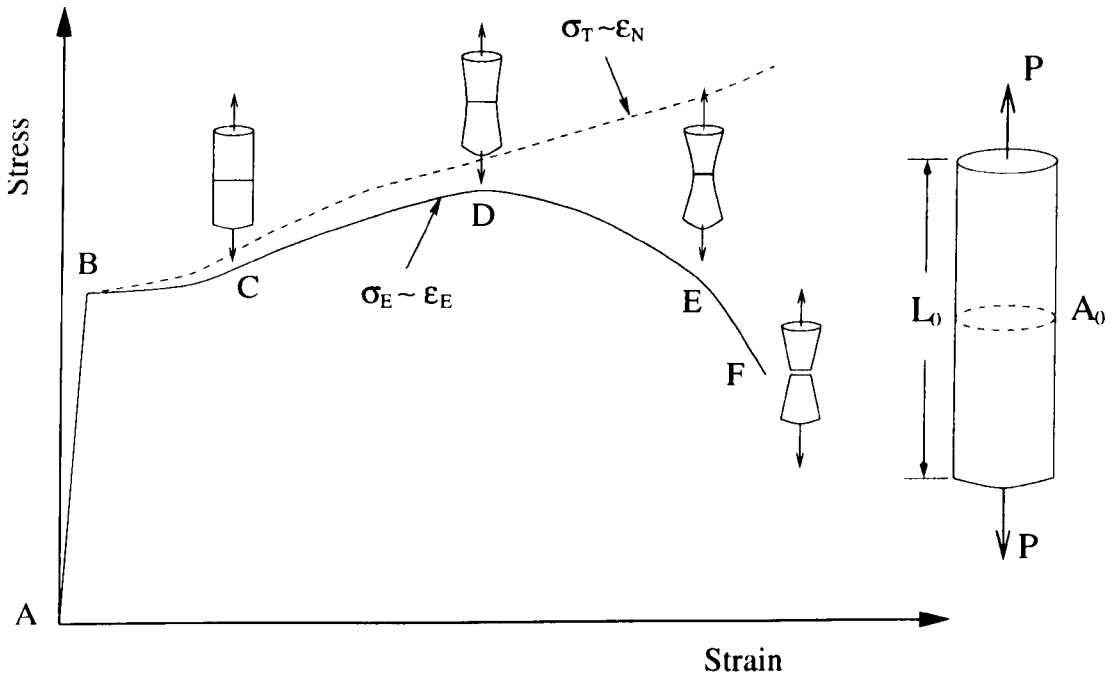

Fig.A2 Uniaxial stress-strain curve to failure.

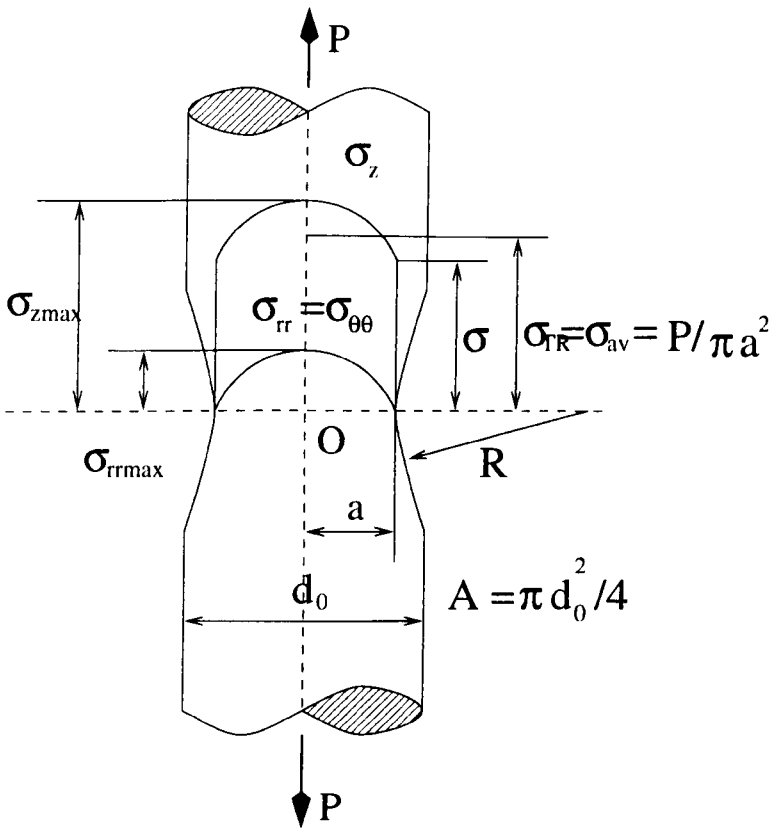

Fig.A3 Stress distributions in the neck of a tensile specimen.

APPENDIX B: STRAIN ENERGY DENSITY FAILURE CRITERION

B.1. Introduction

Many failure criteria have been proposed to predict the initiation of macroscopic material failure under various conditions. Generally speaking, they may be divided into four different types, (a) stress or strain failure criteria; (b) energy type failure criteria; (c) damage failure criteria; (d) empirical failure criteria, and have been used successfully in various failure problems. It appears that the validity of all these failure criteria is restricted to specified types of failure problems. It is necessary to set up a physical basis for further developments of more universal material failure criteria on the macroscopic scale.

The purpose of this Appendix is to fulfil this task by establishing a theoretical framework for a criterion of failure initiation in macroscopic continuum solids. This theoretical framework will embody the following three features, (1) a macroscopic energy density concept to define macroscopic material failure; (2) a correlation between the physical mechanism of macroscopic material failure with the microscopic material behaviour; (3) incorporation of the different failure types including brittle and ductile failures when consideration of material damage effects.

An energy concept to define material failure was proposed initially by Freudenthal(1950). He realised that material failure occurs in different scales simultaneously, which led him to introduce an energy concept to describe material failure. The importance of the energy concept was also emphasized by Gordon(1976).

Furthermore, Freudenthal realised the difference between elastic deformations(related to potential energy) and inelastic deformations(dissipated energy) in an energy type failure criterion, which is expressed by the following statement(pp.20 in Freudenthal(1950))

"Since the process of bond separation which initiates fracture depends on the momentary elastic strain or the potential energy in a different manner from what it

depends on the inelastic strain or the dissipated energy, the elastic and inelastic strain energy must enter the fracture condition separately."

While, Gordon(1976) also pointed out that(pp.71)

"The weakening mechanism, rather than the bond strength, was what really controlled mechanical strength."

Although many types of strain energy failure criteria have been proposed after Freudenthal, most of them didn't distinguish such an important difference between the contributions of elastic strain energy and inelastic strain energy in an energy failure criterion except Lemaitre and Chaboche who expressed a similar viewpoint in their book(pp.402-403 in Lemaitre and Chaboche(1990)). However, they did not progress from this point to set up a general energy type failure criterion.

Section B.2 will establish a theoretical framework of material failure criterion evaluated from Freudenthal(1950)'s original work, which is the specified elastic strain energy density failure criterion. The influence of irreversible process on material cohesive potential described by a dissipative function based on thermodynamics is also discussed in this section. For material ductile failure, this function could be used to describe material failures, and will be defined as dissipative energy density failure criterion, which reduces to several previous successful ductile failure criteria, as discussed in section B.3.

B.2. Strain Energy Density Failure Criterion

B.2.1. Potential and Dissipative Energies in a Mechanical System

The material behaviour in a mechanical system is a complex process involving deformation and damage mechanisms from atomic to macroscopic levels, as shown in Fig.B.1. The input mechanical energy will be either stored or consumed in a mechanical system through different deformation and failure mechanisms. Material deformations and failures at different levels have different physical meanings, which may be related from one level to another by proper statistical methods. Generally speaking, the material behaviour on one level is a collective, or group, behaviour of the material on a sub-level. It is understandable that the general significance of the results is lost unless the interrelation between the observed macroscopic material behaviour and the internal structure in terms of atomic, molecular, or microscopic

phenomena can be established(pp.4 in Freudenthal(1950)). A successful deformation or failure theory should be physically consistent at each material level.

Macroscopical material deformations may be divided into elastic and inelastic deformations, which have different physical mechanisms at the microscopical level. The metal theory at atomic level was set up by Drude and Lorenz when they introduced the free-electron theory of metals, which suggests that in a metallic crystal the valency electrons are detached from their atoms and can move freely between the positive metallic lattice, and the negative free electrons to provide the cohesive strength of the metal. Such a linkage may be regarded as a special case of covalent bonding through a valency electron cloud. The equilibrium spacing between two ions bonded together is determined by a balance between the attraction due to the bond and the repulsion which develops when their outer electron shells begin to overlap each other. Thus, atoms in condensed phase occupy equilibrium positions about the valley of the inter-atomic energy curve(Fig.B.2) determined by the formed atomic bonds(Woo and LI(1993)). Upon the application of external force, the atoms are displaced from their equilibrium positions which changes the potential energy of the system, and which is recoverable with the removal of external force within a certain range of displacement. Macroscopic elastic deformation is a collective behaviour of atomic displacements from their equilibrium positions. And, the macroscopic stress, defined as the material interactions on the level of continuum mechanics, is the collective behaviour of interactions between atomic bonds.

On the other hand, atoms may overcome their energy barriers and move into a new equilibrium valley of free energy with excessive input of external mechanical energies, which leads to the breaking of the previous bonds and re-establishing a new configuration of bonds. Material defects, or material damages, will be formed during this re-bonding process. A collective atomic migration in a stress field causes a slip(or dislocation) in a crystal, whose collective behaviour leads to macroscopic plastic(or inelastic) deformations. Furthermore, the atomic bond may be disrupted by obstructing atomic migrations due to the piled up dislocation barriers during atomic migration process. Therefore, macroscopic inelastic deformation is an important mechanism to weaken the macroscopic material cohesive potential.

It is evident that failure on the atomic level does not imply a material failure

on macroscopic level. However, both the atomic migration and atomic bond disruption cause a change of the material structures, and, therefore, a change of the material macroscopic properties. For ductile materials, void developments are important under certain conditions, which also represents a material structural change from the view point of macroscopic level. The common feature for inelastic deformations and material damages is their irreversibility, which are energy dissipation processes from an energy viewpoint. Thus, the macroscopic failure process of a material should be described by the thermodynamic theory of irreversible processes.

B.2.2. Thermodynamic Foundation of Dissipative Process

Material failure is a process involving thermal and mechanical phenomena from atomic to macroscopic levels, which may be described by various deformation processes in a mechanical system. The thermodynamics of a continuum medium determines the thermal and mechanical behaviours of solid continuum in its deformation and failure process. It has been noted in Section B.2.1 that any material structural changes related to macroscopic failure process may be described by irreversible thermodynamic theory.

The Clausius-Duhem inequality is

$$\sigma_{ij}\dot{\epsilon}_{ij}-\rho(\dot{\Psi}+s\dot{T})-q_i\frac{T,_i}{T}\geq 0 \qquad \text{(B-1)}$$

where the specific free energy Ψ=e-Ts is introduced, in which σ_{ij} is the Cauchy(true) stress, $\dot{\epsilon}_{ij}$ is the rate of deformation, ρ is the material density, e is the specific internal energy of the material, s is the specific entropy, T is temperature, q is the heat flux vector. The specific free energy Ψ is determined completely by σ_{ij} and other state variables, i.e.,

$$\begin{aligned}&\Psi=\Psi(\sigma_{ij}, \text{ other state variables})\\ &\text{or}\quad \Psi=\Psi(\epsilon^{e}_{ij}, \text{ other state variables}).\end{aligned} \qquad \text{(B-2a,b)}$$

In eqs.(B-2a,b), the so-called "other state variables" may be represented by a group of observable and internal variables, T, $V_0=D_{ij}$(as damage internal variables), V_k(k=1,2,... ...)(as plastic internal variables). Thus, we have

$$\Psi=\Psi(\epsilon_{ij}^{e},T,D_{ij},V_k) \quad \text{or} \quad \Psi=\Psi(\epsilon_{ij}-\epsilon_{ij}^{p},T,D_{ij},V_k) \tag{B-3a,b}$$

where, $\varepsilon_{ij}=\varepsilon_{ij}^{e}+\varepsilon_{ij}^{p}$ is employed for simplicity[3]. Eqs(B-3a,b) gives

$$\begin{aligned}\dot{\Psi}&=\frac{\partial\Psi}{\partial\epsilon_{ij}^{e}}\dot{\epsilon}_{ij}^{e}+\frac{\partial\Psi}{\partial T}\dot{T}+\frac{\partial\Psi}{\partial D_{ij}}\dot{D}_{ij}+\frac{\partial\Psi}{\partial V_k}\dot{V}_k\\ \text{or}\quad \dot{\Psi}&=\frac{\partial\Psi}{\partial\epsilon_{ij}}\dot{\epsilon}_{ij}-\frac{\partial\Psi}{\partial\epsilon_{ij}^{p}}\dot{\epsilon}_{ij}^{p}+\frac{\partial\Psi}{\partial T}\dot{T}+\frac{\partial\Psi}{\partial D_{ij}}\dot{D}_{ij}+\frac{\partial\Psi}{\partial V_k}\dot{V}_k.\end{aligned} \tag{B-4a,b}$$

Thus, the Clausius-Duhem inequality, eq.(B-1) predicts

$$\begin{aligned}&\sigma_{ij}=\rho\frac{\partial\Psi}{\partial\epsilon_{ij}},\quad s=-\frac{\partial\Psi}{\partial T}\\ &P_{ij}\dot{\epsilon}_{ij}^{p}+Y_{ij}\dot{D}_{ij}+A_k\dot{V}_k-\frac{1}{T}q_iT_{,i}\geq 0\end{aligned} \tag{B-5a-c}$$

where $P_{ij}=-\rho\partial\Psi/\partial\varepsilon_{ij}^{p}$, $Y_{ij}=-\rho\partial\Psi/\partial D_{ij}$ and $A_k=-\rho\partial\Psi/\partial V_k$ are thermodynamical forces(stresses) corresponding to intrinsic dissipative processes represented by ε_{ij}^{p}, D_{ij} and V_k. σ_{ij}, determined from eq.(B-5a), has a one to one relationship with ε_{ij} for given T, ε_{ij}^{p}, D and V_k within a non-discontinuous stress set. It may be proved that

$$\frac{\partial\Psi}{\partial\epsilon_{ij}}=\frac{\partial\Psi}{\partial\epsilon_{ij}^{e}}=-\frac{\partial\Psi}{\partial\epsilon_{ij}^{p}}, \tag{B-6}$$

and therefore, $P_{ij}=\sigma_{ij}$, which means that the macroscopic Cauchy stress is the thermodynamical force of plastic dissipation when it is represented by plastic strain.

The dissipation in a mechanical system can be described by eq.(B-5c) according to the thermodynamic principles. When intrinsic mechanical dissipation and thermal dissipation due to heat conduction are decoupled, the intrinsic mechanical dissipation rate is expressed by

$$\dot{\phi}_1=P_{ij}\dot{\epsilon}_{ij}^{p}+A_k\dot{V}_k+Y_{ij}\dot{D}_{ij}\geq 0. \tag{B-7}$$

Function $\dot{\phi}_1$ in eq.(B-7) describes an intrinsic dissipative process in a mechanical system, which will be used as an intrinsic scale to measure material's life expectancy

---

[3] In eq.(B-3b), specific free energy is expressed by observable variable ε_{ij} and T and internal variables ε_{ij}^{p}, D_{ij} and V_k. Although eq.(B-3a) and (B-3b) lead to same results, the results derived from eq.(B-3b) can give a symmetrical and elegant expression of thermodynamics forces.

before macroscopic failure.

In a mechanical system, P_{ij}, Y_{ij} and A_k are defined as a group of thermodynamic stresses. Each thermodynamic stress corresponds to an internal variable which introduces a mechanical intrinsic dissipative mechanism. Their contributions to the total mechanical intrinsic dissipation are reflected in eq.(B-7). Generally, these thermodynamic stresses are functions of stress tensor and other internal variables. However, in many cases, thermodynamic stresses depend only on the stress tensor. It has been shown that $P_{ij}=\sigma_{ij}$ in eq.(B-6). In the following analyses, it may be assumed that $Y_{ij}=Y_{ij}(\sigma_{ij})$ and $A_k=A_k(\sigma_{ij})$.

When it is assumed that mechanical dissipation is independent of heat conducting dissipation (see Truesdell and Noll(pp256 in Malvern(1969)). Now, the mechanical dissipative energy density, ϕ_1, and its rate, $\dot{\phi}_1$, are defined by

$$\phi_1=\int_0^{\phi_1} d\phi_1 \quad \text{and} \quad \dot{\phi}_1=\frac{d\phi_1}{dt} \tag{B-8}$$

which may be used to describe the material de-bonding process at the macroscopical level within the scope of a thermodynamic framework.

B.2.3. Specified Elastic strain Energy Density Failure Criterion

According to Freudenthal(1950) and the above discussion the macroscopic material failure criterion may be described by the following statement:

> *When the specified potential strain energy[4] over a given collection of particles of the material[5] exceeds its critical value, which depends on the preceding irreversible dissipative process and some other environmental parameters, the macroscopic material failure occurs in this material collections.*

It is evident that a proper statistical average process is necessary to express

---

[4] The specified potential strain energy may be understood as the specified elastic strain energy which refers to the maximum possible releasable strain energy in the given material collection.

[5] A given collection of material particles can be identified using material(or Lagrangian) descriptions according to initial material configuration. The choice of the size of a given collection of material particles depends on the described physical properties and material constructions.

this failure criterion within the scope of continuum mechanics. It has been shown that, despite the large difference in the nature and structure of materials, there is a great unity displayed in their macroscopic behaviour, described by macroscopic physical quantities, such as material density, stress, strain, etc., which are defined as average values over a representative material configuration. Together with the limitation concept in mathematics, this technique defines all meaningful physical quantities in continuum mechanics at a geometrical point[6]. Here, we assume that such an average technique is valid for describing macroscopic material failure in continuum mechanics. Therefore, the proposed failure criterion may be described by

$$w_s^e = w_{sc}^e(\phi_1, \dot{\phi}_1, T, \sigma_H) \tag{B-9}$$

where , w_s^e is the specified elastic strain energy density defined on the original representative volume[7], w_{sc}^e is its critical value, ϕ_1 and $\dot{\phi}_1$ are the mechanical dissipative energy density defined on the original representative volume of the material and its rate, respectively, T is the temperature and σ_H is the hydrostatic stress value. It should be noted that if Cauchy stress and natural strain are used, the volume change should be considered in calculating w_s^e. Similar principles are applicable to ϕ_1 and $\dot{\phi}_1$.

B.2.4. Material Brittle Failure

Ii is well-known that materials under low temperature or high strain rate tend to fail in a brittle manner with only a small amount of prior plastic flow. In this case, the influence of internal mechanical dissipation, ϕ_1, on w_{sc}^e in equation (B-9) may be neglected. Furthermore, existing investigations have shown that the mechanism of brittle failure, i.e., cleavage, is a mechanism involving the breakage of interatomic bonds. This mode of failure is not very sensitive to temperature and strain rate

---

[6] The geometrical point in continuum mechanics, on which macroscopical physical quantities are defined, should be sufficiently large on the microscopic level. It was pointed out by Hancock and Mackenzie(1976) that failure initiation must involve a minimum amount of material which is characteristic of the scale of physical events involved.

[7] Material mass is more proper to represent the given collection of material particles(Matic et al.(1988)), which is equivalent to using their original geometrical volume due to the conservation of mass.

according to the Ludwik-Davidenkov-Orowan hypothesis(Cottrell(1964)) and the discussions in Dodd and Bai(1987) (pp.51-71) and Polakowski and Ripling(1966) (pp.230). Therefore, the failure criterion, equation (B-9), simplifies for brittle failures to

$$w_s^e = w_{sc}^e \tag{B-10}$$

Within the scope of linear elastic mechanics, the influence of volume change on the specified elastic strain energy density may be neglected because

$$J^e = \frac{3\sigma_H}{E}(1-2\nu) \sim \frac{\sigma_H^c}{E} \sim 10^{-2} \tag{B-11}$$

for most metals, where σ_H^c is the critical value of hydrostatic tensile stress for material failure.

The different choice of a specified elastic strain energy density leads to different types of stress failure criteria which have been used widely to calculate the material strengths in brittle failure analyses.

(1) Maximum Normal Stress Failure Criterion

If material failure is initiated by the potential of strain energy related to the maximum normal stress

$$w_s^e = \frac{\sigma_1^2}{E} - \frac{\nu}{E}(\sigma_1\sigma_2 + \sigma_1\sigma_3) = \frac{1+\nu}{E}\sigma_1^2 - \frac{3\nu\sigma_H}{E}\sigma_1, \tag{B-12}$$

where $\sigma_1 \geq \sigma_2 \geq \sigma_3$ are the principal stresses. Therefore, equation (B-10) is equivalent to

$$\sigma_{max} = \sigma_{1f} \tag{B-13}$$

which is the maximum normal stress failure criterion.

(2) Von-Mises Failure Criterion

When material failure is initiated by the potential of distortion strain energy

as proposed by Freudenthal(1950) (pp.387-394)

$$W_s^e = W_d^e = \frac{4(1+\nu)}{6E}\sigma_e^2, \tag{B-14}$$

equation (B-10) may be expressed by

$$\sigma_e = \sigma_{ef} \tag{B-15}$$

which is the von-Mises or octahedral shearing stress failure criterion.

(3) Maximum Shear Stress Failure Criterion

The elastic strain energy corresponding to the maximum shear stress is

$$W_s^e = \int_0^{\gamma} \tau_{max} d\gamma = \frac{\tau_{max}^2}{2G} = \frac{(\sigma_1 - \sigma_3)^2}{8G}. \tag{B-16}$$

So, equation (B-10) reduces to the maximum shear stress failure criterion, i.e.,

$$\tau_{max} = \frac{\sigma_1 - \sigma_3}{2} = \tau_f \tag{B-17}$$

(4) Hydrostatic Tension Failure Criterion

In this case

$$W_s^e = W_v^e = \frac{3(1-2\nu)}{2E}\sigma_H^2, \tag{B-18}$$

therefore, equation (B-10) is equivalent to

$$\sigma_H = \sigma_H^c \tag{B-19}$$

where σ_H^c is the critical value of the hydrostatic tension stress.

These failure criteria are commonly used to estimate the failure strength of various materials, and may be generalised as a stress type failure criterion

$$f(\sigma_{ij}) = 0 \tag{B-20}$$

which could be simplified further by using material isotropic properties.

This type of failure criterion is suitable for brittle material failure due to its independence of the strain history. The key issue is to define the specified elastic-strain energy density which controls a particular type of brittle failure. More discussion on the stress type failure criteria is presented in Polakowski and Ripling(1966), Dorn(1948) and Nadai(1950) (pp.207-228). Equation (B-20) may also be used in predicting ductile material failures when the influence of deformation history is retained in the failure criterion(Dorn(1948)). Dorn's conclusion is consistent with the present expression in equation (B-9) when the deformation history is understood as an irreversible dissipative process. In a plane stress state, these failure criteria are frequently described by biaxial failure maps in metal forming studies. It should be noted that using a stress type failure criterion to predict a ductile material failure is difficult because of the importance of the strain history effects in ductile failure processes. In a case when the loading path or deformation pattern is certain, a stress type failure criterion may be useful for predicting ductile material failures. This is why biaxial failure maps are used widely in the metal forming industry where the loading path is known for each working process.

B.3. Dissipative Energy Density Failure Criterion Associated With Large Inelastic Deformation and Material Failure

B.3.1. Dissipative Energy Density Failure Criterion

If, w_{sc}^{e} is considered as material strength, it decreases with the irreversible dissipative process, i.e., $\partial w_{sc}^{e}/\partial \phi_1 < 0$. Therefore, material ductile failure is a progressive process represented by the continuous decrease of material strength with the continuation of the dissipative process, which emerges as a natural outcome of excessive internal dissipation in a mechanical system. After a sufficiently large dissipation, which normally corresponds to large inelastic deformations, material failure is controlled mainly by the conducted dissipative process instead of being determined by internal interactions among atoms in the case of small inelastic deformations although these internal interactions are still the active driving force to separate material. Experimental studies by Bridgman(1952) have shown that hydrostatic stress has a strong influence on material failure. A tensile stress triaxiality

decreases the ductility of a material, while a compressive stress triaxiality increases it. Thus, the hydrostatic stress should be considered as an environmental parameter when other elastic actions are neglected in material ductile failure[8]. If Ludwik-Davidenkov-Orowan hypothesis(see Section B.2.4) is applicable for inelastic deformation process, the failure criterion for ductile material failure in large inelastic deformations becomes

$$\phi_1=\phi_{1c}(\sigma_H) \tag{B-21}$$

according to eq.(B-9), where, ϕ_{1c} is the critical value of the mechanical dissipative energy density. Equation (B-21) is the dissipative energy density failure criterion, which may be used in the prediction of material ductile failures under large inelastic deformations.

According to eq.(B-7), the dissipation energy is

$$\phi_1=w^p+w^d-w^v \tag{B-22}$$

where, $w^p=\int\sigma_{ij}d\varepsilon_{ij}^p$ is the inelastic strain energy density, ϕ_1 is the intrinsic dissipative energy density, $w^d=\int BdD$ is the damage dissipation density(from now on, Y_{ij} and D_{ij} in eq.(B-7) are substituted by B and D when the isotropic damage is assumed) and $w^v=\int(-A_k)dV_k$ is the stored energy density of cold work(Chrysochoos and Belmahjoub(1992)). For metals, w^v is the energy of the field of the residual micro-stresses which accompany the increase in the dislocation density. It represents only 5-10% of the term w^p and is often negligible[9](pp.68 in Lemaitre and Chaboche(1990)). Therefore, eq.(B-22) is simplified into

$$\phi_1=w^p+w^d. \tag{B-23}$$

If it is assumed that material plastic flow and material damage are two different physical processes, as shown by Lemaitre and Chaboche(1990), we have

---

[8] Actually, the influence of stress triaxility on material failure(both ductile and brittle) can be considered by including specified elastic strain energy density in eq.(B-9).

[9] For example, a coefficient β=90%-95% is used when calculating the temperature rise due to plastic work.

$$\sigma_{ij}\dot{\epsilon}^{p}_{ij} \geq 0 \quad \text{and} \quad \boldsymbol{B}\dot{\boldsymbol{D}} \geq 0. \tag{B-24a,b}$$

Eqs. (B-24a,b) implicate that the intrinsic dissipation consists of two different types, i.e., plastic dissipation and damage dissipation represented by two monotonously increasing functions, w^p and w^d, and the effects of these two different processes on material failure may be different.

B.3.2. Inelastic Strain Energy Density Failure Criterion

Inelastic strain energy density failure criterion has been used widely in predicting material ductile failures for various purposes. Cockcroft- and Latham(1968) suggested that the critical value of the inelastic strain energy density at fracture is practically constant at moderate strain rates, which was used to study the fracture of solid polymers by Vinh and Khalil(1984). Gillemot(1976) used it to predict the crack initiation in materials. Clift, et al.(1987,1990), employed the finite-element technique and several failure criteria to predict the fracture initiation in a range of simple metal-forming operations. It turns out that only the inelastic strain energy density failure criterion predicts successfully the correct fracture initiation sites, which were observed in the experimental results. An inelastic(or plastic) strain energy density failure criterion was combined with dynamic rigid, perfectly plastic analyses of beams and circular plates by Shen and Jones(1992, 1993a,b) and Jones and Shen(1993), and good agreement was found with the actual dynamic failure in several structural elements. These investigations have shown the validity of this failure criterion in some circumstances. However, many other failure criteria like the damage failure criterion also give encouraging failure predictions. It appears that both the damage failure criterion and the inelastic strain energy density failure criterion work well in many circumstances. A reasonable explanation on this aspect is given throughout the present Appendix.

Based on eq. (B-24a,b), it is concluded that material ductile failure is controlled by two dissipative mechanisms, which are inelastic(or plastic) deformation dissipation and damage dissipation, respectively. Material failure may occur due to either excessive plastic dissipation with small material damage from void development or excessive material damage from void coalescence. It is also possible that two dissipative mechanisms are important for the initiation of failure. If material

failure is mainly controlled by the plastic deformation mechanism, the failure criterion will become a plastic strain energy density failure criterion where the contributions from voids are negligible for material failure. In this case, material incompressibility is approximately valid, i.e., $d\varepsilon_{11}^p+d\varepsilon_{22}^p+d\varepsilon_{33}^p=0$, and therefore,

$$w^p=\int_0^{\epsilon_{ij}^p}\sigma_{ij}d\epsilon_{ij}^p=\int_0^{\epsilon_{ij}^p}s_{ij}d\epsilon_{ij}^p+\int_0^{\epsilon_{ij}^p}\sigma_H(d\epsilon_{11}^p+d\epsilon_{22}^p+d\epsilon_{33}^p)=\int_0^{\epsilon_{eq}^p}\sigma_{eq}d\epsilon_{eq}^p=w_c^p, \quad \text{(B-25)}$$

where, $s_{ij}=\sigma_{ij}-\sigma_H\delta_{ij}$, w_c^p is the critical value of plastic strain energy density determined by experiments. Equation (B-25) is described by generalized plastic work per unit volume in Clift et al.(1987, 1990), and is called (plastic) strain energy density failure criterion in Jones and Shen(1993). Basically, inelastic strain energy density failure criterion is valid for failure initiation controlled mainly by plastic dissipative process.

B.3.3. Continuum Damage Failure Criteria

In this section , we will discuss the situation when the failure process is controlled mainly by material damage dissipation. The microscopic mechanism is the coalescence of voids due to the initiation of unstable flow between the neighbouring voids. In this case, the failure criterion is

$$w^d=w_c^d, \quad \text{or} \quad w^e(\frac{\bar{E}}{E}-1)=w_c^d \quad \text{(B-26)}$$

where $w^d=w^e(\bar{E}/E-1)$ according to damage mechanics, $\bar{E}$ is the Young's modulus of the virgin material, w_c^d is the critical value of the damage dissipation density. The elastic strain energy, w^e, depends on strain hardening(also depends on strain rate hardening if it is significant), hydrostatic stress, σ_H and current Young's modulus, E, while, the current Young's modulus depends on the damage parameter, D. Thus, eq.(B-26) may be expressed by

$$D=D_c(\sigma_H) \quad \text{(B-27)}$$

when material plastic strain hardening is not significant during a damage control failure process. Eq.(B-27) is well-known as damage failure criterion and has been used widely in continuum damage mechanics to predict the initiation of material

ductile failure. The significance of the parameter σ_H on the value of D_c need to be verified by experiments. Alves(1996) examined the influence of σ_H on the critical damage parameter, D_c. It was concluded that the critical damage parameter does not seem to be highly stress state dependent for the mild steel. A similar conclusion was reached by Otsuka et al.(1987) for a structural steel SM41A. However, other evidence gave controversial results(Becker(1987) and Shi et al.(1991)). A discussion on this topic is given by Alves(1996). Strain rate and temperature influences on the critical value of D are not included in eq.(B-27). It was also shown by Alves(1996) that strain rate does not significantly influence the critical damage parameter in the studied problem. However, it is well-known that material ductility decreases with increase of strain rate(and also with decrease of temperature). For a damaged material, material ductility includes both plastic deformation and damage development. Thus, it is highly possible that strain rate and temperature have some influences on the critical damage parameter, which need to be verified by further experiments.

Another potential theory used to predict material failure, is the porous ductile material model established by Gurson(1977) and developed successively by many other authors. In spite of the different modelling procedures used in these two theories, similar concepts are used in both theories to define material failure. In continuum damage mechanics, the surface density of the discontinuity of the material(D) is used to represent material damage and to define material failure by its critical value(D_c). In porous ductile material model, the void volume fraction(f) together with its critical value(f_F) is used to define the material failure. For an isotropic material, there is a relationship between them for a given void type. Therefore, eq.(B-27) can be expressed equivalently by

$$f=f_c(\sigma_H) \tag{B-28}$$

as used in many void growth models(Gurson(1977), Tvergaard(1990)).

The application of eq.(B-27) or eq.(B-28) requires the solution of the evolution equations of a damage index, which depends on the development of macroscopic stress and strain and their histories, and, in turn, the macroscopic stress and strain contain the information of both plastic dissipation and damage dissipation.

Therefore, it is possible to use macroscopic stress and strain to define a failure criterion, which have been proved by existing results.

After defining a dissipative surface, F, which distinguishes the elastic domain from other dissipative responses, the thermodynamical principle and the minimum free energy theorem lead to

$$d\epsilon_{ij}^{p}=d\lambda\frac{\partial F}{\partial\sigma_{ij}} \quad \text{and} \quad dD=d\lambda\frac{\partial F}{\partial B}. \tag{B-29a,b}$$

Substituting $d\lambda$ determined from (B-29a) to eq(B29-b) gives

$$dD=d\epsilon_{e}^{p}\frac{\dfrac{\partial F}{\partial B}}{\sqrt{\dfrac{2}{3}\dfrac{\partial F}{\partial\sigma_{ij}}\dfrac{\partial F}{\partial\sigma_{ij}}}}=Gd\epsilon_{e}^{p}. \tag{B-30}$$

Similar procedures were used by Zheng et al.(1994), in which the potential function F was expressed by

$$F(\sigma_{ij},B)=\sigma_{e}+g(B,\sigma_{m}) \tag{B-31}$$

where $\partial g/\partial\sigma_{e}=0$. However, in their later discussion, $\partial g/\partial B$ was expressed as a function of σ_{e}, which is not consistent with their previous assumption that g is independent of σ_{e}. Furthermore, the Levy-Mises relationship is evaluated from eq.(B-31) by Zheng et al.(1994), which is not valid generally for a porous ductile material, as shown by porous ductile material model(Gurson(1977) and Tvergaard(1990)).

The material damage failure criterion according to eqs.(B-27) and (B-30) may be expressed by

$$D=\int_{0}^{\epsilon_{e}^{p}}Gd\epsilon_{e}^{p}=D_{c}, \tag{B-32}$$

where $G=G(\sigma_{e},\sigma_{H},D)$ is determined by eq.(B-30).

A large group of ductile failure criteria have been proposed in the form of eq.(B-32). Some examples are listed below.

(1) M.Oyane(1972):

$$G=(1+\frac{1}{a_0}\frac{\sigma_m}{\sigma_e})\epsilon_e^{c_0} \tag{B-33}$$

where $\sigma_m=3\sigma_H$, and a_0 and c_0 are material constants.

(2) M.Zheng, et al.(1994):

$$G=\frac{1}{A}\exp(1.5\frac{\sigma_m}{\sigma_e}) \tag{B-34}$$

where A is material constant.

(3) R.Chaouadi, et al.(1994):

$$G=[1+\alpha\frac{\sigma_m}{\sigma_e}\exp(\frac{\sigma_m}{2\sigma_e})]\sigma_e \tag{B-35}$$

where α is material constant.

(4) T.J.Wang(1992a,b, 1993):

$$G=F(\frac{\sigma_H}{\sigma_e},\epsilon_e^p)=kf(\frac{\sigma_H}{\sigma_e})(\epsilon_e^p-\epsilon_0^p)^{k-1} \tag{B-36}$$

where k is a damage coefficient, ε_0^p is the void nucleation strain, and

$$f(\frac{\sigma_H}{\sigma_e})=\frac{2}{3}(1+\nu)+3(1-2\nu)(\frac{\sigma_H}{\sigma_e})^2. \tag{B-37}$$

When k=1 it is identical to Lemaitre and Chaboche(1990)'s results(pp.440).

These failure criteria have been used in many applications when material damage plays an important role during structural failure.

B.4. Applications of Plastic Strain Energy Density Failure Criterion in Dynamic Structural Responses

It has been observed that several structural elements, when subjected to sufficiently large transverse dynamic loads, may fail in one of three principal modes, i.e.,

Mode I : large inelastic deformations,

Mode II: tearing(tensile failure),

and Mode III: transverse shear failure(fracture),

which were first observed for beams(Menkes and Opat(1973), Ross, et al.(1977) and Jones(1976)), and then for square and circular plates(Ross, et al.(1977), Olson, et al.(1993) and Teeling-Smith and Nurick(1991)) and cylindrical shells(Ross, et al.(1977), Opat and Menkes(1974) and Strickland, et al.(1976)). Only Mode II and Mode III relate to actual material failures and some experimental results for failure exhibit the characteristics of combined modes II and III.

A detailed examination of the experimental results reveals that Modes II and III belong to a local tensile failure(Jones(1989)) although with different response features. Therefore, the values of w_c^p for an inelastic strain energy density failure criterion could be determined from a uniaxial tensile test with the proper consideration of strain rate and hydrostatic effects.

Rigid, perfectly plastic simplifications have been used successfully to predict the dynamic response of a wide range of structural elements. It has some advantages in qualitative analysis and saves computer time when compared with numerical simulations. This section is concentrated mainly on the applications of an inelastic strain energy density failure criterion to a beam made from rigid, perfectly plastic material, which, however, may be extended to plates and cylindrical shells.

Generalized stresses and strains could be introduced in order to simplify the analyses of beams and other structural elements. These generalized stresses and strains are defined with respect to the entire cross-section of a beam. However, a Mode II failure, for example, is a local phenomenon, which does not occur simultaneously across the entire cross-section, but develops at a macroscopic point, as illustrated in Fig.B.2(a). Such a macroscopic failure point is always located within a severely deformed zone where a mixture of bending, shearing and tensile deformations exists and which is called a plastic hinge for a rigid, perfectly plastic beam. The inelastic strain energy density at the expected failure point may be expressed as[10]

[10] Here we assume that the deformations corresponding to the bending moment, transverse shearing force and the membrane force are separable.Therefore, the total deformations at a macroscopic point of a beam is the superimposition of the deformations at that point, which correspond to bending moment, transverse shearing force and membrane force defined in a beam cross-section.

$$w^p = w_m + w_s + w_n \quad , \tag{B-38}$$

where w_m, w_s and w_n are the inelastic strain energy densities associated with the bending moment, shearing force and membrane force at the failure point A in Fig.B.2(a), respectively. A rigid, perfectly plastic analysis does not provide any information on the structure of a plastic hinge. However, it is reasonable from an engineering viewpoint to assume that the stresses and deformations associated with bending, shearing and membrane hinges have the uniform distributions in the longitudinal direction within the hinge as shown in Figs.B.2(b-c). Therefore, the inelastic strain energy density failure criterion expressed by equation (B-37) may be cast in the following form

$$W_m + \frac{l_m}{l_s} W_s + \frac{l_m}{l_n} W_n = BHl_m w_c^p \quad , \tag{B-39}$$

because

$$w_m = \frac{W_m}{BHl_m} \quad , w_s = \frac{W_s}{BHl_s} \quad \text{and} \quad w_n = \frac{W_n}{BHl_n} \quad , \tag{B-40a-c}$$

where B and H are the width and thickness of the beam, and W_m, W_s and W_n are the dissipated inelastic energies in the total length of the corresponding plastic hinges which have hinge lengths l_m, l_s and l_n, respectively. The value of w_c^p should be determined from a dynamic uniaxial tensile test. It should be noted that l_m is the average bending hinge length which is defined by the half length of the bending deformation zone, as shown in Fig.B.2. If it is assumed that $l_n = l_m$, then equation (B-39) becomes[11]

$$W^p = W_m + \gamma W_s + W_n = BHl_m w_c^p \quad , \tag{B-41}$$

where $\gamma = l_m / l_s$. Equation (B-41), in principle, may be extended to circular plates, cylindrical shells and other structural members in a similar way. Nonaka(1967) used slip line theory to study the behaviour of beams and obtained the average hinge

[11] No generality is lost when it is assumed that $l_n = l_m$ because membrane force and the associated deformations are uniform along the beam. In this case, W_n is the total inelastic energy corresponding to the membrane force in an average bending hinge length.

length $l_m=H/2$ for a pure bending moment and $l_m=H$ at the beginning of a membrane state.

If $\gamma=1$, equation (B-41) is simplifies to

$$W^P=W_m+W_s+W_n=w_p^c BHl_m=W_c^P \tag{B-42}$$

which is identical to equation (9) in Jones and Shen(1993). However, the assumption $\gamma=1$ requires verification.

Shen and Jones(1992,1993a,b) and Jones and Shen(1993) used the inelastic strain energy density failure criterion described by equation (B-42) to investigate material failures in various structural elements under different dynamic loadings.

In the particular case of a rigid, perfectly plastic beam having a width B and a thickness H, the actual inelastic work absorbed at failure in a plastic hinge having an average length l_m across the beam thickness is

$$W_c^P=BHl_m w_c^P(\dot{\varepsilon}_m) \tag{B-43}$$

where $w_c^P(\dot{\varepsilon}_m)$ is determined from material test, $\dot{\varepsilon}_m$ is the mean strain rate..

The influence of material strain rate sensitivity on the critical value of the inelastic strain energy density is unclear. w_c^P increases with strain rate according to the experimental data in Yu and Jones(1991) for an aluminium alloy. However, other source assumed that the value of w_c^P is insensitive to strain rate(Jones(1989), also discussion in Section 5.1.4). Thus, it is difficult to estimate the influence of strain rate effects on the value of w_c^P and further systematic experiments are required at various strain rates in order to achieve an understanding of this problem.

Shen and Jones(1992,1993a,b) and Jones and Shen(1993) use this procedure to analyze the material failure of impact loaded beams and circular plates. These theoretical results are compared with the corresponding experimental results(Liu and Jones(1987), Yu and Jones(1991) and Teeling-Smith and Nurick(1991)), and have demonstrated the advantages of the strain energy density failure criterion as a more universal failure criterion, which can be combined with various dynamic analysis procedures or numerical finite-element analyses to predict material failure in different types of structural elements.

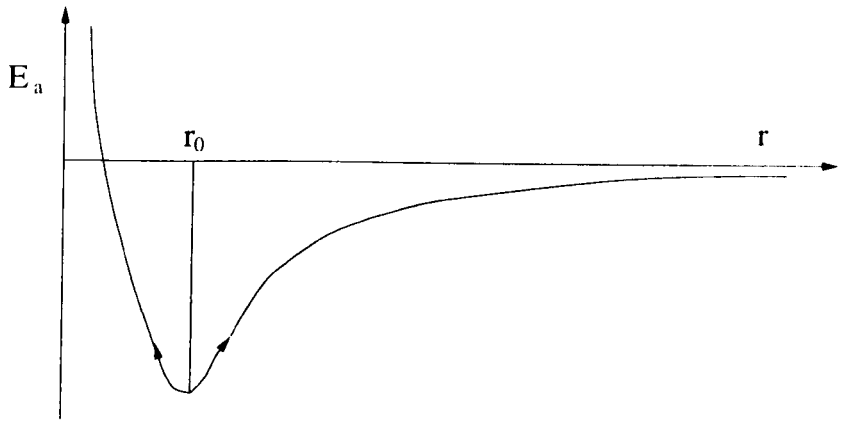

Fig.B.1 The inter-atomic energy curve, r is the distance between atoms.

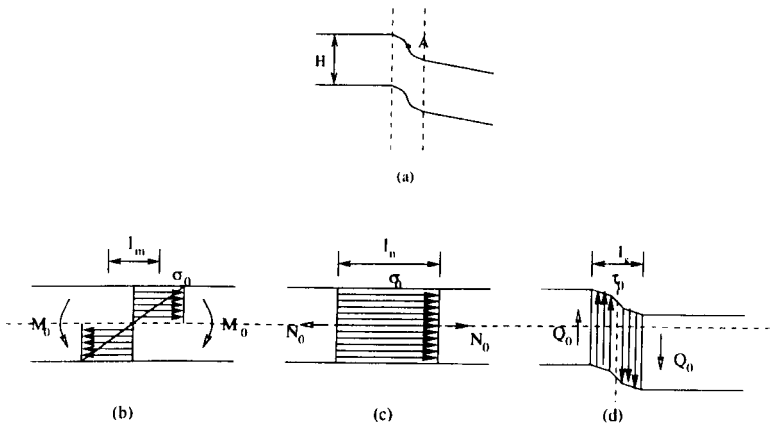

Fig.B.2 (a) Macroscopic failure point in the deformed zone of a beam; (b) Stress and strain distributions under bending; (c) Stress and strain distributions corresponding to membrane force; (d) Transverse shear deformation and stress distributions.

LIST OF TABLES

LIST OF FIGURES

REFERENCES

ABAQUS(1994a), Theory and User's Manual/standard, Version 5.4.
ABAQUS(1994b), Example Problems Manual/standard, Vol.II, Version 5.4, Section 5.2.4-1.
Alves,M.(1996), Damage mechanics applied to structural impact, Ph.D thesis, University of Liverpool.
Ashby,M.F.(1981), Proc. Mat. Sci., Bruce Chalmers Anniversary Volume, pp.1-25.
Atkins,A.G.(1981), Possible explanation for the unexpected departure in hydrostatic tension-fracture strain relations, Metals Sci..
Atkins,A.G.(1988), Scaling in combined plastic flow and fracture, Int. J. Mech. Sci., 30, 173-191.
Awerbuch,J. and Bodner,S.R.(1974), Experimental investigation of normal perforation of projectiles in metallic plates, Int. J. Solids Structures, 10, 685-699.
Azrin,M. and Backofen,W.A.(1970), Met. Trans., 1, 2852-2865.
Bai,Y.L.(1982), Thermo-plastic instability in simple shear, J.Mech. Phys. Solids, 30, 195-207.
Bai,Y.L. and Dodd,B.(1992), Adiabatic shear localization: occurrence, theories and application, Pergamon Press, U.K..
Bammann,D.J., et al.(1993), Failure in ductile materials using finite element methods, in Structural Crashworthiness and Failure, eds. N.Jones and T.Wierzbicki, Elsevier Appl. Sci., England, pp.1-54.
Becker,R.(1987), The effect of porosity distribution on ductile fracture, J. of the Mech. and Phys. of Solids, 35, 577-599.
Bertholf, L.D. and Karnes, C.H.(1975), Two-dimensional analysis of the split-Hopkinson pressure bar system, J. Mech. Phys. Solids, 23, 1-19.
Birch,R.S., Jones,N. and Jouri,W.S.(1988), Performance assessment of an impact rig, Proc. Inst. Mech. Engng., 202(C), 275-285 and 204(C), 8.
Bluhm,J.I. and Morrissey,R.J.(1965), Proc. 1st Int. Conf. on Fracture, eds.T.Yokobori and T.Kawasaki, Sendai, Japan, DII-5, 1739.
Boyer,H.E. and Gall,T.L.(1985), eds, Metals handbook, Desk Edition, A.S.M., Metals Park, Ohio 44073.
Brandes,M.(1972), Mechanical properties of materials under hydrostatic pressure, in Mechanical Behaviour of Materials Under Pressure, eds.H.L.D.Pugh, pp.236-298, Elsevier, Amsterdam.
Bridgman,P.W.(1944), Trans ASM, 32, 553-574.
Bridgman,P.W.(1952), Studies in large plastic flow and fracture, McGraw-Hill.
Brownrigg,A., et al.(1983), The influence of hydrostatic pressure on the flow stress and ductility of a spherodized 1045 steel, Acta Metall., 31, 1141-1150.
Brozzo,P., et al.(1972), A new method for the prediction of formability limits in metal sheets, Sheet Metal Forming and Formability, Proceedings of the 7th biennial Conference of the Int. Deep Drawing Research Group.
Carrol,M.M. and HoltA.C.(1972), Static and dynamic pore-collapse relations for ductile porous materials, J. Appl. Phys., 43, 1626-1636.
Chandrakanth,S. and Pandey,P.C.(1993), A FEM study of ductle failure using

continuum damage model coupled with plasticity, Plastic and Impact Mechanics, ed.N.K.Gupta, Wiley Eastern Limited, New Delhi, pp.173-184.
Chaouadi,R., et al.(1994), Damage work as ductile fracture criterion, Int. J. of Fracture, 66, 155-164.
Chow,C.L. and Wang,J.(1987a), An anisotropic theory of elasticity for continuum damage mechanics, Int. J. of Fracture, 33, 3-16.
Chow,C.L. and Wang,J.(1987b), An inisotropic theory of continuum damage mechanics for ductile fracture, Engng. Fracture Mech., 27, 547-558.
Chow,C.L. and Yang,F.(1991), On one-parameter description of damage state for a brittle material, Engng. Fracture Mech., 40, 335-343.
Chrysochoos,A. and Belmahjoub,F.(1992), Thermographic analysis of thermomechanical coupling, Arch. Mech., 44, 55-68.
Clift,S.E., et al.(1987), Further studies on fracture initiation in plane-strain forging, in applied Solid Mech.-2, eds. A.S.Tooth and J.Spence, Elsevier, Amsterdam.
Clift,S.E., et al.(1990), Fracture prediction in plastic deformation process, Int. J. Mech. Sci., 32, 1-17.
Clifton,R.J.(1983), J. Appl. Mech., 50.
Cockcroft,M.G. and Latham,D.J.(1968), Ductility and the workability of metals, J. Inst. metals, 96, 339.
Cordebois,J.L. and Sidoroff,J.P.(1983), Damage induced elastic anisotropy, Colloque Euromech. 115, Villard de Lans. Also appearing in J.P.Boehler(ed.), Mech. Behaviour of Anisotropic Solids, pp.761-774, Martinus Nijhoff.
Costin,L.S., et al.(1979), Proc. 2nd Conf. Mech.Properties of Materials at High Rates of Strain, ed.J.Harding, pp.90, Adam Hilger, Bristol(original from R.J.Clifton, Report to the NRC Committee on Material Response to Ultrasonic Loading Rates).
Cottrell, A.H.(1964), The mechanical properties of matter, Wiley, London.
Curran,D.R., et al.(1987), Dynamic failure of solids, Phys. reports, 147, 253-388.
Dafalias,Y.F.(1977a), Elasto-plastic coupling within a thermodynamic strain space formulation of plasticity, J. of Non-linear Mech., 12, 327.
Dafalias,Y.F.(1977b), Il'yushin's postulate and resulting thermodynamic conditions on elastoplastic coupling, Int. J. Solids Structs., 13, 239-251.
de Oliveira,J.G. and Jones,N.(1978), Some remarks on the influence of transverse shear on the plastic yielding of structures, *Int. J. Mech. Sci.*, 20, 759-765.
Dodd,B. and Atkins,A.G.(1983), Flow localization in shear deformation of void-containing and void-free solids, Acta Metall., 31, 9-15.
Dodd,B. and Bai,Y.L.(1987), Ductile Fracture and Ductility-with application to metalworking, Academic Press, London.
Dorn,J.E.(1948), The effect of stress state on the fracture strength of metals, in Fracture of Metals, ASM, pp.32-50.
Dragon,A. and Mroz,Z.(1979), A continuum model for plastic-brittle behaviour of rock and concrete, Int. Engng. Sci., 17, 121-137.
Dragon,A.(1985), Plasticity and ductile fracture damage: study of void growth in metals, Engng. Fracture Mechanics., 21, 875-885.
Drucker,D.C.(1951), A more fundamental approach to plastic stress-strain relations, ed. E.Sternberg, *Proc. First U.S. Cong. of Appl. Mech., ASME,* New York, PP.487-491.
Drucker,D.C.(1964), On the postulate of stability of material in the mechanics of

continua, *J. de Mecanique*, 3, 235.
Drugan,W.J. and Shen,Y.(1987), Restrictions on dynamically propagating surfaces of strong discontinuity in elastic-plastic solids, *J. of Mech. Phys. Solids*, 35, 771-787.
Duffy,T.A.(1989), Dynamic rupture of shells, in Structural Failure, eds. T.Wierzbicki and N.Jones, John Wiley & Sons, New York, pp.161-192.
Edelson,B.I. and Baldwin,W.M.(1962), Trans ASM, ASM International, 55, 230.
Embury,J.D. and Leroy,G.H.(1977), Failure maps to metal deformation processes, Fracture 1977, Vol.1, ICF4, Waterloo, Canada, June, 1977, pp.15-42.
Engel,L. and Klingele,H.(1981), Atlas of metal damage, Wolfe Science Books, C.H.Verlag, Munich.
Ferron,G. and Zeghloul,A.(1993), Strain localization and fracture in metal sheets and thin-walled structures, in Structural Crashworthiness and Failure, eds. N.Jones and T.Wierzbicki, Elsevier Appl. Sci., London, pp.131-163.
Follansbee, P.S.(1985), The Hopkinson bar, in ASM Metals Handbook: Vol.8, ASM International, Materials Park, OH, pp.198-203.
Fressengeas,C. and Molinari,A.(1987), Instability and localization of plastic flow in shear at high strain rates, J. Mech. Phys. Solids, 35, 185-211.
Freudenthal,A.M.(1950), The inelastic behaviour of solids, Wiley, Nrw York.
Fyfe,I.M.(1983), Application of Gurson void growth model to dynamic fracture, in MaterialBehaviour under High Stress and Ultra-high Loading Rates, eds.J.Mescall and V.Weiss, Sagamore Army Material research Conf. Proceedings, 29, 309-318.
Fyfe,I.M.(1984), A damage criterion for dynamic ductile failure, in Structural Impact and Crashworthiness, Vol.2, ed.J.Morton, Elsevier, London, 383-394.
Ghosh,A.K.(1976), A criterion for ductile fracture in sheets under biaxial loading, Metall. trans, 7A, 523-533.
Gillemot,L.F.(1976), Criterion of crack initiation and spreading, Engng. Fracture Mech., 8, 239-253.
Gordon,J.E.(1976), The new science of strong materials, 2rd. ed., Penguin Books.
Grady,D.E. and Kipp,M.E.(1987), The growth of unstable thermoplastic shear with application to steady-wave shock compression in solids, J. Mech. Phys. Solids, 35, 95-118.
Grady,D.E.(1992), Properties of an adiabatic shear band process zone, J. Mech. Phys. Solids, 40, 1197-1215.
Griffith,A.A.(1921), The phenomena of rupture and flow in solid, Phil. Trans. Roy. Soc., A221, pp.163-197.
Gurland,J.(1972), Observations on the fracture of cementite particles in a spheroidized 1.05% C steel deformed at room temperature, Acta Metall., 20, 735-741.
Gurson,A.L.(1977), Continuum theory of ductile rupture by void nucleation and growth: Part I-Yield criteria and flow rules for porous ductile media, J. of Engng. Material and Tech., 99, 2-15.
Hancock,J.W. and Mackenzie,A.C.(1976), On the mechanism of ductile failure in high strength steels subjected to multi-axial stress-states, J. Mech. Phys. Solids, 24, 147-169.
Hancock,J.W. and Brown,D.K.(1983), On the role of strain and stress state in ductile failure, J. Mech. Phys. Solids, 31, 1-24.
Hansen,N.R. and Schreyer,H.L.(1994), A thermodynamically consistent framework for theories of elastoplasticity coupled with damage, Int. J. Solids Structs., 31, 359-

389.
Harding,J.(1988), in Impact loading and dynamic behaviour of materials, eds.C.Y.Chiem, et al., Oberursel, Germany, pp.21.
Hecker,S.S.(1976), Exp. studies of yield phenomena in biaxially loaded metals, in Constitutive Equations in Viscoplasticity: Computational and Engng. Aspects, eds.J.A.Stricklin and K.J.Saczalski, pp.1-33, Am. Soc. Mech. Engng., New York.
Hecker,S.S.(1977), Analysis modelling and experimentation, in Formability, eds.S.S.Hecker, et al., pp.105-182, Met. Soc. AIME.
Hecker,S.S.(1978), in Application of Numerical Methods to Forming Processes, eds.H.Armen and R.F.Jones, pp.85-94, ASME AMD-28.
Hill,R.(1950), The mathematical theory of plasticity, Oxford Univ. Press, pp.317-340.
Hodge,Jr.,P.G.(1955), Impact pressure loading of rigid-plastic cylindrical shells, *J. of Mech. Phy. of Solids*, 3, 176-188.
Holmes,B.S., et al.(1993), Modelling the process of failure in structures, in Structural Crashworthiness and Failure, eds.N.Jones and T.Wierzbicki, Elsevier Appl. Sci., London, pp.55-93.
Hopkins,H.G. and Prager,W.(1954), On the dynamics of plastic circular plates, *ZAMP*, 5, 317-330.
Illston,J.M., et al.(1979), Concrete, timber and metals, the nature and behaviour of structural materials, Van Nostrand Reinhold Company, London.
Il'yushin,A.A.(1961), Prik. Mat. Mekh., 25, 503.
Johnson,G.R. and Cook,W.H.(1983), Proc. 7th Int. Symp. Ballistics, Am Def. Prep. Org.(ADPA), Netherlands.
Johnson,J.N.(1981), Dynamic fracture and spallation in ductile solids, J. Appl. Phys., 52, 2812-2825.
Jones,N.(1976), Plastic failure of ductile beam loaded dynamically, Trans. ASME, J. Engng. Ind., 98, 131-136.
Jones,N. and de Oliveira,J.G.(1979), The influence of rotatory inertia and transverse shear on the dynamic plastic behaviour of beams, ASME J. of Appl. Mech., 46, 303-310(1979).
Jones,N. and de Oliveira,J.G.(1980), Dynamic plastic response of circular plates with transverse shear and rotatory inertia, *ASME J. Appl. Mech.*, 47, 27-34.
Jones,N. and de Oliveira,J.G.(1983), Impulsive loading of a cylindrical shell with transverse shear and rotatory inertia, *Int. J. of Solids and Structures*, 19, 263-279.
Jones,N.(1989), Structural impact, Cambridge Univ. Press.
Jones,N.(1989b), Recent studies on the dynamic plastic response of structures, Appl. Mech. Rev., 42, 95-115.
Jones,N.(1989c), On the dynamic inelastic failure of beams, in Structural Failure, eds. T.Wierzbicki and N.Jones, Wiley, New York, pp.133-159.
Jones,N.(1989d), Some comments on the modelling of material properties for dynamic structural plasticity, in Mechanical Properties of Materials at High rates of Strain, ed.J.Harding, Institute of Phys. Conf. Series No.102, Bristol, pp.435-445.
Jones,N.(1993), Material properties for structural impact problems, in Advances in Materials and Their Applications, ed.P.Rama Rao, Wiley Eastern Limited, New Delhi, 151-163.
Jones,N. and Shen,W.Q.(1993), Criteria for the inelastic rupture of ductile metal beams subjected to large dynamic loadings, in Structural Crashworthiness and Failure,

eds.N.Jones and T.Wierzbicki, Elsevier Appl. Sci., London, pp.96-130.
Jones,N., Kim,S.B. and Li,Q.M.(1997),Response and failure of ductile circular plates struck by a mass, J. of Pressure Vessel Tech., Vol.119, 332-342.
Jouri,W.S. and Jones,N.(1988), The impact behaviour of aluminium alloy and mild steel double-shear specimens, Int. J. Mech. Sci., 30, 153-172.
Ju,J.W.(1989), On energy-based coupled elastoplastic damage theories: constitutive modelling and computational aspects, Int. J. Solids Struct., 25, 803-833.
Kachanov,L.M.(1958), Time of the rupture process under creep conditions, IVZ Akad Nauk, SSSR., Otd Tech. Nauk, No.8, pp.26-31.
Kachanov,L.M.(1986), Introduction to continuum damage mechanics, Martinus Nijhoff Dordricht.
Kachanov,L.M..(1994), Elastic solids with many cracks and related problems, in J.W.Hutchinson and T.Y.Wu, eds., Advances in Pllied Mechanics, pp.259-445, Academic Press, Inc..
Kalthoff,J.F., et al.(1987), Failure mode transition at high rates of loading, Proc. of the Int. Conf. on Impact Loading and Dynamic Behaviour of Materials, ed. C.Y.Chiem, et al., Bremen, Deutsche Gesellschaft fur Metallkunde, DGM, pp.185-196.
Kalthoff,J.F.(1990), Transition in the failure behaviour of dynamically shear loaded cracks, Proc. of the 11th US National Conf. of Appl. Mech., ed.C.F.Chen, TUCSON, Arizona, May, pp.5247-5250.
Kattan,P.I. and Voyiadjis,G.Z.(1990), A coupled theory of damage mechanics and finite strain elasto-plasticity--I, damage and elastic deformations, Int. J. Engng. Sci., 28, 421-435.
Keeler,S.P. and Backofen,W.A.(1963), Plastic instability and fracture in sheets stretched over rigid punches, Trans. ASM, 56, 25-48.
Klepaczko,J.R.(1994), Plastic shearing at high and very high strain rate, J. De Physique, Colloque C8, pp35-40.
Koiter,W.T.(1953), Stress-strain relations, uniqueness and variational theorems for elastic-plastic materials with a singular yield surface, *Quarterly of Appl. Math.*, 11, 350-354.
Korhonen,A.S.(1978), On the theories of sheet metal necking and forming limits, ASME J. Engng. Mat. Tech., 100, 303-309.
Krajcinovic,D.(1985), Continuum damage mechanics revisited: basic concepts and definitions, ASME, J. Appl. Mech., 52, 829-834.
Krajcinovic,D.(19?), Constitutive theories for solids with defective microstructure, in Damage Mech. and Continuum Modelling, ed.N.Stubbs and D.Krajcinovic, pp.39-56, ASCE.
Lee,E.H. and Symonds,P.S.(1952), Large plastic deformation of beams under transverse impact, *ASME J. of Appl. Mech.*, 19, 308-314.
Lemaitre,J.(1971), Evaluation of dissipation and damage in metals, Proc. I.C.M., Vol.1, Kyoto, Japan.
Lemaitre,J. and Chaboche,J.L.(1990), Mechanics of solid materials, Cambridge University Press, Cambridge.
Li,Q.M. and Jones,N.(1991), Influence of boundary conditions on the blast loading of beams and circular plates, in Appl. Solid Mech.-4, eds.A.R.S.Ponter and A.C.F.Cocks, Elsevier Appl. Sci., London, pp.52-71.

Li,Q.M. and Jones,N.(1994), Blast loading of fully clamped circular plates with transverse shear effects, Int. J. Solids Structures, 31, 1861-1876.
Li,Q.M. and Jones,N.(1995a), Blast loading of fully clamped beams with transverse shear effects, Mechanics of Structures and Machines, 23, 59-86.
Li,Q.M. and Jones,N.(1995b), blast loading of a "short" cylindrical shell with transverse shear effects, Int. J. Impact Engng., 16, 331-353.
Liu,J.H. and Jones,N.(1987), Experimental investigation of clamped beams struck transversely by a mass, Int. J. Impact Engng., 6, 303-335.
Liu,J.H. and Jones,N.(1988), Dynamic response of a rigid plastic clamped beam struck by a mass at any point on the span, Int. J. Solids Struct., 24, 251-270.
Ludwik,P.(1927), The meaning of flow and rupture resistance in material testing, Zeitschrift Vereines deutsher Ingenieure, 71, 1532-1538.
Mai,Y.W.(1993), On the plane-stress essential fracture work in plastic failure of ductile materials, Int. J. Mech. Sci., 35, pp.995-1005.
Malvern,L.E.(1969), Introduction to the mechanics of a continuous medium, Prentice-Hall, New Jersey.
Marchand,A. and Duffy,J.(1988), An experimental study of the formation process of adiabatic shear bands in a structural steel, J. Mech. Phys. Solids, 36, 251-283.
Matic,P., et al.(1988), The relation of tensile specimen size and geometry effects to unique constitutive parameters for ductile materials, Proc. R. Soc. Lond. A417, 309-333.
McClintock,F.A.(1968), A criterion for ductile fracture by the growth of holes, J. of Appl. Mech., 35, 363-371.
McClintock,F.A.(1993), Necking in plane strain under bending with constant tension, J. Mech. Phys. Solids, 41, 1327-1343.
Menkes,S.B. and Opat,H.J.(1973), Broken beams, Exp. Mech., 13, 480-486.
Meyers,M.A.(1994), Dynamic behavior of materials, John Wiley & Sons Inc, New york.
Molinari,A. and Clifton,R.J.(1987), Analytic characterization of shear localization in thermo-visco-plastic materials, ASME, J. Appl. Mech., 54, 806-812.
Nadai,A.(1950), Theory of flow fracture of solids, Vol.1, McGraw-Hill Book Comp., London.
Needleman,A.(1994), Computational modelling of material failure, Appl. Mech. Rev., 47(6), Part 2, S34-S42.
Nemat-Nasser,S.(1988), Discontinuities in elastic-plastic solids, *Mechanics of Material*, 7, 215-229.
Nonaka,T.(1967), Some interaction effects in a problem of plastic beam dynamics, Part 1-3, ASME, J. Appl. Mech., 34, 623-643.
Nonaka,T.(1977), Shear and bending response of a rigid-plastic beam to blast-type loading, *Ingenieur-Archiv*, 46, 35-52.
Norris,D.M., et al.(1978a), A computer simulation of the tension test, J. Mech. Phys. Solids, 26, 1-19.
Norris,D.M., et al.(1978b), A plastic strain mean-stress criterion for ductile fracture, J. Engng. Material Tech., 100, 279-286.
Nowacki,W.K.(1978), *Stress waves in non-elastic solids*, Pergamon Press.
Oliferuk,W.(1993), Rate of energy storage and microstructure evolution during the tensile deformation of austenitic steel, Material Sci. and Engng., A161, 55-63.

Olson,M.D., et al.(1993), Deformation and rupture of blast loaded square plates---predictions and experiments, Int. J. Impact Engng., 13, 279-291.
Opat,H.J. and Menkes,S.M.(1974), Hard point failure in relationship to lethality, Tech. Rept. 4738, Picatinny Arsenal, Dover, NJ.
Osacada,K., et al.(1981), Ductile fracture of carbon steel under cold metal forming conditions(3rd report, effects of deformation mode and deformation history on ductile fracture strain), Bull. JSME, 24, 534-539.
Otsuka,A, et al.(1987), Relationship between ductile crack initiation and void volume fraction, Nuclear Engng. and Design, 105, 121-129.
Oyane,M.(1972), Criteria of ductile fracture strain, Bulletin of the JSME, 15, 1507-1513.
Pan,J., et al.(1983), Localization of deformation in rate sensitive porous plastic solids, Int. J. Fracture, 21, 261-278.
Polakowski,N.H. and Ripling,E.J.(1966), Strength and structure of engineering materials, Prentice-Hall, Englewood Cliffs, N.J..
Prigogine,I. and Stengers,I(1984), Order out of chaos, man's new dialogue with nature, Flamingo.
Ramesh, K.T. and Narasimhan, S.(1996), Finite deformations and the dynamic measurement of radial strains in compression Kolsky bar experiments, Int. J. Solids Struct., 33, 3723-3738.
Rice,J.R. and Tracey,D.M.(1969), On the ductile enlargement of voids in triaxial stress fields, J. Mech. Phys. Solids, 17, 201-217.
Rice,J.R.(1971), Inelastic constitutive relations for solids: an internal-variable theory and its application to metal plasticity, J. Mech. Phys. Solids, 19, 433-455.
Ross,C.A., et al.(1977), Response and failure of simple structural elements subjected to blast loading, Shock and Vib. Digest, 9, 15-26.
Roy,G.Le, et al.(1981), A model of ductile fracture based on the nucleation and growth of voids, Acta Metall., 29, 1509-1522.
Sachs,G.(1948), Effect of strain on fracture, in Fracturing of metals, pp.51-67, ASM, Cleveland, Ohio.
Shen,W.Q. and Jones,N.(1992), A failure criterion for beams under impulsive loading, Int. J. Impact Engng., 12, 101-121 and 329.
Shen,W.Q. and Jones,N.(1993), Dynamic plastic response and failure of a clamped beam struck transversely by a mass, Int. J. Solid Structures, 30, 1631-1648.
Shen,W.Q. and Jones,N.(1993b), Dynamic response and failure of fully clamped circular plates under impulsive loading, Int. J. Impact Engng., 13, 259-278.
Shi,Y.W., et al.(1991), Void growth at ductile crack initiation of a structural steel, Engng. Fracture Mech., 39, 37-44.
Shockey,D.A., et al.(1981), in Shock Waves and High-strain Rate Phenomena in Metals: Concepts and Application, eds. M.A.Meyers and L.E.Murr, Plenum Press, New York, pp.129.
Sih,G.C.(1985), Mechanics and physics of energy density theory, Theoretical and Appl. Mech., 4, 157-173.
Sih,G.C. and Ho,J.W.(1993a), Rigid-plastic and damage behaviour in metal forming: Part I-theoretical development, Theoretical and Appl. Mech., 18, 193-210.
Sih,G.C. and Ho,J.W.(1993b), Rigid-plastic and damage behaviour in metal forming: Part II-model prediction, Theoretical and Appl. Mech., 18, 211-246.

Simo,J.C. and Ju,J.W.(1987), Stress and strain based continuum damage models, Part I and II, Int. J. Solids and Struct., 23, 821-869.
Spretnak,J.W.(1974), AFML-TR-74-160.
Stricklan,W.S., et al.(1976), Failure of aluminum cylindrical shells subjected to transverse blast loadings, 47th Shock and Vib. Symp., Albuquerque, N.M..
Symonds,P.S.(1968), Plastic shear deformation in dynamic load problems, in Engng. Plasticity, eds. J.Heyman and F.A.Leckie, Cambridge Univ. Press, Cambridge, pp.647-664.
Taylor,G.I. and Quinney,H.(1934), The latent energy remaining in a metal after cold working, Proc. R. Soc., A413, 307-326.
Teeling-Smith,R.G. and Nurick,G.N.(1991), The deformation and tearing of thin circular plates subjected to impulsive loads, Int. J. Impact Engng., 11, 77-91.
Timoshenko,S.(1956), Strength of Materials, Part II, Advanced Theory and Problems, 3rd ed., Robert E.Krieger Pub. Comp., New York, pp.420-427.
Tvergaard,V.(1981), Influence of voids on shear band instabilities under plane strain conditions, Int. J. Fracture, 17, 389-407.
Tvergaard,V. and Needleman,A.(1984), Analysis of the cup-cone fracture in a round tensile bar,Acta Metall., 32, 157-169.
Tvergaard,V.(1990), Material failure by void coalescence, in Advances in Appl. Mech., eds.J.W.Hutchinson and T.Y.Wu, Academic Press, 27, 83-151.
Van Stone,R.H., et al.(1983), Microstructural aspects of fracture by dimpled rupture, Int. Metals Reviews, 30, 157-179.
von Karman,T.(1911), Z. Vereins deutscher Ing., 55, 1749-1757.
Voyiadjis,G.Z., et al.(1990), A coupled theory of damage mechanics and finite strain elasto-plasticity--II, damage and finite strain plasticity, Int. J. Engng. Sci., 28, 505-524.
Voyiadjis,G.Z. and Kathan,P.I.(1992), A plastic-damage theory for large deformation of solids--I, theoretical formulation, Int. J. Engng. Sci., 30, 1089-1108.
Walter,J.W.(1992), Numerical experiments on adiabatic shear band formation in one dimension, Int. J. of Plasticity, 8, 657-693.
Wang,L.L., et al.(1988), The dependence of adiabatic shear banding on strain-rate, strain and temperature, J. De Physique, Colloque C3, 207-214.
Wang,L.L., et al.(1994), A macro- and microscopic study of adiabatic shearing extension of mode-II crack at dynamic loading, J. De Physique, Colloque C8, 465-470.
Wang,L.L. and Jones,N.(1996), An analysis of the shear failure of rigid-linear hardening beams under impulsive loading, Acta Mechanica Sinica, .
Wang,T.J.(1992a), Unified CDM model and local criterion for ductile fracture-I: unified CDM model for ductile fracture, Engng. Fracture Mech., 42, 177-183.
Wang,T.J.(1992b), Unified CDM model and local criterion for ductile fracture-II: ductile fracture local criterion based on the CDM model, Engng. Fracture Mech., 42, 185-193.
Wang,T.J.(1994), Further investigation of a new continuum damage mechanics criterion for ductile fracture: experimental verification and applications, Engng. Fracture Mech., 48, 217-230.
Wang,Z.P. and Zheng,J.(1994), Dynamic failure in ductile porous materials, Engng. Fracture Mech., 49, 61-74.

Wen,H.M. and Jones,N.(1994), Experimental investigation into the dynamic plastic response and perforation of a clamped circular plate struck transversely by a mass, J. Mech. Engng. Sci., proc. I. Mech. E., 208(C), 113-137.
Wen,H.M., et al.(1995a), Deformation and failure of clamped beams under low speed impact loading, Int. J. of Impact Engng., 16, 435-454.
Wen,H.M., et al.(1995b), Failure maps of clamped beams under impulsive loading, Mech. Struct. Machine, 23, 453-472.
Wen,H.M., et al.(1995c), A note on clamped circular plates under impulsive loading, Mech. Struct. Machine, 23, 331-342.
Wen,H.M.(1996), Deformation and tearing of clamped work-hardening beams subjected to impulsive loading, Int. J. Impact Engng., 18, 425-433.
Wen,H.M. and Jones,N.(1996), Low-velocity perforation of punch-impact-loaded metal plates, J. of Pressure Vessel Tech., 118, 181-187.
Woo,C.W. and Li,D.L.(1993), A universal physically consistent definition of material damage, Int. J. Solids Struct., 30, 2097-2108.
Wright,T.W. and Walter,J.W.(1987), On stress collapse in adiabatic shear bands, J. Mech. Phys., Solids, 35, 701-720.
Wright,T.W. and Ockendon,H.(1996), A scaling law for the effect of inertia on the formation of adiabatic shear bands, Int. J. of Plasticity, 12, 927-934.
Woolman,J. and Mottram,R.A.(1966), The mechanical and physical properties of the British standard En steels, Vol.2, Pergamon Press, London.
Youngdahl,C.K.(1971), Influence of pulse shape on the final plastic deformation of a circular plate, *Int. J. Solids Struct.*, 7, 1127-1142.
Yu,J.L. and Jones,N.(1989), Numerical simulation of a clamped beam under impact loading, Computers and Structures, 32, 281-293.
Yu,J.L. and Jones,N.(1991), Further experimental investigations on the failure of clamped beams under impact loads, Int. J. Solids Structures, 27, 1113-1137.
Yu,J.L. and Jones,N.(1997), Numerical simulation of impact loaded steel beams and the failure criteria, Int. J. Solids Structures, 34(30).
Zbib,H.M. and Jubran,T.S.(1992), Dynamic shear banding: a three-dimensional analysis, Int. J. of Plasticity, 8, 619-641.
Zener,C.(1948), The micro-mechanism of fracture, in Fracturing of Metals, ed. G.Sachs, American Society for Metals, Cleveland, Ohio, pp.3-31.
Zener,C. and Holloman,J.H.(1944), Effect of strain rate upon plastic flow of steel, J.Appl. Phys., 15, pp.22.
Zhang,K.S. and Zheng,C.Q.(1990), Microvoid multistage nucleating model and its application in analyses of micro damage and fracture, Engng. Fracture Mech., 37, 621-629.
Zheng,M., et al.(1994), On the ductile damage theory, Int. J. of Fracture, 67, R87-R92.
Zhu,G., et al.(1986), Estimation of the plastic structural response under impact, *Int. J. of Impact Engng.*, 4, 271-282.